frontiers | Research Topics

Advances in predicting future adverse coronary events: the role of cardiovascular imaging and coronary physiology indices

Edited by
Michail Papafaklis, Italo Porto and Sara Seitun

Published in
Frontiers in Cardiovascular Medicine

ISSN 1664-8714
ISBN 978-2-8325-5530-9
DOI 10.3389/978-2-8325-5530-9

About Frontiers

Frontiers is more than just an open access publisher of scholarly articles: it is a pioneering approach to the world of academia, radically improving the way scholarly research is managed. The grand vision of Frontiers is a world where all people have an equal opportunity to seek, share and generate knowledge. Frontiers provides immediate and permanent online open access to all its publications, but this alone is not enough to realize our grand goals.

Frontiers journal series

The Frontiers journal series is a multi-tier and interdisciplinary set of open-access, online journals, promising a paradigm shift from the current review, selection and dissemination processes in academic publishing. All Frontiers journals are driven by researchers for researchers; therefore, they constitute a service to the scholarly community. At the same time, the *Frontiers journal series* operates on a revolutionary invention, the tiered publishing system, initially addressing specific communities of scholars, and gradually climbing up to broader public understanding, thus serving the interests of the lay society, too.

Dedication to quality

Each Frontiers article is a landmark of the highest quality, thanks to genuinely collaborative interactions between authors and review editors, who include some of the world's best academicians. Research must be certified by peers before entering a stream of knowledge that may eventually reach the public - and shape society; therefore, Frontiers only applies the most rigorous and unbiased reviews. Frontiers revolutionizes research publishing by freely delivering the most outstanding research, evaluated with no bias from both the academic and social point of view. By applying the most advanced information technologies, Frontiers is catapulting scholarly publishing into a new generation.

What are Frontiers Research Topics?

Frontiers Research Topics are very popular trademarks of the *Frontiers journals series*: they are collections of at least ten articles, all centered on a particular subject. With their unique mix of varied contributions from Original Research to Review Articles, Frontiers Research Topics unify the most influential researchers, the latest key findings and historical advances in a hot research area.

Find out more on how to host your own Frontiers Research Topic or contribute to one as an author by contacting the Frontiers editorial office: frontiersin.org/about/contact

Advances in predicting future adverse coronary events: the role of cardiovascular imaging and coronary physiology indices

Topic editors

Michail Papafaklis — University of Patras, Greece

Italo Porto — University of Genoa, Italy

Sara Seitun — San Martino Polyclinic Hospital IRCCS, Italy

Citation

Papafaklis, M., Porto, I., Seitun, S., eds. (2024). *Advances in predicting future adverse coronary events: the role of cardiovascular imaging and coronary physiology indices*. Lausanne: Frontiers Media SA. doi: 10.3389/978-2-8325-5530-9

Table of contents

frontiers | Frontiers in Cardiovascular Medicine

TYPE Editorial
PUBLISHED 09 May 2023
DOI 10.3389/fcvm.2023.1206076

OPEN ACCESS

EDITED AND REVIEWED BY
Christos Bourantas,
Queen Mary University of London,
United Kingdom

*CORRESPONDENCE
Michail I. Papafaklis
m.papafaklis@yahoo.com

RECEIVED 14 April 2023
ACCEPTED 26 April 2023
PUBLISHED 09 May 2023

CITATION
Seitun S, Porto I and Papafaklis MI (2023) Editorial: Advances in predicting future adverse coronary events: the role of cardiovascular imaging and coronary physiology indices. Front. Cardiovasc. Med. 10:1206076. doi: 10.3389/fcvm.2023.1206076

Editorial: Advances in predicting future adverse coronary events: the role of cardiovascular imaging and coronary physiology indices

Sara Seitun[1], Italo Porto[2,3] and Michail I. Papafaklis[4]*

[1]Department of Radiology, IRCCS Ospedale Policlinico San Martino, Genova, Italy, [2]Department of Internal Medicine, University of Genova, Genova, Italy, [3]Cardiology Unit, Cardio-Thoracic and Vascular Department, IRCCS Ospedale Policlinico San Martino, Genova, Italy, [4]Catheterization and Hemodynamic Unit, Alexandra University Hospital, Athens, Greece

KEYWORDS

angiography, computed tomography coronary angiogram (CTCA), intravascular imaging (IVUS), optical coherence tomogaphy, cardiac MRI (CMR), coronary artery disease, acute coronary syndrome (ACS), fractional flow reserve (FFR)

Editorial on the Research Topic
Advances in predicting future adverse coronary events: the role of cardiovascular imaging and coronary physiology indices

Atherosclerotic coronary artery disease (CAD) remains the leading cause of morbidity and mortality worldwide (1). CAD is the consequence of a multistep and multifactorial process, in which chronic inflammation is involved at every stage. The clinical manifestations of the disease are extremely variable, ranging from subclinical atherosclerosis to plaque progression and acute coronary events. During the last decade, both non-invasive and invasive imaging techniques, as well as assessment of coronary physiology and hemodynamics have provided significant prognostic information. This Research Topic focuses on the prognostic role of cardiovascular imaging and coronary physiology indices for the identification of high-risk patients and coronary lesions. The studies included in this Research Topic address (1) the prognostic implications of non-invasive anatomic and functional imaging techniques (2), new physiologic markers of ischemia (3), new machine-learning assisted analysis of coronary thrombosis (4), the prognostic role of vascular biomarkers in specific subsets of patients, and (5) the advanced diagnostic and prognostic role of invasive intracoronary imaging.

Over the past decade, coronary computed tomography angiography (CCTA) has emerged as a first-line non-invasive imaging modality for the evaluation of patients with suspected CAD, receiving multiple Class 1 recommendations by both the American and European guidelines (2, 3).

The state-of-the-art minireview article by Emfietzoglou et al. addresses the major fields of application of CCTA and future perspectives with new technology such as photon-counting technique with intrinsic spectral capabilities at high contrast and spatial resolution. Besides coronary stenosis assessment, CCTA may evaluate plaque burden and nonobstructive high-risk coronary plaques to predict the risk of future coronary events and to guide targeted treatment and initiation of appropriate preventive therapy. CCTA may also provide the hemodynamic assessment of the coronary lesion via the CT-derived

fractional flow reserve (FFR) and myocardial perfusion for guiding treatment decisions. Finally, recent fields of research are the computation of coronary endothelial shear stress, a marker of the initiation and progression of atherosclerosis, and the pericoronary fat attenuation as a sensor of coronary inflammation.

Our series also included several relevant original research articles. The original research by Lee et al. evaluated the prognostic impact of anatomic and hemodynamic plaque characteristics as assessed by CCTA in predicting subsequent coronary events (DESTINY Study). They analyzed 158 patients who underwent CCTA for suspected CAD within 6–36 months before percutaneous coronary intervention (PCI) for acute myocardial infarction (MI) or unstable angina and 62 age- and sex-matched patients without PCI as the control group. They concluded that high-risk plaque characteristics (HRPCs: low attenuation plaque, positive remodeling, napkin-ring sign, spotty calcification, minimal luminal area <4 mm^2, or plaque burden ≥70%) and hemodynamic parameters [per-vessel FFR (FFRCT), per-lesion ΔFFRCT, and percent ischemic myocardial mass] added incremental prognostic value to clinical factors. Moreover, HRPCs provided more incremental predictability than clinical risk factors alone among vessels with negative FFRCT but not among vessels with positive FFRCT.

Intravascular ultrasound (IVUS) is a useful tool for accurate assessment of coronary lesion complexity and for optimization of stent implantation during PCI. Several meta-analyses of large observational and randomized studies have shown that (IVUS) guidance may improve short and long-term clinical outcomes compared to angiography guidance alone (4–7). However, outside of trials, IVUS use remains highly heterogenous and often low. Tindale et al. analyzed the real-world use and outcomes in PCI-naive patients undergoing IVUS-guided intervention in a specialist heart hospital in the UK. They performed a retrospective analysis of prospectively collected data from 10,574 consecutive patients. Only 4.3% of patients underwent IVUS, with a median follow-up of 4.6 years. There was no difference in survival or major adverse cardiac events (MACE) on both matched and adjusted analysis, although this may well be explained by significant selection bias and the high-risk population. The underuse of IVUS in routine interventional practice is multifactorial, with lack of training, individual operator experience, greater procedural time, and cost barrier being the most reported factors limiting its use (8).

The case report of Krcmar et al. is a great example of how intracoronary imaging with optical coherence tomography (OCT) can guide highly complex procedures, by providing exquisite anatomical details and three-dimensional images. They described a rare and potentially fatal complication of chronic stent loss in the left main and its migration into the left circumflex artery ostium during PCI. This complication was not immediately noticed by the operator, but 5 months later was successfully resolved by OCT guidance with the crushing technique. OCT provided useful information on the exact position and endothelialisation within the undeployed stent.

Coronary flow capacity (CFC) is a relatively new potentially important physiologic marker of ischemia for guiding PCI (9). Hamaya et al. evaluated the determinants and prognostic implications of the changes of thermodilution method-derived CFC status following PCI. In a total of 450 patients with chronic coronary syndrome (CCS), CFC changes following PCI were largely determined by the pre-PCI CFC status and were associated with a lower risk of incident target vessel failure.

Myocardial strain analysis assessed by cardiac magnetic resonance (CMR) feature tracking has emerged as a simple post-processing technique to assess myocardial motion and deformation and has shown to provide additional incremental prognostic value compared to traditional functional parameters in various cardiovascular disease settings (10). Zhuang et al. demonstrated that left ventricular strain and strain rate detected by CMR feature tracking were independent predictors of survival in 78 asymptomatic patients with repaired tetralogy of Fallot who required pulmonary valve replacement.

The original study by Ma et al. analyzed the predictive value of plasma big endothelin-1 (big ET-1) for the occurrence of adverse cardiovascular events in a cohort of patients with in-stent restenosis (ISR) and diabetes mellitus after PCI with drug-eluting stents. Big ET-1 is a 39-amino acid propeptide that is cleaved into the biologically active ET-1. ET-1 is a potent vasoconstrictor, both in large vessels and in the microcirculation, with intramyocardial vessels being very sensitive to its actions. The predictive value of increased circulating ET-1 levels has been shown in most cardiovascular diseases, leading ET-1 to be considered as a likely mediator of excessive vasoconstriction, endothelial dysfunction, cardiac remodeling, and age-associated inflammation (11). At 3-year follow-up, Ma et al demonstrated that big ET-1 improved the predictive value for MACEs over traditional and angiographic risk factors in patients with ISR and diabetes ($n = 795$) but not in non-diabetic patients with ISR ($n = 998$). Therefore, elevated big ET-1 may identify a group of stented patients with diabetes and ISR who are at particular risk for worse outcomes.

ST-segment elevation acute coronary syndrome (STEACS) typically occurs due to occlusive coronary thrombus formation superimposed on a ruptured or eroded atherosclerotic plaque. Kotronias et al. performed an interesting prospective OxAMI (Oxford Acute Myocardial Infarction) study evaluating the pathobiology of coronary thrombosis in patients with STEACS. Thrombus composition has relevant prognostic information since it has been shown that macroscopically red (erythrocyte-rich) thrombi are associated with an adverse prognostic outcome compared to macroscopically white (platelet-rich) thrombi (12). Kotronias et al included 306 patients presenting with STEACS who underwent manual thrombectomy during primary PCI. They used a novel method utilizing spatially resolved reflectance spectroscopy combined with machine-learning approaches for the characterization and quantification of aspirated coronary thrombosis. In a sub-set of 36 patients, they assessed invasive [index of coronary microvascular resistance (IMR)] and non-invasive [microvascular obstruction (MVO) at CMR] indices of coronary microvascular injury. They demonstrated that this novel analytical approach enabled the quantification of thrombus composition, including automated quantification of thrombus area within the images. Finally, the derived reflectance spectral

signatures of coronary thrombi were correlated with microvascular injury phenotyping, as measured by MVO and IMR.

In conclusion, the articles included in this Research Topic are small but important steps in our understanding of CAD, adding new knowledge about the prognostic role of different imaging techniques, coronary physiology indices, and cardiovascular biomarkers. In the coming years, it is expected that further work could provide a deeper insight into the pathophysiology of coronary atherosclerotic process with the ultimate aim to improve patient outcomes, reduce the burden of cardiovascular disease and aid in the development of new therapeutic strategies.

Author contributions

All authors listed have made a substantial, direct, and intellectual contribution to the work and approved it for publication.

Conflict of interest

The authors declare that the research was conducted in the absence of any commercial or financial relationships that could be construed as a potential conflict of interest.

Publisher's note

References

1. Tsao CW, Aday AW, Almarzooq ZI, Alonso A, Beaton AZ, Bittencourt MS, et al. Heart disease and stroke statistics-2022 update: a report from the American Heart Association. *Circulation*. (2022) 145:e153–639. doi: 10.1161/CIR.0000000000001052

2. Knuuti J, Wijns W, Saraste A, Capodanno D, Barbato E, Funck-Brentano C, et al. 2019 ESC guidelines for the diagnosis and management of chronic coronary syndromes. *Eur Heart J*. (2020) 41:407–77. doi: 10.1093/eurheartj/ehz425; Erratum in: Eur Heart J. (2020) 41:4242.

3. Gulati M, Levy PD, Mukherjee D, Amsterdam E, Bhatt DL, Birtcher KK, et al. 2021 AHA/ACC/ASE/CHEST/SAEM/SCCT/SCMR guideline for the evaluation and diagnosis of chest pain: a report of the American college of cardiology/American heart association joint committee on clinical practice guidelines. *Circulation*. (2021) 144:e368–454. doi: 10.1161/CIR.0000000000001029; Erratum in: Circulation. (2021) 144:e455.

4. Choi KH, Song YB, Lee JM, Lee SY, Park TK, Yang JH, et al. Impact of intravascular ultrasound-guided percutaneous coronary intervention on long-term clinical outcomes in patients undergoing complex procedures. *JACC Cardiovasc Interv*. (2019) 12:607–20. doi: 10.1016/j.jcin.2019.01.227

5. Hong SJ, Mintz GS, Ahn CM, Kim JS, Kim BK, Ko YG, et al. Effect of intravascular ultrasound-guided drug-eluting stent implantation: 5-year follow-up of the IVUS-XPL randomized trial. *JACC Cardiovasc Interv*. (2020) 13:62–71. doi: 10.1016/j.jcin.2019.09.033

6. Dykun I, Babinets O, Hendricks S, Balcer B, Puri R, Al-Rashid F, et al. Utilization of IVUS improves all-cause mortality in patients undergoing invasive coronary angiography. *Atheroscler Plus*. (2021) 43:10–7. doi: 10.1016/j.athplu.2021.07.001

7. Buccheri S, Franchina G, Romano S, Puglisi S, Venuti G, D'Arrigo P, et al. Clinical outcomes following intravascular imaging-guided versus coronary angiography-guided percutaneous coronary intervention with stent implantation: a systematic review and Bayesian network meta-analysis of 31 studies and 17,882 patients. *JACC Cardiovasc Interv*. (2017) 10:2488–98. doi: 10.1016/j.jcin.2017.08.051

8. Koskinas KC, Nakamura M, Räber L, Colleran R, Kadota K, Capodanno D, et al. Current use of intracoronary imaging in interventional practice- results of a European association of percutaneous cardiovascular interventions (EAPCI) and Japanese association of cardiovascular interventions and therapeutics (CVIT) clinical practice survey. *Circ J*. (2018) 82:1360–8. doi: 10.1253/circj.CJ-17-1144

9. Murai T, Stegehuis VE, van de Hoef TP, Wijntjens GWM, Hoshino M, Kanaji Y, et al. Coronary flow capacity to identify stenosis associated with coronary flow improvement after revascularization: a combined analysis from DEFINE FLOW and IDEAL. *J Am Heart Assoc*. (2020) 9:e016130. doi: 10.1161/JAHA.120.016130

10. Xu J, Yang W, Zhao S, Lu M. State-of-the-art myocardial strain by CMR feature tracking: clinical applications and future perspectives. *Eur Radiol*. (2022) 32:5424–35. doi: 10.1007/s00330-022-08629-2

11. Jankowich M, Choudhary G. Endothelin-1 levels and cardiovascular events. *Trends Cardiovasc Med*. (2020) 30:1–8. doi: 10.1016/j.tcm.2019.01.007

12. Quadros AS, Cambruzzi E, Sebben J, David RB, Abelin A, Welter D, et al. Red versus white thrombi in patients with ST-elevation myocardial infarction undergoing primary percutaneous coronary intervention: clinical and angiographic outcomes. *Am Heart J*. (2012) 164:553–60. doi: 10.1016/j.ahj.2012.07.022

frontiers in Cardiovascular Medicine

CASE REPORT
published: 10 February 2022
doi: 10.3389/fcvm.2022.825542

Case Report: Optical Coherence Tomography Usage for Treatment of the Chronically Lost Stent in the Left Main Coronary Artery

Tomislav Krcmar[1], Ivana Grgic Romic[1], Vjekoslav Tomulic[1], Tomislav Jakljevic[1], Luka Bastiancic[1] and Ivan Zeljkovic[2]*

[1] Deparment of Cardiology, Rijeka University Hospital Centre, Rijeka, Croatia, [2] Department of Cardiology, Sestre Milosrdnice University Hospital Centre, Zagreb, Croatia

Acute adverse outcomes of a stent loss during percutaneous coronary intervention (PCI) are well described, however, data on long-term consequences are scarce, especially with intravascular imaging. We report a case of a coronary stent loss in the left main and ostial left circumflex artery (LCx) bifurcation and its migration into the LCx ostium during PCI procedures. This rare complication, which was not immediately noticed, was verified and successfully resolved 5 months after using optical coherence tomography and right trans-radial access. Considering the infrequency of this complication, few cases have been reported, however, our case has several distinct specificities. We aim to encourage the crushing technique in cases of chronic stent loss when the retrieval is not an option and highlight the optical coherence tomography (OCT) value in imaging and evaluation of similar complex settings.

Keywords: optical coherence tomography, intravascular imaging, stent loss, left main, crush technique, percutaneous coronary intervention (complex PCI)

OPEN ACCESS

Edited by:
Michail Papafaklis, University Hospital of Ioannina, Greece

Reviewed by:
Makoto Araki, Massachusetts General Hospital and Harvard Medical School, United States
Antonios Karanasos, Hippokration General Hospital, Greece

****Correspondence:***
Ivana Grgic Romic
ivana.grgic.ri@gmail.com

Specialty section:
This article was submitted to Cardiovascular Imaging, a section of the journal Frontiers in Cardiovascular Medicine

Received: *30 November 2021*
Accepted: *10 January 2022*
Published: *10 February 2022*

Citation:
Krcmar T, Grgic Romic I, Tomulic V, Jakljevic T, Bastiancic L and Zeljkovic I (2022) Case Report: Optical Coherence Tomography Usage for Treatment of the Chronically Lost Stent in the Left Main Coronary Artery. Front. Cardiovasc. Med. 9:825542. doi: 10.3389/fcvm.2022.825542

INTRODUCTION

Unnoticed loss of an unexpanded stent during percutaneous coronary intervention (PCI) is a rare and potentially fatal complication, with decreasing incidence in recent years (1–3). A number of mechanisms for stent loss have been suggested, mostly involving coronary anatomy and technical procedural specificities (3–5). Acute adverse outcomes are well described, however, data on long-term consequences of chronically lost stent is scarce, especially with intravascular imaging (1, 5, 6).

We report a case of an unnoticed coronary stent loss in the left main and ostial left circumflex artery (LCx) bifurcation during a primary PCI, which was successfully treated after 5 months with the usage of optical coherence tomography (OCT).

CASE DESCRIPTION

A 48-year-old male patient, a smoker without a history of chronic diseases, presented with an acute myocardial infarction without ST elevation (NSTEMI) to a local hospital. Urgent coronary angiography demonstrated sub-occlusion (99% stenosis) in the midportion of the dominant right coronary artery (RCA) (**Figure 1A**) and significant distal LCx (90% stenosis) lesion (**Figure 1B**).

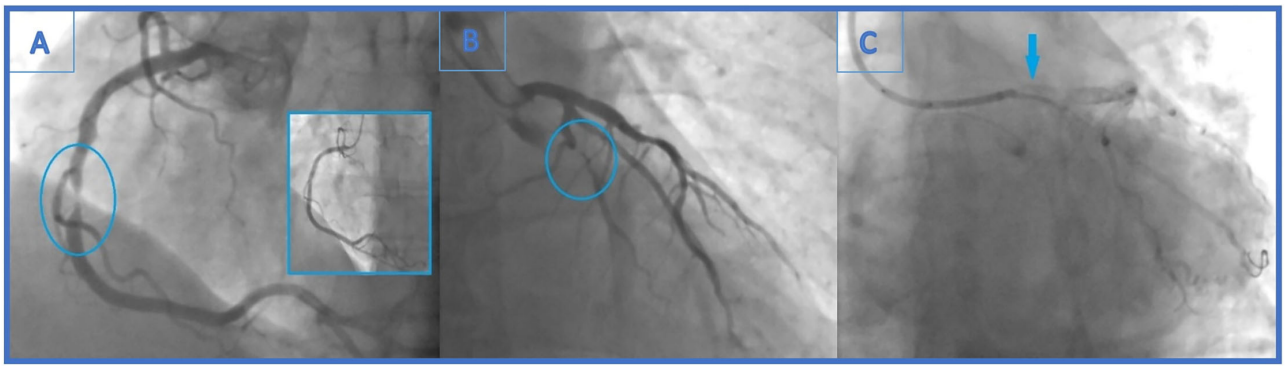

FIGURE 1 | (A) Urgent coronary angiography with significant mid-right coronary artery stenosis (99%)-the culprit lesion and final angiographic result in the little window. **(B)** Distal left circumflex artery (LCx) lesion left unsolved (90% stenosis). **(C)** Angiogram showing stent falling from the balloon and darting into the LCx ostium. It is seen as linear radio-opaque object in the LM/LCx.

Primary percutaneous coronary intervention (PCI) was undertaken using a Judkins-right 4 cm guiding catheter with side holes (Cordis, Milpitas, CA, USA). Employing a 0.014 in balanced middleweight (BMW) guidewire (Abbott Vascular, Santa Clara, CA, USA), drug eluting stent (DES) Xience Prime (3.5 × 15 mm, Abbott Vascular) was successfully implanted in a culprit RCA lesion (**Figure 1A**). Intervention was pursued on the distal LCx lesion with 6 French (Fr) Extra backup guiding (EBU) catheter 3.75 cm (Medtronic, Minneapolis, MN, USA) and BMW guidewire (Abbott Vascular). After predilatation with non-compliant (NC) balloons (Traveler 1.20 × 8 mm and 2.0 × 8 mm, Abbot Vascular), Xience Prime stent (3.0 × 12 mm, Abbot Vascular) could not cross the lesion and the intervention was aborted. Echocardiographic examination showed mildly hypertrophic myocardium with no regional wall abnormalities and left ventricular ejection fraction of 60%. After 3 days of uneventful hospitalization, the patient was released.

After 4 months, the patient reported effort angina (Canadian Cardiac Society—CCS class 2), and the stress-ECG test showed signs of ischaemia. Coronary angiography revealed newly formed, highly significant ostial (95%) LCx stenosis (LM 0.0.1 lesion according to Medina classification) (**Figure 2A**). Previously known distal LCx stenosis (90%) was also shown.

Intervention was pursued through 6F EBU catheter 3.5 cm (Medtronic). The first obtuse marginal artery (OM1) and LCx were wired with BMW (Abbot Vascular) in OM1 and BMW Universal II (Abbot Vascular) in LCx. Distal LCx lesion was pre-dilatated with non-compliant (NC) balloons (Traveler 2.5 × 15 mm and 2.0 × 20 mm, Abbot Vascular), after which Resolute Onyx stent (2.75 × 26 mm, Medtronic) was placed. Ostial LCx lesion was predilated [up to 22 atmosphere (atm)] with an NC balloon (Traveler 2.5 × 15 mm, Abbot Vascular) and Resolute Onyx stent (3.0 × 12 mm, Medtronic) was implanted in proximal LCx (**Figure 2C**).

Carefully observing the final result, a linear radiopaque object was seen in the distal segment of the left main coronary artery (LMCA), which has not been verified before. At that point, the operator suspected that the ostial LCx stent had crushed an earlier lost stent which was protruding from the proximal LCx to the distal LMCA (**Figure 2B**). Afterwards, the first angiography film was viewed, and it was seen how the stent went loose from the wire and darted into the LCx ostium (**Figure 1C**). Further evaluation was indicated, but this time in our facility using an intravascular imaging modality with the idea to precisely visualize lost stent, its position, and endothelialisation.

The patient came back to our facility 1 month after the second coronary angiography due to lack of the OCT catheter (caused primarily by financial reasons), and without an urgent indication since there was no angiographic or clinical sign of coronary blood-flow obstruction. The right radial artery was used for introducing the OCT catheter (Dragonfly DUO Imaging Catheter, St. Jude Medical, Sylmar, CA, USA) into the coronary arteries. Coronary stents in the proximal LCx and in the mid-RCA were found completely patent. The lack of OCT imaging prior to the first LCx PCI is a limitation as it precluded optimal visualization of the complication.

OCT visualised undeployed stent protruding (approximately 50% of the stent) from the ostium of LCx to distal segment of LMCA, not causing a significant stenosis (**Figure 3A**). The lost stent was partially endothelialised (proximal 50% in the LMCA, distal part in the LCx was partially crushed 1 month earlier) (**Figure 3B**). There was no sign of thrombus formation around or inside the lost stent. Since the distal part of the lost stent was crushed with a stent deployed into a proximal LCx segment during the second coronary intervention, stent deployment from the LMCA to the left anterior descending coronary artery (LAD) with crushing of both the proximal 50% of lost stent and a small part of protruding proximal LCx stent was planned. Using a 7 Fr EBU catheter 3.5 cm Launcher (Medtronic), the stenosis was crossed with a 0.014 in guidewire (Hi-Torque BMW Universal II, Abbot Vascular) and positioned to the distal segment of LAD. "Ultra-thin strut" DES Orsiro (4.0 × 22 mm, Biotronik, Lake Oswego, OR, USA) was deployed into the LMCA ostium to proximal LAD with a mini crush of proximal LCx stent and protruding LCx undeployed stent struts. Then, a Runthrough Hypercoat guidewire (Terumo Europe NV, Lueven, Belgium)

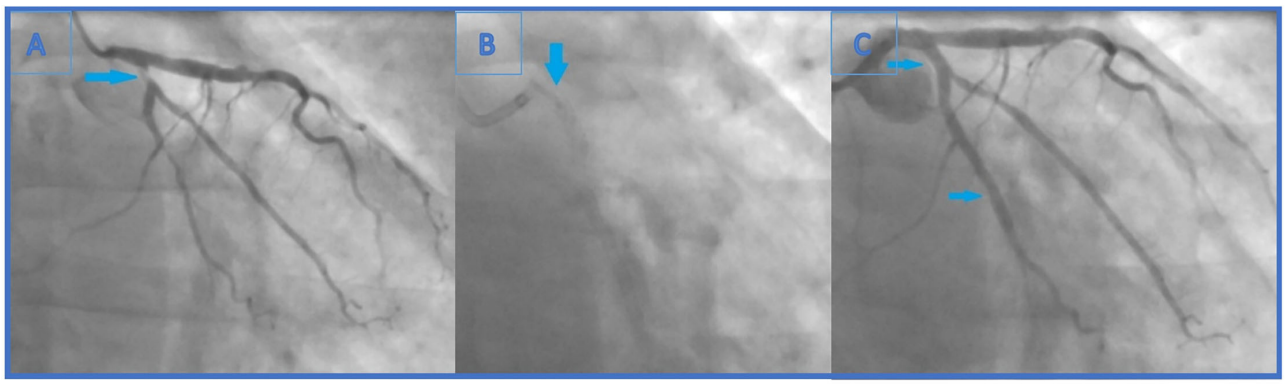

FIGURE 2 | (A) Second coronary angiography revealed newly formed, highly significant ostial (95%) (Medina 0.0.1) LCx stenosis. Also, previously known distal LCx stenosis (90%) was shown. **(B)** The end of the second intervention (angiography without iodinated contrast): the lost stent in the left main coronary artery (arrow). The distal part of the lost stent (part in the LCx, 70% of its length) is crushed with the proximal LCx stent. **(C)** The end of the second intervention where proximal and distal LCx stenosis were solved (arrows indicating lesion sites where the stents were implanted).

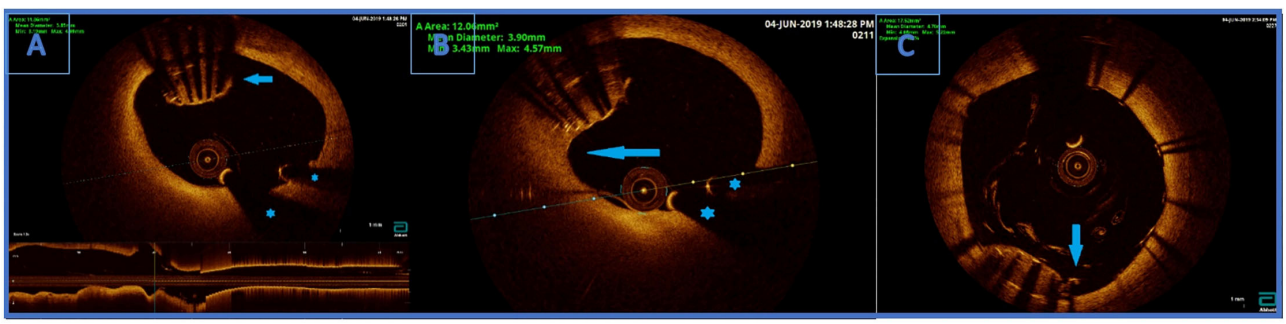

FIGURE 3 | (A) Optical coherence tomography (OCT) finding an undeployed part of the lost stent in the left main artery. There are no signs of thrombosis around the stent. Below is the longitudinal view of the left main OCT. *Wire artifacts. **(B)** Optical coherence tomography image. Partially endothelialised (arrow) part of the undeployed stent in the LM. **(C)** OCT showing good apposition of the new stent and a successfully crushed part of the undeployed stent. Arrow indicating a single non fully apposed strut.

was crossed through stent struts in the proximal LCx. After struts dilatation (up to 22 atm) with a semi-compliant (SC) balloon (Maverick 2.5 × 15 mm, Boston Scientific, Marlborough, MA, USA), an additional kissing balloon post dilatation was necessary. It was performed with a semi-compliant (SC) balloon (14 atm) (Maverick 3.0 × 15 mm, Boston Scientific) in LAD and an NC balloon (12 atm) (Emerge 2.75 × 8 mm, Boston Scientific Corp., Natick, MA, USA) in LCx, resulting in the lost stent being crushed between the LAD wall and the new stent in LMCA/LAD.

The procedure was finalized with a proximal optimisation technique (POT) in LMCA with an NC balloon (Quantum 4.5 × 8 mm, Boston Scientific). Final angiography showed TIMI III flow (**Figure 4**) and OCT demonstrated well-apposed stent struts with a crushed lost stent in LMCA (**Figure 3C**; **Supplementary Video** with final OCT pullback from LAD to LM). The patient had an uneventful recovery and is still in follow-up. Dual antiplatelet therapy with ticagrelor (90 mg two times daily) and acetylsalicylic acid (100 mg one time daily) was continued for 12 months after the intervention. Currently, the patient is prescribed ticagrelor (60 mg two times daily) together with acetylsalicylic acid (100 mg once daily) for an additional 12 months. Afterwards, the plan is to recommend acetylsalicylic acid lifelong (100 mg once daily) and a vascular dose of rivaroxaban (2.5 mg two times daily).

DISCUSSION

We presented a case of a coronary stent loss and its migration into the LCx ostium during an attempt of its distal segment revascularisation. A rare complication was not immediately noticed by the operator, but was OCT verified 5 months later and was successfully resolved using the right trans-radial access. Considering the infrequency of this complication, few cases have been reported in the literature, however, our case has several distinct specificities (1–7).

Firstly, the lost stent was located in the LMCA, a rare location described in only several cases so far (1, 5, 7). More importantly, this was a chronic stent loss, while earlier cases were describing acute management of stent loss in LMCA (1–4, 7, 8). In addition,

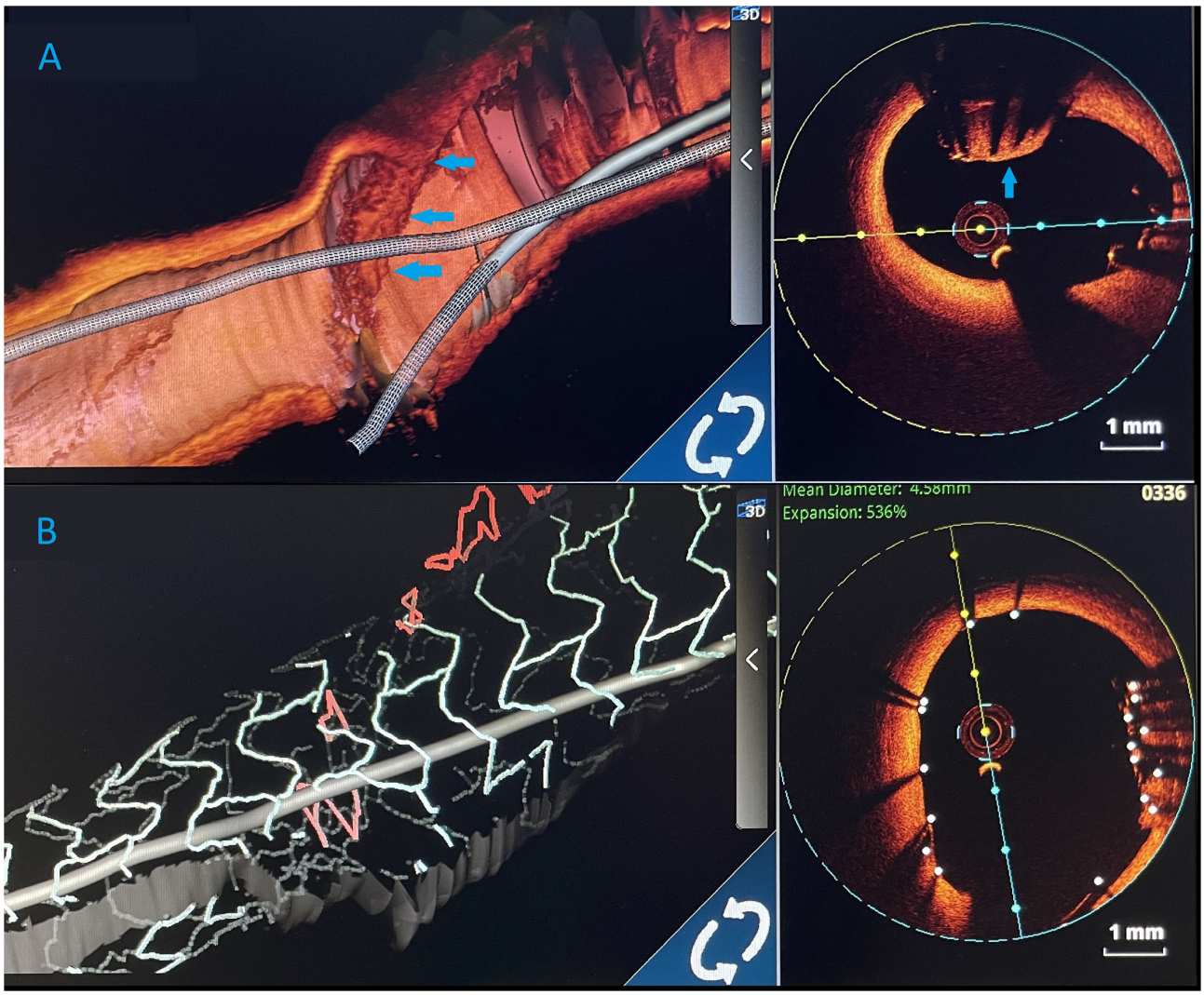

FIGURE 4 | Three-dimensional (3D) images. **(A)** 3D render of an optical coherence tomography (OCT) showing an undeployed lost stent (blue arrows) in the left main artery. **(B)** Optical coherence tomography 3D view. After LM stent implantation, lost stent (blue arrows) is successfully crushed against the left main artery wall.

most reports describe management of acutely noticed and treated stent losses, while in our case, long-term consequences are seen, which are not well known (2, 3, 5, 7).

Secondly, it is generally advised to avoid stent crush or deployment within the LMCA or at a bifurcation lesion for the sake of the restenosis risk (1, 9). However, retrieval of the lost stent was not an option in our case since the distal half was already crushed with the stent deployed into the proximal LCx segment 1 month before. Retrieval of the lost stent can be efficacious with various non-surgical methods, including the small-balloon technique, which is the most frequently used one, double-wire technique, and loop-snare technique (1, 2, 4, 9, 10). Hence, new stent deployment from LMCA to LAD, with crushing of both proximal 50% of the lost stent and a small part of stent protruding to proximal LCx, was planned. The operator considered that the option of stenting from LAD to the LM is a better option than the stenting from LCx. The reason is that in case of stenting from LCx to LM, part of proximal LCx would have four layers of stents (lost stent crushed earlier, ostial LCx stent implanted during second procedure, and a new stent from LCx to the LM). Also, the LCx artery is narrower than the LM and LAD, hence the result of post dilatation and POT would be less optimal.

Brilakis et al. suggested that in cases in which the lost stent cannot be retrieved, deploying or crushing the stent may be a good alternative with good clinical outcomes (4). In another study, lost stents were crushed against the vessel wall in two patients with no major cardiac complications (9).

Thirdly, according to a retrospective study, patients who encountered stent loss had a higher incidence of bleeding,

requiring transfusion and causing a need for coronary artery bypass surgery, both not noted in our case (2).

Fourthly, in most cases, the stent was lost due to not crossing the stenosis and being damaged while trying, hence becoming dissociated from its delivery system (1, 4, 10, 11). In our case, one can only speculate that the stent was lost because of the high friction caused by vessel angulation and inadequate guiding of the catheter position. In addition, the operator was not aware of this happening during the initial procedure. Thus, operators should be reminded to check the complete condition of the stent system after unsuccessful deployment, especially if this was the case due to the (heavy) calcification of the lesion and/or anatomical specificities (tortuosity, angulation $>90^{\circ}$, bi/trifurcation, etc.) (1–4, 10, 11). Interestingly, 5 months after its loss, the stent was only partially covered by intima with no signs of thrombus formation. This could be explained by dual antiplatelet therapy usage and a normal left ventricle ejection fraction (LVEF 60%) (5–9, 12). The reason the stent could not cross during the initial intervention but did cross at the time of the recurrent event is probably due to: better lesion preparation, more experienced operator, and the partial endothelialisation of the lost stent. We chose OCT over intravascular ultrasound (IVUS) because of its superior resolution imaging, giving a better characterization of neointimal tissue (6, 13, 14). Finally, besides the risk of stent crushing in the critical coronary segment, this complex coronary intervention was entirely performed using only right radial access, while most other similar cases were using femoral access (1–12).

In conclusion, we encourage the crushing technique in cases of chronic stent loss when the retrieval is not an option, along with highlighting the OCT value in imaging and evaluation of similar complex settings. This complex procedure can be done using a transradial approach without affecting the safety or efficacy. Operators should be reminded to check the complete condition of the stent system after an unsuccessful deployment, regardless of the reason.

DATA AVAILABILITY STATEMENT

The original contributions presented in the study are included in the article/**Supplementary Material**, further inquiries can be directed to the corresponding author/s.

ETHICS STATEMENT

Ethical review and approval was not required for the study on human participants in accordance with the local legislation and institutional requirements. The patients/participants provided their written informed consent to participate in this study. Written informed consent was obtained from the individual(s) for the publication of any potentially identifiable images or data included in this article.

AUTHOR CONTRIBUTIONS

TK performed the intervention together with VT and LB. IG and TJ drafted the manuscript. IZ contributed to manuscript design, drafting, and critical revision. All authors have critically read and reviewed this article, approved the version to be published, and agreed to be accountable for all aspects of the work in ensuring that questions related to the accuracy or integrity of any part of the work are appropriately investigated and resolved.

SUPPLEMENTARY MATERIAL

The Supplementary Material for this article can be found online at: https://www.frontiersin.org/articles/10.3389/fcvm.2022.825542/full#supplementary-material

REFERENCES

1. Alomar ME, Michael TT, Patel VG, Altomare CG, Rangan BV, Cipher D, et al. Stent loss and retrieval during percutaneous coronary interventions: a systematic review and meta-analysis. *J Invasive Cardiol.* (2013) 25:637–41. doi: 10.1016/s0735-1097(13)61649-6
2. Kammler J, Leisch F, Kerschner K, Kypta A, Steinwender C, Kratochwill H, et al. Long-term follow-up in patients with lost coronary stents during interventional procedures. *Am J Cardiol.* (2006) 98:367–9. doi: 10.1016/j.amjcard.2006.01.105
3. Nikolsky E, Gruberg L, Pechersky S, Kapeliovich M, Grenadier E, Amikam S, et al. Stent deployment failure: reasons, implications, and short- and long-term outcomes. *Catheter Cardiovasc Interv.* (2003) 59:324–8. doi: 10.1002/ccd.10543
4. Brilakis ES, Best PJ, Elesber AA, Barsness GW, Lennon RJ, Holmes DR Jr, et al. Incidence, retrieval methods, and outcomes of stent loss during percutaneous coronary intervention: a large single-center experience. *Catheter Cardiovasc Interv.* (2005) 66:333–40. doi: 10.1002/ccd.20449
5. Ronchard T, Combaret N, Malcles G, Motreff P, Souteyrand G. Identification of undeployed stent in the left main coronary artery after 3 years on optical coherence tomography. *Circ J.* (2018) 82:1972–3. doi: 10.1253/circj.CJ-17-0985
6. Cockburn J, Wilkes N, Figtree G, Ward M, Bhindi R, Hansen P. Use of optical coherence tomography to guide treatment of an undeployed stent trapped in the right coronary artery to cover a proximal stent outflow dissection. *Int J Cardiol.* (2013) 167:e163–6. doi: 10.1016/j.ijcard.2013.04.172
7. Fam JM, den Dekker W, de Graaf P , Regar E. An unusual case of stent-in-stent thrombosis. *JACC Cardiovasc Interv.* (2015) 8:e261–2. doi: 10.1016/j.jcin.2015.07.039
8. Stajić Z. Stent dislodgement in the distal left main coronary artery and its successful management with balloon crushing technique. *Vojnosanit Pregl.* (2015) 72:454–7. doi: 10.2298/VSP131006008S
9. Yang DH, Woo SI, Kim DH, Park SD, Jang JH, Kwan J, et al. Two dislodged and crushed coronary stents: treatment of two simultaneously dislodged stents using crushing techniques. *Korean J Intern Med.* (2013) 28:718–23. doi: 10.3904/kjim.2013.28.6.718
10. Eggebrecht H, Haude M, von Birgelen C, Oldenburg O, Baumgart D, Herrmann J, et al. Nonsurgical retrieval of embolized coronary stents. *Catheter Cardiovasc Interv.* (2000) 51:432–40. doi: 10.1002/1522-726X(200012)51:4<432::AID-CCD12>3.0.CO;2-1
11. Yang Soon C, Chong E, Sangiorgi GM. A challenging case of dislodged stent retrieval with the use of Goose neck snare kit. *Catheter Cardiovasc Interv.* (2010) 75:630–3. doi: 10.1002/ccd.22283
12. Silva Marques J, Leite L, Oliveira-Santos M, Matos V. Subclinical thrombosis of a chronically lost stent. *Eur Heart J.* (2017) 38:920. doi: 10.1093/eurheartj/ehw657

13. Hussain F, Moussa T. Migration of an embolized deployed stent from the left main with subsequent crushing: a new use for the IVUS catheter? *J Invasive Cardiol.* (2010) 22:E19–22.
14. Prati F, Guagliumi G, Mintz GS, Costa M, Regar E, Akasaka T, et al. Expert review document part 2: Methodology, terminology and clinical applications of optical coherence tomography for the assessment of interventional procedures. *Eur Heart J.* (2012) 33:2513–20. doi: 10.1093/eurheartj/ehs095

Conflict of Interest: The authors declare that the research was conducted in the absence of any commercial or financial relationships that could be construed as a potential conflict of interest.

Publisher's Note: All claims expressed in this article are solely those of the authors and do not necessarily represent those of their affiliated organizations, or those of the publisher, the editors and the reviewers. Any product that may be evaluated in this article, or claim that may be made by its manufacturer, is not guaranteed or endorsed by the publisher.

frontiers | Frontiers in Cardiovascular Medicine

ORIGINAL RESEARCH
published: 23 May 2022
doi: 10.3389/fcvm.2022.871450

Anatomic and Hemodynamic Plaque Characteristics for Subsequent Coronary Events

Seung Hun Lee[1†], David Hong[2†], Neng Dai[3], Doosup Shin[4], Ki Hong Choi[2], Sung Mok Kim[5], Hyun Kuk Kim[6], Ki-Hyun Jeon[7], Sang Jin Ha[8], Kwan Yong Lee[9], Taek Kyu Park[2], Jeong Hoon Yang[2], Young Bin Song[2], Joo-Yong Hahn[2], Seung-Hyuk Choi[2], Yeon Hyeon Choe[5], Hyeon-Cheol Gwon[2], Junbo Ge[3] and Joo Myung Lee[2]*

[1] Division of Cardiology, Department of Internal Medicine, Chonnam National University Hospital, Chonnam National University Medical School, Gwangju, South Korea, [2] Division of Cardiology, Department of Internal Medicine, Heart Vascular Stroke Institute, Samsung Medical Center, Sungkyunkwan University School of Medicine, Seoul, South Korea, [3] Department of Cardiology, Shanghai Institute of Cardiovascular Diseases, Zhongshan Hospital, Fudan University, Shanghai, China, [4] Division of Cardiovascular Medicine, Department of Internal Medicine, University of Iowa Carver College of Medicine, Iowa City, IA, United States, [5] Department of Radiology, Cardiovascular Imaging Center, Heart Vascular Stroke Institute, Samsung Medical Center, Sungkyunkwan University School of Medicine, Seoul, South Korea, [6] Department of Internal Medicine and Cardiovascular Center, Chosun University Hospital, University of Chosun College of Medicine, Gwangju, South Korea, [7] Division of Cardiovascular Medicine, Department of Internal Medicine, Seoul National University Bundang Hospital, Seongnam, South Korea, [8] Division of Cardiology, Department of Internal Medicine, Gangneung Asan Hospital, University of Ulsan College of Medicine, Gangneung, South Korea, [9] Cardiovascular Center and Cardiology Division, Seoul St. Mary's Hospital, The Catholic University of Korea, Seoul, South Korea

OPEN ACCESS

Edited by:
Sara Seitun,
San Martino Polyclinic Hospital IRCCS, Italy

Reviewed by:
Leandro Slipczuk,
Montefiore Health System, United States
Andreas Mitsis,
Medical School, University of Cyprus, Cyprus
Stefano Benenati,
San Martino Hospital (IRCCS), Italy

***Correspondence:**
Joo Myung Lee
drone80@hanmail.net;
joomyung.lee@samsung.com

[†]These authors have contributed equally to this work

Specialty section:
This article was submitted to Coronary Artery Disease, a section of the journal Frontiers in Cardiovascular Medicine

Received: 08 February 2022
Accepted: 19 April 2022
Published: 23 May 2022

Citation:
Lee SH, Hong D, Dai N, Shin D, Choi KH, Kim SM, Kim HK, Jeon K-H, Ha SJ, Lee KY, Park TK, Yang JH, Song YB, Hahn J-Y, Choi S-H, Choe YH, Gwon H-C, Ge J and Lee JM (2022) Anatomic and Hemodynamic Plaque Characteristics for Subsequent Coronary Events. Front. Cardiovasc. Med. 9:871450. doi: 10.3389/fcvm.2022.871450

Objectives: While coronary computed tomography angiography (CCTA) enables the evaluation of anatomic and hemodynamic plaque characteristics of coronary artery disease (CAD), the clinical roles of these characteristics are not clear. We sought to evaluate the prognostic implications of CCTA-derived anatomic and hemodynamic plaque characteristics in the prediction of subsequent coronary events.

Methods: The study cohort consisted of 158 patients who underwent CCTA with suspected CAD within 6–36 months before percutaneous coronary intervention (PCI) for acute myocardial infarction (MI) or unstable angina and age-/sex-matched 62 patients without PCI as the control group. Preexisting high-risk plaque characteristics (HRPCs: low attenuation plaque, positive remodeling, napkin-ring sign, spotty calcification, minimal luminal area <4 mm^2, or plaque burden $\geq$70%) and hemodynamic parameters (per-vessel fractional flow reserve [FFRCT], per-lesion ΔFFR_{CT}, and percent ischemic myocardial mass) were analyzed from prior CCTA. The primary outcome was a subsequent coronary event, which was defined as a composite of vessel-specific MI or revascularization for unstable angina. The prognostic impact of clinical risk factors, HRPCs, and hemodynamic parameters were compared between vessels with (160 vessels) and without subsequent coronary events (329 vessels).

Results: Vessels with a subsequent coronary event had higher number of HRPCs (2.6 ± 1.4 vs. 2.3 ± 1.4, $P = 0.012$), lower FFR_{CT} (0.76 ± 0.13 vs. 0.82 ± 0.11, $P < 0.001$), higher ΔFFR_{CT} (0.14 ± 0.12 vs. 0.09 ± 0.08, $P < 0.001$), and higher percent ischemic myocardial mass (29.0 ± 18.5 vs. 26.0 ± 18.4, $P = 0.022$) than

those without a subsequent coronary event. Compared with clinical risk factors, HRPCs and hemodynamic parameters showed higher discriminant abilities for subsequent coronary events with ΔFFR_{CT} being the most powerful predictor. HRPCs showed additive discriminant ability to clinical risk factors (c-index 0.620 vs. 0.558, $P = 0.027$), and hemodynamic parameters further increased discriminant ability (c-index 0.698 vs. 0.620, $P = 0.001$) and reclassification abilities (NRI 0.460, IDI 0.061, $P < 0.001$ for all) for subsequent coronary events. Among vessels with negative FFR_{CT} (>0.80), adding HRPCs into clinical risk factors significantly increased discriminant and reclassification abilities for subsequent coronary events (c-index 0.687 vs. 0.576, $P = 0.005$; NRI 0.412, $P = 0.002$; IDI 0.064, $P = 0.001$) but not for vessels with positive FFR_{CT} (≤0.80).

Conclusion: In predicting subsequent coronary events, both HRPCs and hemodynamic parameters by CCTA allow better prediction of subsequent coronary events than clinical risk factors. HRPCs provide more incremental predictability than clinical risk factors alone among vessels with negative FFR_{CT} but not among vessels with positive FFR_{CT}.

Clinical Trial Registration: PreDiction and Validation of Clinical CoursE of Coronary Artery DiSease With CT-Derived Non-INvasive HemodYnamic Phenotyping and Plaque Characterization (DESTINY Study), NCT04794868.

Keywords: coronary artery disease, coronary CT angiography, myocardial ischemia, vulnerable plaques, prognosis

INTRODUCTION

Identification of patients with coronary atherosclerotic disease (CAD) at high risk of acute coronary syndrome (ACS) and who may benefit from intensified preventive measures has been of major interest (1). Since postmortem studies provided insights into plaque vulnerability and rupture as the major causes of ACS and sudden cardiac death, various imaging modalities have been used to identify characteristics of vulnerable plaques, which are prone to rupture (high-risk plaque characteristics [HRPCs]) (2–6).

Nevertheless, given the limited predictive value of HRPCs alone in the prediction of subsequent coronary events, (7) contemporary practice has been guided by the hemodynamic significance of CAD determined by invasive physiologic indexes, such as fractional flow reserve (FFR) (8), but not by HRPCs. Recent studies have suggested the importance of both hemodynamic significance and plaque vulnerability in CAD and their complementary roles in the progression of the disease and the development of ACS (9). Comprehensive assessment of CAD has become possible in clinical practice with recent advances in coronary computed tomography angiography (CCTA) and computational fluid dynamics (CFD), which allow simultaneous noninvasive assessment of anatomic plaque characteristics (4–6) and hemodynamic significance of CAD (10).

However, studies on the clinical role of the comprehensive evaluation of these features are limited, and it is still unclear whether integrating various aspects of the pathophysiology of CAD would increase the predictability of subsequent coronary events (9). Furthermore, it would be important to better understand the prognostic implications and the potential role of utilizing HRPCs in contemporary CAD management. In this regard, this study sought to evaluate (1) prognostic implications of combined analysis of CCTA-derived HRPCs and hemodynamic parameters in the prediction of subsequent coronary events and (2) differential prognostic implications of CCTA-derived HRPCs according to the hemodynamic significance of CAD.

MATERIALS AND METHODS

Study Design and Population

To evaluate the prognostic impact of anatomic and hemodynamic plaque characteristics on subsequent coronary events, this study enrolled two separate patient populations (the ACS cohort and the negative control cohort) (**Figure 1**). The ACS cohort included consecutive patients who underwent CCTA within 6–36 months before percutaneous coronary intervention (PCI) for acute myocardial infarction (MI) or unstable angina admitted to Samsung Medical Center between 2003 and 2019. The negative control cohort included age-/sex-matched patients who underwent CCTA within 6–36 months before invasive coronary angiography for suspected stable angina but did not undergo PCI because there was no significant lesion at the time of angiography. In both cohorts, CCTA was performed under the judgment of the

Abbreviations: ACS, acute coronary syndrome; CAD, coronary atherosclerotic disease; CCTA, coronary computed tomography angiography; CFD, computational fluid dynamics; FFR_{CT}, fractional flow reserve by coronary computed tomography angiography; HR, hazard ratio; HRPCs, high-risk plaque characteristics; MI, myocardial infarction; PCI, percutaneous coronary intervention.

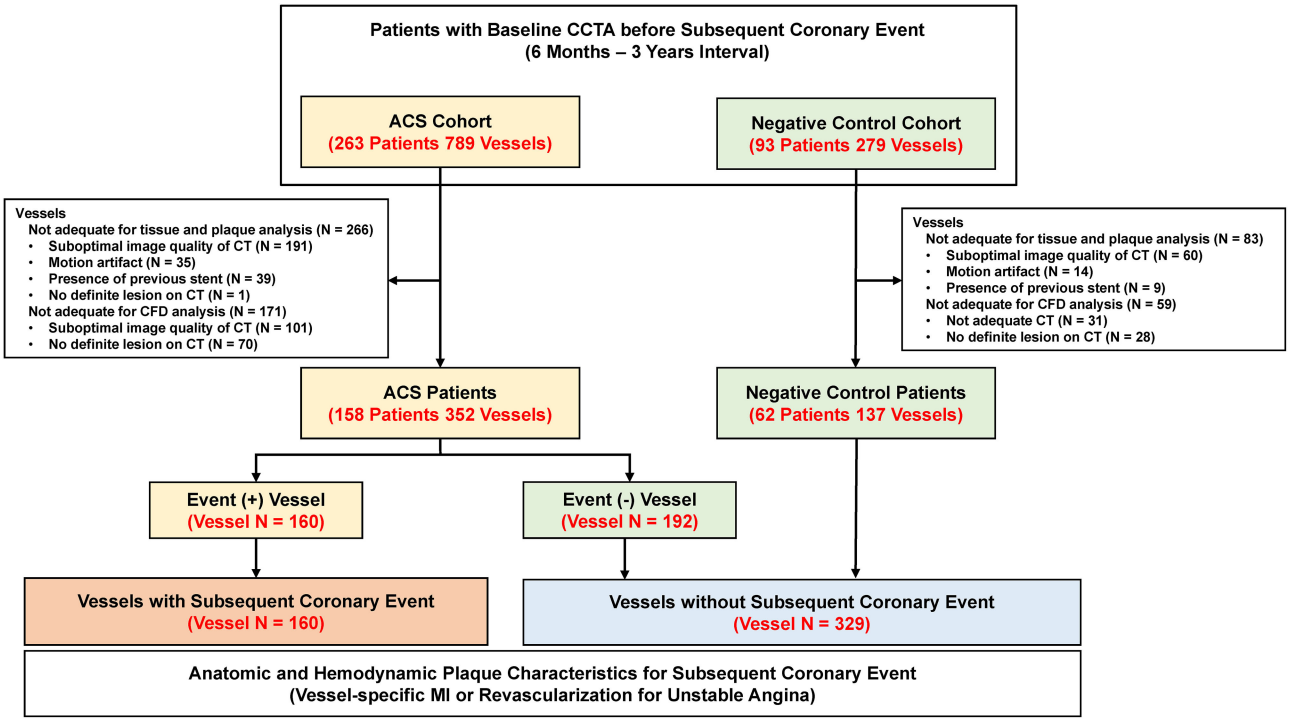

FIGURE 1 | Study flow. This study enrolled two separate patient populations (ACS and negative control cohort). The ACS cohort included consecutive patients who underwent CCTA within 6–36 months before PCI for acute myocardial infarction or unstable angina. The negative control cohort included age-/sex-matched patients who underwent CCTA within 6–36 months before invasive coronary angiography for suspected stable angina but did not undergo PCI because there was no significant lesion at the time of angiography. A total of 489 vessels (160 vessels with subsequent coronary event and 329 vessels without subsequent coronary event) were finally included in the study. ACS, acute coronary syndrome; CCTA, coronary computed tomography angiography; CFD, computational fluid dynamics; CT, computed tomography; PCI, percutaneous coronary intervention.

respective physicians as a routine clinical evaluation for suspected CAD. In addition, the operators were blinded to the detailed core laboratory analyses of anatomic and hemodynamic plaque characteristics at the time of invasive angiography.

In the ACS cohort, patients without clear culprit lesions in invasive angiography, intravascular ultrasound, or optical coherence tomography were excluded. Additional exclusion criteria were patients with ACS caused by in-stent restenosis, vessels with stents before CCTA, previous history of coronary artery bypass grafting, and type 2 myocardial infarction due to other general medical conditions. In both ACS and negative control cohorts, patients with unavailable CCTA images or suboptimal image quality for the analysis of plaque characteristics or CFD were excluded by the CCTA core laboratory (Elucid Bioimaging, Inc., Boston, MA, USA) or the CFD core laboratory (Shanghai Institute of Cardiovascular Diseases, Shanghai, China), respectively. The study protocol was approved by the institutional review board of Samsung Medical Center. This study was conducted in accordance with the Declaration of Helsinki and registered on clinicaltrials.gov (PreDiction and Validation of Clinical CoursE of Coronary Artery DiSease With CT-Derived Non-INvasive HemodYnamic Phenotyping and Plaque Characterization [DESTINY Study], NCT02374775).

Analysis of Anatomic Plaque Characteristics in CCTA

Coronary computed tomography angiography images were obtained in accordance with the Society of Cardiovascular Computed Tomography Guidelines on Performance of CCTA, with 64-channel scanner (GE Healthcare, Milwaukee, WI, USA) or 128-channel dual-source scanner platforms (Siemens Medical System, Forchheim, Germany) with electrocardiographic gating (11). A standardized protocol for heart rate control with beta-blockers and sublingual nitroglycerin was administered. All CCTA images were analyzed regarding anatomic plaque characteristics in a blinded fashion using histologically validated plaque quantification software (vascuCAP, clinical edition) at a core laboratory (Elucid Bioimaging, Inc., Boston, MA, USA) (12).

For anatomic severity, diameter stenosis, area stenosis, minimum lumen area (MLA), and lesion length were measured. Whole vessel and plaque tissue characterization were performed by defining the vessel wall into different components: calcified tissue, intra-plaque hemorrhage, lipid-rich necrotic core, matrix, or perivascular adipose tissue (13). Plaque burden was defined as the ratio of wall area divided by the overall vessel area (12, 13). Any lesions with diameter stenosis >30% were selected for plaque tissue characterization. In cases of multiple lesions in the same target vessel, the lesion with the greatest diameter stenosis

was selected as the representative lesion. The presence of the following HRPCs was analyzed according to the definitions from previous studies: (1) low attenuation plaque (average density ≤30 Hounsfield units [HU].); (2) positive remodeling (lesion diameter/reference diameter ≥1.1); (3) napkin-ring sign (ring-like attenuation pattern with peripheral high attenuation tissue surrounding a central lower attenuation portion); and (4) spotty calcification (average density >130 HU and diameter <3 mm) (4, 5). In this analysis, HRPCs were defined by combining both qualitative and quantitative parameters based on previous studies with the presence of any of the following features: low attenuation plaque, positive remodeling, napkin-ring sign, spotty calcification, MLA <4 mm^2, or plaque burden ≥70% (2–5).

Analysis of Hemodynamic Plaque Characteristics in CCTA

Hemodynamic parameters derived from CCTA were analyzed in a blinded fashion at a core laboratory (Zhongshan Hospital, Shanghai, China) using a commercialized offline software system (RuiXin-FFR, version 1.0, Raysight Medical, Shenzhen, China). First, three-dimensional anatomical computational models of the coronary tree were reconstructed from CCTA images. Second, patient-specific boundary conditions were obtained from the CCTA images. Third, hemodynamics parameters were solved by CFD-based FFR_{CT} calculation. Detailed methods of three-dimensional model reconstruction and CFD-based FFR_{CT} calculation are described in the **Supplementary Appendix**. Briefly, coronary models were constructed using segmentation algorithms that extracted the luminal surface of the epicardial coronary arteries and branches. Coronary flow and pressure were computed by solving the Navier–Stokes equations, assuming that blood is approximated as a Newtonian fluid. Boundary conditions for hyperemia were derived from myocardial mass, vessel sizes at each outlet, and the response of the microcirculation to adenosine. As with plaque tissue characterization, only lesions with a diameter stenosis of >30% were selected for the computation of hemodynamic parameters. For this study, three hemodynamic parameters were used, namely, per-vessel FFR_{CT}, per-lesion delta FFR_{CT} (ΔFFR_{CT}), and per-vessel percent ischemic myocardial mass. First, FFR_{CT} was defined as the ratio of mean downstream coronary pressure (P_d) and the aortic pressure (P_a) derived from the CFD analysis under a simulated hyperemic condition. Second, ΔFFR_{CT} was defined by computing the difference in FFR_{CT} values at the proximal and distal sites of each lesion. Third, the percent ischemic myocardial mass of each vessel segment was defined as the ratio between the myocardial mass subtended beyond the point at which the vessel's FFR_{CT} is ≤0.80 and the entire vessel segment (14). Myocardial mass was computed using a stem-and-crown model (15, 16), which is based on allometric scaling between the length of the coronary arterial tree and myocardial mass (15, 16).

Data Collection and Clinical Outcomes

Clinical data were collected by reviewing electronic medical records. All angiograms were analyzed, and culprit lesions were determined in a blinded fashion at core laboratories (Samsung Medical Center, Seoul, Korea). The primary outcome was a subsequent coronary event, which was defined as a composite of vessel-specific MI or revascularization for unstable angina. The definition of clinical outcomes was in accordance with the Academic Research Consortium. Acute MI was defined according to the universal definition of MI (17).

Statistical Analysis

Data were analyzed on a per-patient basis for clinical characteristics and on a per-vessel basis for anatomic and hemodynamic plaque characteristics and vessel-specific clinical outcomes. For per-patient analyses, the Student's *t*-test and the chi-square test were used to compare continuous and categorical variables, respectively. For per-vessel analyses, a generalized estimating equation was used to adjust for intra-subject variability among vessels from the same patient. An analysis of variance test was used to compare differences in the number of clinical risk factors and hemodynamic parameters according to the classification by the number of HRPCs.

The discriminant function of clinical characteristics and anatomic and hemodynamic plaque characteristics for the primary outcome were evaluated using the c-index and 95% confidence interval (CI) in receiver operating curve analysis. Optimal cutoff values for HRPCs and hemodynamic parameters were determined based on receiver operating curve analysis and results of previous studies (5, 8, 9). Diagnostic performance was presented as sensitivity, specificity, positive predictive value, negative predictive value, and diagnostic accuracy. Incremental predictability of HRPCs and hemodynamic parameters for the primary outcome was compared using a global chi-square estimated by the likelihood ratio test. The cumulative incidence of the primary outcome was presented as Kaplan–Meier estimates and compared using a log-rank test. To adjust for the interrogated vessels within the same patient, multivariable marginal Cox proportional hazards regression was used to calculate the adjusted hazard ratio (HR) and 95% CI. Adjusted covariables were age, sex, hypertension, diabetes mellitus, dyslipidemia, chronic kidney disease, and current smoker. The assumption of proportionality was assessed graphically using a log minus log plot, and all Cox proportional hazard models satisfied the proportional hazards assumption.

Three prediction models were constructed to assess the incremental prognostic value of HRPCs and hemodynamic parameters: (1) model 1: clinical risk factors; (2) model 2: model 1 + individual components of HRPCs; and (3) model 3: model 2 + hemodynamic parameters. Clinical risk factors included age, sex, hypertension, diabetes mellitus, dyslipidemia, chronic kidney disease, and current smoker. Hemodynamic parameters included FFR_{CT}, ΔFFR_{CT}, and percent ischemic myocardial mass. Discriminant ability was compared using the c-index, and reclassification performance was compared using the relative integrated discrimination improvement (IDI) and category-free net reclassification index (NRI). Subgroup analysis was performed to assess the differential prognostic implications of HRPCs according to hemodynamic significance. Vessels were divided into subgroups according to optimal cutoff values of FFR_{CT} and ΔFFR_{CT}, and the incremental prognostic value for the primary outcome of HRPCs was evaluated in each subgroup.

TABLE 1 | Baseline clinical characteristics.

Variables	Total patient (*N* = 220)	ACS patient (*N* = 158)	Negative control patient (*N* = 62)	*P*-value
Demographics				
Age, years	65.5 ± 10.2	65.2 ± 10.6	66.2 ± 9.3	0.488
Men	179 (81.4)	131 (82.9)	48 (77.4)	0.454
CCTA—ICA Interval	554.3 ± 268.2	535.7 ± 260.7	601.9 ± 282.9	0.100
Clinical presentation				<0.001
ST-segment elevation myocardial infarction	10 (4.5)	10 (6.3)	0 (0.0)	
Non-ST-segment elevation myocardial infarction	17 (7.7)	17 (10.8)	0 (0.0)	
Unstable angina	131 (59.5)	131 (82.9)	0 (0.0)	
Stable angina	62 (28.2)	0 (0.0)	62 (100.0)	
Cardiovascular risk factors				
Hypertension	160 (72.7)	113 (71.5)	47 (75.8)	0.635
Diabetes mellitus	131 (59.5)	94 (59.5)	37 (59.7)	>0.999
Dyslipidemia	93 (42.3)	63 (39.9)	30 (48.4)	0.318
Chronic kidney disease	15 (6.8)	11 (7.0)	4 (6.5)	>0.999
Current smoker	42 (19.1)	30 (19.0)	12 (19.4)	>0.999
History of percutaneous coronary intervention	25 (11.4)	24 (15.2)	1 (1.6)	0.009
History of myocardial infarction	12 (5.5)	10 (6.3)	2 (3.2)	0.561
History of cerebrovascular accident	34 (15.5)	24 (15.2)	10 (16.1)	>0.999
History of peripheral vascular disease	14 (6.4)	9 (5.7)	5 (8.1)	0.734
Medical treatment after CCTA before clinical event				
Antiplatelet agent	167 (75.9)	123 (77.8)	44 (71.0)	0.369
ACEI or ARB	100 (45.5)	70 (44.3)	30 (48.4)	0.692
Beta blocker	81 (36.8)	59 (37.3)	22 (35.5)	0.919
Calcium channel blocker	84 (38.2)	59 (37.3)	25 (40.3)	0.799
Statin	146 (66.4)	104 (65.8)	42 (67.7)	0.910
Ezetimibe	8 (3.6)	7 (4.4)	1 (1.6)	0.546
Echocardiographic findings				
Left ventricular ejection fraction, %	62.2 ± 9.5	61.9 ± 9.9	63.2 ± 8.5	0.428

Data are presented as mean ± standard deviation or number (%).
ACEI, angiotensin-converting enzyme inhibitor; ACS, acute coronary syndrome; ARB, angiotensin receptor blocker; CCTA, coronary computed tomography angiography; ICA, invasive coronary angiography.

All analyses were two-sided, and *P*-values <0.05 were considered statistically significant. Statistical analyses were performed using R version 4.0.3 (R Foundation for Statistical Computing, Vienna, Austria).

RESULTS

Characteristics of Patients

A total of 220 patients with 489 vessels were selected for the current analyses (**Figure 1**). Among them, 158 patients (71.8%) were from the ACS cohort and 62 (28.2%) were from the negative control cohort. In the ACS cohort, 17.1 and 82.9% of patients presented with acute MI and unstable angina, respectively. Among the ACS cohort, 160 vessels had subsequent coronary events and 192 vessels were non-culprit vessels. With 137 vessels from the negative control cohort, a total of 329 vessels were not related to subsequent coronary events. The mean interval between CCTA and invasive coronary angiography was 554.3 ± 268.2 days. In the comparison of the clinical characteristics of patients, there was no significant difference in demographics, cardiovascular comorbidities, or profiles of medical treatment after CCTA (**Table 1**).

Anatomic and Hemodynamic Plaque Characteristics

Table 2 shows the comparison of anatomic and hemodynamic plaque characteristics between 160 vessels with subsequent coronary events and 329 vessels without subsequent coronary events. In addition, **Supplementary Table 1** presents the anatomical and hemodynamic plaque characteristics of 137 vessels from the negative control cohort. Vessels with subsequent coronary events showed significantly lower MLA and higher plaque burden than vessels without events. Regarding anatomic plaque characteristics, vessels with subsequent coronary events showed a significantly higher proportion of low attenuation plaque, MLA <4 mm^2, and plaque burden at lumen area ≥70% than vessels without events. As a result, vessels with subsequent coronary events had a higher number of HRPCs (2.6 ± 1.4 vs. 2.3 ± 1.4, $P = 0.009$) than vessels without events. There was no significant difference in other individual components of the

TABLE 2 | Anatomic and hemodynamic plaque characteristics.

Variables	Total Vessels (*N* = 489)	Vessels with subsequent coronary event (*N* = 160)	Vessels without subsequent coronary event (*N* = 329)	*P*-value
Interrogated Vessels				0.002
Left anterior descending artery	189 (38.7)	79 (49.4)	110 (33.4)	
Left circumflex artery	143 (29.2)	35 (21.9)	108 (32.8)	
Right coronary artery	157 (32.1)	46 (28.8)	111 (33.7)	
Anatomical severity				
Diameter stenosis, %	54.4 ± 18.2	58.4 ± 18.2	52.6 ± 17.9	0.001
Area stenosis, %	63.1 ± 19.3	66.6 ± 19.0	61.4 ± 19.3	0.006
Minimum lumen area, mm^2	1.8 ± 1.4	1.5 ± 1.2	1.9 ± 1.4	0.002
Lesion length, mm	22.5 ± 17.2	24.4 ± 16.9	21.6 ± 17.3	0.175
Whole vessel tissue characterization				
Plaque burden, %	80.2 ± 12.6	82.9 ± 11.5	78.9 ± 13.0	0.001
Calcified volume, %	4.3 ± 5.5	4.4 ± 5.3	4.3 ± 5.6	0.919
Maximum calcified area, %	24.8 ± 22.4	24.4 ± 20.9	25.0 ± 23.1	0.781
Intra-plaque hemorrhage volume, mm^3	4.2 ± 7.8	4.8 ± 10.0	4.0 ± 6.4	0.374
Maximum intra-plaque hemorrhage area, mm^2	0.73 ± 0.96	0.77 ± 0.91	0.71 ± 0.99	0.565
Lipid-rich necrotic core volume, mm^3	1.4 ± 3.9	1.9 ± 5.0	1.2 ± 3.2	0.150
Maximum lipid-rich necrotic core area, mm^2	0.35 ± 0.68	0.41 ± 0.77	0.32 ± 0.63	0.202
Perivascular adipose tissue volume, %	30.2 ± 12.6	31.8 ± 12.4	29.4 ± 12.6	0.060
Vessel length, mm	75.2 ± 35.4	75.2 ± 33.8	75.2 ± 36.2	0.984
Target plaque tissue characterization				
Plaque burden, %	82.2 ± 11.9	85.5 ± 9.9	80.5 ± 12.5	<0.001
Calcified volume, %	11.6 ± 8.1	10.6 ± 8.2	12.1 ± 8.1	0.119
Maximum calcified area, %	32.8 ± 20.9	31.1 ± 20.1	33.6 ± 21.3	0.278
Intra-plaque hemorrhage volume, mm^3	2.3 ± 4.6	3.1 ± 6.2	2.0 ± 3.5	0.087
Maximum intra-plaque hemorrhage area, mm^2	0.60 ± 0.87	0.76 ± 1.03	0.52 ± 0.77	0.037
Lipid-rich necrotic core volume, mm^3	1.2 ± 3.6	1.7 ± 5.1	1.0 ± 2.5	0.179
Maximum lipid-rich necrotic core area, mm^2	0.31 ± 0.63	0.36 ± 0.71	0.29 ± 0.58	0.363
High-risk plaque characteristics				
Low attenuation plaque	102 (20.9)	46 (28.8)	56 (17.0)	0.004
Positive remodeling	211 (43.1)	75 (46.9)	136 (41.3)	0.288
Napkin-ring sign	80 (16.4)	27 (16.9)	53 (16.1)	0.933
Spotty calcification	334 (68.3)	113 (70.6)	221 (67.2)	0.505
Minimum lumen area $<4mm^2$	401 (82.0)	140 (87.5)	261 (79.3)	0.037
Plaque burden at lumen area ≥70%	29 (5.9)	16 (10.0)	13 (4.0)	0.014
Number of HRPCs	2.4 ± 1.4	2.6 ± 1.4	2.3 ± 1.4	0.009
Number of HRPCs ≥3	236 (48.3)	92 (57.5)	144 (43.8)	0.006
Hemodynamic plaque characteristics				
FFR_{CT}	0.80 ± 0.12	0.76 ± 0.13	0.82 ± 0.11	<0.001
ΔFFR_{CT}	0.11 ± 0.10	0.14 ± 0.12	0.09 ± 0.08	<0.001
Ischemia myocardial mass, %	26.9 ± 18.5	29.0 ± 18.5	26.0 ± 18.4	0.022

Data are presented as mean ± standard deviation, median (Q1–Q3), or number (%).
FFR_{CT}, fractional flow reserve by coronary computed tomography angiography; HRPCs, high-risk plaque characteristics.

whole vessel and plaque tissue characterization between the two groups.

In terms of hemodynamic plaque characteristics, vessels with subsequent coronary events had lower FFR_{CT} (0.76 ± 0.13 vs. 0.82 ± 0.11, $P < 0.001$), higher ΔFFR_{CT} (0.14 ± 0.12 vs. 0.09 ± 0.08, $P < 0.001$), and higher percent ischemic myocardial mass (29.0 ± 18.5 vs. 26.0 ± 18.4, $P = 0.022$) than vessels without events. There was a significant association between the number of HRPCs and the number of clinical risk factors, FFR_{CT}, ΔFFR_{CT}, and percent ischemic myocardial mass. With an increased number of HRPCs, there was a significant increase in the number of clinical risk factors, ΔFFR_{CT}, and percent ischemic myocardial mass and a significant decrease in FFR_{CT} (overall $P < 0.001$ for all comparisons) (**Supplementary Figure 1**).

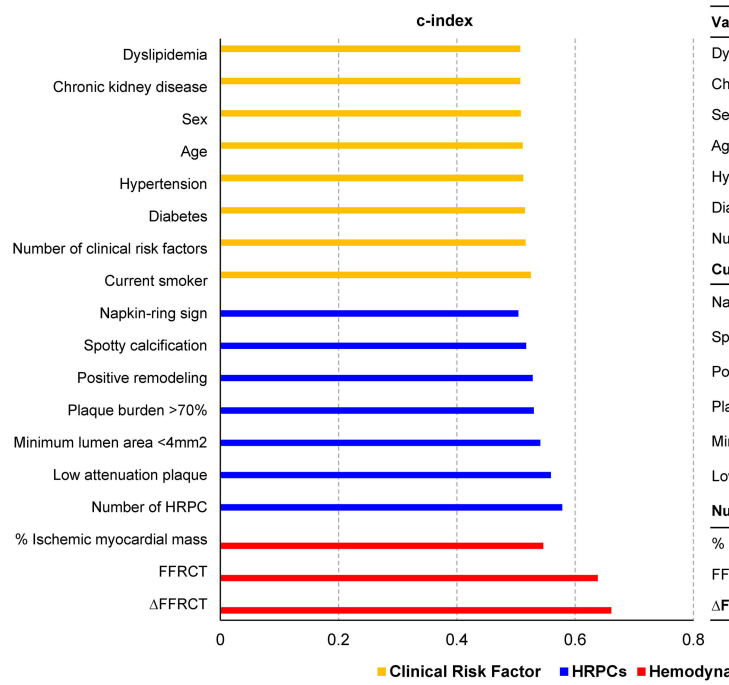

Variables	c-index	95% CI	P value
Dyslipidemia	0.507	0.460 - 0.553	0.517
Chronic kidney disease	0.507	0.482 - 0.532	0.414
Sex	0.508	0.472 - 0.544	0.563
Age	0.511	0.455 - 0.567	0.715
Hypertension	0.512	0.469 - 0.554	0.640
Diabetes	0.515	0.468 - 0.561	0.722
Number of clinical risk factors	0.516	0.463 - 0.570	0.747
Current smoker	**0.525**	**0.488 - 0.562**	**Reference**
Napkin-ring sign	0.504	0.469 – 0.539	0.002
Spotty calcification	0.517	0.474 – 0.561	0.002
Positive remodeling	0.528	0.481 – 0.575	0.006
Plaque burden >70%	0.530	0.505 – 0.556	0.067
Minimum lumen area < 4mm^2	0.541	0.507 – 0.575	0.105
Low attenuating plaque	0.559	0.518 – 0.599	0.414
Number of HRPCs	**0.578**	**0.525 – 0.630**	**Reference**
% Ischemic myocardial mass	0.546	0.492 – 0.601	<0.001
FFR_{CT}	0.638	0.586 – 0.689	0.229
ΔFFR_{CT}	**0.661**	**0.609 – 0.712**	**Reference**

FIGURE 2 | Comparison of discrimination abilities of clinical risk factors, HRPCs, and hemodynamic parameters for subsequent coronary events. Discrimination abilities of clinical risk factors (green bar), HRPCs (blue bar), and hemodynamic parameters (red bar) for subsequent coronary events are presented as c-index and 95% CI. For various variables in each group, the c-index comparison was performed with the variable with the highest c-index in each group. CI, confidence interval; FFR_{CT}, fractional flow reserve by coronary computed tomography angiography; HRPCs, high-risk plaque characteristics.

Prognostic Implications of Individual Anatomic and Hemodynamic Plaque Characteristics

Compared with clinical risk factors, individual components of HRPCs and hemodynamic parameters showed higher discriminant abilities for subsequent coronary events. Among anatomic and hemodynamic parameters, ΔFFR_{CT} showed the highest c-index to predict subsequent coronary events (c-index 0.661, 95% CI: 0.609–0.712) (**Figure 2**).

Optimal cutoff values of hemodynamic parameters and the number of HRPCs for predicting subsequent coronary events were $FFR_{CT} \leq 0.80$, $\Delta FFR_{CT} \geq 0.06$, percent ischemic myocardial mass $\geq$ 40%, and the number of HRPCs $\geq$ 3 (**Supplementary Table 2**). When the risk of subsequent coronary events was compared according to optimal cutoff values of hemodynamic parameters and the number of HRPCs, vessels with $FFR_{CT} \leq 0.80$, $\Delta FFR_{CT} \geq 0.06$, percent ischemic myocardial mass $\geq$40%, and the number of HRPCs $\geq$3 were independently associated with an increased risk of subsequent coronary events than vessels with $FFR_{CT} > 0.80$, $\Delta FFR_{CT} < 0.06$, percent ischemic myocardial mass <40%, and the number of HRPCs < 3, respectively (**Figure 3** and **Table 3**).

However, the positive predictive value and diagnostic accuracy of each hemodynamic parameter and the number of HRPCs were modest to predict subsequent coronary events as individual parameters (**Supplementary Table 2**). Nevertheless, the addition of percent ischemic myocardial mass, HRPCs, FFR_{CT}, and ΔFFR_{CT} into clinical risk factors showed a stepwise increase in predictability for subsequent coronary events (**Figure 4**). Among anatomic and hemodynamic parameters, ΔFFR_{CT} showed the highest incremental predictability of the other variables ($P <$ 0.001 for comparisons with the others).

Prediction Models for Subsequent Coronary Events

Table 4 and **Supplementary Figure 2** show the comparison of discriminant and reclassification abilities of three models for the prediction of subsequent coronary events. Compared with model 1 with clinical risk factors, additional integration of HRPCs into model 1 (model 2) showed higher discriminant ability (c-index 0.620 vs. 0.558, $P = 0.027$) and higher reclassification ability (NRI 0.269, $P = 0.004$; IDI 0.037, $P < 0.001$). Model 3, which included additional integration of hemodynamic parameters in model 2, further improved model 2 in terms of discriminant ability (c-index 0.698 vs. 0.620, $P = 0.001$) and reclassification ability (NRI 0.460, $P < 0.001$; IDI 0.061, $P < 0.001$) (**Table 4** and **Supplementary Figure 2**). Furthermore, a simplified model (c-index 0.680, 95% CI: 0.630–0.731) was constructed by selecting only the variables with the best discriminant abilities among HRPCs (low attenuating plaque) and hemodynamic variables (ΔFFR_{CT}), respectively, and adding them to clinical risk factors showed similar discriminant ability to model 3 (c-index 0.680 vs. 0.698, $P = 0.234$).

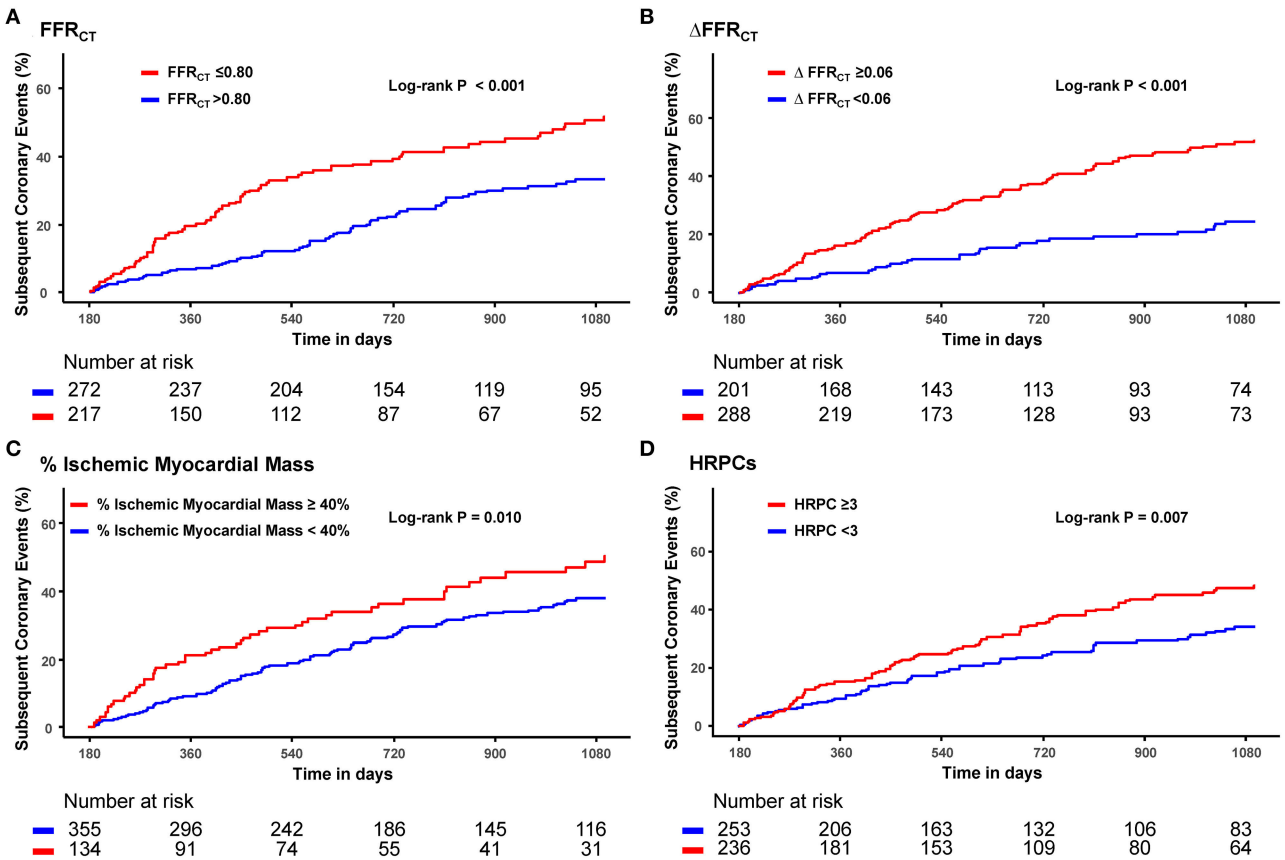

FIGURE 3 | Cumulative incidence of subsequent coronary events according to FFR$_{CT}$, ΔFFR$_{CT}$, % ischemic myocardial mass, and HRPCs. Cumulative incidence of subsequent coronary events according to optimal cutoff values of **(A)** FFR$_{CT}$, **(B)** ΔFFR$_{CT}$, **(C)** % ischemic myocardial mass, and **(D)** HRPCs. FFR$_{CT}$, fractional flow reserve by coronary computed tomography angiography; HRPCs, high-risk plaque characteristics.

TABLE 3 | Cumulative incidence of subsequent coronary events according to hemodynamic parameters and HRPCs.

Variables		Cumulative Incidence*	Unadjusted HR (95% CI)	*P*-value	Adjusted HR† (95% CI)	*P*-value
FFR$_{CT}$	**≤0.80**	51.7% (88)	1.96 (1.44–2.68)	<0.001	2.05 (1.49–2.82)	<0.001
	>0.80	33.2% (72)				
ΔFFR$_{CT}$	**≥0.06**	52.1% (122)	2.61 (1.81–3.76)	<0.001	2.75 (1.94–3.89)	<0.001
	<0.06	24.5% (38)				
% Ischemic myocardial mass	**≥40**	50.3% (52)	1.54 (1.10–2.14)	0.011	1.59 (1.14–2.21)	0.006
	<40	37.8% (108)				
HRPCs	**≥3**	48.3% (92)	1.54 (1.13–2.11)	0.007	1.59 (1.16–2.18)	0.004
	<3	34.2% (68)				

*Values are % (n) unless otherwise indicated. *Cumulative incidence of clinical outcomes presented as Kaplan–Meier estimates. †Adjusted variables in the multivariable marginal Cox regression model were age, sex, hypertension, diabetes, dyslipidemia, chronic kidney disease, and current smoker.*
CI, confidence interval; FFR$_{CT}$, fractional flow reserve by coronary computed tomography angiography; HR, hazard ratio; HRPCs, high-risk plaque characteristics.

Differential Prognostic Implication of HRPCs According to Hemodynamic Significance

To evaluate the differential prognostic implications of HRPCs according to hemodynamic significance, target vessels were stratified according to their hemodynamic significance determined by the optimal cutoff value of FFR$_{CT}$ ≤ 0.80 vs. >0.80 or ΔFFR$_{CT}$ ≥ 0.06 vs. <0.06. In vessels with FFR$_{CT}$ ≤ 0.80, there was no significant difference in the distribution of HRPCs among vessels with or without subsequent coronary events. Conversely, in vessels with FFR$_{CT}$ > 0.80, the vessels with subsequent coronary events

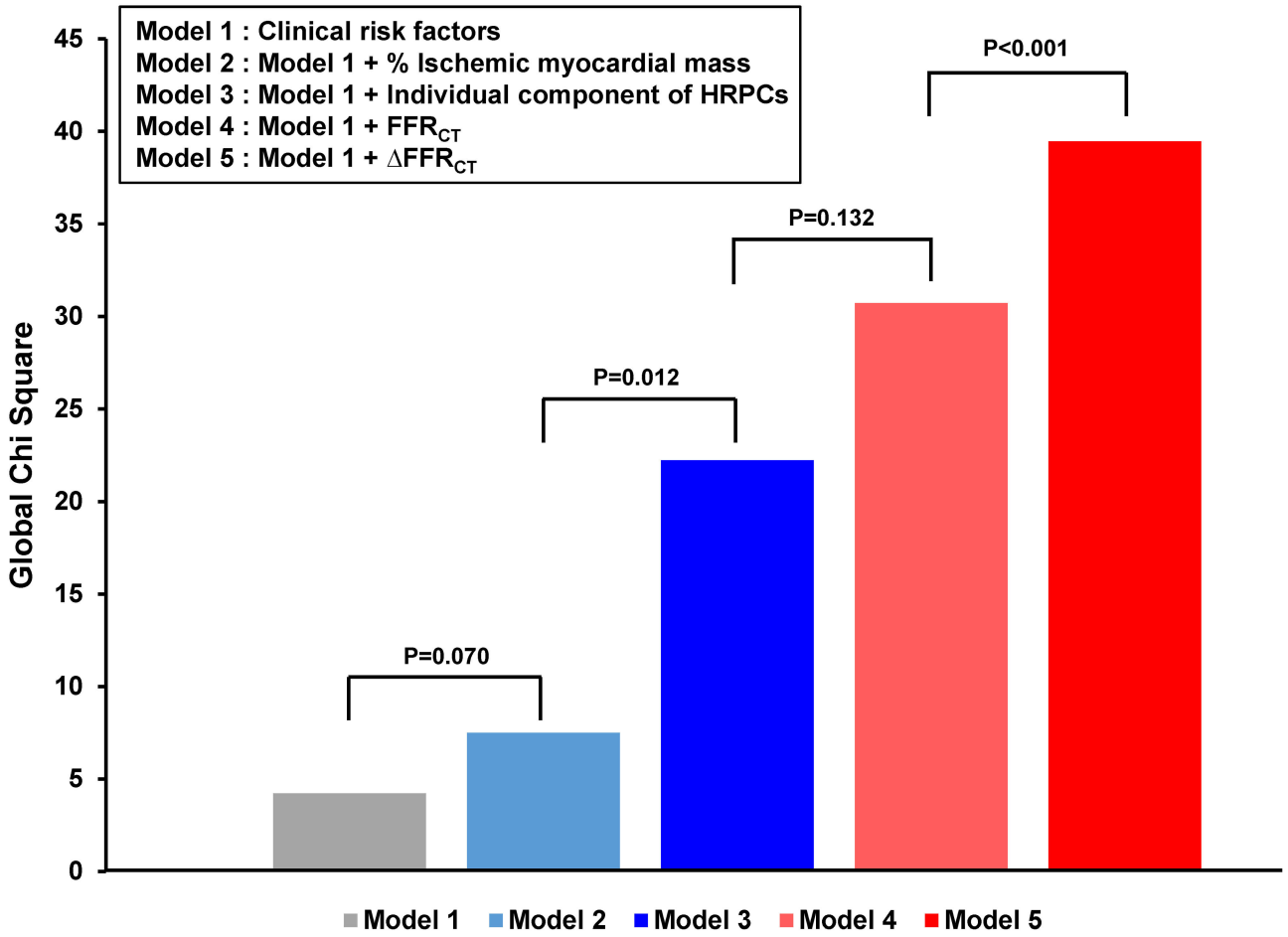

FIGURE 4 | Incremental prognostic impact of HRPCs and hemodynamic parameters for subsequent coronary events. The addition of percent ischemic myocardial mass, HRPCs, ΔFFR_{CT}, and ΔFFR_{CT} into clinical risk factors showed increased predictability for subsequent coronary events. Clinical risk factors included age, sex, hypertension, diabetes mellitus, dyslipidemia, chronic kidney disease, and current smoker. HRPCs included low attenuation plaque, positive remodeling, napkin-ring sign, spotty calcification, minimum luminal area <4 mm^2, or plaque burden ≥70%. FFR_{CT}, fractional flow reserve by coronary computed tomography angiography; HRPCs, high-risk plaque characteristics.

TABLE 4 | Comparison of prediction models for subsequent coronary events.

Models*	c-index	Difference with previous model				
		c-index comparison *P*-value	NRI	*P*-value	IDI	*P*-value
Model 1	0.558 (0.504–0.611)					
Model 2	0.620 (0.566–0.674)	0.027	0.269 (0.084–0.455)	0.004	0.037 (0.019–0.055)	<0.001
Model 3	0.698 (0.648–0.747)	0.001	0.460 (0.277–0.644)	<0.001	0.061 (0.036–0.085)	<0.001

**Models are constructed as follows: model 1: clinical risk factors; model 2: model 1 + individual component of HRPCs; and model 3: model 2 + hemodynamic parameters. Components of clinical risk factors, hemodynamic parameters, and HRPCs are as follows: Clinical risk factors: age, sex, hypertension, diabetes, dyslipidemia, chronic kidney disease, and current smoker; Hemodynamic parameters: % ischemic myocardial mass, FFR_{CT}, and ΔFFR_{CT}; HRPCs: low attenuation plaque, positive remodeling, napkin-ring sign, spotty calcification, minimum lumen area <4 mm^2, and plaque burden at lumen area ≥70%.*

FFR_{CT}, fractional flow reserve by coronary computed tomography angiography; HRPCs, high-risk plaque characteristics; IDI, relative integrated discrimination improvement; NRI, category-free net reclassification index.

showed a significantly higher proportion of low attenuating plaque and plaque burden ≥70% and showed a higher number of HRPCs (**Supplementary Table 3**). Stratified analysis by ΔFFR_{CT} showed similar results, and the number of HRPCs was significantly higher in vessels with subsequent coronary events only among vessels with $\Delta FFR_{CT} < 0.06$.

Conversely, there was no significant difference in the number of HRPCs among vessels with $\Delta FFR_{CT} \geq 0.06$ (**Supplementary Table 4**).

When the risk of subsequent coronary events was compared according to the number of HRPCs, a significantly higher risk of subsequent coronary events in vessels with HRPCs ≥ 3 than in vessels with HRPCs < 3 was observed only among vessels with negative FFR_{CT} or ΔFFR_{CT} (**Figure 5**). In addition, integration of HRPCs significantly improved discriminant and reclassification abilities for subsequent coronary events only in vessels with negative hemodynamic significance ($FFR_{CT} > 0.80$; 0.687 vs. 0.576, $P = 0.005$; NRI 0.412, $P = 0.002$; IDI 0.064, $P = 0.001$; $\Delta FFR_{CT} < 0.06$; 0.733 vs. 0.623, $P = 0.034$; NRI 0.620, $P < 0.001$; IDI 0.075, $P = 0.001$) (**Figure 6**).

DISCUSSION

This study evaluated (1) the prognostic implications of CCTA-derived anatomic and hemodynamic plaque characteristics to predict subsequent coronary events, and (2) the differential prognostic implications of anatomic plaque characteristics according to the hemodynamic significance of CAD. The main findings are as follows: First, HRPCs and hemodynamic parameters showed higher discriminant abilities for subsequent coronary events than clinical risk factors, with ΔFFR_{CT} being the most powerful predictor. Second, HRPCs showed additive discriminant and reclassification abilities to clinical risk factors in the prediction of subsequent coronary events, which were further increased by adding hemodynamic parameters. Third, the prognostic impact of HRPCs was significant among vessels with negative hemodynamic significance ($FFR_{CT} > 0.80$ or $\Delta FFR_{CT} < 0.06$) but not among those with positive hemodynamic significance ($FFR_{CT} \leq 0.80$ or $\Delta FFR_{CT} \geq 0.06$).

Risk Stratification for Subsequent Coronary Events Using CCTA

Identification of patients at increased risk of ACS who may benefit from intensified preventive measures has been a major challenge, and previous studies have consistently shown that prediction based on clinical risk factors is insufficient for adequate individual risk assessment (1). In contemporary practice, patients with suspected ischemic heart disease are commonly evaluated by noninvasive stress testing, which determines the need for invasive coronary angiography (8). However, the revascularization is not indicated in two-third of the cases sent for invasive coronary angiography due to anatomically or hemodynamically nonobstructive stenosis in epicardial coronary arteries (18). Previous studies demonstrated that those nonobstructive CAD could be accompanied by major adverse cardiovascular events including ACS (19), and the treatment strategy based on noninvasive stress testing did not significantly reduce the risk of ACS or ACS-related mortality compared with medical treatment alone (20, 21).

Conversely, recent trials showed that CCTA-based evaluation of CAD provided better risk stratification of high-risk patients and improved prognosis compared with standard care (22). Furthermore, multiple studies showed that CCTA-derived anatomic plaque characteristics (MLA, plaque burden, positive remodeling, low-attenuation plaque, napkin-ring sign, and spotty calcification) could provide additional information on the risk of ACS (4, 5). In addition, other studies presented the prognostic implications of CCTA-derived hemodynamic parameters. The prognostic value of FFR_{CT} has been confirmed for up to 5 years in several studies (10, 23, 24). Of note, in the ADVANCE registry, with the largest sample size ($N = 5083$), patients with negative $FFR_{CT} > 0.80$ showed a significantly lower risk of cardiac death or MI than those with $FFR_{CT} \leq 0.80$ at 1 year (0.2% vs. 0.8%, $P = 0.01$) (10). The EMERALD study retrospectively evaluated 72 patients who had undergone CCTA before ACS events and compared CCTA-derived anatomic and hemodynamic plaque characteristics (FFR_{CT}, ΔFFR_{CT}, wall shear stress, and axial plaque stress) between the culprit and non-culprit vessels. In this study, plaques with adverse anatomic and hemodynamic characteristics had a significantly higher risk of ACS than those without (9). Despite the lack of a negative control group not presenting with ACS being a major limitation of the EMERALD study, the results supported the potential role of CCTA-based anatomic and hemodynamic plaque characteristics for better identification of high-risk patients. However, studies on the clinical role of the comprehensive evaluation of these features over clinical risk factors have been limited. Furthermore, there has been limited study, which evaluated the differential prognostic implications of CCTA-derived HRPCs according to the hemodynamic significance of CAD.

Increased Predictability by CCTA-Derived Anatomic and Hemodynamic Plaque Evaluation

As with previous studies (1), discriminant ability of clinical risk factors to predict subsequent coronary events was limited, and the c-index of clinical risk factors was lower than that of most CCTA-derived anatomic plaque characteristics. Among the CCTA-derived anatomic plaque characteristics, plaque burden $\geq$70%, MLA < 4 mm^2, and low attenuation plaque showed higher discrimination abilities for subsequent coronary events than any individual clinical risk factor or other parameters of HRPCs. As with previous results from the 3V-FFR-FRIENDS study (5), the number of HRPCs showed a higher discrimination ability than either individual parameters of HRPCs or clinical risk factors.

More importantly, CFD-derived hemodynamic parameters were more predictive for subsequent coronary events than clinical risk factors or HRPCs. The three CFD-derived hemodynamic parameters evaluated in this study, namely, FFR_{CT}, ΔFFR_{CT}, and percent ischemic myocardial mass, represent different aspects of hemodynamic significance in the target vessel territory. The FFR_{CT} represents the severity of myocardial ischemia, whereas the percent ischemic myocardial

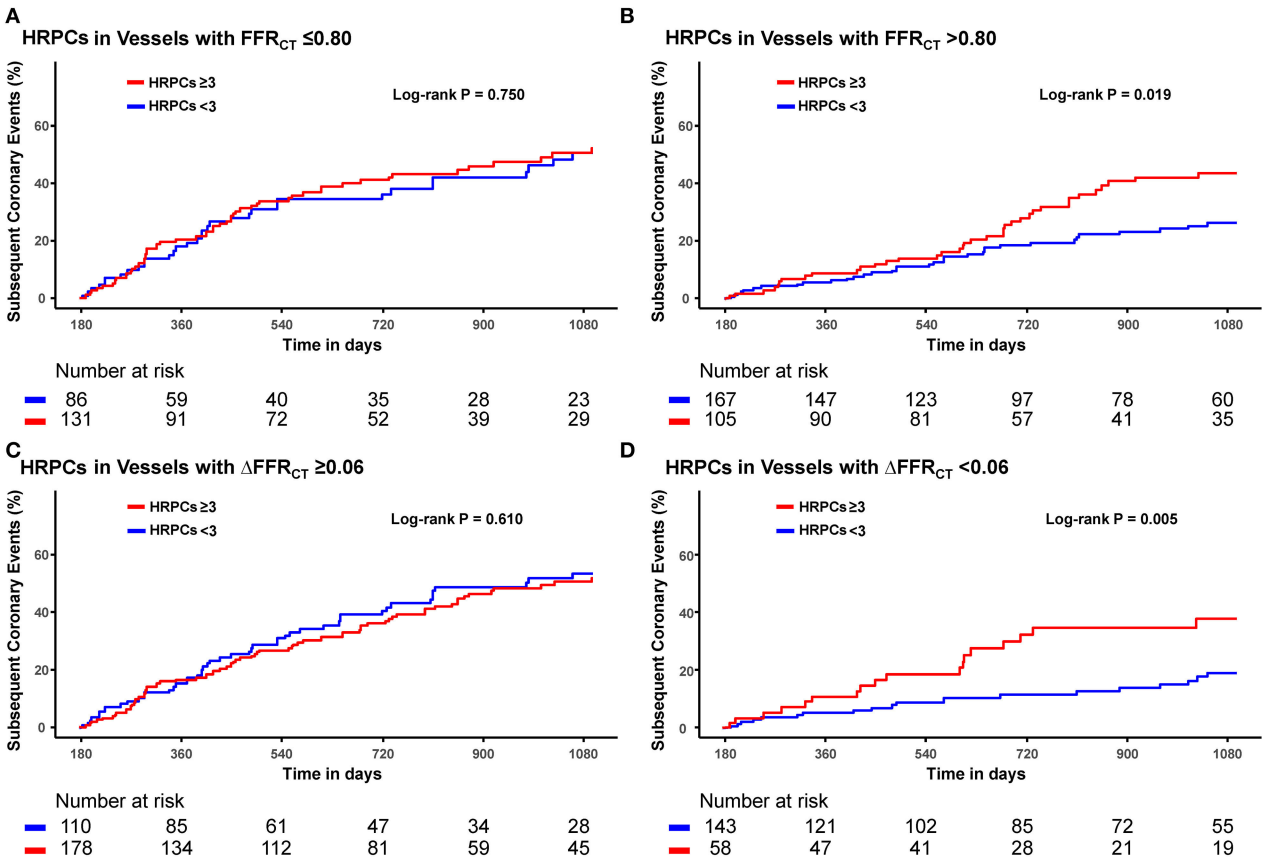

FIGURE 5 | Differential prognostic impact of HRPCs for subsequent coronary events according to hemodynamic parameters. Differential prognostic impact of number of HRPCs of ≥3 is evaluated in vessels with **(A)** FFR_{CT} ≤0.80, **(B)** FFR_{CT} >0.80 **(C)** ΔFFR_{CT} ≥0.06, and **(D)** ΔFFR_{CT} <0.06. Abbreviations: FFR_{CT}, fractional flow reserve by coronary computed tomography angiography; HRPCs, high-risk plaque characteristics.

mass represents the extent of myocardial ischemia. Furthermore, FFR_{CT} reflects cumulative hemodynamic deprivation of the entire target vessel, representing vessel-level significance, whereas ΔFFR_{CT} reflects the severity of local stenosis within the target vessel, representing lesion-level significance. Among these hemodynamic parameters, the discrimination abilities of FFR_{CT} and ΔFFR_{CT} were significantly higher than those of any clinical risk factors, individual HRPCs, or the number of HRPCs. These results support the contemporary practice guidelines that recommend treatment decisions based on the hemodynamic significance of the target lesion (8). Of note, ΔFFR_{CT} showed the highest discriminant ability for subsequent coronary events, suggesting that lesion-level hemodynamic significance may be the most important determinant of subsequent coronary events among other anatomic and hemodynamic parameters, including vessel-level FFR_{CT}.

In the prediction of subsequent coronary events, CCTA-derived HRPCs and CFD-derived hemodynamic parameters showed incremental predictability when added to clinical risk factors. The final model with clinical risk factors, HRPCs, and hemodynamic parameters showed significantly increased discrimination and reclassification abilities. Considering that CCTA enables simultaneous assessment of both HRPCs and hemodynamic parameters without additional scans or invasive procedures, radiation exposure, or use of hyperemic agents, it would be a practical diagnostic and prognostic stratification tool for patients with suspected CAD who may need intensive medical treatment to prevent plaque progression and rupture. Further study is warranted to incorporate this concept into daily practice.

Differential Prognostic Implications of HRPCs According to Hemodynamic Significance

Previous studies showed that there were associations among lesion severity, anatomic plaque characteristics, and hemodynamic lesion severity (2, 3, 5, 25). Similarly, we found that HRPCs were significantly associated with hemodynamic parameters, namely, FFR_{CT}, ΔFFR_{CT}, and percent ischemic myocardial mass. These associations can differ in each patient/lesion due to numerous patient- or lesion-specific parameters such as plaque content, presence of positive or negative remodeling, lesion location, or variation in coronary flow and microvascular function. Nevertheless,

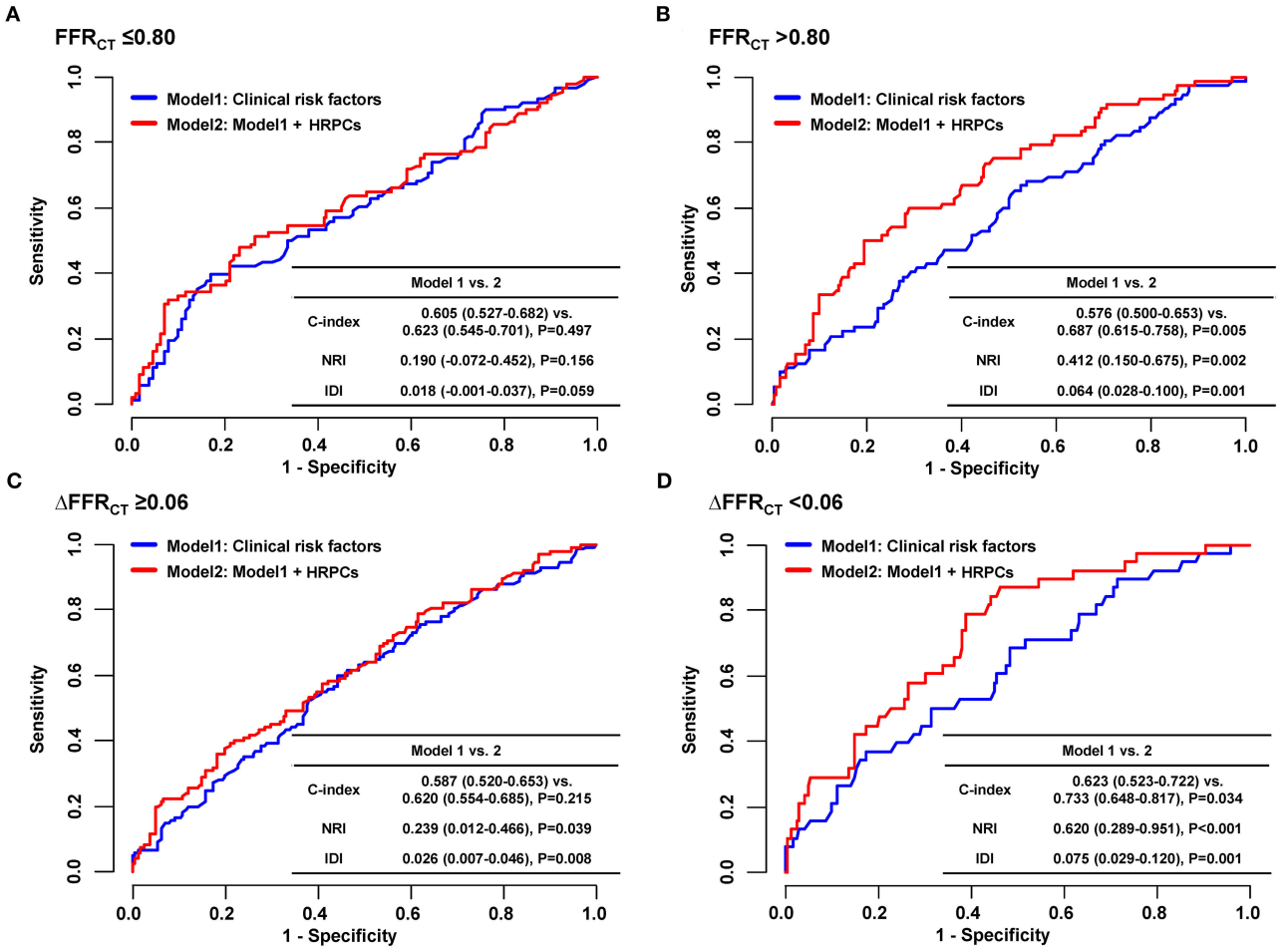

FIGURE 6 | Incremental prognostic value of HRPCs for subsequent coronary events according to hemodynamic parameters. To assess incremental discriminatory and reclassification abilities of HRPCs in addition to clinical risk factors for subsequent coronary events, two models were constructed as follows: model 1: clinical risk factors (age, sex, hypertension, diabetes mellitus, dyslipidemia, chronic kidney disease, and current smoker) and model 2: clinical risk factors + HRPCs (low attenuation plaque, positive remodeling, napkin-ring sign, spotty calcification, minimal luminal area <4 mm^2, or plaque burden ≥70%). Incremental discriminatory and reclassification abilities of HRPCs were evaluated in vessels with **(A)** FFR$_{CT}$ ≤ 0.80, **(B)** FFR$_{CT}$ > 0.80, **(C)** ΔFFR$_{CT}$ ≥ 0.06, and **(D)** ΔFFR$_{CT}$ < 0.06. FFR$_{CT}$, fractional flow reserve by coronary computed tomography angiography; HRPCs, high-risk plaque characteristics; IDI, relative integrated discrimination improvement; NRI, category-free net reclassification index.

since current guidelines recommend treatment decisions based on hemodynamic significance but not the anatomic plaque characteristics, there has been an ongoing debate regarding the prognostic significance of HRPCs in lesions with negative hemodynamic significance. A recent 3V-FFR-FRIENDS study demonstrated that, among deferred vessels with FFR >0.80, those with ≥3 HRPCs showed a significantly higher risk of vessel-specific MI, revascularization, or cardiac death at 5 years compared with those with <3 HRPCs (5).

In this study, there was no additional role for HRPCs in predicting subsequent coronary events in vessels with positive hemodynamic significance (FFR$_{CT}$ ≤ 0.80 or ΔFFR$_{CT}$ < 0.06). Conversely, in vessels with negative hemodynamic significance, the presence of ≥3 HRPCs was independently associated with a higher risk of subsequent coronary events, and HRPCs showed an incremental discrimination ability when added to clinical risk factors. These results imply that additional evaluation of CCTA-based anatomic plaque characteristics in hemodynamically insignificant lesions might improve risk stratification in patients with CAD. Since ischemia-based imaging assessments with noninvasive stress tests cannot detect CAD without hemodynamic significance, CCTA-based anatomic plaque assessment would be helpful to select individuals at elevated risk for subsequent coronary events who could have been underdiagnosed by the stress tests. Furthermore, considering the differential prognostic implications of HRPCs according to hemodynamic significance, it should be further evaluated whether intensive medical therapy and/or preemptive PCI in hemodynamically insignificant lesions with HRPCs can induce stabilization of plaque characteristics (26) and eventually improve patient prognosis. Current ongoing trials (PREVENT [NCT02316886]

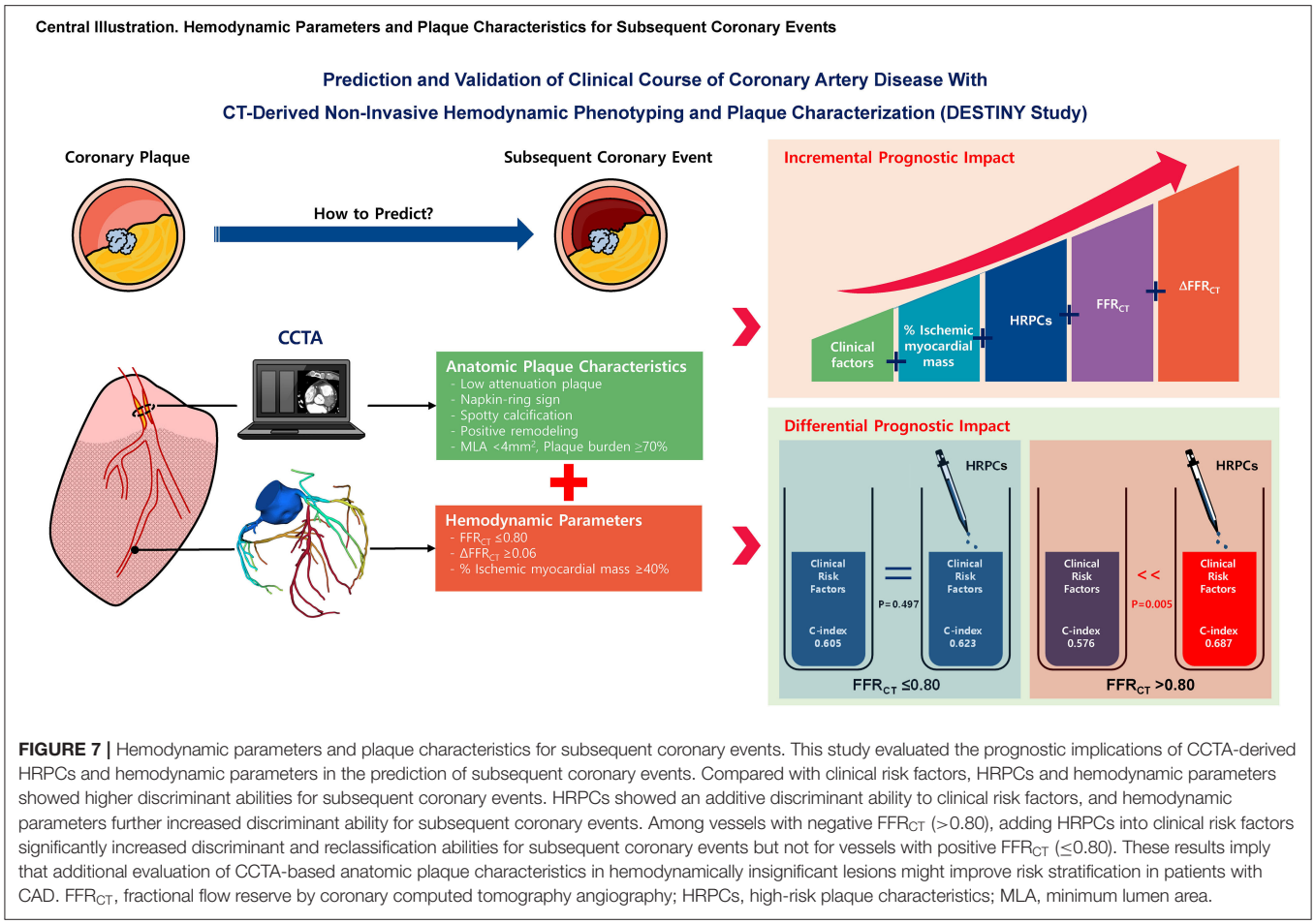

FIGURE 7 | Hemodynamic parameters and plaque characteristics for subsequent coronary events. This study evaluated the prognostic implications of CCTA-derived HRPCs and hemodynamic parameters in the prediction of subsequent coronary events. Compared with clinical risk factors, HRPCs and hemodynamic parameters showed higher discriminant abilities for subsequent coronary events. HRPCs showed an additive discriminant ability to clinical risk factors, and hemodynamic parameters further increased discriminant ability for subsequent coronary events. Among vessels with negative FFR_{CT} (>0.80), adding HRPCs into clinical risk factors significantly increased discriminant and reclassification abilities for subsequent coronary events but not for vessels with positive FFR_{CT} (≤0.80). These results imply that additional evaluation of CCTA-based anatomic plaque characteristics in hemodynamically insignificant lesions might improve risk stratification in patients with CAD. FFR_{CT}, fractional flow reserve by coronary computed tomography angiography; HRPCs, high-risk plaque characteristics; MLA, minimum lumen area.

and PROSPECT II [NCT02171065]) will help to clarify this issue.

Limitations

Some limitations should be acknowledged. First, this study has limitations related to the observational design of the study. Consequently, confounding bias may occur due to measured and unmeasured variables. Second, only patients who underwent invasive coronary angiography 6–36 months after CCTA were included in the study, which may have caused selection bias. Therefore, the current results may not be generalized to an overall population who underwent CCTA. Further external validation is needed in future studies. Third, vessels that were not suitable for anatomic and hemodynamic plaque characteristics analyses were excluded. This may also have caused selection bias. In particular, vessels with severe calcification were excluded from the analysis as they were considered suboptimal for plaque characterization. Fourth, the decision to perform CCTA and PCI was left to the operator's discretion. Fifth, neither group received adequate preventive medication according to the current consensus. However, this might reflect real-world practice and show the natural course of the patients. Sixth, it should be noted that the overall accuracy of models to predict future ACS occurrences was not very high. This might reflect the complex nature of the underlying mechanism of ACS.

CONCLUSION

In predicting subsequent coronary events, both HRPCs and hemodynamic parameters by CCTA allow for better prediction of subsequent coronary events than clinical risk factors alone. HRPCs provide incremental predictability than clinical risk factors among vessels with negative FFR_{CT} but not among vessels with positive FFR_{CT} (**Figure 7**).

DATA AVAILABILITY STATEMENT

The datasets presented in this article are not readily available because data cannot be shared publicly due to the privacy of individuals that participated in the study. The data will be shared on reasonable request to the corresponding author. Requests to access the datasets should be directed to JL, drone80@hanmail.net.

ETHICS STATEMENT

The studies involving human participants were reviewed and approved by Samsung Medical Center. The patients/participants provided their written informed consent to participate in this study.

AUTHOR CONTRIBUTIONS

SL, DH, and JL: conception, design, analysis, interpretation of data, drafting and revising of the manuscript, and final approval of the manuscript submitted. ND, DS, KC, SK, HK, K-HJ, SH, KL, TP, JY, YS, S-HC, YC, H-CG, and JG: interpretation of data, revising of the manuscript, and final approval of the manuscript submitted. All authors contributed to the article and approved the submitted version.

SUPPLEMENTARY MATERIAL

The Supplementary Material for this article can be found online at: https://www.frontiersin.org/articles/10.3389/fcvm.2022.871450/full#supplementary-material

REFERENCES

1. D'Agostino RB, Vasan RS, Pencina MJ, Wolf PA, Cobain M, Massaro JM, et al. General cardiovascular risk profile for use in primary care: the framingham heart study. *Circulation.* (2008) 117:743–53. doi: 10.1161/CIRCULATIONAHA.107.699579
2. Stone GW, Maehara A, Lansky AJ, de Bruyne B, Cristea E, Mintz GS, et al. A prospective natural-history study of coronary atherosclerosis. *N Engl J Med.* (2011) 364:226–35. doi: 10.1056/NEJMoa1002358
3. Cheng JM, Garcia-Garcia HM, de Boer SP, Kardys I, Heo JH, Akkerhuis KM, et al. In vivo detection of high-risk coronary plaques by radiofrequency intravascular ultrasound and cardiovascular outcome: results of the atheroremo-ivus study. *Eur Heart J.* (2014) 35:639–47. doi: 10.1093/eurheartj/eht484
4. Motoyama S, Ito H, Sarai M, Kondo T, Kawai H, Nagahara Y, et al. Plaque Characterization by coronary computed tomography angiography and the likelihood of acute coronary events in mid-term follow-up. *J Am Coll Cardiol.* (2015) 66:337–46. doi: 10.1016/j.jacc.2015.05.069
5. Lee JM, Choi KH, Koo BK, Park J, Kim J, Hwang D, et al. Prognostic implications of plaque characteristics and stenosis severity in patients with coronary artery disease. *J Am Coll Cardiol.* (2019) 73:2413–24. doi: 10.1016/j.jacc.2019.02.060
6. Chang HJ, Lin FY, Lee SE, Andreini D, Bax J, Cademartiri F, et al. Coronary Atherosclerotic Precursors of Acute Coronary Syndromes. *J Am Coll Cardiol.* (2018) 71:2511–22. doi: 10.1016/j.jacc.2018.02.079
7. Koskinas KC, Ughi GJ, Windecker S, Tearney GJ, Raber L. Intracoronary imaging of coronary atherosclerosis: validation for diagnosis, prognosis and treatment. *Eur Heart J.* (2016) 37:524–35a-c. doi: 10.1093/eurheartj/ehv642
8. Knuuti J, Wijns W, Saraste A, Capodanno D, Barbato E, Funck-Brentano C, et al. 2019 Esc guidelines for the diagnosis and management of chronic coronary syndromes. *Eur Heart J.* (2020) 41:407–77. doi: 10.1093/eurheartj/ehz425
9. Lee JM, Choi G, Koo BK, Hwang D, Park J, Zhang J, et al. Identification of high-risk plaques destined to cause acute coronary syndrome using coronary computed tomographic angiography and computational fluid dynamics. *JACC Cardiovasc Imaging.* (2019) 12:1032–43. doi: 10.1016/j.jcmg.2018.01.023
10. Patel MR, Norgaard BL, Fairbairn TA, Nieman K, Akasaka T, Berman DS, et al. 1-year impact on medical practice and clinical outcomes of ffrct: the advance registry. *JACC Cardiovasc Imaging.* (2020) 13:97–105. doi: 10.1016/j.jcmg.2019.03.003
11. Taylor AJ, Cerqueira M, Hodgson JM, Mark D, Min J, O'Gara P, et al. Accf/Scct/Acr/Aha/Ase/Asnc/Nasci/Scai/Scmr 2010 appropriate use criteria for cardiac computed tomography. a report of the American College of Cardiology Foundation Appropriate Use Criteria Task Force, the Society of Cardiovascular Computed Tomography, the American College of Radiology, the American Heart Association, the American Society of Echocardiography, the American Society of Nuclear Cardiology, the North American Society for Cardiovascular Imaging, the Society for Cardiovascular Angiography and Interventions, and the Society for Cardiovascular Magnetic Resonance. *J Cardiovasc Comput Tomogr.* (2010) 4:407 e1-33. doi: 10.1016/j.jcct.2010.11.001
12. van Assen M, Varga-Szemes A, Schoepf UJ, Duguay TM, Hudson HT, Egorova S, et al. Automated plaque analysis for the prognostication of major adverse cardiac events. *Eur J Radiol.* (2019) 116:76–83. doi: 10.1016/j.ejrad.2019.04.013
13. Buckler AJ, Karlöf E, Lengquist M, Gasser TC, Maegdefessel L, Perisic Matic L, et al. Virtual transcriptomics: noninvasive phenotyping of atherosclerosis by decoding plaque biology from computed tomography angiography imaging. *Arterioscler Thromb Vasc Biol.* (2021) 41:1738–50. doi: 10.1161/ATVBAHA.121.315969
14. Ihdayhid AR, Norgaard BL, Achenbach S, Khav N, Gaur S, Leipsic J, et al. Ischemic myocardial burden subtended by computed tomography-derived fractional flow reserve (Approach(Ffrct)): an exploratory analysis on diagnostic performance. *JACC Cardiovasc Imaging.* (2020) 13:2264–7. doi: 10.1016/j.jcmg.2020.05.008
15. West GB, Brown JH, Enquist BJ. A General model for the origin of allometric scaling laws in biology. *Science.* (1997) 276:122–6. doi: 10.1126/science.276.5309.122
16. Kim HY, Doh JH, Lim HS, Nam CW, Shin ES, Koo BK, et al. Identification of coronary artery side branch supplying myocardial mass that may benefit from revascularization. *JACC Cardiovasc Interv.* (2017) 10:571–81. doi: 10.1016/j.jcin.2016.11.033
17. Thygesen K, Alpert JS, Jaffe AS, Chaitman BR, Bax JJ, Morrow DA, et al. Fourth universal definition of myocardial infarction (2018). *J Am Coll Cardiol.* (2018) 72:2231–64. doi: 10.1016/j.jacc.2018.08.1038
18. Patel MR, Peterson ED Dai D, Brennan JM, Redberg RF, Anderson HV, et al. Low diagnostic yield of elective coronary angiography. *N Engl J Med.* (2010) 362:886–95. doi: 10.1056/NEJMoa0907272
19. Fishbein MC, Siegel RJ. How big are coronary atherosclerotic plaques that rupture? *Circulation.* (1996) 94:2662–6. doi: 10.1161/01.CIR.94.10.2662
20. Sedlis SP, Hartigan PM, Teo KK, Maron DJ, Spertus JA, Mancini GB, et al. Effect of Pci on long-term survival in patients with stable ischemic heart disease. *N Engl J Med.* (2015) 373:1937–46. doi: 10.1056/NEJMoa1505532
21. Maron DJ, Hochman JS, Reynolds HR, Bangalore S, O'Brien SM, Boden WE, et al. Initial invasive or conservative strategy for stable coronary disease. *N Engl J Med.* (2020) 382:1395–407. doi: 10.1056/NEJMoa1915922
22. Investigators S-H, Newby DE, Adamson PD, Berry C, Boon NA, Dweck MR, et al. Coronary Ct angiography and 5-year risk of myocardial infarction. *N Engl J Med.* (2018) 379:924–33. doi: 10.1056/NEJMoa1805971
23. Douglas PS, De Bruyne B, Pontone G, Patel MR, Norgaard BL, Byrne RA, et al. 1-Year outcomes of Ffrct-guided care in patients with suspected coronary disease: the platform study. *J Am Coll Cardiol.* (2016) 68:435–45. doi: 10.1016/j.jacc.2016.05.057
24. Norgaard BL, Terkelsen CJ, Mathiassen ON, Grove EL, Botker HE, Parner E, et al. Coronary Ct angiographic and flow reserve-guided management of patients with stable ischemic heart disease. *J Am Coll Cardiol.* (2018) 72:2123–34. doi: 10.1016/j.jacc.2018.07.043

25. Driessen RS, Stuijfzand WJ, Raijmakers PG, Danad I, Min JK, Leipsic JA, et al. Effect of plaque burden and morphology on myocardial blood flow and fractional flow reserve. *J Am Coll Cardiol.* (2018) 71:499–509. doi: 10.1016/j.jacc.2017.11.054
26. Andelius L, Mortensen MB, Nørgaard BL, Abdulla J. Impact of statin therapy on coronary plaque burden and composition assessed by coronary computed tomographic angiography: a systematic review and meta-analysis. *Eur Heart J Cardiovasc Imaging.* (2018) 19:850–8. doi: 10.1093/ehjci/jey012

Conflict of Interest: JL received a Research Grant from St. Jude Medical (Abbott Vascular) and Philips Volcano.

The remaining authors declare that the research was conducted in the absence of any commercial or financial relationships that could be construed as a potential conflict of interest.

Publisher's Note: All claims expressed in this article are solely those of the authors and do not necessarily represent those of their affiliated organizations, or those of the publisher, the editors and the reviewers. Any product that may be evaluated in this article, or claim that may be made by its manufacturer, is not guaranteed or endorsed by the publisher.

frontiers | Frontiers in Cardiovascular Medicine

ORIGINAL RESEARCH
published: 26 May 2022
doi: 10.3389/fcvm.2022.854107

Predictive Value of Plasma Big Endothelin-1 in Adverse Events of Patients With Coronary Artery Restenosis and Diabetes Mellitus: Beyond Traditional and Angiographic Risk Factors

Yue Ma, Tao Tian, Tianjie Wang, Juan Wang, Hao Guan, Jiansong Yuan, Lei Song, Weixian Yang* and Shubin Qiao**

Research Center for Coronary Heart Disease, Fuwai Hospital, National Center for Cardiovascular Diseases, Chinese Academy of Medical Sciences and Peking Union Medical College, Beijing, China

OPEN ACCESS

Edited by:
Michail Papafaklis, University Hospital of Ioannina, Greece

Reviewed by:
Felice Gragnano, University of Campania Luigi Vanvitelli, Italy
Vojislav Giga, University of Belgrade, Serbia

***Correspondence:**
Shubin Qiao
qsbfw@sina.com
Weixian Yang
wxyang2009@sina.com
Lei Song
drsong@vip.163.com

Specialty section:
This article was submitted to Coronary Artery Disease, a section of the journal Frontiers in Cardiovascular Medicine

Received: *13 January 2022*
Accepted: *28 April 2022*
Published: *26 May 2022*

Citation:
Ma Y, Tian T, Wang T, Wang J, Guan H, Yuan J, Song L, Yang W and Qiao S (2022) Predictive Value of Plasma Big Endothelin-1 in Adverse Events of Patients With Coronary Artery Restenosis and Diabetes Mellitus: Beyond Traditional and Angiographic Risk Factors. Front. Cardiovasc. Med. 9:854107. doi: 10.3389/fcvm.2022.854107

Background: Patients with diabetes are a high-risk group for coronary in-stent restenosis (ISR), so it would be valuable to identify biomarkers to predict their prognosis. The plasma big endothelin-1 (big ET-1) level is closely related to cardiovascular adverse events; however, for patients with ISR and diabetes who undergo percutaneous coronary intervention (PCI), whether big ET-1 is independently correlated with prognosis is still uncertain.

Methods: Patients with drug-eluting stent (DES) restenosis who underwent successful re-PCI from January 2017 to December 2018 at the Chinese Academy of Medical Sciences Fuwai Hospital were enrolled and followed up for 3 years. The patients were divided into the tertiles of baseline big ET-1. The primary end points were major adverse cardiovascular events (MACEs): cardiac death, non-fatal myocardial infarction (MI), target lesion revascularization (TLR), and stroke. A Cox multivariate proportional hazard model and the C-statistic were used to evaluate the potential predictive value of big ET-1 beyond traditional and angiographic risk factors.

Results: A total of 1,574 patients with ISR were included in this study, of whom 795 were diabetic. In patients with ISR and diabetes, after an average follow-up of 2.96 ± 0.56 years, with the first tertile of big ET-1 as a reference, the hazard ratio [HR] (95% CI) of MACEs after adjustment for traditional and angiographic risk factors was 1.24 (0.51–3.05) for the second tertile and 2.60 (1.16–5.81) for the third. Big ET-1 improved the predictive value for MACEs over traditional risk factors (C-statistic: 0.64

vs. 0.60, $p = 0.03$). Big ET-1 was not significantly associated with the risk of MACEs in patients without diabetes.

Conclusion: Increased plasma big ET-1 was associated with a higher risk of adverse cardiovascular prognosis independent of traditional and angiographic risk factors, and therefore, it might be used as a predictive biomarker, in patients with ISR and diabetes.

Keywords: coronay artery disease, in-stent restenosis, big endothelin-1 (big ET-1), diabetes mellitus, cardiovascular prognosis

INTRODUCTION

Diabetes mellitus is an important risk factor for the development of cardiovascular diseases, such as coronary artery disease (CAD), cerebrovascular disease, and peripheral artery disease (1, 2). Cardiovascular disease is the main cause of death in diabetic patients (3). The total number of diabetic patients in the world is predicted to increase to 592 million by 2035 (4). Coronary artery in-stent restenosis (ISR), a complication that is unpreventable in patients with percutaneous coronary intervention (PCI), refers to lesions with a vascular diameter stenosis rate ≥50% in the stent and/or within 5 mm of both edges of the stent (5). Although drug-eluting stent (DES) implantation improves the long-term prognosis of patients, ISR is still a serious problem (6, 7). Patients with diabetes are a high-risk group for ISR (8, 9). Therefore, it will be valuable to identify biomarkers with predictive value for the prognosis of patients with ISR and diabetes.

Endothelin-1 (ET-1) is a 21-amino-acid polypeptide that is produced by vascular endothelial cells. It is the most effective vasoconstrictor in the cardiovascular system and has the characteristic of long-lasting action (10). ET-1 and its receptors mediate pathophysiological processes, such as inflammation, oxidative stress, endothelial dysfunction, and insulin resistance, leading to the occurrence and progression of diabetes and atherosclerotic diseases (11). Due to the instability of ET-1 in plasma, its clinical application as a biomarker is limited (12). Big ET-1, as the precursor of ET-1, has a longer half-life and can be used as a surrogate indicator to reflect the ET-1 level (12). Big ET-1 has a useful predictive value in patients with three-vessel CAD, stable CAD, young myocardial infarction (MI), acute myocardial infarction (AMI), and diabetes (13–16); however, little is known about its clinical predictive value in patients with ISR and diabetes, a more vulnerable population of patient with CAD. Therefore, this study is aimed to identify the potential association between big ET-1 and clinical prognosis and determine whether big ET-1 has an incremental effect on risk prediction beyond traditional and angiographic risk factors in patients with ISR and diabetes.

Abbreviations: ISR, in-stent restenosis; Big ET-1, big endothelin-1; PCI, percutaneous coronary intervention; DES, drug-eluting stent; MI, myocardial infarction; AMI, acute myocardial infarction; MACEs, Major adverse cardiovascular events; TLR, target lesion revascularization; HR, hazard ratio; CI, confidence interval; CAD, coronary artery disease; OGTT, oral glucose tolerance test; HbA1c, glycosylated hemoglobin A1c; BMI, body mass index; TIA, transient ischemic attack; CABG, coronary artery bypass grafting; LVEF, left ventricular ejection fraction; LVDD, left ventricular diastolic diameter; TnI, troponin I; TG, triglycerides; TC, total cholesterol; LDL-c, low-density lipoprotein cholesterol; HDL-c, high-density lipoprotein cholesterol; ELISA, enzyme-linked immunosorbent assay; TVR, target vessel revascularization; ST, stent thrombosis; LM, left main artery; LAD, left anterior descending; LCX, left circumflex; RCA, right coronary artery; CEC, clinical events committee.

METHODS

Study Population

There were 35,649 patients with CAD who underwent successful PCI at the Chinese Academy of Medical Sciences Fuwai Hospital from January 2017 to December 2018, of whom 6.42% of patients (n = 2,289) who were diagnosed with DES restenosis were consecutively enrolled in this study. The diagnosis of ISR was based on the presence of lesions in the coronary stent and/or within 5 mm of an edge of the stent, with a vascular diameter stenosis rate ≥50%. According to the angiographic characteristics, it can be divided into four types: type I occurs when the stent or the stent edge is ≤ 10 mm, type II is a diffuse ISR confined to stents >10 mm, type III is a diffuse ISR >10 mm beyond the edge of the stent, and type IV is a completely occlusive ISR (5). Diabetes was diagnosed in patients who met any of the following criteria: fasting blood glucose ≥7.0 mmol/L without any caloric intake for at least 8 h; oral glucose tolerance test (OGTT) with a glucose load of 75 g anhydrous glucose for 2 h; blood glucose ≥11.1 mmol/L; glycosylated hemoglobin ≥6.5%; and random blood glucose ≥11.1 mmol/L in patients with typical symptoms of hyperglycemia (17). The patients were divided into diabetic and non-diabetic groups according to whether they had a diagnosis of diabetes. The exclusion criteria were as follows: a history of diabetes, lack of fasting blood glucose or glycosylated hemoglobin information, lack of plasma big ET-1 test results, and lack of complete follow-up information. The process of selection and exclusion is shown in **Figure 1**. This study complied with the Declaration of Helsinki and was approved by the ethics review committee. All patients signed an informed consent form.

Data Collection

In addition to demographic data, patients' traditional and angiographic risk factors were both collected.

Traditional risk factors include body mass index (BMI), hypertension, hyperlipidemia, diabetes, smoking history, thyroid disease, stroke or transient ischemic attack (TIA), history of peripheral artery disease, chronic kidney failure, and coronary artery bypass grafting (CABG).

Angiographic risk factors include ISR lesion position, ISR angiographic type, pre-Thrombolysis in Myocardial Infarction

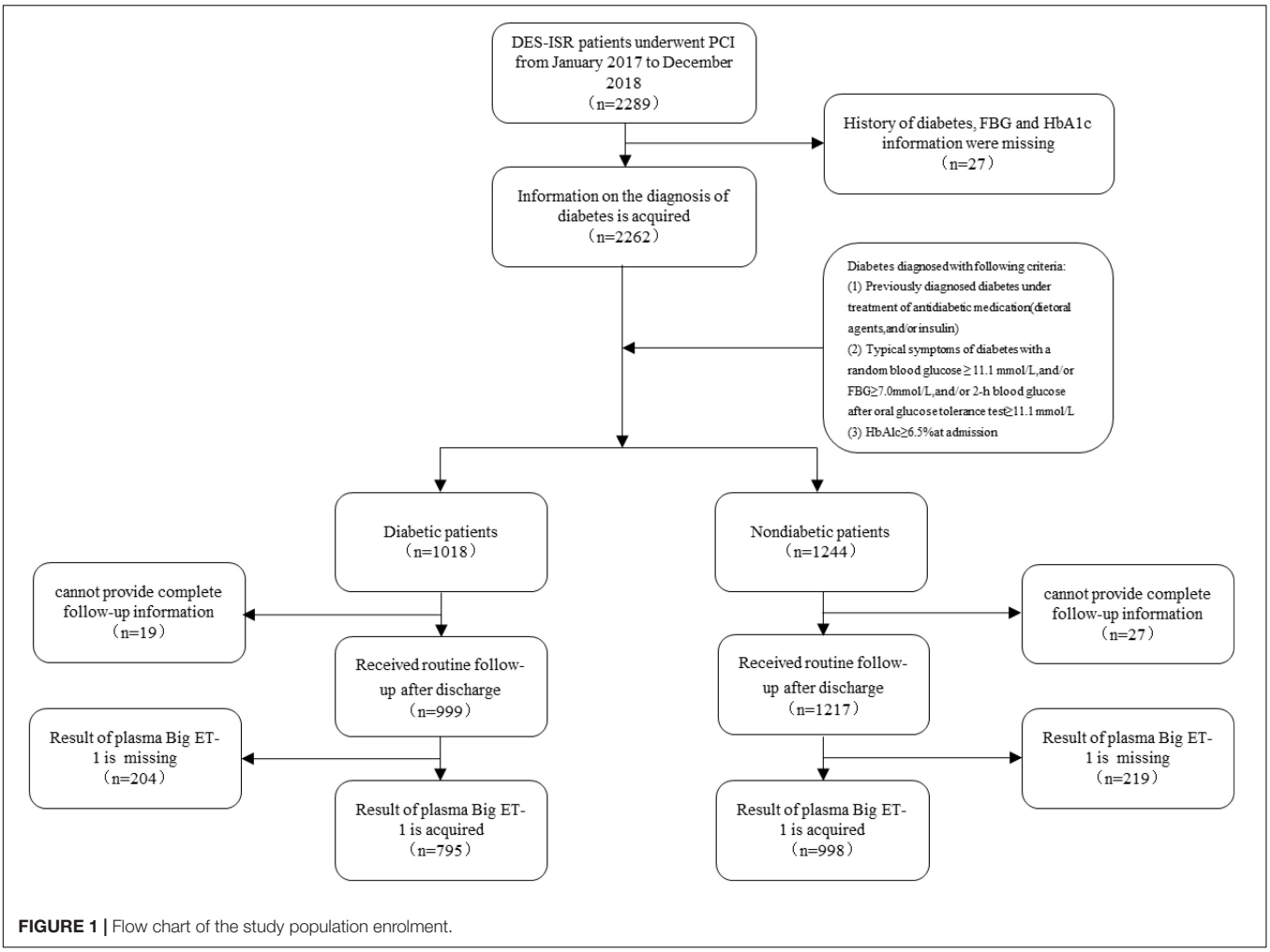

FIGURE 1 | Flow chart of the study population enrolment.

(TIMI) flow, reference vessel diameter, target lesion length, diameter stenosis rate, and the presence of special types of lesions, such as calcification, occlusion, ostial lesion, thrombus, angulated lesion, and concentric lesion and the number of target lesions. The coronary angiography results were interpreted by two experienced cardiovascular intervention doctors.

The big ET-1 detection method involved drawing 5 ml of fasting venous blood from a vacuum ethylenediaminetetraacetic acid (EDTA) anticoagulant tube, centrifuging at 3,000 r/min for 10 min within 1 h after blood collection, and analyzing the sample by enzyme-linked immunosorbent assay (ELISA) (BIOMEDICA, Austria). The reference value range of big ET-1 was <0.25 pmol/L, and the detection sensitivity was 0.02 pmol/L.

Follow-Up and End Point Event

The patients were followed up for 3 years by uniformly trained staff through a telephone follow-up or outpatient follow-up. The primary end point was major adverse cardiovascular events (MACEs), which included cardiogenic death, non-fatal MI, target lesion revascularization (TLR), and stroke. Cardiac death was defined as death directly caused by cardiovascular disease. Secondary end points included all-cause death, target vessel revascularization (TVR), stent thrombosis (ST), and hemorrhage. Hemorrhage was defined as intracranial hemorrhage, hemoglobin drop ≥50 g/L, or hematocrit drop ≥15% caused by hemorrhage.

Statistical Analysis

SPSS 23.0 and R language 3.5.1 statistical software were used to analyze the data. The Kolmogorov-Smirnov normality test was performed on continuous variables. Data with a normal distribution are represented by $\bar{x}\pm s$ and were compared between groups using the independent sample *t*-test; data with a non-normal distribution are represented by M (Q1, Q3) and were compared using the Wilcoxon rank-sum test. Categorical variables are expressed as percentages, and the χ^2 test was used for comparisons between groups. Prior to association analyses, variables with skewed distributions were natural log-transformed. Univariate and multivariate Cox proportional hazard models were used to determine the predictors of the end point event, and the risk is expressed as the hazard ratio (HR) with its 95% confidence interval (CI). All variables with a value of $p < 0.2$ were included in a stepwise Cox regression

($p < 0.2$ as entry criterion and $p > 0.1$ as removal criterion) for identifying potential outcome-specific independent predictors, which were treated as covariates in the ensuing multivariate analyses between big ET-1 and outcomes. The interaction between diabetic status and big ET-1 was tested by adding a product term in the multivariate Cox models. Kaplan-Meier curves were drawn to analyze the survival rate, and the log-rank test was used to compare the difference in survival rate between big ET-1 tertiles. A multivariable-adjusted survival curve was also plotted. A restricted cubic spline was used to analyze the dose-effect relationship between big ET-1 and prognostic events. The C-statistic was calculated to demonstrate the predictive value of big ET-1 for prognostic events when compared with those of traditional and angiographic risk factors. All tests were two-tailed, and differences were considered statistically significant at $p < 0.05$.

RESULTS

Baseline Characteristics of the Study Population

The current study finally enrolled 1,793 participants, with a mean age of 60.79 ± 9.77 years and a male proportion of 80.76% (n = 1,448). Patients were stratified into two groups according to the diagnosis of diabetes. Patients with diabetes exhibited significantly higher big ET-1 levels than non-diabetic patients (0.23 vs. 0.26, $p < 0.001$). There was no difference between the diabetes group and the non-diabetic group in terms of sex, hyperlipidemia, smoking, thyroid disease, peripheral vascular disease, or other traditional risk factors ($p > 0.05$). The incidence of hypertension, previous stroke, and the levels of N-terminal (NT)-pro-B-type natriuretic peptide (BNP) were higher, and levels of uric acid and high-density lipoprotein cholesterol (HDL-c) were lower in diabetic patients ($p < 0.05$). Both diabetic patients and non-diabetic patients had the left anterior descending (LAD) as the main vessel of the ISR lesion. These groups showed no significant difference in the distribution of angiographic risk factors, such as reference vessel diameter, target lesion length, diameter stenosis rate, special lesion, angiographic type, and pre-TIMI flow (all $p > 0.05$). There was no difference in the medications that were used for the treatment of CAD between the groups (all $p > 0.05$; **Table 1**). There was no difference in the characteristics between the enrolled and excluded patients (**Supplementary Table 1**).

Clinical Outcomes

During the average follow-up time of 2.96 ± 0.56 years, 54 patients in the diabetes group (6.79%) experienced MACEs, and 141 patients in the total sample (7.86%) had a secondary end point event. There were 83 patients in the non-diabetic group (8.32%) with MACEs, and 88 patients (8.82%) had secondary end point events. There was no statistically significant difference in the incidence of composite end point events between the two groups ($p > 0.05$), although the incidence of stroke was higher while the incidence of cardiac death was lower in the diabetes group ($p < 0.05$; **Table 2**).

Kaplan-Meier Analysis

Among the diabetic patients, the incidence of MACEs in the big ET-1 tertile 3 was higher than that in the other two tertiles (log-rank $p = 0.043$), and the incidence of secondary end point events was slightly but not significantly higher than that in the other two groups (log-rank $p = 0.083$). Among the non-diabetic patients, the incidence of MACEs (log-rank $p = 0.140$) and the incidence of secondary end point events were not significantly different between the big ET-1 tertiles (log-rank $p = 0.074$; **Figure 2**).

Stepwise Cox Regression of Traditional and Angiographic Predictors

Univariate Cox regression analysis for traditional and angiographic variables was performed separately for MACEs and secondary end points. Then, all variables with $p < 0.2$ were entered into the multivariable Cox regression analysis for MACEs and secondary end points following the stepwise method for identifying independent predictors. We found that big ET-1 had an independent predictive value in diabetic patients. In addition, angulated lesions, history of CABG, low-density lipoprotein cholesterol (LDL-c), reference vessel diameter, thyroid disease, early ISR, and non-ISR lesion intervention were also associated with the prognosis of ISR patients with diabetes mellitus. All detailed results from the univariate and multivariable analyses are shown in **Supplementary Tables 2–5**.

Interaction Between Big ET-1 and Diabetes

When adding big ET-1 (as a continuous variable), a diagnosis of diabetes, and the interaction term of big ET-1 × diagnosis of diabetes (big ET-1 × diabetes) into a Cox regression, after adjusting for traditional and angiographic risk factors, we found that the interaction term was statistically significant for predicting both MACEs and the secondary end points (p for interaction < 0.0001). The significant interaction between big ET-1 and the diagnosis of diabetes indicates that diabetes diagnosis could modify the relationship between big ET-1 and the adverse cardiovascular prognosis. When adding big ET-1 as a categorical variable into a Cox regression analysis, after adjusting for traditional and angiographic risk factors, the interaction term was again statistically significant for predicting both MACEs (p for interaction = 0.008) and the secondary end points (p for interaction = 0.012; **Table 3**).

Relationship Between Big ET-1 and Cardiovascular Prognosis

In the diabetic patients, a one-unit increase in log-transformed big ET-1 was associated with a 105% increase in the risk of MACE (HR = 2.05, 95% CI: 1.36–3.09, $p = 0.001$) and a 98% increase in the risk of secondary end point events (HR = 1.98, 95% CI: 1.29–3.03, $p = 0.002$) after adjusting for age, sex, angulated lesion, history of CABG, LDL-c, reference vessel diameter, thyroid disease, early ISR, and non-ISR lesion intervention as potential traditional and angiographic factors input from the stepwise Cox regression analysis. When we grouped patients into the tertiles of big ET-1 level, compared with the first tertile, the second and

TABLE 1 | Baseline, lesion, and intervention characteristics of patients with coronary artery restenosis.

	Total (*n* = 1,793)	Diabetic patients (*n* = 795)	Non-diabetic patients (*n* = 998)	*P*-value
Demographic data				
Age, years	60.79 ± 9.77	61.39 ± 9.03	60.32 ± 10.31	0.0213
Sex, male, n (%)	1,448 (80.76)	631 (79.37)	817 (81.86)	0.1835
BMI, kg/m^2	26.07 ± 3.14	26.43 ± 3.03	25.79 ± 3.20	<0.0001
Cardiovascular risk factors, n (%)				
Hypertension	1,218 (67.97)	594 (74.81)	624 (62.53)	<0.0001
Hyperlipidemia	1,678 (98.36)	750 (98.17)	928 (98.51)	0.5757
Smoking	1,139 (65.54)	493 (63.78)	646 (66.94)	0.1676
Other disease, n (%)				
Pre-myocardial infarction	629 (35.08)	287 (36.10)	342 (34.27)	0.4193
Thyroid disease	64 (3.57)	24 (3.02)	40 (4.01)	0.2621
Stroke or TIA	220 (12.27)	116 (14.59)	104 (10.42)	0.0075
Peripheral vascular disease	196 (10.93)	88 (11.07)	108 (10.82)	0.8675
Chronic kidney failure	20 (1.12)	13 (1.64)	7 (0.70)	0.0614
History of CABG	75 (4.18)	39 (4.91)	36 (3.61)	0.1725
Clinical presenting, n (%)				0.9738
ACS	833 (46.46)	369 (46.42)	464 (46.49)	
CCS	960 (53.54)	426 (53.58)	534 (53.51)	
Examination				
LVEF, %	60.62 ± 7.58	60.21 ± 7.58	60.95 ± 7.58	0.0809
LVDD, mm	49.05 ± 5.42	49.12 ± 5.19	48.98 ± 5.61	0.6448
TnI, ng/L	0.02 (0.00, 0.07)	0.03 (0.00, 0.07)	0.02 (0.00, 0.07)	0.1005
Creatinine, μmol/L	82.52 (72.20, 93.71)	82.65 (72.00, 93.42)	82.27 (73.00, 94.00)	0.6320
Uric acid, μmol/L	350.35 (291.20, 407.85)	335.29 (278.20, 392.00)	359.00 (306.00, 416.35)	<0.0001
TG, mmol/L	1.48 (1.00, 2.05)	1.50 (1.20, 2.10)	1.47 (1.00, 2.04)	0.1566
TC, mmol/L	3.71 (3.20, 4.41)	3.68 (3.20, 4.39)	3.71 (3.20, 4.44)	0.2470
HDL-C, mmol/L	1.06 (1.00, 1.24)	1.03 (0.80, 1.23)	1.08 (1.00, 1.25)	0.0004
LDL-C, mmol/L	2.14 (1.80, 2.71)	2.12 (1.60, 2.71)	2.15 (1.80, 2.71)	0.4423
NT-proBNP, pg/mL	113.20 (51.80, 294.40)	125.10 (54.20, 338.60)	106.80 (49.80, 260.50)	0.0049
Big ET-1, pmol/L	0.24 (0.20, 0.35)	0.26 (0.20, 0.37)	0.23 (0.20, 0.33)	<0.0001
Big ET-1 in tertiles, n (%)				
Tertile 1	540 (30.12)	194 (24.40)	346 (34.67)	<0.0001
Tertile 2	615 (34.30)	269 (33.84)	346 (34.67)	<0.0001
Tertile 3	638 (35.58)	332 (41.76)	306 (30.66)	<0.0001
ISR duration, years	6.50 (5.40, 7.57)	6.56 (5.60, 7.61)	6.46 (5.20, 7.57)	0.2086
ISR duration type*, n (%)				0.1147
Early ISR	67 (3.74)	36 (4.53)	31 (3.11)	
Later ISR	1,726 (96.26)	759 (95.47)	967 (96.89)	
ISR lesion position, n (%)				
LM	44 (2.45)	20 (2.52)	24 (2.40)	0.8801
LAD	733 (40.88)	320 (40.25)	413 (41.38)	0.6284
LCX	247 (13.78)	104 (13.08)	143 (14.33)	0.4466
RCA	571 (31.85)	273 (34.34)	298 (29.86)	0.0431
Graft bypass	8 (0.45)	5 (0.63)	3 (0.30)	0.4785
ISR lesion features				
Reference vessel diameter, mm	3.04 ± 0.47	3.02 ± 0.46	3.06 ± 0.47	0.1423
Target lesion length, mm	26.71 ± 19.38	26.55 ± 18.84	26.84 ± 19.82	0.7688
Diameter stenosis rate, %	88.78 ± 9.77	89.02 ± 9.84	88.59 ± 9.71	0.3939
Special lesion, n (%)				
Calcification	777 (51.08)	358 (52.34)	419 (50.06)	0.3763
Occlusion	325 (21.05)	141 (20.35)	184 (21.62)	0.5409
Ostial lesion	205 (13.39)	95 (13.85)	110 (13.02)	0.6351
Thrombus	20 (1.34)	10 (1.49)	10 (1.22)	0.6560

(Continued)

TABLE 1 | (Continued)

	Total (*n* = 1,793)	Diabetic patients (*n* = 795)	Non-diabetic patients (*n* = 998)	*P*-value
Angulated lesion	466 (25.99)	212 (26.67)	254 (25.45)	0.5598
Concentric lesion	271 (15.11)	108 (13.58)	163 (16.33)	0.1066
Diffuse lesion	1,078 (60.12)	461 (57.99)	617 (61.82)	0.1497
Angiographic type, n (%)				0.9099
Type I	85 (4.74)	40 (5.03)	45 (4.51)	
Type II	670 (37.37)	300 (37.74)	370 (37.07)	
Type III	708 (39.49)	313 (39.37)	395 (39.58)	
Type IV	330 (18.40)	142 (17.86)	188 (18.84)	
Pre TIMI flow, n (%)				0.8481
Class 0	326 (18.18)	140 (17.61)	186 (18.64)	
Class 1	62 (3.46)	26 (3.27)	36 (3.61)	
Class 2	134 (7.47)	57 (7.17)	77 (7.72)	
Class 3	1,271 (70.89)	572 (71.95)	699 (70.04)	
ISR intervention strategy, n (%)				
DCB	782 (43.61)	341 (42.89)	441 (44.19)	0.5827
DES	1,011 (56.39)	454 (57.11)	557 (55.81)	0.5827
Non-ISR lesion intervention, n (%)	469 (26.16)	222 (27.92)	247 (24.75)	0.1286
Number of target lesion, n (%)				0.0509
1	1,324 (73.84)	573 (72.08)	751 (75.25)	
2	396 (22.09)	180 (22.64)	216 (21.64)	
3	73 (4.07)	42 (5.28)	31 (3.11)	
Medicine treatment, n (%)				
Aspirin	1,735 (96.77)	764 (96.10)	971 (97.29)	0.1557
P_2Y_{12} receptor inhibitor	1,749 (97.55)	774 (97.36)	975 (97.70)	0.6469
Statin	1,737 (96.88)	771 (96.98)	966 (96.79)	0.8206

**Early ISR refers to a duration less than 1 year, and late ISR refers to a duration greater than 1 year; angulated lesion is defined as a lesion with an angle greater than or equal to 45° between the proximal and distal segments; patients were grouped in tertiles according to big ET-1: first (big ET-1 < 0.20 pmol/L), second (0.20 pmol/L ≤ big ET-1 < 0.31 pmol/L), and third (big ET-1 ≥ 0.31 pmol/L).*

LVEF, left ventricular ejection fraction; LVDD, left ventricular diastolic diameter; TnI, troponin I; TG, triglycerides; TC, total cholesterol; HDL-c, high-density lipoprotein cholesterol; LDL-c, low-density lipoprotein cholesterol.

TABLE 2 | Follow-up of patients with coronary artery restenosis.

	Total (*n* = 1,793)	Diabetic patients (*n* = 795)	Non-diabetic patients (*n* = 998)	*P*-value
Time of follow-up (years, $\bar{x} \pm s$)	2.96 ± 0.56	2.96 ± 0.56	2.95 ± 0.55	0.7608
MACE, n (%)	137 (7.64)	54 (6.79)	83 (8.32)	0.2275
Cardiac death, n (%)	26 (1.45)	6 (0.75)	20 (2.00)	0.0279
Non-fatal MI, n (%)	12 (0.67)	4 (0.50)	8 (0.80)	0.4413
TLR, n (%)	85 (4.74)	33 (4.15)	52 (5.21)	0.2943
Stroke, n (%)	18 (1.00)	13 (1.64)	5 (0.50)	0.0167
Secondary endpoints, n (%)	141 (7.86)	53 (6.67)	88 (8.82)	0.0928
All-cause death, n (%)	42 (2.34)	15 (1.89)	27 (2.71)	0.2549
TVR, n (%)	82 (4.57)	32 (4.03)	50 (5.01)	0.3213
ST*, n (%)	7 (0.39)	1 (0.13)	6 (0.60)	0.1411
Hemorrhage, n (%)	21 (1.17)	8 (1.01)	13 (1.30)	0.5623

**All presented with probable stent thrombosis.*

third tertiles had HRs of 1.24 (0.51–3.05) and 2.60 (1.16–5.81) for MACE and 0.97 (0.40–2.37) and 2.00 (0.91–4.41) for secondary end point outcomes, respectively, after multivariable adjustment (see **Table 4** and **Figure 3**). The HRs (with their 95% CIs) of all covariates in the model are shown in **Supplementary Table 6**. The results of the subgroup analysis are shown in **Supplementary Figures 1, 2**.

Big ET-1 was not significantly associated with the risk of MACEs or secondary end point events in patients without diabetes, whether in univariate or multivariate

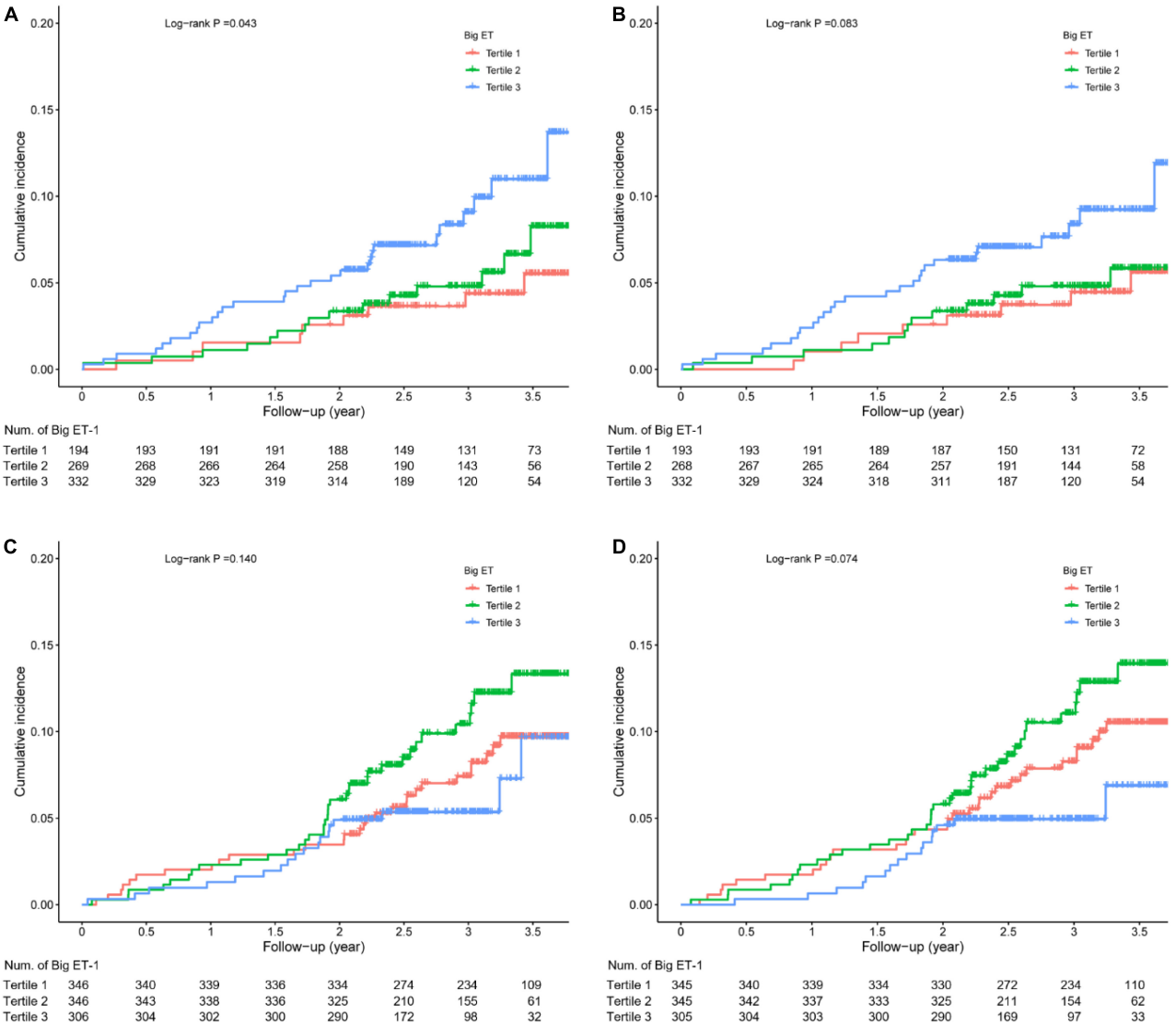

FIGURE 2 | Kaplan-Meier survival analysis. **(A)** Major adverse cardiovascular events (MACE) in diabetic patients; **(B)** secondary end points in diabetic patients; **(C)** MACE in non-diabetic patients; and **(D)** secondary end points in non-diabetic patients.

analysis (all $p > 0.05$; see **Table 5** and **Figure 3**). All results of the multivariate Cox analysis are shown in **Supplementary Table 7**.

Dose-Response Relationship Between big ET-1 and Cardiovascular Prognosis

The restricted cubic spline analysis after adjustment for traditional and angiographic risk factors showed that the relationships between big ET-1 and MACE and secondary end point events were both linear in the diabetic group. The risk of MACEs and secondary end point events was increased with increasing big ET-1, and the trend was statistically significant ($p = 0.005$ and 0.011, respectively), while the test for a non-linear relationship was not statistically significant ($p = 0.106$ and 0.517, respectively; **Figure 4**).

Incremental Predictive Value of Big ET-1 for an Adverse Prognosis

Big ET-1 alone showed a similar predictive value for MACEs as a model incorporating traditional risk factors, with respective C-statistics of 0.60 (0.52–0.68) and 0.60 (0.53–0.68) (p for difference = 0.54). Adding big ET-1 to the model with traditional risk factors, a moderate but statistically significant increase in the C-statistic was observed (0.64 (0.56–0.72) vs. 0.60 (0.53–0.68), $\triangle$C-statistic = 0.03, p for difference = 0.03). Similarly, big ET-1 showed additional predictive value for the secondary end point events when added to traditional risk factors [0.67 (0.59–0.75) vs. 0.63 (0.56–0.71), $\triangle$C-statistic = 0.03, p for difference = 0.02]. However, adding big ET-1 to the model with traditional and angiographic risk factors yielded no significant increase in the C-statistic (**Table 6**).

TABLE 3 | Interaction between big endothelin-1 and diabetes in the prognosis of MACEs and secondary end points.

	Wald chi-square value*	*P*-value*	Wald chi-square value**	*P*-value**
MACE				
Big ET-1	3.58	0.058	4.56	0.103
Diabetes	8.46	0.004	1.95	0.163
Big ET-1 × Diabetes	13.07	<0.0001	9.61	0.008
Age	3.53	0.06	3.61	0.057
Sex	5.35	0.021	4.87	0.027
BNP	5.28	0.022	6.76	0.009
Diameter stenosis rate	1.83	0.177	1.63	0.201
Thyroid disease	4.53	0.033	4.36	0.037
Secondary endpoints				
Big ET-1	2.93	0.087	4.86	0.088
Diabetes	6.23	0.013	1.4	0.236
Big ET-1 × Diabetes	12.55	<0.0001	8.82	0.012
Age	1.07	0.302	1.16	0.282
Sex	3.1	0.078	2.85	0.092
BNP	5.71	0.017	7.48	0.006
Diameter stenosis rate	6.12	0.013	5.78	0.016

**Big endothelin-1 (ET-1) as a continuous variable. **Big ET-1 as a categorical variable, age, sex, and variables found as independent predictors in the overall population were adjusted. Big ET-1 and B-type natriuretic peptide (BNP) were natural log-transformed.*

TABLE 4 | Cox proportional hazards models for prognosis in diabetic patients.

	Univariate		Multivariate	
	HR (95% CI)	*P*-value	HR (95% CI)	*P*-value
MACE				
Big ET-1*	1.85 (1.26–2.72)	0.002	2.05 (1.36–3.09)	0.001
Big ET-1 tertile 1	Reference	–	Reference	–
Big ET-1 tertile 2	1.35 (0.59–3.09)	0.477	1.24 (0.51–3.05)	0.634
Big ET-1 tertile 3	2.32 (1.09–4.92)	0.029	2.60 (1.16–5.81)	0.02
Secondary endpoints				
Big ET-1*	1.77 (1.19–2.63)	0.005	1.98 (1.29–3.03)	0.002
Big ET-1 tertile 1	Reference	–	Reference	–
Big ET-1 tertile 2	1.06 (0.46–2.43)	0.893	0.97 (0.40–2.37)	0.948
Big ET-1 tertile 3	1.93 (0.93–4.04)	0.079	2.00 (0.91–4.41)	0.084

**Big endothelin-1 (ET-1) was natural log-transformed. Major adverse cardiovascular events (MACE) model adjusted for age, sex, angulated lesion, history of coronary artery bypass grafting [CABG], low-density lipoprotein cholesterol [LDL-c], reference vessel diameter, thyroid disease. Secondary end points model adjusted for age, sex, angulated lesion, history of CABG, early ISR, and non-ISR lesion intervention.*

DISCUSSION

This study analyzed the predictive value of big ET-1 for the occurrence of adverse cardiovascular events in a cohort of patients with ISR and diabetes mellitus after PCI. The main findings are as follows: (1) patients with ISR and diabetes have higher levels of big ET-1 than non-diabetic patients. (2) Patients with ISR and diabetes who have higher big ET-1 levels have a higher incidence of MACEs than patients with ISR and diabetes with lower levels of big ET-1. (3) Increased plasma big ET-1 level is correlated with a worse prognosis of patients with ISR and diabetes, it has good predictive value even after adjusting for traditional and angiographic risk factors. (4) The level of big ET-1 is linearly correlated with the occurrence of MACEs in patients with ISR and diabetes. (5) The addition of big ET-1 to the traditional cardiovascular risk prediction model significantly improves the ability to stratify prognostic risk for patients with ISR and diabetes.

Although diabetic patients often have other risk factors at the same time, diabetes itself is a powerful independent risk factor for cardiovascular events. Increased blood glucose levels, insulin resistance, hyperlipidemia, inflammation, and thrombosis accelerate the formation of atherosclerosis, leading diabetic patients to become a high-risk group for ISR (1–3, 8, 18).

The level of big ET-1 is closely related to cardiovascular events and is used as a risk predictor of cardiovascular disease (19). The role of big ET-1 in hypertension, diabetes, and myocardial hypertrophy is manifested in poor cardiovascular remodeling, which is caused by an increase in left ventricular mass (20–22). Big ET-1 also helps to predict the risk of congestive heart failure and death in the general population (23, 24). It has predictive value in patients with chronic heart failure (25), and its predictive value is not inferior to those of hemodynamic monitoring indicators (26). In patients with arrhythmia and cardiomyopathy, high big ET-1 level has a certain predictive value for death, malignant arrhythmia, heart transplantation, and other adverse events (27–30).

Big ET-1 has good predictive value for the prognosis of patients with CAD. Zhang et al. observed 6,150 patients with three-vessel CAD and found that a high big ET-1 level is an independent risk factor for long-term mortality, indicating that it has good predictive value in patients with severe CAD (14). Zhou et al. followed up 3,154 patients with stable CAD and 565 patients with AMI who were younger than 35 years old and found that the occurrence of vascular events was closely correlated with the big ET-1 level (13, 15). Yip et al. established a prospective cohort of 186 cases of ST-segment elevation myocardial infarction (STEMI). Big ET-1 was a strong predictor of the independent composite end point of severe deterioration of cardiac function and death within 30 days after emergency PCI (31). Gao et al. in 822 patients with STEMI combined with diabetes, found that the level of big ET-1 had a strong correlation with no reflow after emergency PCI and with the long-term prognosis, indicating that it has a strong predictive value in patients with CAD and diabetes (16). However, there has been no previous research on the relationship between big ET-1 and the prognosis of patients with ISR.

Our study is the first to discover the important predictive value of big ET-1 level for the cardiovascular prognosis, beyond traditional and angiographic risk factors, in patients with ISR and diabetes, though this is in line with the results of previous studies; i.e., high big ET-1 levels predict a poor outcome. The mechanism of action of big ET-1 in the prognosis of patients with ISR and diabetes is still inconclusive, but it may be related to the following factors: (1) overexpression of big ET-1 aggravates

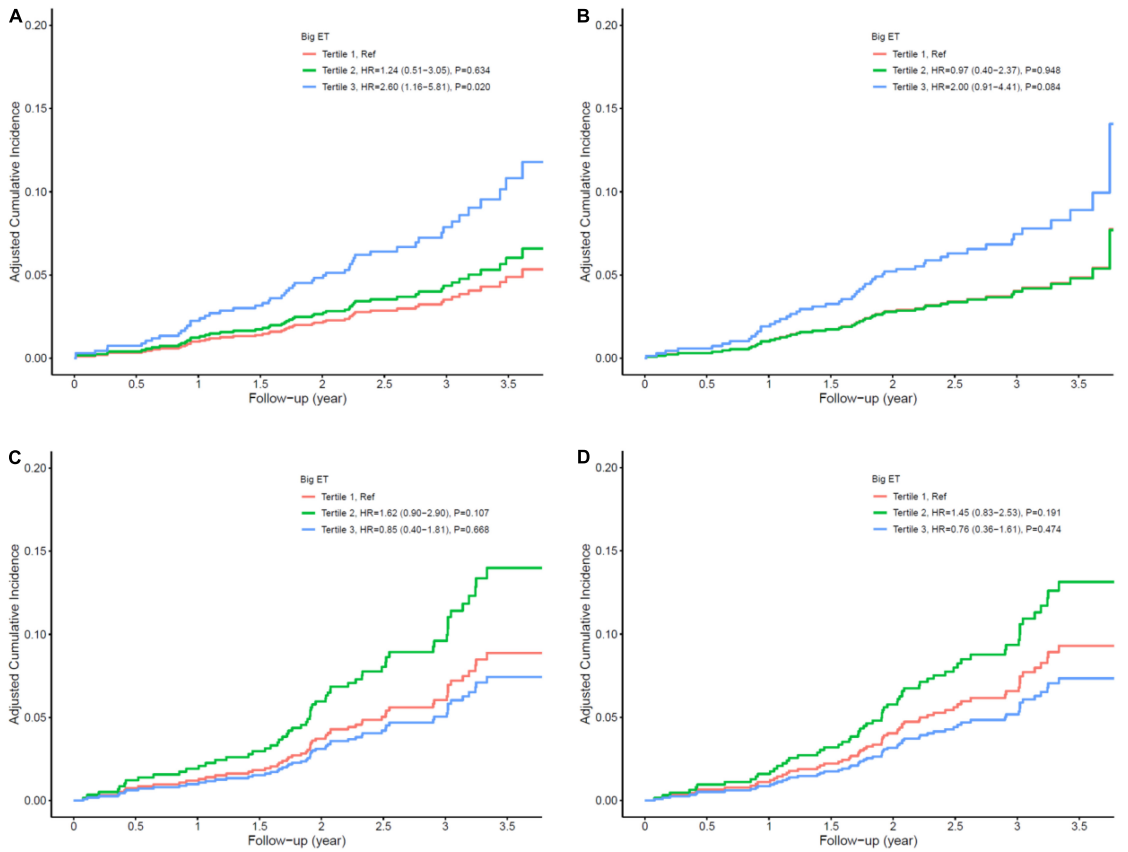

FIGURE 3 | Cox multivariate survival analysis. **(A)** Major adverse cardiovascular events (MACE) in diabetic patients; **(B)** secondary end points in diabetic patients; **(C)** MACE in non-diabetic patients; **(D)** secondary end points in non-diabetic patients.

diabetes-induced vascular endothelial dysfunction by inducing oxidative stress (32), which clinically can manifest as hyperplasia of the neointima or neovascular atherosclerosis in the stent (33).

TABLE 5 | Cox proportional hazards models for prognosis in non-diabetic patients.

	Univariate		Multivariate	
	HR (95% CI)	***P*-value**	**HR (95% CI)**	***P*-value**
MACE				
Big ET-1*	0.84 (0.55–1.28)	0.415	0.82 (0.50–1.33)	0.418
Big ET-1 tertile 1	Reference	–	Reference	–
Big ET-1 tertile 2	1.42 (0.87–2.32)	0.16	1.62 (0.90–2.90)	0.107
Big ET-1 tertile 3	0.85 (0.47–1.53)	0.581	0.85 (0.40–1.81)	0.668
Secondary endpoints				
Big ET-1*	0.74 (0.49–1.13)	0.162	0.82 (0.50–1.33)	0.417
Big ET-1 tertile 1	Reference	–	Reference	–
Big ET-1 tertile 2	1.31 (0.81–2.11)	0.266	1.45 (0.83–2.53)	0.191
Big ET-1 tertile 3	0.67 (0.37–1.23)	0.195	0.76 (0.36–1.61)	0.474

**Big endothelin-1 (ET-1) was natural log-transformed. Major adverse cardiovascular events (MACE) model adjusted for age, sex, left ventricular ejection fraction (LVEF), in-stent restenosis (ISR) duration, hypertension, drug-eluting stent (DES) intervention, total cholesterol (TC), and diameter stenosis rate. Secondary end points model adjusted for age, sex, high-density lipoprotein cholesterol (HDL-c), TC, reference vessel diameter, target lesion length, and diameter stenosis rate.*

(2) Big ET-1 can promote the synthesis of inflammatory microglia in diabetic patients (34) and downregulate inflammatory activity to accelerate the progression of atherosclerosis (35). (3) Big ET-1 mediates the increase in nitric oxide production and the uncoupling of calcium signaling to aggravate the contraction of small blood vessels in diabetic patients (36–38), thereby causing angina pectoris due to coronary microcirculation disorder. (4) Big ET-1 alone or together with other agonists can cause platelet activation, and activated platelets can also stimulate endothelial cells to release big ET-1 (39), which leads to the formation of ST. (5) A long-term increase in big ET-1 can cause cerebrovascular accidents in patients with pre-arteriosclerosis (40), and serious cerebrovascular accidents can cause death. These proposed mechanisms are based on reasoning from population characteristics, so the specific pathophysiological mechanisms need to be empirically clarified.

In terms of clinical application value, our findings come from real-world patients with ISR and diabetes. Our study found that traditional and angiographic risk factors, such as an angulated lesion, history of CABG, LDL-C, reference vessel diameter, thyroid disease, early ISR, and non-ISR lesion intervention, had predictive value for adverse cardiovascular events in patients with ISR and diabetes. Moreover, after adjusting for the traditional and angiographic risk factors, big

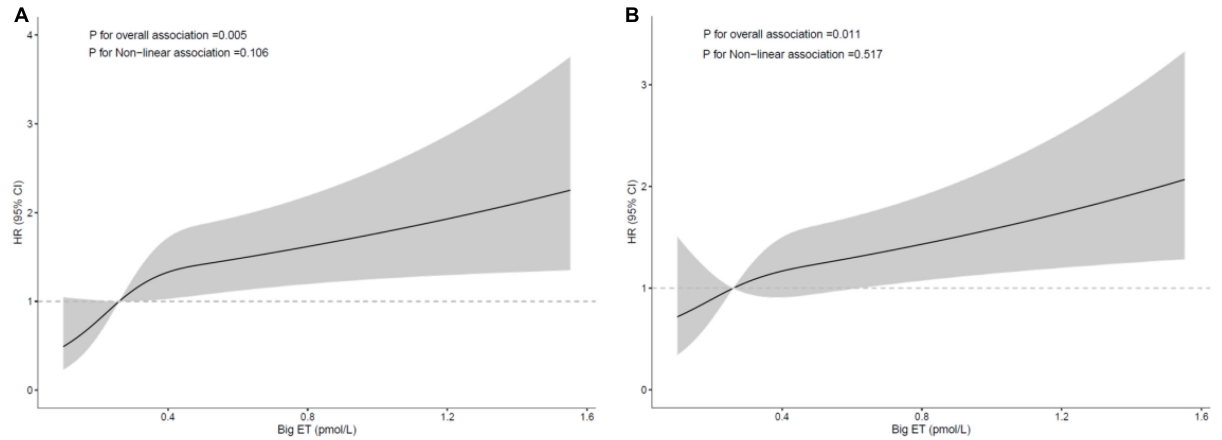

FIGURE 4 | Restricted cubic spline curve for the risk in diabetic patients according to big ET-1; **(A)** major adverse cardiovascular events [MACE; adjusted for age, sex, left ventricular ejection fraction (LVEF), in-stent restenosis (ISR) duration, hypertension, drug-eluting stent (DES) intervention, total cholesterol (TC), and diameter stenosis rate]; **(B)** secondary end points [adjusted for age, sex, high-density lipoprotein cholesterol (HDL-c), TC, reference vessel diameter, target lesion length, and diameter stenosis rate].

TABLE 6 | C-statistics of traditional risk factors and big ET-1 in patients with diabetes.

	MACE			Secondary end points		
	C-statistic (95% CI)	**ΔC-statistic**	***P*-value**	**C-statistic (95% CI)**	**ΔC-statistic**	***P*-value**
Model 1*	0.60 (0.53–0.68)	Reference	–	0.63 (0.56–0.71)	Reference	–
Model 2*	0.64 (0.56–0.72)	0.033	0.03	0.67 (0.59–0.75)	0.035	0.02
Model 3*	0.68 (0.60–0.75)	Reference	–	0.66 (0.57–0.74)	Reference	–
Model 4*	0.68 (0.60–0.76)	0.005	0.32	0.66 (0.57–0.74)	0.002	0.46

**Model 1: traditional risk factors [age, sex, BMI, smoking, hypertension, hyperlipidemia, stroke or transient ischemic attack (TIA), and left ventricular ejection fraction (LVEF)]; Model 2: traditional risk factors + big endothelin-1 (ET-1); Model 3: traditional and angiographic risk factors [major adverse cardiovascular events (MACE) model adjusted for age, sex, LVEF, in-stent restenosis (ISR) duration, hypertension, DES intervention, total cholesterol (TC), and diameter stenosis rate]. Secondary end points [model adjusted for age, sex, high-density lipoprotein cholesterol (HDL-c), TC, reference vessel diameter, target lesion length, and diameter stenosis rate]; Model 4: traditional and angiographic risk factors + big ET-1.*

ET-1 still showed independent predictive value, and the increase in big ET-1 was linearly correlated with the increase in the incidence of adverse cardiovascular events. After adding the biomarker big ET-1 to the traditional cardiovascular risk factor model, the C-statistic increased significantly, indicating that big ET-1 can significantly improve the predictive ability of adverse cardiovascular events in diabetic patients. Although the C-statistic was not significantly improved by adding angiographic risk factors, possibly because the sample size was not large enough and the positive rate of angiographic risk factors was low, this does not negate the predictive value of big ET-1, as traditional risk factors are more accessible to clinicians than angiographic risk factors, especially in patients who cannot undergo coronary angiography. The results of our study are of great value in the risk stratification of patients and the detection of high-risk patients (those with big ET-1 $>$ 0.31 pmol/L), so they can guide the formulation of individualized medication choices and revascularization treatment plans for patients, which may improve their life expectancy.

Specific types of DES might yield a more favorable prognosis in terms of target-lesion failure in diabetic patients. The SUGER study showed that Cre8 EVO stents might be superior to Resolute Onyx stents in reducing target lesion failure (41). Drug-coated balloon (DCB) implantation for *de novo* lesions in diabetic patients has demonstrated a lower incidence of TVR than DES implantation (42, 43), which means DCBs are more advantageous in diabetic patients.

This study has some limitations: (1) this was a single-center, observational clinical study, so the external validity of the results is limited. Since the study primarily included Chinese patients, the results and conclusions only apply to Asians and need to be confirmed in other populations in prospective multicenter studies. (2) There was little information on the specific causes of death for the end point events, and the deaths whose causes could not be determined were not all cardiovascular deaths. Prognostic events were adjudicated by physicians but not the clinical events committee (CEC). As the CEC provides a more standardized and independent outcome assessment (44), prognostic events should be adjudicated by the CEC in future study designs. (3) Most studies on big ET-1 and cardiovascular prognosis, such as this study, have been in Chinese patients. Due to the differences in metabolic levels between different races, future studies should be done in multiple centers treating different races. (4) The prognostic analysis of this study was based on the detection of big

ET-1 in a single plasma sample. It might be better to take multiple samples and use their average.

CONCLUSION

Increased plasma big ET-1 was associated with a higher risk of adverse cardiovascular prognosis independent of traditional and angiographic risk factors, and therefore it might be used as a prognostic/predictive biomarker in patients with ISR and diabetes.

DATA AVAILABILITY STATEMENT

The raw data supporting the conclusions of this article will be made available by the authors, without undue reservation.

ETHICS STATEMENT

The studies involving human participants were reviewed and approved by the Clinical Research Ethics Committee of Chinese Academy of Medical Sciences Fuwai Hospital. The patients/participants provided their written informed consent to participate in this study. Written informed consent was obtained from the individual(s) for the publication of any potentially identifiable images or data included in this article.

AUTHOR CONTRIBUTIONS

YM made substantial contributions to study design, data collection, data analysis, and manuscript writing. JY, LS, WY, and SQ made substantial contributions to study design and intellectual direction. TT, TW, JW, and HG made contributions to data collection and analysis. All authors read and approved the final manuscript.

FUNDING

This work was supported by the grant from the National Key Research and Development Program of China (2018YFB1107102).

SUPPLEMENTARY MATERIAL

The Supplementary Material for this article can be found online at: https://www.frontiersin.org/articles/10.3389/fcvm.2022.854107/full#supplementary-material

REFERENCES

1. Cosentino F, Grant PJ, Aboyans V, Bailey CJ, Ceriello A, Delgado V, et al. 2019 ESC guidelines on diabetes, pre-diabetes, and cardiovascular diseases developed in collaboration with the EASD. *Eur Heart J.* (2020) 41:255–323.
2. Glovaci D, Fan W, Wong ND. Epidemiology of diabetes mellitus and cardiovascular disease. *Curr Cardiol Rep.* (2019) 21:21.
3. Dal Canto E, Ceriello A, Ryden L, Ferrini M, Hansen TB, Schnell O, et al. Diabetes as a cardiovascular risk factor: an overview of global trends of macro and micro vascular complications. *Eur J Prev Cardiol.* (2019) 26:25–32. doi: 10.1177/2047487319878371
4. Guariguata L, Whiting DR, Hambleton I, Beagley J, Linnenkamp U, Shaw JE. Global estimates of diabetes prevalence for 2013 and projections for 2035. *Diabetes Res Clin Pract.* (2014) 103:137–49. doi: 10.1016/j.diabres.2013.11.002
5. Mehran R, Dangas G, Abizaid AS, Mintz GS, Lansky AJ, Satler LF, et al. Angiographic patterns of in-stent restenosis: classification and implications for long-term outcome. *Circulation.* (1999) 100:1872–8. doi: 10.1161/01.cir.100.18.1872
6. Bonaa KH, Mannsverk J, Wiseth R, Aaberge L, Myreng Y, Nygard O, et al. Drug-eluting or bare-metal stents for coronary artery disease. *N Engl J Med.* (2016) 375:1242–52.
7. Zhu Y, Liu K, Chen M, Liu Y, Gao A, Hu C, et al. Triglyceride-glucose index is associated with in-stent restenosis in patients with acute coronary syndrome after percutaneous coronary intervention with drug-eluting stents. *Cardiovasc Diabetol.* (2021) 20:137. doi: 10.1186/s12933-021-01332-4
8. Scheen AJ, Warzee F, Legrand VM. Drug-eluting stents: meta-analysis in diabetic patients. *Eur Heart J.* (2004) 25:2167–8.
9. Paramasivam G, Devasia T, Jayaram A, UK AR, Rao MS, Vijayvergiya R, et al. In-stent restenosis of drug-eluting stents in patients with diabetes mellitus: clinical presentation, angiographic features, and outcomes. *Anatol J Cardiol.* (2020) 23:28–34. doi: 10.14744/AnatolJCardiol.2019.72916
10. Davenport AP, Hyndman KA, Dhaun N, Southan C, Kohan DE, Pollock JS, et al. Endothelin. *Pharmacol Rev.* (2016) 68:357–418.
11. Pernow J, Shemyakin A, Bohm F. New perspectives on endothelin-1 in atherosclerosis and diabetes mellitus. *Life Sci.* (2012) 91:507–16. doi: 10.1016/j.lfs.2012.03.029
12. Papassotiriou J, Morgenthaler NG, Struck J, Alonso C, Bergmann A. Immunoluminometric assay for measurement of the C-terminal endothelin-1 precursor fragment in human plasma. *Clin Chem.* (2006) 52:1144–51. doi: 10.1373/clinchem.2005.065581
13. Zhou BY, Gao XY, Zhao X, Qing P, Zhu CG, Wu NQ, et al. Predictive value of big endothelin-1 on outcomes in patients with myocardial infarction younger than 35 years old. *Per Med.* (2018) 15:25–33. doi: 10.2217/pme-2017-0044
14. Zhang C, Tian J, Jiang L, Xu L, Liu J, Zhao X, et al. Prognostic value of plasma big endothelin-1 level among patients with three-vessel disease: a cohort study. *J Atheroscler Thromb.* (2019) 26:959–69. doi: 10.5551/jat.47324
15. Zhou BY, Guo YL, Wu NQ, Zhu CG, Gao Y, Qing P, et al. Plasma big endothelin-1 levels at admission and future cardiovascular outcomes: a cohort study in patients with stable coronary artery disease. *Int J Cardiol.* (2017) 230:76–9. doi: 10.1016/j.ijcard.2016.12.082
16. Gao R, Wang J, Zhang S, Yang G, Gao Z, Chen X. The value of combining plasma D-dimer and endothelin-1 levels to predict no-reflow after percutaneous coronary intervention of ST-segment elevation in acute myocardial infarction patients with a type 2 diabetes mellitus history. *Med Sci Monit.* (2018) 24:3549–56. doi: 10.12659/MSM.908980
17. American Diabetes Association [ADA]. Diagnosis and classification of diabetes mellitus. *Diabetes Care.* (2014) 37:S81–90.
18. Flaherty JD, Davidson CJ. Diabetes and coronary revascularization. *JAMA.* (2005) 293:1501–8.
19. Jankowich M, Choudhary G. Endothelin-1 levels and cardiovascular events. *Trends Cardiovasc Med.* (2020) 30:1–8.
20. Peng T, Li X, Hu Z, Yang X, Ma C. Predictive role of endothelin in left ventricular remodeling of chronic kidney disease. *Ren Fail.* (2018) 40:183–6. doi: 10.1080/0886022X.2018.1455586
21. Valero-Munoz M, Li S, Wilson RM, Boldbaatar B, Iglarz M, Sam F. Dual Endothelin-A/Endothelin-B receptor blockade and cardiac remodeling in heart failure with preserved ejection fraction. *Circ Heart Fail.* (2016) 9:e003381. doi: 10.1161/CIRCHEARTFAILURE.116.003381
22. Lindman BR, Davila-Roman VG, Mann DL, McNulty S, Semigran MJ, Lewis GD, et al. Cardiovascular phenotype in HFpEF patients with or without diabetes: a RELAX trial ancillary study. *J Am Coll Cardiol.* (2014) 64:541–9. doi: 10.1016/j.jacc.2014.05.030

23. Yokoi K, Adachi H, Hirai Y, Enomoto M, Fukami A, Ogata K, et al. Plasma endothelin-1 level is a predictor of 10-year mortality in a general population: the Tanushimaru study. *Circ J.* (2012) 76:2779–84. doi: 10.1253/circj.cj-12-0469
24. Jankowich MD, Wu WC, Choudhary G. Association of elevated plasma endothelin-1 levels with pulmonary hypertension, mortality, and heart failure in African American individuals: the Jackson heart study. *JAMA Cardiol.* (2016) 1:461–9. doi: 10.1001/jamacardio.2016.0962
25. Pousset F, Isnard R, Lechat P, Kalotka H, Carayon A, Maistre G, et al. Prognostic value of plasma endothelin-1 in patients with chronic heart failure. *Eur Heart J.* (1997) 18:254–8.
26. Pacher R, Stanek B, Hulsmann M, Koller-Strametz J, Berger R, Schuller M, et al. Prognostic impact of big endothelin-1 plasma concentrations compared with invasive hemodynamic evaluation in severe heart failure. *J Am Coll Cardiol.* (1996) 27:633–41. doi: 10.1016/0735-1097(95)00520-x
27. Fan P, Zhang Y, Lu YT, Yang KQ, Lu PP, Zhang QY, et al. Prognostic value of plasma big endothelin-1 in left ventricular non-compaction cardiomyopathy. *Heart.* (2021) 107:836–41. doi: 10.1136/heartjnl-2020-317059
28. Wang Y, Tang Y, Zou Y, Wang D, Zhu L, Tian T, et al. Plasma level of big endothelin-1 predicts the prognosis in patients with hypertrophic cardiomyopathy. *Int J Cardiol.* (2017) 243:283–9. doi: 10.1016/j.ijcard.2017.03.162
29. Wu S, Yang YM, Zhu J, Ren JM, Wang J, Zhang H, et al. The association between plasma big endothelin-1 levels at admission and long-term outcomes in patients with atrial fibrillation. *Atherosclerosis.* (2018) 272:1–7. doi: 10.1016/j.atherosclerosis.2018.02.034
30. Cinar T, Hayiroglu M, Cicek V, Orhan AL. A new marker for ventricular tachyarrhythmias in patients with postinfarction left ventricular aneurysm: big endothelin-1. *Anatol J Cardiol.* (2020) 23:193–4. doi: 10.14744/AnatolJCardiol.2020.46595
31. Yip HK, Wu CJ, Chang HW, Yang CH, Yu TH, Chen YH, et al. Prognostic value of circulating levels of endothelin-1 in patients after acute myocardial infarction undergoing primary coronary angioplasty. *Chest.* (2005) 127:1491–7. doi: 10.1378/chest.127.5.1491
32. Idris-Khodja N, Ouerd S, Mian MOR, Gornitsky J, Barhoumi T, Paradis P, et al. Endothelin-1 overexpression exaggerates diabetes-induced endothelial dysfunction by altering oxidative stress. *Am J Hypertens.* (2016) 29:1245–51. doi: 10.1093/ajh/hpw078
33. Nakazawa G, Otsuka F, Nakano M, Vorpahl M, Yazdani SK, Ladich E, et al. The pathology of neoatherosclerosis in human coronary implants bare-metal and drug-eluting stents. *J Am Coll Cardiol.* (2011) 57:1314–22. doi: 10.1016/j.jacc.2011.01.011
34. Abdul Y, Jamil S, He L, Li W, Ergul A. Endothelin-1 (ET-1) promotes a proinflammatory microglia phenotype in diabetic conditions. *Can J Physiol Pharmacol.* (2020) 98:596–603. doi: 10.1139/cjpp-2019-0679
35. Wolf D, Ley K. Immunity and inflammation in atherosclerosis. *Circ Res.* (2019) 124:315–27.
36. Ergul A. Endothelin-1 and diabetic complications: focus on the vasculature. *Pharmacol Res.* (2011) 63:477–82. doi: 10.1016/j.phrs.2011.01.012
37. Abdelhalim MA. Effects of big endothelin-1 in comparison with endothelin-1 on the microvascular blood flow velocity and diameter of rat mesentery in vivo. *Microvasc Res.* (2006) 72:108–12. doi: 10.1016/j.mvr.2006.04.007
38. Kalani M. The importance of endothelin-1 for microvascular dysfunction in diabetes. *Vasc Health Risk Manag.* (2008) 4:1061–8. doi: 10.2147/vhrm.s3920
39. Jagroop IA, Daskalopoulou SS, Mikhailidis DP. Endothelin-1 and human platelets. *Curr Vasc Pharmacol.* (2005) 3:393–9.
40. Novo G, Sansone A, Rizzo M, Guarneri FP, Pernice C, Novo S. High plasma levels of endothelin-1 enhance the predictive value of preclinical atherosclerosis for future cerebrovascular and cardiovascular events: a 20-year prospective study. *J Cardiovasc Med (Hagerstown).* (2014) 15:696–701. doi: 10.2459/JCM.0000000000000121
41. Romaguera R, Salinas P, Gomez-Lara J, Brugaletta S, Gomez-Menchero A, Romero MA, et al. Amphilimus- versus zotarolimus-eluting stents in patients with diabetes mellitus and coronary artery disease (SUGAR trial). *Eur Heart J.* (2021). [Epub ahead of print]. doi: 10.1093/eurheartj/ehab790
42. Wohrle J, Scheller B, Seeger J, Farah A, Ohlow MA, Mangner N, et al. Impact of diabetes on outcome with drug-coated balloons versus drug-eluting stents: the BASKET-SMALL 2 trial. *JACC Cardiovasc Interv.* (2021) 14:1789–98. doi: 10.1016/j.jcin.2021.06.025
43. Jeger RV, Eccleshall S, Wan Ahmad WA, Ge J, Poerner TC, Shin ES, et al. Drug-coated balloons for coronary artery disease: third report of the international DCB consensus group. *JACC Cardiovasc Interv.* (2020) 13:1391–402. doi: 10.1016/j.jcin.2020.02.043
44. Leonardi S, Branca M, Franzone A, McFadden E, Piccolo R, Juni P, et al. Comparison of investigator-reported and clinical event committee-adjudicated outcome events in GLASSY. *Circ Cardiovasc Qual Outcomes.* (2021) 14:e006581. doi: 10.1161/CIRCOUTCOMES.120.006581

Conflict of Interest: The authors declare that the research was conducted in the absence of any commercial or financial relationships that could be construed as a potential conflict of interest.

frontiers | Frontiers in Cardiovascular Medicine

ORIGINAL RESEARCH
published: 15 June 2022
doi: 10.3389/fcvm.2022.901941

Robust Association Between Changes in Coronary Flow Capacity Following Percutaneous Coronary Intervention and Vessel-Oriented Outcomes and the Implication for Clinical Practice

Rikuta Hamaya[1,2], Taishi Yonetsu[3], Kodai Sayama[4], Kazuki Matsuda[4], Hiroki Ueno[4], Tatsuhiro Nagamine[4], Toru Misawa[4], Masahiro Hada[3], Masahiro Hoshino[4], Tomoyo Sugiyama[4], Tetsuo Sasano[3] and Tsunekazu Kakuta[4]**

[1] Division of Preventive Medicine, Department of Medicine, Brigham and Women's Hospital and Harvard Medical School, Boston, MA, United States, [2] Department of Epidemiology, Harvard T.H. Chan School of Public Health, Boston, MA, United States, [3] Department of Cardiology, Tokyo Medical and Dental University, Tokyo, Japan, [4] Department of Cardiology, Tsuchiura Kyodo General Hospital, Tsuchiura, Japan

Background: Coronary flow capacity (CFC) is a potentially important physiologic marker of ischemia for guiding percutaneous coronary intervention (PCI) indication, while the changes through PCI have not been investigated.

Objectives: To assess the determinants and prognostic implication of delta CFC, defined as the change in the CFC status following PCI.

Materials and Methods: From a single-center registry, a total of 450 patients with chronic coronary syndrome (CCS) who underwent fractional flow reserve (FFR)-guided PCI with pre-/post-PCI invasive coronary physiological assessments were included. Associations between PCI-related changes in thermodilution method-derived CFC categories and incident target vessel failure (TVF) were assessed.

Results: The mean (*SD*) age was 67.1 (10.0) years and there were 75 (16.7%) women. Compared with patients showing no change in CFC categories after PCI, patients with category worsened, +1, +2, and +3 category improved had the hazard ratio (95% *CI*) for incident TVF of 2.27 (0.95, 5.43), 0.85 (0.33, 2.22), 0.45 (0.12, 1.63), and 0.14 (0.016, 1.30), respectively (*p* for linear trends = 0.0051). After adjustment for confounders, one additional change in CFC status was associated with 0.61 (0.45, 0.83) times the hazard of TVF. CFC changes were largely predicted by the pre-PCI CFC status.

Conclusion: Coronary flow capacity changes following PCI, which was largely determined by the pre-PCI CFC status, were associated with the lower risk of incident TVF in patients with CCS who underwent PCI. The CFC changes provide a mechanistic explanation on potential favorable effect of PCI on reducing vessel-oriented outcome in lesions with reduced CFC and low FFR.

Keywords: coronary flow capacity, coronary flow reserve, percutaneous coronary intervention, fractional flow reserve, coronary artery disease

OPEN ACCESS

Edited by:
Sara Seitun,
Radiology Unit, San Martino Polyclinic Hospital (IRCCS), Italy

Reviewed by:
Matteo Tebaldi,
Azienda Ospedaliero Universitaria – Cardiology Unit, Italy
Sergio Berti,
Toscana Gabriele Monasterio Foundation, Italy
Yuxiang Dai,
Fudan University, China
Jan Piek,
Amsterdam University Medical Center, Netherlands

****Correspondence:***
Rikuta Hamaya
rktrocky@gmail.com
Tsunekazu Kakuta
kaz@joy.email.ne.jp

Specialty section:
This article was submitted to Coronary Artery Disease, a section of the journal Frontiers in Cardiovascular Medicine

Received: *22 March 2022*
Accepted: *18 May 2022*
Published: *15 June 2022*

Citation:
Hamaya R, Yonetsu T, Sayama K, Matsuda K, Ueno H, Nagamine T, Misawa T, Hada M, Hoshino M, Sugiyama T, Sasano T and Kakuta T (2022) Robust Association Between Changes in Coronary Flow Capacity Following Percutaneous Coronary Intervention and Vessel-Oriented Outcomes and the Implication for Clinical Practice. Front. Cardiovasc. Med. 9:901941. doi: 10.3389/fcvm.2022.901941

INTRODUCTION

Globally, clinical practice is getting toward choosing a deferral of percutaneous coronary intervention (PCI) in patients with chronic coronary syndrome (CCS) given comparative effectiveness of PCI against medical therapy (1–4) with respect to patient outcomes. PCI is a costly procedure with potential adverse effects (5), and hence the patient selection for the intervention should be very strict especially intending to reduce future adverse events. On the contrary, deferring all elective PCIs in patients with CCS might be too simplistic, given evidence showing the effects of fractional flow reserve (FFR)-guided PCI on reducing spontaneous myocardial infarction or future revascularization (6, 7), and the prognostic benefit of PCI differential according to several factors (1, 2, 8). Recently, PCI is principally guided by FFR or instantaneous wave-free ratio (iFR), whereas integrating complementary characteristics for the purpose is emergingly warranted to tailor the intervention and maximize the clinical benefit.

Coronary flow capacity (CFC) is a relatively new, theoretically grounded physiological index that represents ischemia due to coronary flow limitation (9–12). Reduced CFC is a condition with low coronary flow reserve [CFR; hyperemic coronary flow (hCF) divided by resting CF] combined with slow hyperemic CF rather than fast resting CF. CFC holds interesting prognostic information where severely reduced CFC does not necessarily implicate elevated risk for future cardiovascular events if treated by PCI, whereas low CFR does regardless of PCI treatment (12, 13). Thus, reduced CFC may highlight a reversible feature of ischemic burden through revascularization, and we have previously reported the potential utility of CFC in guiding PCI to improve the overall prognostic benefit (12, 13). However, the change in CFC status following PCI, which is an important measure of assessing the impact of PCI with respect to the flow restoration and the consequent impact on clinical courses, has not been investigated.

In the present study, to fill the knowledge gap, we aimed to assess the prognostic implication of delta CFC, defined as the changes of CFC status following PCI. We also evaluated the predictability of delta CFC. We hypothesized that delta CFC would be associated with vessel-related outcomes and it would be predominantly determined by the pre-PCI CFC status.

MATERIALS AND METHODS

Population

From January 2011 to April 2019, patients with known CCS who underwent PCI with the measurements of both pre- and post-PCI comprehensive coronary physiological assessments at Tsuchiura Kyodo General Hospital were identified from the institutional database. We excluded patients with indications for revascularization of ≥2 vessels, angiographically significant left main disease, previous CABG, renal insufficiency with baseline creatinine > 2.0 mg/dl, decompensated heart failure, cardiogenic shock, acute myocardial infarction, atrial fibrillation, extremely tortuous, or calcified coronary arteries, vessels with visible collateral development or ostial stenosis, and unreliable physiological assessment including CFR < 0.5 or CFR > 7. We did not exclude on the basis of the extent of stenosis outside of the above criteria, while subtotal lesions in which invasive physiological assessment could not be conducted were not included. The institutional ethics committee approved the study protocol. All patients provided written informed consent for enrollment in the institutional database for potential future investigations. All patient data and procedural details were obtained from medical records. The study complies with the Declaration of Helsinki.

Percutaneous Coronary Intervention and Multivessel Disease

Percutaneous coronary intervention was indicated according to clinical practice guidelines at the time of the procedure with necessarily presence of ischemia evaluated by FFR, stress echocardiogram, cardiac magnetic resonance tomography, coronary computed tomography, single-photon emission computerized tomography, or the combinations, and agreement between ≥2 board-certified cardiologists. The diseased vessel was defined as main branches having ≥50% stenosis on visual assessment, and multi-vessel disease corresponded to coronary arteries with ≥2 angiographical diseased vessels.

Coronary Physiological Assessment

Coronary physiological assessment was performed using thermodilution methods by using PressureWire (Abbott Vascular, St Paul, MN, United States) before and after PCI. After intracoronary nitrate (100 or 200 μg) administration, resting and hyperemic thermodilution curves were obtained in triplicate using three injections (3–4 ml each) of room-temperature saline, and the inverse of the average basal (bTmn) and hyperemic mean transit times (hTmn) were calculated. Hyperemia was induced by intravenous infusion of adenosine 5′-triphosphate (140–160 mg/kg/min). In vessels with tandem lesions, we optimized the treatment strategy in a standard way and conducted physiological assessment as follows: place the wire at the most distal of a target vessel to assess FFR, treat lesions where greater FFR step-up was observed, assess post-PCI physiological indices, and add PCI to residual treatable lesions with apparent FFR step-up (and if so again assess post-PCI physiological indices).

Fractional flow reserve was calculated as the ratio of mean distal coronary pressure (Pd) to mean aortic pressure (Pa) during maximal hyperemia. Basal (bCF) and hyperemic coronary flow (hCF) were defined as the inverse of bTmn and hTmn, respectively (14). CFR was calculated as the ratio of hyperemic to basal coronary flow. IMR was defined as hyperemic Pd * hTmn or hyperemic Pa * hTmn * [(1.35 * ratio of mean distal-to-aortic coronary pressure)–0.32] as detailed in elsewhere (15).

Abbreviations: bCF, basal coronary flow; bTmn, basal mean transit time; CFC, coronary flow capacity; CFR, coronary flow reserve; FFR, fractional flow reserve; hCF, hyperemic coronary flow; hTmn, hyperemic mean transit time; PCI, percutaneous coronary intervention; TVF, target vessel failure.

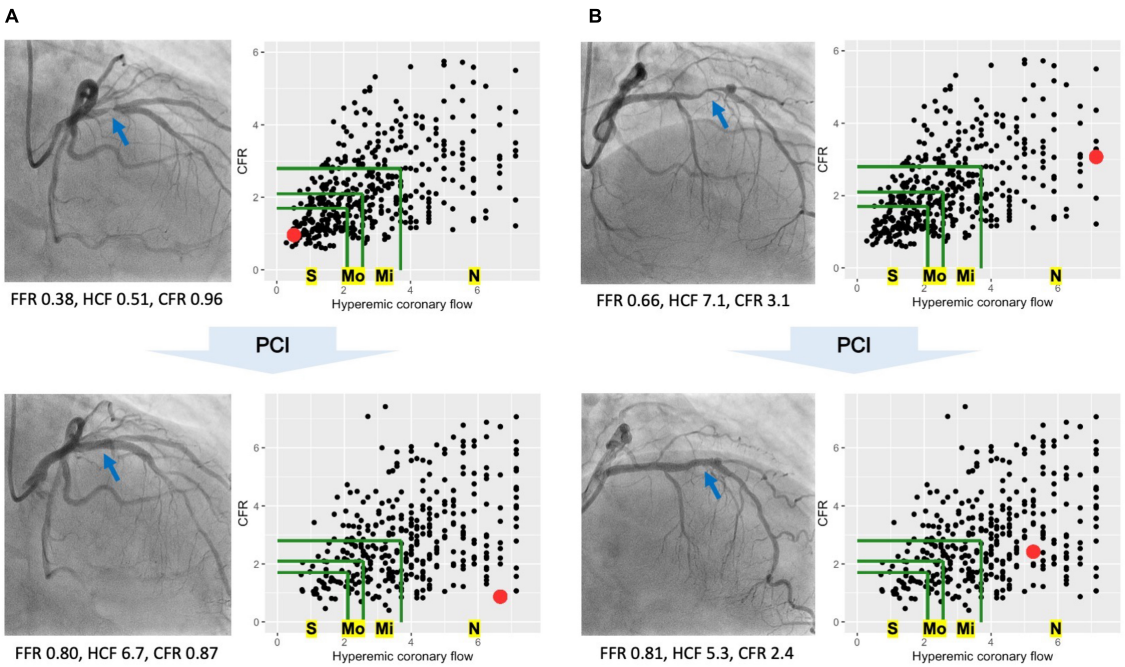

FIGURE 1 | Coronary flow capacity (CFC) changes in two representative cases. Two representative cases showing distinct CFC changes following percutaneous coronary intervention (PCI). In each cine image, blue arrows indicate the culprit lesions in the left anterior descending arteries. Each scatter plot shows CFC map, where each dot representing one vessel is mapped according to the hyperemic coronary flow (hCF, x-axis) and coronary flow reserve (CFR, y-axis). Green lines are the boundaries of CFC categories; the bounded most inner to outer areas are corresponded to severely reduced (S), moderately reduced (Mo), mildly reduced (Mi), and normal CFC (N), respectively. Red dots in the CFC maps represent the cases of each cine image. **(A)** PCI increased the hCF from 0.51 to 6.7 with a little effect on CFR, leading to the improvement in CFC categories from severely reduced to normal ones. Benefit of PCI would be expected in such cases with greater CFC improvement (i.e., lower risk of target-vessel failure). **(B)** PCI did not let changes in CFC categories; pre-PCI normal to post-PCI normal CFC. In such cases with no CFC improvement following PCI, the improvement in fractional flow reserve (FFR) might indicate the modification in the epicardial lesions but not the coronary flow restoration, potentially highlighting the limited benefit of PCI.

TABLE 1 | Baseline characteristics by pre-revascularization CFC status.

Pre-PCI CFC	Severely reduced CFC *N* = 99	Moderately reduced CFC *N* = 63	Mildly reduced CFC *N* = 96	Normal CFC *N* = 192	SMD
Age, year	69.3 (10.7)	68.9 (10.6)	68.4 (9.3)	64.9 (9.3)	0.24
Female	25 (25.3)	8 (12.7)	14 (14.6)	28 (14.6)	0.16
Smoking					0.15
Never	72 (72.7)	52 (82.5)	77 (80.2)	143 (74.5)	
Past	25 (25.3)	10 (15.9)	17 (17.7)	45 (23.4)	
Current	2 (2.0)	1 (1.6)	2 (2.1)	4 (2.1)	
Hypertension	67 (67.7)	48 (76.2)	74 (77.1)	128 (66.7)	0.15
Diabetes	44 (44.4)	29 (46.0)	34 (35.4)	74 (38.5)	0.13
Hypercholestrolemia	53 (53.5)	36 (57.1)	55 (57.3)	138 (71.9)	0.23
eGFR, mL/min/1.73 m^2	60 (24)	63 (24)	63 (22)	67 (22)	0.16
Left ventricular EF $\leq$ 50%	16 (16.2)	7 (11.1)	20 (20.8)	23 (12.0)	0.15
Multivessel disease	38 (38.4)	18 (28.6)	33 (34.4)	49 (25.5)	0.16
Vessel location					0.25
Right coronary artery	23 (23.2)	17 (27.0)	19 (19.8)	29 (15.1)	
Left anterior descending artery	67 (67.7)	34 (54.0)	65 (67.7)	138 (71.9)	
Left circumflex artery	9 (9.1)	12 (19.0)	12 (12.5)	25 (13.0)	
FFR, unit	0.61 [0.53, 0.69]	0.68 [0.60, 0.74]	0.72 [0.66, 0.75]	0.73 [0.69, 0.77]	0.78
CFR, unit	1.12 [0.96, 1.33]	1.76 [1.28, 1.90]	2.18 [1.64, 2.39]	3.12 [2.42, 3.94]	1.67
IMR, unit	41.0 [34.9, 56.1]	27.4 [23.4, 39.7]	20.9 [17.8, 29.8]	15.0 [11.0, 20.5]	0.96
Baseline coronary flow, unit	1.03 [0.74, 1.27]	1.14 [0.77, 1.70]	1.34 [0.98, 1.83]	1.28 [0.87, 2.17]	0.43
Hyperemic coronary flow, unit	1.15 [0.83, 1.49]	2.04 [1.44, 2.27]	2.78 [2.13, 3.12]	4.08 [3.03, 5.56]	1.81

Values are n (%) for categorical variables and mean (SD) or median (IQR) for continuous variables.
CFC, coronary flow capacity; CFR, coronary flow reserve; EF, ejection fraction; FFR, fractional flow reserve; IMR, index of microvascular resistance; PCI, percutaneous coronary intervention; SMD, standardized mean difference.

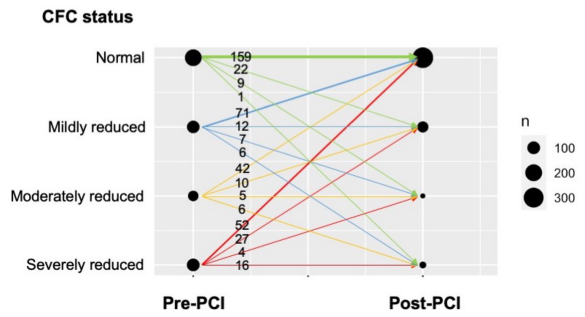

FIGURE 2 | Changes in CFC following PCI in the present cohort. The plot visualizes the number of patients with respect to pre-PCI CFC, post-PCI CFC, and the change. Numbers indicate the number of patients corresponding to the CFC changes, illustrated as the arrows. Thickness of the arrows and circles reflect the number of patients in each CFC change and each pre-/post-CFC categories, respectively. The majority of the patients improved their CFC status into normal after PCI, while the proportion was smaller in those with pre-PCI reduced CFC.

Definition of Coronary Flow Capacity

Coronary flow capacity is a concept incorporating decreased CFR and reduced hyperemic coronary flow originally proposed in PET (9). Most previous studies characterized CFC status as severely reduced, moderately reduced, mildly reduced, and normal, linking them to definite, potential, unlikely, and no ischemia, respectively (10, 12, 16, 17). We defined the CFC status in line with previously published largest study using thermodilution technique (12); normal CFC as CFR $\geq$ 2.80 with hCF $\geq$ 3.70; mildly reduced CFC as CFR $<$ 2.80 and $\geq$2.10, combined with hCF $<$ 3.70 and $\geq$2.56; moderately reduced CFC as CFR $<$ 2.10 and $\geq$1.70, and 1/Tmn $<$ 2.56 and $\leq$2.00; and severely reduced CFC otherwise (CFR $<$ 1.70 and hCF $<$ 2.00). The same criteria were applied for the pre- and post-PCI physiological assessments. **Figure 1** illustrates the changes of CFC status before/after PCI in two representative cases.

Delta Coronary Flow Capacity

We ranked CFC categories as (1) for severely reduced, (2) for moderately reduced, (3) for mildly reduced, and (4) for normal. Delta CFC was defined as a numeric difference between post-PCI CFC minus pre-PCI CFC rank, ranging from -3 to +3; for example, +3 reflects the changes from severely reduced to normal CFC following PCI.

Clinical Follow-Up

Patients were followed-up by outpatient clinic visits or by telephone contact to ascertain the occurrence of target vessel failure (TVF), defined as a composite of cardiac death, acute MI not clearly attributable to a non-target vessel (target-vessel MI; TVMI), and clinically driven revascularization of the target (PCI-treated) vessel (target-vessel revascularization; TVR). All

TABLE 2 | Characteristics by categories of CFC changes following PCI.

CFC change	Worsened *N* = 52	No change *N* = 192	+1 category improved *N* = 85	+2 category improved *N* = 69	+3 category improved *N* = 52	SMD
Age, year	67.8 (9.4)	65.9 (9.6)	67.9 (9.5)	68.7 (10.3)	67.9 (12.1)	0.11
Female	9 (17.3)	30 (15.6)	13 (15.3)	8 (11.6)	15 (28.8)	0.19
Smoking						0.16
Never	41 (78.8)	147 (76.6)	67 (78.8)	52 (75.4)	37 (71.2)	
Past	11 (21.2)	41 (21.4)	16 (18.8)	15 (21.7)	14 (26.9)	
Current	0 (0.0)	4 (2.1)	2 (2.4)	2 (2.9)	1 (1.9)	
Hypertension	34 (65.4)	136 (70.8)	62 (72.9)	47 (68.1)	38 (73.1)	0.088
Diabetes	27 (51.9)	80 (41.7)	26 (30.6)	29 (42.0)	19 (36.5)	0.20
Hypercholestrolemia	37 (71.2)	130 (67.7)	50 (58.8)	35 (50.7)	30 (57.7)	0.26
eGFR, mL/min/1.73 m^2	64 (24)	65 (23)	63 (25)	63 (23)	63 (21)	0.045
Left ventricular EF $\leq$ 50%	6 (11.5)	26 (13.5)	17 (20.0)	12 (17.4)	5 (9.6)	0.15
Multivessel disease	12 (23.1)	53 (27.6)	34 (40.0)	18 (26.1)	21 (40.4)	0.21
Vessel location						0.22
Right coronary artery	7 (13.5)	35 (18.2)	18 (21.2)	17 (24.6)	11 (21.2)	
Left anterior descending artery	42 (80.8)	130 (67.7)	56 (65.9)	41 (59.4)	35 (67.3)	
Left circumflex artery	3 (5.8)	27 (14.1)	11 (12.9)	11 (15.9)	6 (11.5)	
FFR, unit	0.72 [0.68, 0.77]	0.72 [0.69, 0.77]	0.72 [0.65, 0.75]	0.66 [0.59, 0.72]	0.56 [0.47, 0.63]	0.84
CFR, unit	2.52 [1.84, 3.17]	2.90 [1.93, 3.76]	2.12 [1.63, 2.38]	1.36 [1.09, 1.81]	1.17 [0.96, 1.37]	1.21
IMR, unit	19.1 [14.4, 26.6]	15.8 [11.2, 24.7]	21.8 [18.9, 31.5]	34.6 [25.1, 44.9]	38.3 [34.0, 51.6]	0.72
Baseline coronary flow, unit	1.27 [0.87, 2.11]	1.23 [0.87, 2.01]	1.30 [0.99, 1.69]	1.12 [0.72, 1.49]	0.99 [0.75, 1.22]	0.39
Hyperemic coronary flow, unit	2.90 [2.31, 4.09]	3.85 [2.56, 5.26]	2.70 [2.08, 3.12]	1.52 [1.12, 2.04]	1.07 [0.83, 1.50]	1.32
Pre-PCI CFC (%)						3.19
Severely reduced	33 (63.5)	159 (82.8)	0 (0.0)	0 (0.0)	0 (0.0)	
Moderately reduced	13 (25.0)	12 (6.2)	71 (83.5)	0 (0.0)	0 (0.0)	
Mildly reduced	6 (11.5)	5 (2.6)	10 (11.8)	42 (60.9)	0 (0.0)	
Normal	0 (0.0)	16 (8.3)	4 (4.7)	27 (39.1)	52 (100.0)	

Values are n (%) for categorical variables and mean (SD) or median (IQR) for continuous variables.
CFC, coronary flow capacity; CFR, coronary flow reserve; EF, ejection fraction; FFR, fractional flow reserve; IMR, index of microvascular resistance; PCI, percutaneous coronary intervention; SMD, standardized mean difference.

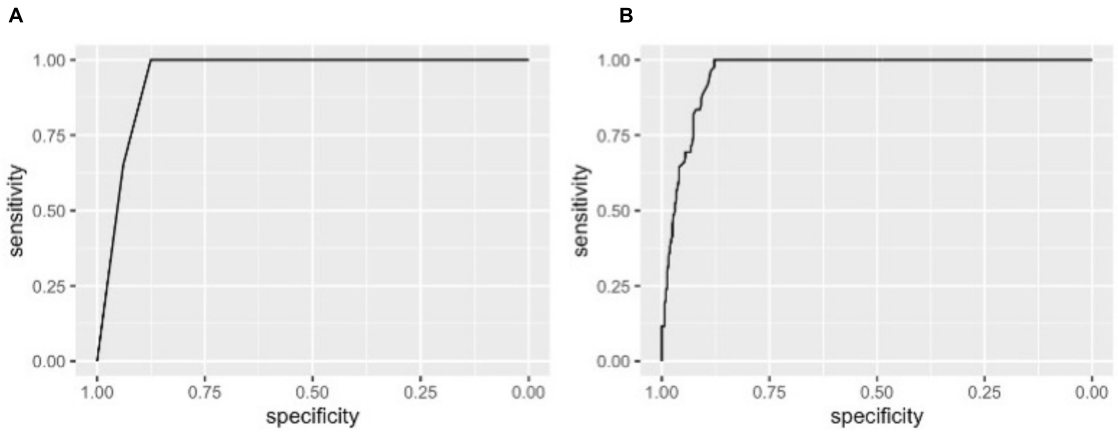

FIGURE 3 | Receiver operating characteristic (ROC) curves for improvement in CFC by ≥2 categories following PCI. The ROC curves showing the discrimination of CFC improvement by ≥2 categories by pre-PCI CFC alone **(A)** and CFC plus FFR **(B)**. Area under the curves (*AUCs*) (95% *CI*) were 0.95 (0.93, 0.97) and 0.96 (0.94, 0.98) in panels **(A,B)**, respectively. Note, at the best cutoffs, the specificity was 100% because such improvement could only be observed in patients with pre-PCI severely or moderately reduced CFC.

TABLE 3 | Prediction of CFC improvement by various pre-PCI information.

	A. CFC improvement with ≥2 categories			
	Variable	**AUC (95% CI)**	**Sensitivity**	**Specificity**
Age	Continuous	0.55 (0.49, 0.61)	0.31	0.82
Sex	Discrete	0.52 (0.48, 0.56)	0.19	0.84
Smoking	3 categories	0.52 (0.47, 0.57)	0.26	0.78
Hypertension	Discrete	0.50 (0.45, 0.55)	0.30	0.71
Diabetes	Discrete	0.50 (0.45, 0.55)	0.60	0.40
Hypercholestrolemia	Discrete	0.56 (0.51, 0.61)	0.46	0.66
eGFR	Continuous	0.49 (0.43, 0.55)	0.49	0.57
Left ventricular EF ≤ 50%	Discrete	0.50 (0.47, 0.54)	0.86	0.15
Multivessel disease	Discrete	0.51 (0.46, 0.56)	0.32	0.70
FFR	Continuous	0.77 (0.72, 0.82)	0.72	0.73
CFR	Continuous	0.87 (0.84, 0.90)	0.96	0.69
IMR	Continuous	0.83 (0.80, 0.87)	0.89	0.68
Baseline coronary flow	Continuous	0.62 (0.57, 0.68)	0.78	0.45
Hyperemic coronary flow	Continuous	0.90 (0.87, 0.93)	0.98	0.74
Pre-PCI CFC	4 categories	0.95 (0.93, 0.97)	1.00	0.88

B. Continuous delta CFC (changes in category ranks)	
	***R*-squared**
Age	0.008
Sex	0.00
Smoking	0.001
Hypertension	0.00
Diabetes	0.006
Hypercholestrolemia	0.015
eGFR	0.001
LVEF ≤ 50%	0.002
Multivessel disease	0.009
FFR	0.12
CFR	0.28
IMR	0.11
Baseline coronary flow	0.041
Hyperemic coronary flow	0.30
Pre-PCI CFC	0.49

(Continued)

patient-reported adverse events were verified by evaluating hospital records or contacting the treating cardiologist or general practitioner. All events were checked at least twice by different experienced cardiologists.

Statistical Analysis

Continuous variables are presented as mean (*SD*) or median (Q1, Q3) and categorical variables are presented as counts (percentages). Missing values in covariates were imputed by classification and regression tree methods. Baseline characteristics according to the pre-PCI CFC status or CFC changes following PCI were compared based on the standardized mean differences (SMD).

The predictability of CFC changes was assessed for each pre-PCI characteristics, respectively, with use of area under the curve (*AUC*), sensitivity and specificity at the best cutoffs, and receiver operating characteristic (*ROC*) curves. The prediction for the continuous delta CFC was evaluated with the use of *R*-squared values.

Hazard ratios (*HRs*) of incident TVF were estimated by the COX proportional hazard models, either for categorical CFC changes [worsened, no change (reference), +1 to +3 categories improved] or of continuous delta CFC (per one category change). The *p*-values for linear trends were calculated from the COX models for continuous delta CFC. Models were adjusted for age (continuous), sex (men/women), diabetes (yes/no), vessel location (left anterior descending/left circumflex/right coronary artery), multivessel disease (yes/no), and FFR (continuous). Associations between pre- or post-PCI CFC categories and incident TVF were also assessed similarly. Relevant Kaplan–Meier curves were also computed.

The discrimination ability of incident TVF was assessed by various nested logistic regression models; Model 1 included age, sex, diabetes, vessel location, and multivessel disease; Model 2 was Model 1 plus pre-PCI FFR; Model 3 was Model 2 plus pre-PCI CFR (continuous); and Model 4 was

TABLE 3 | (Continued)

C. ≥3 CFC categories improvement (i.e., severely reduced to normal CFC)

	AUC (95% CI)	Sensitivity	Specificity
Age	0.55 (0.46, 0.64)	0.37	0.77
Sex	0.57 (0.50, 0.63)	0.29	0.85
Smoking	0.53 (0.46, 0.60)	0.27	0.79
Hypertension	0.51 (0.45, 0.58)	0.73	0.30
Diabetes	0.52 (0.45, 0.59)	0.63	0.41
Hypercholestrolemia	0.52 (0.45, 0.60)	0.42	0.63
eGFR	0.54 (0.45, 0.63)	0.33	0.79
LVEF ≤ 50%	0.53 (0.48, 0.57)	0.90	0.15
Multivessel disease	0.55 (0.48, 0.63)	0.40	0.71
FFR	0.83 (0.77, 0.90)	0.77	0.80
CFR	0.87 (0.84, 0.91)	1.00	0.70
IMR	0.83 (0.79, 0.88)	0.88	0.71
Baseline coronary flow	0.64 (0.57, 0.71)	0.81	0.49
Hyperemic coronary flow	0.90 (0.87, 0.93)	1.00	0.73
Pre-PCI CFC	0.94 (0.93, 0.96)	1.00	0.88

D. ≥1 CFC category improvement

	AUC (95% CI)	Sensitivity	Specificity
Age	0.56 (0.51, 0.62)	0.58	0.55
Sex	0.51 (0.47, 0.54)	0.17	0.84
Smoking	0.51 (0.47, 0.55)	0.24	0.77
Hypertension	0.51 (0.47, 0.55)	0.71	0.30
Diabetes	0.54 (0.49, 0.58)	0.64	0.44
Hypercholestrolemia	0.56 (0.52, 0.61)	0.44	0.68
eGFR	0.52 (0.46, 0.57)	0.46	0.60
LVEF ≤ 50%	0.52 (0.48, 0.55)	0.17	0.87
Multivessel disease	0.54 (0.50, 0.59)	0.35	0.73
FFR	0.69 (0.64, 0.74)	0.56	0.76
CFR	0.81 (0.77, 0.85)	0.98	0.57
IMR	0.79 (0.75, 0.83)	0.81	0.66
Baseline coronary flow	0.58 (0.52, 0.63)	0.75	0.43
Hyperemic coronary flow	0.83 (0.80, 0.87)	1.00	0.53
Pre-PCI CFC	0.91 (0.88, 0.94)	1.00	0.79

***A,C,D**: Sensitivity and specificity are at the best cutoffs.*
***B:** R-squared was calculated for continuous changes in CFC categories, ranging –3 to +3.*
CFC, coronary flow capacity; CFR, coronary flow reserve; EF, ejection fraction; FFR, fractional flow reserve; IMR, index of microvascular resistance; PCI, percutaneous coronary intervention.

Model 3 plus delta CFC (in ranks, ranging from -3 to +3). The improvements in the discrimination were assessed by net reclassification improvement (NRI) and integrated discrimination improvement (IDI).

The *p*-value for linear trend was calculated to estimate the statistical significance of the association of CFC in ranks (ranging from 1 to 4) or delta CFC (ranging from -3 to +3) and incident TVF in the COX proportional hazard models. Two-sided *p* values for linear trends < 0.05 were considered statistically significant. All analyses were conducted using R 4.0.3 (The R Foundation).

RESULTS

Baseline Characteristics

A total of 450 patients with a clinical indication for revascularization and with 450 vessels with one coronary lesion indicated for and amenable to revascularization (1 vessel/subject) were included in the present analysis, and the mean (*SD*) age was 67.1 (10.0) years and there were 75 (16.7%) women. Median (Q1, Q3) FFR and CFR were 0.70 (0.63, 0.75) and 2.00 (1.33, 2.95), respectively. A total of 99, 63, 96, and 192 patients were classified as having severely reduced, moderately reduced, mildly reduced, and normal CFC status at baseline.

Table 1 summarizes the patient characteristics according to pre-PCI CFC status. The worse CFC status was associated with generally worse coronary physiologic profile. Medians (*IQRs*) FFR, CFR, and IMR were 0.62 (0.54, 0.69), 1.17 (1.03, 1.36), and 40.6 (35.0, 55.6) in patients with severely reduced CFC, and 0.73 (0.69, 0.78), 3.05 (2.28, 3.81), and 14.9 (11.0, 19.8) in those with normal CFC, respectively.

Coronary Flow Capacity Changes Following Percutaneous Coronary Intervention

Figure 2 illustrates the changes in CFC categories following PCI. In every pre-PCI CFC status, the majority were improved into normal CFC after PCI, leading to a total of 324 (80%) patients having post-PCI normal CFC status. Worse pre-PCI CFC status was associated with a higher probability of having worse post-PCI CFC status; for example, post-PCI moderately or severely reduced CFC was observed in 20 (24%), 11 (19%), 13 (14%), and 10 (6%) patients in pre-PCI severely reduced, moderately reduced, mildly reduced, and normal CFC status, respectively.

Characteristics of each delta CFC category are summarized in **Table 2**. Worsening, no change, +1, +2, and +3 rank changes in CFC categories following PCI were observed in *N* = 52, 192, 85, 69, and 52 patients, respectively. There were no clear trends

TABLE 4 | Associations of CFC changes following PCI in ranks and detailed outcomes.

CFC change	Worsened *N* = 52	No change *N* = 192	+1 category improved *N* = 85	+2 category improved *N* = 69	+3 category improved *N* = 52
Target-vessel failure	9 (17.3)	16 (8.3)	6 (7.1)	4 (5.8)	1 (1.9)
Cardiac death	1 (1.9)	1 (0.5)	0 (0.0)	1 (1.4)	0 (0.0)
Target-vessel myocardial infarction	4 (7.7)	5 (2.6)	3 (3.5)	0 (0.0)	0 (0.0)
Target-vessel revascularization	4 (7.7)	10 (5.2)	3 (3.5)	3 (4.3)	1 (1.9)

Values are n (%).
Target-vessel failure is a compostie of cardiac death, target-vessel myocardial infarction, and target-vessel revascularization.
CFC, coronary flow capacity; PCI, percutaneous coronary intervention.

TABLE 5 | Association between CFC changes following PCI and incident target vessel failure.

	A. Association between CFC changes and incident TVF						
CFC change	**Continuous (per one category)**	**Worsened**	**No change**	**+1 category improved**	**+2 category improved**	**+3 category improved**	***P*-trend**
TVF case/*N*		9/52	16/192	6/85	4/69	1/52	
Unadjusted HR	0.67 (0.50, 0.88)	2.27 (0.95, 5.43)	ref	0.85 (0.33, 2.22)	0.45 (0.12, 1.63)	0.14 (0.016, 1.30)	0.0051
Multivariate-adjusted HR	0.61 (0.45, 0.83)						0.0017

B. Coefficients in the multivariate regression models for CFC changes

	HR	**95% CI**
Delta CFC, per category	0.62	0.47, 0.83
Age, per year	1.00	0.97, 1.04
Female	0.81	0.31, 2.15
LAD versus RCA	0.74	0.34, 1.59
LCx versus RCA	0.35	0.07, 1.61
Diabetes	0.85	0.43, 1.67
Multivessel disease	1.14	0.56, 2.32
FFR, per 0.01 unit	0.97	0.94, 1.01

*HRs were estimated using COX proportional hazard models categorical CFC changes with no change as the reference **(A)** and CFC improvement in ranks (ranging -3 to +3) **(A,B)**.*

Multivariate models were adjusted for age (continuous), sex (male/female), diabetes (yes/no), vessel location (LAD/LCx/RCA), multivessel disease (yes/no), and FFR (continuous).

P-value for linear trend (P-trend) was calculated to estimate the statistical significance of the association between delta CFC (ranging -3 to +3) and incident TVF in the COX proportional hazard models.

CFC, coronary flow capacity; FFR, fractional flow reserve; HR, hazard ratio; LAD, left anterior descending artery; LCx, left circumflex artery; PCI, percutaneous coronary intervention; RCA, right coronary artery; TVF, target-vessel failure.

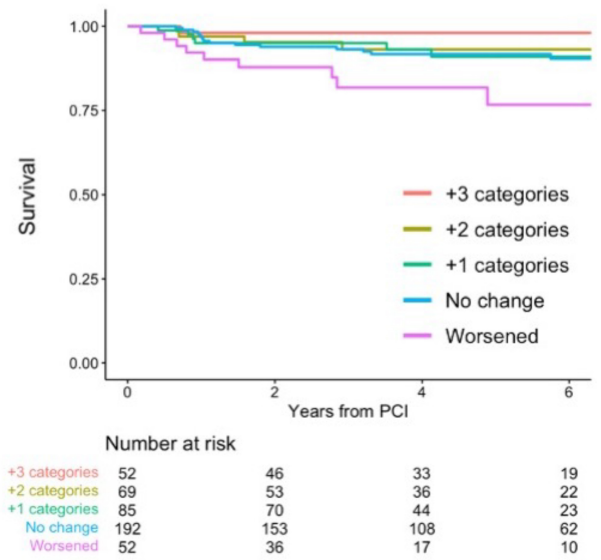

FIGURE 4 | Survival from target-vessel failure (TVF) according to CFC changes. Kaplan–Meier curves showing survival from TVF according to the changes in CFC following PCI. CFC changes were categorized as worsened (-3 to -1 categories change), no change, +1, +2, or +3 categories improvement. Numbers indicate the number of patients at risk.

in demographics across the groups, while lower FFR, CFR and hyperemic coronary flow, higher IMR, and worse CFC profiles were associated with greater CFC improvement. Those with worsened CFC after PCI were characterized with a relatively higher proportion of LAD lesions, while no other clear differences were found comparing with the patients with no changes in CFC.

Prediction of Coronary Flow Capacity Changes

The pre-PCI CFC status, although it has only 4 categories, was highly predictive of the improvement in CFC status following PCI, with AUC (95% *CI*) of 0.95 (0.93, 0.97) for ≥2 categories improvement (**Figure 3A**). The sensitivity was 100% because such improvement can only be possible in vessels with pre-PCI moderately or severely reduced CFC. Additional consideration of FFR had little influence on the discrimination (*AUC* [95% *CI*]: 0.96 [0.94, 0.98], **Figure 3B**). Other non-physiological characteristics were not comparatively predictive (**Table 3A**). Notedly, 48.6% of the variability of continuous delta CFC was explained solely by pre-PCI CFC, while only 12.4% by FFR (**Table 3B**). Results on the predictions for ≥1 and ≥3 CFC categories improvement were summarized in **Tables 3C,D**, which is consistently supporting the critical role of pre-PCI CFC in the predictions.

Association Between Delta Coronary Flow Capacity and Incident Target Vessel Failure

During a median follow-up of 4.3 (*IQR*: 2.5, 6.9) years, a total of 36 events were confirmed. Associations between CFC changes and detailed outcomes are summarized in **Table 4**. Patients with worsened, unchanged, +1, +2, and +3 improved CFC categories had the TVF risk of 17.3, 8.3, 7.1, 5.8, and 1.9%, respectively. Approximately 10% of the patients with worsened CFC had

TABLE 6 | Association between pre- and post-PCI CFC and incident target vessel failure.

	A. Association between pre-PCI CFC and incident TVF					
Pre-PCI CFC	**Continuous (per one category)**	**Severely reduced**	**Moderately reduced**	**Mildly reduced**	**Normal**	***P*-trend**
TVF case/*N*		5/99	6/63	8/96	17/192	
Unadjusted HR	1.14 (0.86, 1.52)	0.56 (0.20, 1.51)	1.15 (0.45, 2.93)	0.98 (0.42, 2.27)	ref	0.33
Multivariate-adjusted HR	1.25 (0.88, 1.77)					0.22

B. Coefficients in the multivariate regression models for pre-PCI CFC

	HR	**95% CI**
Pre-PCI CFC, per category	1.25	0.88, 1.77
Age, per year	1.00	0.97, 1.04
Female	0.85	0.32, 2.23
LAD versus RCA	0.77	0.36, 1.67
LCx versus RCA	0.31	0.07, 1.47
Diabetes	0.96	0.49, 1.89
Multivessel disease	1.09	0.54, 2.21
FFR, per 0.01 unit	0.98	0.94, 1.03

C. Association between post-PCI CFC and incident TVF

Post-PCI CFC	**Continuous (per one category)**	**Severely reduced**	**Moderately reduced**	**Mildly reduced**	**Normal**	***P*-trend**
TVF case/*N*		6/29	2/25	8/72	20/324	
Unadjusted HR	0.66 (0.49, 0.88)	3.83 (1.54, 9.57)	1.38 (0.32, 5.89)	2.07 (0.91, 4.70)	ref	0.0050
Multivariate-adjusted HR	0.65 (0.48, 0.88)					0.0055

D. Coefficients in the multivariate regression models for post-PCI CFC

	HR	**95% CI**
Post-PCI CFC, per category	0.65	0.48, 0.88
Age, per year	0.99	0.96, 1.03
Female	0.79	0.30, 2.09
LAD versus RCA	0.84	0.39, 1.81
LCx versus RCA	0.40	0.09, 1.90
Diabetes	0.80	0.40, 1.61
Multivessel disease	1.08	0.53, 2.20
FFR, per 0.01 unit	1.00	0.97, 1.04

*HRs were estimated using COX proportional hazard models for categorical pre-PCI CFC with normal CFC as the reference **(A)**, continuous pre-PCI CFC in ranks (ranging 1–4) (**A,B**), categorical post-PCI CFC with normal CFC as the reference **(C)**, continuous post-PCI CFC in ranks (ranging 1–4) **(C,D)**.*
Multivariate models were adjusted for age (continuous), sex (male/female), diabetes (yes/no), vessel location (LAD/LCx/RCA), multivessel disease (yes/no), and FFR (continuous).
P-value for linear trend was calculated to estimate the statistical significance of the association between CFC in ranks (ranging 1–4) and incident TVF in the COX proportional hazard models.
CFC, coronary flow capacity; FFR, fractional flow reserve; HR, hazard ratio; LAD, left anterior descending artery; LCx, left circumflex artery; PCI, percutaneous coronary intervention; RCA, right coronary artery; TVF, target-vessel failure.

cardiac death or TVMI, whereas only one TVR event was observed in the 52 patients with +3 CFC categories improvement. Compared with no change in CFC categories after PCI, patients with category worsened, +1, +2, and +3 category improved had the hazard ratio (*HR*) (95% *CI*) for incident TVF of 2.27 (0.95, 5.43), 0.85 (0.33, 2.22), 0.45 (0.12, 1.63), and 0.14 (0.016, 1.30), respectively (*p* for linear trends = 0.0051; **Table 5**). After adjustment for confounders, one additional improvement in CFC status was associated with 0.61 (0.45, 0.83) times the hazard of TVF (*p* for linear trends = 0.0017). **Figure 4** depicts the relevant Kaplan–Meier curves.

No survival differences were observed according to distinct pre-PCI CFC status with a multivariable-adjusted *HR* of 1.25 (0.88, 1.77) for one rank higher CFC category (**Tables 6A**,**B** and **Figure 5A**). There were significant associations between post-PCI CFC and incident TVF (**Tables 6C**,**D** and **Figure 5B**).

Table 7 shows the prediction of incident TVF by various nested models and the metrics for the improvement in the discrimination. Models comprised solely of demographics had *AUC* (95% *CI*) of 0.57 (0.47, 0.67) and the further consideration of pre-PCI FFR and pre-PCI CFR did not improve the discrimination. The model additionally including delta CFC had higher *AUC* (0.71 [95% *CI*: 0.62, 0.79]) and the discrimination was well improved compared with the model without delta CFC (*NRI*: 0.47 [95% *CI*: 0.14, 0.81] and *IDI*: 0.035 [95% *CI*: 0.011, 0.060]).

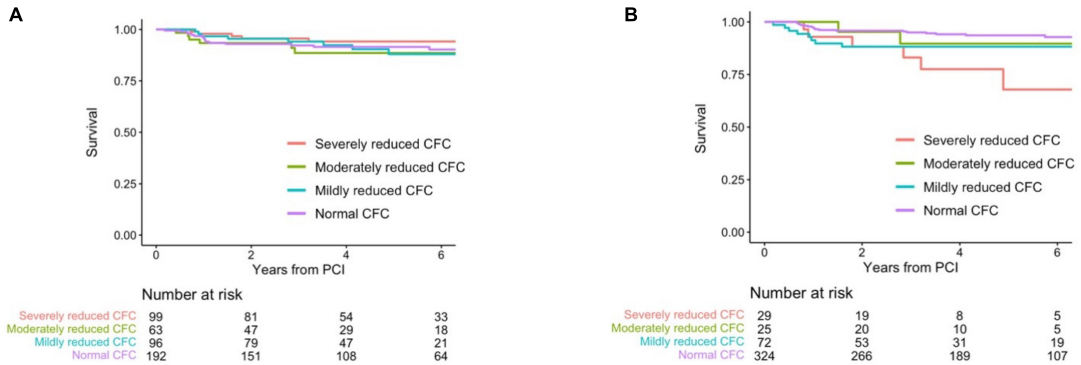

FIGURE 5 | Kaplan–Meier curves showing survival from TVF according to the post-PCI CFC categories. Kaplan–Meier curves showing survival from TVF according to pre- **(A)** and post-CFC status **(B)**. CFC status was categorized as severely reduced, moderately reduced, mildly reduced, and normal. Numbers indicate the number of patients at risk.

TABLE 7 | Prediction incident target vessel failure based on pre-PCI information.

	AUC (95% CI)	Comparator of NRI/IDI analyses	Continuous NRI (95% CI)	IDI (95% CI)
Model 1: Demographics	0.57 (0.47, 0.67)	–	–	–
Model 2: Model 1 + pre-PCI FFR	0.57 (0.47, 0.67)	Model 1	0.00 (–0.33, 0.33)	0.000 (0.000, 0.000)
Model 3: Model 2 + pre-PCI CFR	0.59 (0.50, 0.68)	Model 2	–0.01 (–0.35, 0.33)	0.002 (–0.002, 0.006)
Model 4: Model 3 + delta CFC	0.71 (0.62, 0.79)	Model 3	0.47 (0.14, 0.81)	0.035 (0.011, 0.060)

Models were based on logistic regressions for incident target vessel failure.
Model 1 included age, sex, diabetes, vessel location, and multivessel disease; Model 2 was Model 1 plus pre-PCI FFR; Model 3 was Model 2 plus pre-PCI CFR (continuous); and Model 4 was Model 3 plus delta CFC (in ranks, ranging –3 to +3).
AUC, area under the curve; CFC, coronary flow capacity; CFR, coronary flow reserve; IDI, integrated discrimination improvement; NRI, net reclassification improvement; PCI, percutaneous coronary intervention.

DISCUSSION

In the present study, the changes in CFC status following PCI were robustly associated with incident TVF in patients with the CCS. The change was largely determined by the pre-PCI CFC status. Furthermore, no association between pre-PCI CFC and incident TVF was observed, suggesting prognostic benefits of PCI in patients with reduced CFC categories. This study provides a mechanistic explanation on potential favorable effects of PCI on reducing vessel-oriented outcomes in lesions with reduced CFC, supporting a use of CFC, in addition to FFR, in guiding PCI to maximize the benefit. A summary of the present study was illustrated in **Figure 6**.

Although FFR well captures the severity of epicardial atherosclerosis, the index does not directly incorporate the information on coronary flow and microvascular resistance. CFR has been attracted as a potential flow-related marker that could guide PCI, while a recent prospective study did not observe the role (18). This is partly because low CFR is a heterogeneous condition with varied resting and hyperemic coronary flow status (18). The physiological benefit of PCI primarily lies in modifying the hyperemic flow limitation (19–21). CFC is an integrated concept of CFR and hyperemic coronary flow, and thus low FFR combined with reduced CFC highlights hyperemic coronary flow limitation-based ischemia due to epicardial atherosclerosis, where PCI could maximally offer the physiological benefit. In accordance with the theoretical basis, we have previously showed a differential prognostic effect of PCI according to the CFC status in registry data (13). The present study further supports the role of CFC by highlighting the impact of changes in CFC status following PCI, a direct representation of the

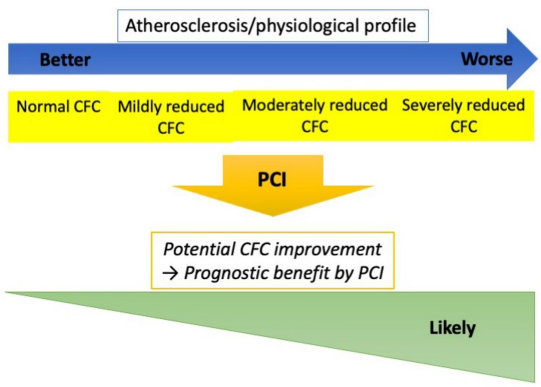

FIGURE 6 | Study summary. Worse CFC status was associated with higher atherosclerotic risk and worse coronary physiological profile. However, the clinical courses were similar across the pre-PCI CFC if treated by elective PCI, while the changes in CFC following PCI were robustly associated with the risk of TVF. Furthermore, CFC changes are largely determined by the pre-PCI status. These observations implicate that lesions with reduced CFC could potentially attain greater CFC improvement by PCI, and consequently the lowered risk of vessel-oriented adverse events. CFC could thus serve as guidance for elective PCI indication, which needs to be evaluated in studies comparing PCI versus medical therapy in reduced CFC lesions.

improvement in coronary flow and ischemic burden; notedly, TVF was observed in only 1 out of 52 patients whose CFC status changed from severely reduced to normal. The pre-PCI CFC status largely offers the prediction of the changes, supportive of the usage in guiding PCI.

From another aspect, current FFR-guidance might indicate too many stable vessels for revascularization in which the physiological benefit from PCI could not be expected. In particular, lesions with low FFR and normal CFC, comprising 43% of vessels in the present registry, hardly anticipates coronary flow restoration or reduction of ischemic burden, and thus these might better be treated medically with respect to prognostic advantage and possibly to symptomatic relief. Although there is a correlation between FFR and CFC, FFR only explains 12% of the variability of CFC changes, supportive of the merit of integrating CFC for guiding PCI indication in addition to FFR. Additionally, while this study demonstrated a clear prognostic contribution of the changes in the regional CFC following PCI, the impact of PCI on the global coronary flow property could be different as we previously described (19, 22, 23). Further consideration of global physiological indices might lead to better identification of patients with CCS who would likely benefit from the intervention.

The study has several limitations. The present analysis is based on a single-center registry and as such the generalizability is limited. The moderate sample size prevents rigorous adjustments of confounders. However, such adjustments could make the estimate further away from null, as higher CFC improvement can occur in patients with pre-PCI reduced CFC, which categories were generally associated with higher atherosclerotic risks and worse physiological profiles. Thermodilution methods could overestimate CFR compared with Doppler-technique (24). Finally, the present study does not directly indicate the usefulness of CFC in guiding PCI but offers an explanation on the potential mechanisms, i.e., improvement in CFC status. Another study is needed to demonstrate the prognostic impact of FFR plus CFC-guided compared with FFR only-guided PCI in a larger population.

CONCLUSION

Changes in CFC categories following PCI was associated with lower risk of incident TVF in patients with CCS who underwent PCI. The pre-PCI CFC status was a sole strong predictor for the CFC changes. This study provides a mechanistic explanation on a potential favorable effect of PCI on reducing vessel-oriented outcome in lesions with reduced CFC and low FFR.

DATA AVAILABILITY STATEMENT

The raw data supporting the conclusions of this article will be made available by the authors, without undue reservation.

ETHICS STATEMENT

The studies involving human participants were reviewed and approved by Tsuchiura Kyodo General Hospital Ethics Committee. The patients/participants provided their written informed consent to participate in this study.

AUTHOR CONTRIBUTIONS

RH: concept, design, drafting of the manuscript, and statistical analysis. All authors: acquisition, analysis, or interpretation of data. TK: critical revision of the manuscript for important intellectual content, administrative, technical, or material support, and supervision. All authors contributed to the article and approved the submitted version.

REFERENCES

1. Maron DJ, Hochman JS, Reynolds HR, Bangalore S, O'Brien SM, Boden WE, et al. Initial invasive or conservative strategy for stable coronary disease. *N Engl J Med.* (2020) 382:1395–407.
2. Bangalore S, Maron DJ, O'Brien SM, Fleg JL, Kretov EI, Briguori C, et al. Management of coronary disease in patients with advanced kidney disease. *N Engl J Med.* (2020) 382:1608–18.
3. Boden WE, O'Rourke RA, Teo KK, Hartigan PM, Maron DJ, Kostuk WJ, et al. Optimal medical therapy with or without PCI for stable coronary disease. *N Engl J Med.* (2007) 356:1503–16. doi: 10.1056/NEJMoa070829
4. Frye RL, August P, Brooks MM, Hardison RM, Kelsey SF, MacGregor JM, et al. A randomized trial of therapies for type 2 diabetes and coronary artery disease. *N Engl J Med.* (2009) 360:2503–15.
5. Ueki Y, Otsuka T, Bär S, Koskinas KC, Heg D, Häner J, et al. Frequency and outcomes of periprocedural MI in patients with chronic coronary syndromes undergoing PCI. *J Am Coll Cardiol.* (2022) 79:513–26. doi: 10.1016/j.jacc.2021.11.047
6. Zimmermann FM, Omerovic E, Fournier S, Kelbæk H, Johnson NP, Rothenbühler M, et al. Fractional flow reserve-guided percutaneous coronary intervention vs. medical therapy for patients with stable coronary lesions: meta-analysis of individual patient data. *Eur Heart J.* (2019) 40:180–6. doi: 10.1093/eurheartj/ehy812
7. Xaplanteris P, Fournier S, Pijls NHJ, Fearon WF, Barbato E, Tonino PAL, et al. Five-year outcomes with PCI guided by fractional flow reserve. *N Engl J Med.* (2018) 379:250–9. doi: 10.1056/NEJMoa1803538
8. De Bruyne B, Pijls NH, Kalesan B, Barbato E, Tonino PA, Piroth Z, et al. Fractional flow reserve-guided PCI versus medical therapy in stable coronary disease. *N Engl J Med.* (2012) 367:991–1001. doi: 10.1056/NEJMoa1205361
9. Johnson NP, Gould KL. Integrating noninvasive absolute flow, coronary flow reserve, and ischemic thresholds into a comprehensive map of physiological severity. *JACC Cardiovasc Imaging.* (2012) 5:430–40. doi: 10.1016/j.jcmg.2011.12.014
10. van de Hoef TP, Echavarría-Pinto M, van Lavieren MA, Meuwissen M, Serruys PW, Tijssen JG, et al. Diagnostic and prognostic implications of coronary flow capacity: a comprehensive cross-modality physiological concept in ischemic heart disease. *JACC Cardiovasc Interv.* (2015) 8:1670–80. doi: 10.1016/j.jcin.2015.05.032
11. Gould KL, Johnson NP. Coronary physiology beyond coronary flow reserve in microvascular angina: JACC state-of-the-art review. *J Am Coll Cardiol.* (2018) 72:2642–62. doi: 10.1016/j.jacc.2018.07.106
12. Hamaya R, Yonetsu T, Kanaji Y, Usui E, Hoshino M, Yamaguchi M, et al. Diagnostic and prognostic efficacy of coronary flow capacity obtained using

pressure-temperature sensor-tipped wire-derived physiological indices. *JACC Cardiovasc Interv.* (2018) 11:728–37. doi: 10.1016/j.jcin.2018.01.249
13. Hamaya R, Lee JM, Hoshino M, Yonetsu T, Koo BK, Escaned J, et al. Clinical outcomes of fractional flow reserve-guided percutaneous coronary intervention by coronary flow capacity status in stable lesions. *EuroIntervention.* (2020) 17:e301–8. doi: 10.4244/EIJ-D-20-00401
14. Fearon WF, Balsam LB, Farouque HM, Caffarelli AD, Robbins RC, Fitzgerald PJ, et al. Novel index for invasively assessing the coronary microcirculation. *Circulation.* (2003) 107:3129–32. doi: 10.1161/01.CIR.0000080700.98607.D1
15. Yong AS, Layland J, Fearon WF, Ho M, Shah MG, Daniels D, et al. Calculation of the index of microcirculatory resistance without coronary wedge pressure measurement in the presence of epicardial stenosis. *JACC Cardiovasc Interv.* (2013) 6:53–8. doi: 10.1016/j.jcin.2012.08.019
16. de Winter RW, Jukema RA, van Diemen PA, Schumacher SP, Driessen RS, Stuijfzand WJ, et al. The impact of coronary revascularization on vessel-specific coronary flow capacity and long-term outcomes: a serial [15O]H2O positron emission tomography perfusion imaging study. *Eur Heart J Cardiovasc Imaging.* (2022) 23:743–52. doi: 10.1093/ehjci/jeab263
17. Murai T, Stegehuis VE, van de Hoef TP, Wijntjens GWM, Hoshino M, Kanaji Y, et al. Coronary flow capacity to identify stenosis associated with coronary flow improvement after revascularization: a combined analysis from DEFINE FLOW and ideal. *J Am Heart Assoc.* (2020) 9:e016130. doi: 10.1161/JAHA.120.016130
18. Johnson NP, Matsuo H, Nakayama M, Eftekhari A, Kakuta T, Tanaka N, et al. Combined pressure and flow measurements to guide treatment of coronary stenoses. *JACC Cardiovasc Interv.* (2021) 14:1904–13. doi: 10.1016/j.jcin.2021.07.041
19. Hamaya R, Sugano A, Kanaji Y, Fukuda T, Kanno Y, Yonetsu T, et al. Absolute myocardial blood flow after elective percutaneous coronary intervention evaluated on phase-contrast cine cardiovascular magnetic resonance imaging. *Circ J.* (2018) 82:1858–65. doi: 10.1253/circj.CJ-17-1449
20. Hamaya R, Kanaji Y, Usui E, Hoshino M, Murai T, Yonetsu T, et al. Improvement of fractional flow reserve after percutaneous coronary intervention does not necessarily indicate increased coronary flow. *Eur Cardiol.* (2019) 14:10–2. doi: 10.15420/ecr.2018.27.2
21. Kanaji Y, Murai T, Yonetsu T, Usui E, Araki M, Matsuda J, et al. Effect of elective percutaneous coronary intervention on hyperemic absolute coronary blood flow volume and microvascular resistance. *Circ Cardiovasc Interv.* (2017) 10:e005073. doi: 10.1161/CIRCINTERVENTIONS.117.005073
22. Hamaya R, Fukuda T, Sugano A, Kanaji Y, Hada M, Kanno Y, et al. Impact of regional functional ischemia on global coronary flow reserve in patients with stable coronary artery disease. *J Cardiol.* (2019) 73:263–70. doi: 10.1016/j.jjcc.2018.12.005
23. Kanaji Y, Yonetsu T, Hamaya R, Murai T, Usui E, Hoshino M, et al. Impact of elective percutaneous coronary intervention on global absolute coronary flow and flow reserve evaluated by phase-contrast cine-magnetic resonance imaging in relation to regional invasive physiological indices. *Circ Cardiovasc Interv.* (2018) 11:e006676. doi: 10.1161/CIRCINTERVENTIONS.118.006676
24. Everaars H, de Waard GA, Driessen RS, Danad I, van de Ven PM, Raijmakers PG, et al. Doppler flow velocity and thermodilution to assess coronary flow reserve: a head-to-head comparison with [(15)O]H(2)O PET. *JACC Cardiovasc Interv.* (2018) 11:2044–54. doi: 10.1016/j.jcin.2018.07.011

Conflict of Interest: The authors declare that the research was conducted in the absence of any commercial or financial relationships that could be construed as a potential conflict of interest.

Publisher's Note: All claims expressed in this article are solely those of the authors and do not necessarily represent those of their affiliated organizations, or those of the publisher, the editors and the reviewers. Any product that may be evaluated in this article, or claim that may be made by its manufacturer, is not guaranteed or endorsed by the publisher.

frontiers | Frontiers in Cardiovascular Medicine

TYPE Mini Review
PUBLISHED 15 July 2022
DOI 10.3389/fcvm.2022.920119

OPEN ACCESS

EDITED BY
Sara Seitun,
San Martino Polyclinic Hospital IRCCS, Italy

REVIEWED BY
Chiara De Biase,
Centro Sanitario Locale Napoli 1 Centro, Italy
Alberto Clemente,
Gabriele Monasterio Tuscany Foundation (CNR), Italy
Cesare Mantini,
University of Studies G. d'Annunzio Chieti and Pescara, Italy

*CORRESPONDENCE
Polydoros N. Kampaktsis
pkampaktsis@yahoo.com

SPECIALTY SECTION
This article was submitted to Cardiovascular Imaging, a section of the journal Frontiers in Cardiovascular Medicine

RECEIVED 14 April 2022
ACCEPTED 28 June 2022
PUBLISHED 15 July 2022

CITATION
Emfietzoglou M, Mavrogiannis MC, Samaras A, Rampidis GP, Giannakoulas G and Kampaktsis PN (2022) The role of cardiac computed tomography in predicting adverse coronary events.
Front. Cardiovasc. Med. 9:920119.
doi: 10.3389/fcvm.2022.920119

The role of cardiac computed tomography in predicting adverse coronary events

Maria Emfietzoglou[1], Michail C. Mavrogiannis[1], Athanasios Samaras[2], Georgios P. Rampidis[2], George Giannakoulas[2] and Polydoros N. Kampaktsis[3]*

[1]Division of Cardiovascular Medicine, Radcliffe Department of Medicine, University of Oxford, John Radcliffe Hospital, Oxford, United Kingdom, [2]Aristotle University of Thessaloniki, Thessaloniki, Greece, [3]Division of Cardiology, Columbia University Irving Medical Center, New York, NY, United States

Cardiac computed tomography (CCT) is now considered a first-line diagnostic test for suspected coronary artery disease (CAD) providing a non-invasive, qualitative, and quantitative assessment of the coronary arteries and pericoronary regions. CCT assesses vascular calcification and coronary lumen narrowing, measures total plaque burden, identifies plaque composition and high-risk plaque features and can even assist with hemodynamic evaluation of coronary lesions. Recent research focuses on computing coronary endothelial shear stress, a potent modulator in the development and progression of atherosclerosis, as well as differentiating an inflammatory from a non-inflammatory pericoronary artery environment using the simple measurement of pericoronary fat attenuation index. In the present review, we discuss the role of the above in the diagnosis of coronary atherosclerosis and the prediction of adverse cardiovascular events. Additionally, we review the current limitations of cardiac computed tomography as an imaging modality and highlight how rapid technological advancements can boost its capacity in predicting cardiovascular risk and guiding clinical decision-making.

KEYWORDS

cardiac computed tomography, coronary artery disease, coronary artery calcium score, perivascular fat, computational fluid dynamics, adverse coronary events

Introduction

Cardiac computed tomography (CCT) has emerged in the last decade as an important non-invasive modality for the evaluation of coronary artery disease (CAD) with actively expanding indications. Initial research led to the establishment of a coronary artery calcium score (CACS) for improved risk stratification of asymptomatic patients with intermittent probability for adverse atherosclerotic events; a CACS of zero is associated with low rates of future adverse events (1). Similarly, CCT angiography (CCTA) was shown to be a reliable modality for ruling out CAD in low-risk patients who present to the emergency room with chest pain, leading additionally to decreased length of stay (2). Further studies examined the role of cardiac CCTA in the evaluation of suspected CAD in patients with stable angina. The non-invasive anatomic assessment

was compared to standard of care non-invasive functional assessment as an additional or standalone modality (3, 4). The addition of CCTA resulted in a lower risk for long-term coronary death or myocardial infarction, as the increased sensitivity of CCTA for the detection of coronary atherosclerosis led to higher rates of guideline-directed preventive therapy initiation. The use of CCTA as a standalone modality resulted in similar outcomes compared to stress testing or invasive coronary angiography (5). These results highlighted that CCTA is an excellent non-invasive modality for the evaluation of suspected CAD in symptomatic patients; in fact, the latest European Society of Cardiology (ESC) guidelines give a class I recommendation for cardiac CCTA for the evaluation of stable CAD (6). Additionally, however, these results underline the importance of complementary functional assessment that so far had been obtained by stress testing and invasive indices. The latter represents an active area of research in CCTA that could improve its prognostic value for coronary events in patients where coronary atherosclerosis is diagnosed (7, 8). Parallel to the above, a significant number of studies focused on the potential role of CCTA for the identification of "vulnerable plaques", i.e., coronary atherosclerosis sites that would be associated with a much higher chance of plaque rupture and thrombotic events (9). Although today, the focus has switched to the "vulnerable patient" (10), assessment of high-risk plaques remains important. Finally, CCTA has recently been pivotal in understanding the role of perivascular adipose tissue in atherosclerosis (11) and how associated pericoronary inflammation can be used as a novel prognostic index of adverse coronary outcomes (12) (Figure 1).

In the current review, we aim to delineate the contribution of CCT in predicting future adverse cardiovascular outcomes across different clinical scenarios. First, we discuss how CCT can quantitatively assess coronary calcium, the degree of luminal stenosis and total plaque burden, and how these are related to adverse events. We then discuss the role of CCTA based-plaque characterization and its clinical role. Furthermore, we summarize the current state of functional and hemodynamic assessment *via* CCTA including endothelial shear stress. We elaborate on the role of perivascular fat inflammation in relation to CCTA. Finally, we appraise the limitations of CCT and discuss how technological advances can enhance the capability of CCT in cardiovascular risk prediction in the near future.

Coronary artery calcium score

CCT allows quantification of plaque calcium burden by measuring the Agatston score (13). CACS is based on a low radiation dose, non-contrast CT (14) and represents a simple, quick, inexpensive, and reproducible test. CACS has shown to correlate well with long-term risk of cardiac events when used as a binary or categorical number (1, 15–18). For example, the 10-year risk for adverse atherosclerotic events of a 65-year-old male with hyperlipidemia and medically treated hypertension is over 10%. If the same individual has a CACS of zero, then the risk becomes 3.5%. Importantly, the predictive value of CACS is incremental to that of traditional risk factors and risk calculators that have included CACS have outperformed established risk scores, such as the Framingham score and the 2013 American College of Cardiology (ACC)/American Heart Association (AHA) risk estimator (19). Today, CACS is an established way to better assess the Atherosclerotic Cardiovascular Disease (ASCVD) risk of asymptomatic individuals that otherwise fall into intermediate risk and start appropriate risk factor modification therapy (class IIb recommendation in European Society of Cardiology guidelines and IIa in ACC/AHA). The serial use of CACS is less clear, particularly in patients who are on statin therapy (20).

Nevertheless, the clinical application of CACS must take into account the pre-test probability of CAD, even when CACS is zero, as plaque can be non-calcified, particularly in younger, high-risk patients. Along these lines, clinical decisions for symptomatic patients should not be based solely on CACS, and in fact, CACS is not recommended in that scenario, as shown in the CORE64 trial where >10% of symptomatic patients with CACS of zero had obstructive CAD (21).

Anatomic assessment

Stenosis and plaque volume

Established applications of anatomic assessment *via* CCTA include the evaluation of symptomatic patients with suspected CAD. The degree of luminal stenosis as well as the presence of obstructive disease on CCTA, defined as >70% stenosis, correlate very well with mortality risk (22, 23). CCTA exhibits moderate to high sensitivity and specificity in discriminating lesion severity (24), with diagnostic accuracy curbed mainly by technical artifacts and limitations. Nevertheless, anatomic assessment with CCTA in the ISCHEMIA trial effectively ruled out left main disease, while clinical and stress testing were weak predictors (25). On the other hand, the advantage of CCTA compared to invasive angiography is the more precise evaluation of the presence and extent of non-obstructive lesions. This is clinically important since it has been shown that recurrent adverse events, specifically cardiovascular death, cardiac arrest, myocardial infarction, or unstable angina, arise from equally from culprit and non-culprit lesions during an index hospitalization (26). In fact, non-culprit lesions frequently cause mild stenoses. In contrast, severe plaque burden has been associated with adverse outcomes regardless of the degree of luminal stenosis (27). Of note, total plaque burden in asymptomatic individuals with type-2 diabetes has demonstrated additional prognostic value for cardiac events compared to clinical risk assessment and CACS (28). Coronary

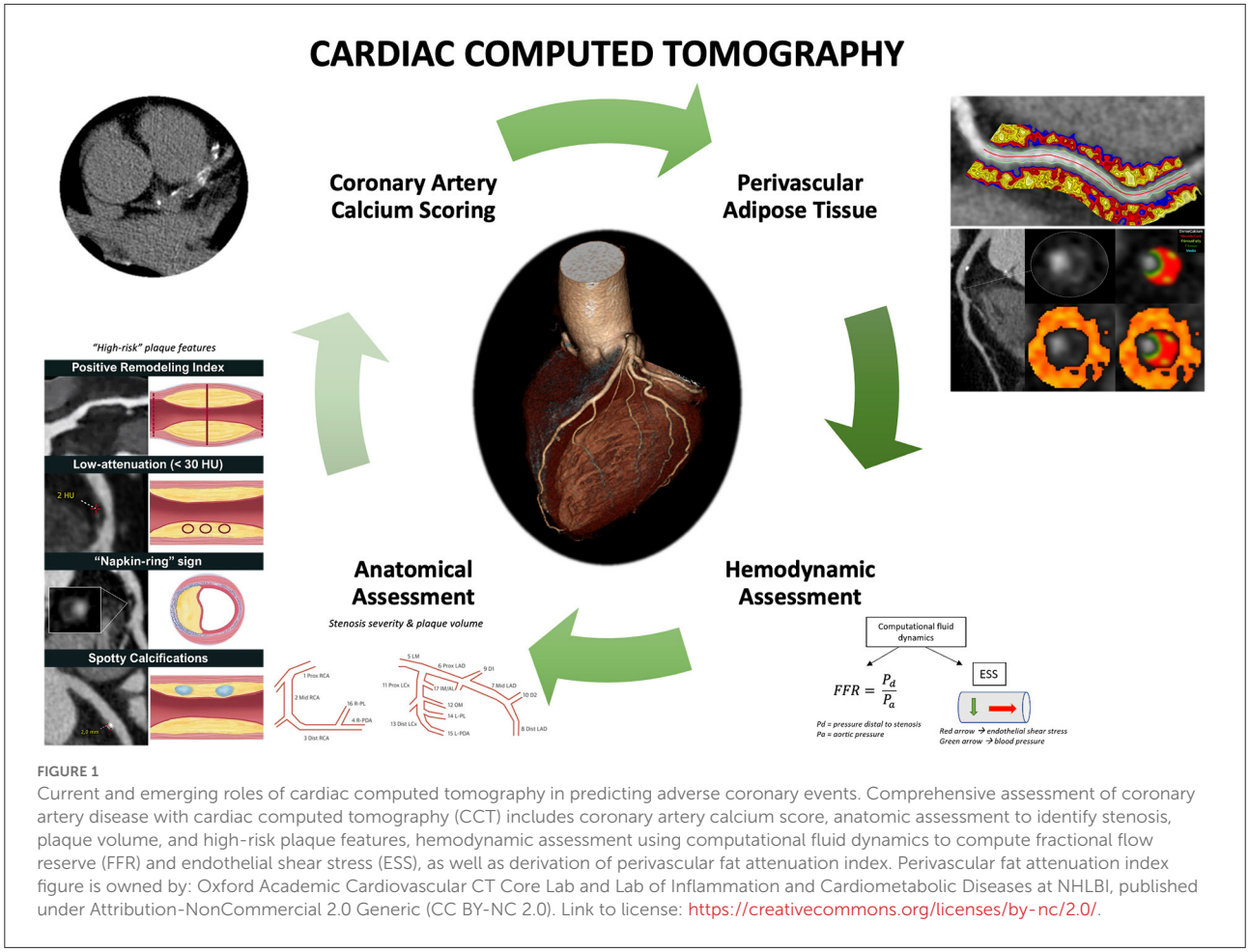

FIGURE 1
Current and emerging roles of cardiac computed tomography in predicting adverse coronary events. Comprehensive assessment of coronary artery disease with cardiac computed tomography (CCT) includes coronary artery calcium score, anatomic assessment to identify stenosis, plaque volume, and high-risk plaque features, hemodynamic assessment using computational fluid dynamics to compute fractional flow reserve (FFR) and endothelial shear stress (ESS), as well as derivation of perivascular fat attenuation index. Perivascular fat attenuation index figure is owned by: Oxford Academic Cardiovascular CT Core Lab and Lab of Inflammation and Cardiometabolic Diseases at NHLBI, published under Attribution-NonCommercial 2.0 Generic (CC BY-NC 2.0). Link to license: https://creativecommons.org/licenses/by-nc/2.0/.

plaque burden on CCTA has also been shown to correlate with levels of high-sensitivity cardiac troponin T (hs-cTnT) in patients that were ruled out for myocardial infarction or even in asymptomatic patients. Even mild CAD has been associated with quantifiable circulating levels of hs-cTnT (29). As evidenced by *in vitro* studies, these elevated levels of hs-cTnT are not necessarily corresponding to myocardial necrosis, but they suggest that there is sufficient ischemia to result in cell stress, activation of caspase-3, cleavage, and release of cTnT (30). Possible mechanisms of ischemia are physical exercise, emotional stress, dislodgement of thrombi in coronary microvasculature and plaque erosion (31). CCTA-derived parameters can also be directly used for non-invasive evaluation of atherosclerotic features. For instance, positive remodeling of a plaque as well as non-calcified plaque volume have both been associated with increased risk for acute coronary syndromes (ACS) in a meta-analysis of 18 CCTA studies (32). Additional prognostic information could be obtained by serial examinations, as plaque progression has been associated with increased risk for ACS. However, serial CCTAs result in cumulative radiation exposure and are currently not recommended as standard of care. Studies are attempting to identify predictors of coronary plaque progression based on features of a baseline CCTA (33).

High-risk plaques: Characteristics and prognostic value

The concept of high-risk or "vulnerable" plaques is that certain anatomic plaque characteristics can predict plaque rupture, erosion, and thus future thrombotic events. The concept originated from thin cap fibroatheromas, i.e., plaques with a necrotic or lipid core and a thin layer of overlying epithelial cells, which were associated with higher risk of adverse events (34). High-risk characteristics have been identified using CCTA include positive remodeling, low attenuation, spotty calcification, and the "napkin-ring" sign (35). Interestingly, these features respond well to statin use and may regress in serial scans (36). The greatest challenge in the application of these high-risk features is the complex natural history of coronary

atherosclerosis itself; most plaque ruptures or erosions are now thought to be asymptomatic events that lead to plaque growth (37). In addition, it has been shown that coronary plaques have dynamic morphology and thin cap fibroatheromas may involve into thick cap fibroatheromas, i.e., lower risk plaques, at follow up (38). Equally importantly, symptomatic plaque rupture or erosion is determined by additional hemodynamic local factors such as endothelial shear stress, as well as systemic factors that determine the individual's thrombophilic state (38); thus prediction of clinically meaningful events is extremely complex and "vulnerable" plaques cannot be easily targeted for revascularization (10). Nevertheless, it is worth discussing the CCTA-derived characteristics of "vulnerable" plaques and their association with coronary events.

Positive remodeling is defined as the compensatory enlargement of the outer vessel wall at the site of an atherosclerotic lesion as the plaque burden increases (39). From a histopathological perspective, this enlargement results from macrophage infiltration and a large amount of necrotic core. CCTA can reliably measure and quantify positive remodeling using an index defined as the ratio of the vessel cross-sectional area at the site of maximal stenosis and the average of proximal and distal reference cross-sectional areas. A threshold of 1.1 is typically preferred in the assessment of CCTA images (40). Several studies have shown that a higher positive remodeling index can identify thin cap fibroatheroma (41, 42), as well as culprit lesions in ACS, but not in stable angina (43). In a prospective study including 74 participants with ACS or stable angina undergoing CCTA, positive remodeling was found in 96% of patients with ACS and ruptured fibrous caps, but only in 20% of those with ACS and intact fibrous caps and in 14% of individuals with stable angina (p <0.001) (44).

Low attenuation (<30 Hounsfield units) is typically used to easily describe plaques with a large lipid-rich necrotic core, as lipids typically have the lowest CCTA attenuation value. Ruptured plaques tend to have lower attenuation compared to stable lesions (44), while a lower plaque attenuation has been found in patients with ACS compared to those with stable angina (45). In a prospective study by Ozaki et al. including patients with ACS or stable angina, low attenuation plaques were more frequently observed in individuals with ACS and ruptured fibrous caps than in those with ACS and intact fibrous cap and those with stable angina (88, 40, and 18%, respectively; $p = 0.001$) (44). However, it is important to note that the CT attenuation value of a plaque may be influenced by various factors, including the concentration of the contrast agent, plaque burden, slice thickness, image noise, and tube voltage (46). Moreover, although fibrous tissue typically has higher attenuation values compared to lipids, there is a substantial overlap of densities often rendering their distinction from a CCTA impossible (47). Therefore, a reliable differentiation of lipid-rich and fibrous-rich plaques based on CCTA-attenuation remains challenging.

"Napkin-ring" sign. Refers to a specific plaque attenuation pattern with is a central area of low CCTA attenuation in contact with the arterial lumen surrounded by a ring-like higher attenuation plaque tissue (48). The central low attenuation corresponds to a large necrotic core, while the surrounding are of higher CCTA attenuation corresponds to fibrous plaque tissue, both of which are important predictors of plaque rupture (49). Napkin-ring sign is more frequent in thin cap fibroatheromas identified by optic coherence tomography (OCT) (41), and is strongly associated with future adverse cardiac events, independently from other high-risk plaque features (50). In a prospective study of 895 patients, the hazard ratio (HR) of ACS in patients with napkin-ring sign was 5.55 ($p < 0.001$) indicating a strong and statistically significant association (50). Although napkin ring signs seems to be a specific feature of rupture-prone plaques, its sensitivity remains relatively modest and thus, further in-depth analysis of plaque attenuation patterns is warranted.

Spotty calcifications are defined as <3 mm calcifications in plaques with a density of more than 130 Hounsfield units (51). Calcification marks local inflammation, which can exert mechanical effects on the plaque that make it susceptible to rupture (52). Spotty calcification has been associated with accelerated atherosclerosis progression in individuals with stable angina pectoris (53), while it has also been associated to culprit plaques in patients with ACS (54). In a study including 38 patients with ACS and 33 with stable angina pectoris, spotty calcification was significantly more frequent in ACS lesions (63 vs. 21%, $p < 0.001$), while large calcification was observed less frequently in ACS lesions than in stable angina (22 vs. 55%; $p < 0.05$) (43). An important limitation is that CCTA cannot visualize micro-calcifications that are smaller than 0.5 mm in diameter which are thought to be a common feature of unstable coronary lesions (55, 56).

Hemodynamic assessment

Fractional flow reserve

CCTA cannot reliably say whether a lesion is mild, moderate, or severe and thus, current research is focused on achieving a complementary functional assessment of coronary plaques that so far has been obtained by stress testing and invasive indices. If successful, it would tremendously improve the prognostic value of CCTA. Functional flow reserve (FFR) is defined as the ratio between the maximum achievable blood flow in the presence of coronary stenosis and the theoretical maximum flow if the stenosis was not present (57). FFR is measured invasively using pressure wires in the coronary arteries. Invasive FFR >0.75–0.8 indicates hemodynamically non-significant stenosis for which percutaneous coronary intervention can be deferred (58). Recent advantages have allowed a non-invasive calculation of FFR using

CCTA and computational fluid dynamics. A negative CT-FFR, i.e., a value above a specific cut-off, carries the promise of safely deferring invasive angiography in patients with stable angina (59). However, CT-FFR has its limitations and introduces an error of its own, while an evidence-based cut-off value for non-invasive FFR is yet to be defined. In a small study of almost 190 patients with suspected CAD and intermediate coronary lesions, CT-FFR >0.8 was used to defer invasive angiography; patients had no adverse events occurring during a median follow-up of 12 months (60). In another study of around 250 patients that presented with acute chest pain and no known CAD, revascularization was deferred when CT-FFR was >0.8 with no difference in occurrence of major adverse cardiac events (61). Current evidence suggests that a dichotomous decision can be made for CT-FFR higher than 0.80 as well as for values equal or lower than 0.70, whereas for the range between 0.71 and 0.80 remains a "gray zone" and referral to invasive angiography should be considered individually (62).

Myocardial perfusion

Another technique that can add functional information in CCT is myocardial computed tomography perfusion (CTP) (63). Moreover, dynamic CTP offers absolute quantification of myocardial blood flow, as in positron-emission tomography (PET) (64). Multicenter studies have demonstrated that myocardial CTP can provide incremental diagnostic value over CCTA alone for the identification of hemodynamically significant coronary artery disease (63, 65), similar to that of magnetic resonance perfusion (65). Additionally, dynamic CTP has been shown to be superior to machine learning empowered CT-FFR for identifying obstructive lesions (66). Dynamic myocardial CTP also has incremental predictive value over CCTA or clinical risk factors for the prediction of future major adverse cardiac events, allowing for improved risk stratification (67, 68). In one study, myocardial blood flow derived from dynamic CTP was the strongest predictor for major adverse cardiovascular events outperforming high risk plaque features and CT-FFR (69).

Endothelial shear stress

Endothelial shear stress (ESS) is the frictional force produced when blood flows through an artery and has proven to trigger biological signaling in the endothelium (70). Physiologic ESS, typically found in straight vascular regions, upregulates anti-inflammatory genes and is atheroprotective. Low ESS, often found at branch points, bifurcations, and regions of high curvature, initiates cellular pathways that promote inflammation and are considered to be atherogenic (71). Specifically in native arteries, low ESS has been associated with the initiation and progression of atherosclerosis, development of high-risk plaque characteristics, need for revascularization, and major adverse cardiovascular events (26, 72). In stented arteries, low ESS has been correlated with neo-intima hyperplasia and neo-atherosclerosis, which can ultimately lead to further adverse cardiovascular events, including stent restenosis (73, 74). ESS is a promising hemodynamic index that can be evaluated using CCTA and computational fluid dynamics. As the lower imaging resolution of CCTA can have an impact on the accuracy of the estimated ESS, higher-resolution models reconstructed from a fusion of CCTA with intravascular imaging techniques, such as intravascular ultrasound (IVUS) and OCT, have been developed (75). Studies using CCTA-based models have shown that ESS assessment can provide incremental value in discriminating coronary segments more likely to exhibit atherosclerotic disease progression (76). In the Exploring the Mechanism of Plaque Rupture in Acute Coronary Syndrome Using Coronary CT Angiography and Computational Fluid Dynamics (EMERALD) study including 72 patients with ACS that had previously underwent CCTA, hemodynamic assessment, including ESS evaluation, provided additional value in identification of high-risk plaques that had ultimately caused ACS (72). However, further information on the clinical utility of CCTA-ESS remains to be seen.

Perivascular adipose tissue

Recent evidence suggests that perivascular adipose tissue (PVAT) is linked to atherosclerosis as a key regulator and sensor of coronary inflammation (77, 78). PVAT lies in proximity with the vascular wall and plays an important role in the pathogenic process of atherosclerosis by regulating the local microenvironment through the release of a variety of substances, such as bioactive adipokines, cytokines, and chemokines (77, 79). Pericoronary fat attenuation index (FAI) is a novel CCTA-derived biomarker based on the concept that spatial changes in composition induced by inflammation cause a shift in CT attenuation toward more negative HU values (80). FAI is increased in patients with CAD compared to healthy individuals and is particularly increased around culprit lesions of patients presenting with ACS (80). In the Cardiovascular Risk Prediction using Computed Tomography (CRISP-CT) study, two independent cohorts with a total of 3,912 participants undergoing CCT were used to derive and validate the prognostic value of perivascular fat attenuation mapping (12). Based on the results, higher FAI values around proximal right coronary artery and left anterior descending artery were also associated with a higher risk for all-cause death and cardiac death (12). Finally, although FAI has been shown to be modifiable, as it decreased significantly when measured 5 weeks after an index event (80), whether risk-reduction therapies, such as statins, can reverse FAI is yet to be investigated. Future incorporation of CCT derived

TABLE 1 Cardiac computed tomography derived parameters: pros, cons, and clinical value.

Parameters	Pros	Cons	Clinical value
CACS	- Low radiation - No contrast - Quick - Inexpensive - Reproducible	- Unclear value of serial CCT assessments - Must consider pre-test probability of CAD	- Good correlation with long-term risk of cardiac events - Incremental predictive value on top of traditional risk factors
Anatomic assessment			
Stenosis and plaque volume	- Precise evaluation of presence and extent of non-obstructive lesions	- CCTA has moderate to high sensitivity and specificity in lesion severity	- Degree of stenosis correlates well with mortality risk - Severe plaque burden correlates with adverse cardiac outcomes - Plaque progression on serial CCTAs correlates with risk of ACS
High-risk plaque features		- Dynamic morphology of plaques not captured - Need to consider additional thrombophilic factors	- Predict plaque rupture/ erosion - Respond well to statin use
Positive remodeling			- Correlates with TCFA and culprit lesions in ACS
Low attenuation		- Influenced by contrast concentration, plaque burden, slice thickness, image noise, tube voltage - Challenging distinction of lipid vs. fibrous-rich plaques	- Lower attenuation in ruptured plaques and in ACS compared to stable lesions and stable angina
Napkin-ring sign	- Good specificity	- Modest sensitivity	- Correlates with TCFA and future cardiac events
Spotty calcification		- Micro-calcifications cannot be visualized with CCTA	- Correlates with accelerated CAD progression and culprit plaques in ACS
Hemodynamic assessment			
FFR	- Functional assessment of lesion	- Gray zone; No evidence-based cut-off value	- FFR > 0.75–0.8 indicates hemodynamically significant stenosis - Negative CT-FFR can safely defer invasive angiography
CTP	- Identification of of myocardial perfusion defects - Detection of hemodynamically significant stenosis		- Absolute quantification of myocardial blood flow similar to PET - Incremental diagnostic value over CCTA alone and CT-FFR for the identification of hemodynamically significant CAD - Incremental predictive value over CCTA, CT-FFR, or clinical risk factors for the prediction of future major adverse cardiac events
ESS		- Lower accuracy (except if CCTA is fused with intracoronary imaging techniques)	- In native arteries: associated with initiation and progression of atherosclerosis, development of high-risk plaques, need for revascularization, and major adverse events - In stented arteries: associated with neo-intima hyperplasia and neo-atherosclerosis
PVAT		- No data available regarding risk-reduction therapies (e.g., statins)	- Higher FAI associated with: ○ CAD ○ ACS culprit lesions ○ All-cause mortality ○ Cardiac mortality

CACS, Coronary artery calcium score; CCT, Cardiac computed tomography; CAD, Coronary artery disease; CCTA, Cardiac computed tomography angiography; ACS, Acute coronary syndromes; TCFA, thin cap fibroatheroma; FFR, Fractional flow reserve; CT-FFR, Computed tomography-FFR; CTP, Computed tomography perfusion; PET, Positron emission tomography; ESS, Endothelial shear stress; PVAT, Perivascular adipose tissue; FAI, Fat attenuation index.

indices describing perivascular adipose tissue inflammation may improve risk assessment in patients with CAD (Table 1).

Current limitations

Despite its many strengths, CCT for the evaluation of CAD has a few limitations. First, a variety of factors can introduce noise, therefore limiting image quality. Examples include increased heart rate, arrhythmias, high-density materials (e.g., calcium, stents), high body mass index, and poor patient cooperation (e.g., movement, inappropriate breath control). It is typical for calcifications to appear falsely enlarged due to blooming or partial volume artifacts and thus, result in overestimation of the extent of CAD (81). Studies have shown that CCT may provide conflicting results with overestimation or underestimation of the lumen area when compared to IVUS (82, 83). For these reasons, invasive coronary angiography remains the gold standard for coronary lesions and in many cases, CCT can only be used as a gatekeeper to more invasive testing. Additionally, different scanners, protocols, and technical parameters can lead to a variation of results and false interpretations (84). Regarding the use of CCT, another important concern is exposure to radiation and the risk of cancer (85). Furthermore, the contrast required for CCTA carries the risk of contrast-induced nephropathy (86). Finally, as CCT and CCTA are primarily anatomic modalities that assess coronary stenosis, plaque burden and characteristics, the addition of a functional test to increase diagnostic accuracy is often clinically useful (87, 88). In other words, a multimodality or hybrid imaging approach to CAD can be pursued in the appropriate clinical setting.

Cardiac computed tomography and "omics": Radiomics, proteomics, and lipidomics

The development of radiomics, as well as the integration of proteomics and lipidomics with CCT images, show promise for increased diagnostic and prognostic performance of CCT images, yielding potentially important clinical benefits. In fact, a radiomic-based machine learning model to identify advanced atheromatous lesions was found to be superior when compared to visual assessment (89). Similarly, in the CRISP-CT study, radiomic mapping of the perivascular fat was shown to offer incremental value for predicting adverse cardiac events compared to traditional risk profile assessment or presence of high-risk plaque features (90). Additionally, several studies have screened the proteome aiming to investigate whether specific proteins can relate to the presence or extent of coronary atherosclerosis. To illustrate, in a CCTA-based cohort, four proteins involved in vascular processes were found to be specifically associated with either low or high CAD burden (91). Similarly, other studies have assessed the association between lipid profiles with atherosclerotic plaque findings (92). In general, the new era of proteomics and lipidomics could provide a deeper insight to the atherosclerotic process beyond traditional risk factors as well as identify potential and novel treatment targets promising a more individualized patient care in the future.

Dual-energy and photon-counting computed tomography

In the past few years, new CCT techniques such as dual-energy CCT and photon-counting CCT have aimed at improving the spatial resolution and the contrast-to-noise ratio of CT scanners (93). Dual-energy CCT uses two CCT datasets acquired with different photon spectra and tube potentials. With regards to CAD, it can enhance luminal assessment, evaluation of atherosclerotic plaque composition and evaluation of myocardial perfusion (94). Future studies are still needed to ensure wide external validation and existence of incremental clinical value when compared to already established technology. Photon-counting CCT allow for direct detection of incident X-ray photons, in contrast to energy-integrating scanners (i.e., those currently used in clinical practice), which are based on light photon detectors that are converted to electric signals at scintillation layer (95). This allows for increased signal to noise ratio, which in turn allows for better image quality, decreased radiation doses and elimination of beam hardening artifacts. In addition, photon-counting CCT could enhance the ability of the CCT scanner to detect different combinations of contrast agents, such as atherosclerotic plaque-specific nanoparticles (96). Although photon-counting CCT holds a great promise for the future, its access is currently limited to a few centers, and many technical challenges still need to be overcome prior to wide implementation.

Conclusion and future perspectives

CCT has become more widely available and is currently viewed as a first-line diagnostic test CAD. In certain asymptomatic patients, it also provides improved risk stratification, guiding prevention of future adverse events. Further research on image processing could bridge the diagnostic accuracy gap between invasive and non-invasive coronary angiography in regards to grading of calcified plaques and hemodynamic evaluation of lesions. Evaluation of pericoronary fat inflammation could also be broadly adopted for the prediction of future adverse events. In addition, technologic developments aiming at reducing radiation (90) could result in the expansion of CCTA and

help clarify the role of serial scanning. New techniques, such as dual-energy CCT and photon-counting CCT also hold promise at achieving higher spatial resolution and improving contrast-to-noise ratio. Finally, incorporating CCT and CCTA with machine learning and computational fluid dynamics could lead to more precise and individualized risk assessment.

Author contributions

All authors contributed to the writing and revision of the manuscript and approved the final manuscript.

Funding

MINOCA-GR study (Role of CCT in the diagnostic evaluation and risk stratification of patients with myocardial infarction and non-obstructive coronary arteries), an investigator-initiated study, supported by Menarini Hellas S.A (Ref. No. 27.11.2020/72059).

Conflict of interest

The authors declare that the research was conducted in the absence of any commercial or financial relationships that could be construed as a potential conflict of interest.

Publisher's note

All claims expressed in this article are solely those of the authors and do not necessarily represent those of their affiliated organizations, or those of the publisher, the editors and the reviewers. Any product that may be evaluated in this article, or claim that may be made by its manufacturer, is not guaranteed or endorsed by the publisher.

References

1. Budoff MJ, Young R, Lopez VA, Kronmal RA, Nasir K, Blumenthal RS, et al. Progression of coronary calcium and incident coronary heart disease events: MESA (multi-ethnic study of atherosclerosis). *J Am Coll Cardiol.* (2013) 61:1231–9. doi: 10.1016/j.jacc.2012.12.035

2. Hoffmann U, Truong QA, Schoenfeld DA, Chou ET, Woodard PK, Nagurney JT, et al. Coronary CT angiography versus standard evaluation in acute chest pain. *N Engl J Med.* (2012) 367:299–308. doi: 10.1056/NEJMoa1201161

3. Investigators SCOT-HEART, Newby DE. Adamson PD, Berry C, Boon NA, Dweck MR, et al. Coronary CT angiography and 5-year risk of myocardial infarction. *N Engl J Med.* (2018) 379:924–33. doi: 10.1056/NEJMoa1805971

4. Douglas PS, Hoffmann U, Patel MR, Mark DB, Al-Khalidi HR, Cavanaugh B, et al. Outcomes of anatomical versus functional testing for coronary artery disease. *N Engl J Med.* (2015) 372:1291–300. doi: 10.1056/NEJMoa1415516

5. Group DT, Maurovich-Horvat P, Bosserdt M, Kofoed KF, Rieckmann N, Benedek T, et al. CT or invasive coronary angiography in stable chest pain. *N Engl J Med.* (2022). 386:1591–602. doi: 10.1056/NEJMoa2200963

6. Knuuti J, Wijns W, Saraste A, Capodanno D, Barbato E, Funck-Brentano C, et al. 2019 ESC Guidelines for the diagnosis and management of chronic coronary syndromes. *Eur Heart J.* (2020) 41:407–77. doi: 10.1093/eurheartj/ehz425

7. Min JK, Leipsic J, Pencina MJ, Berman DS, Koo BK, van Mieghem C, et al. Diagnostic accuracy of fractional flow reserve from anatomic CT angiography. *JAMA.* (2012) 308:1237–45. doi: 10.1001/2012.jama.11274

8. Marwan M. Computational fluid dynamics: can computed tomography imaging compete with cath-lab physiology? *Cardiovasc Res.* (2019) 115:e41–3. doi: 10.1093/cvr/cvz059

9. Lu G, Ye W, Ou J, Li X, Tan Z, Li T, et al. Coronary computed tomography angiography assessment of high-risk plaques in predicting acute coronary syndrome. *Front Cardiovasc Med.* (2021) 8:743538. doi: 10.3389/fcvm.2021.743538

10. Arbab-Zadeh A, Fuster V. From detecting the vulnerable plaque to managing the vulnerable patient: JACC state-of-the-art review. *J Am Coll Cardiol.* (2019) 74:1582–93. doi: 10.1016/j.jacc.2019.07.062

11. Mancio J, Oikonomou EK, Antoniades C. Perivascular adipose tissue and coronary atherosclerosis. *Heart.* (2018) 104:1654–62. doi: 10.1136/heartjnl-2017-312324

12. Oikonomou EK, Marwan M, Desai MY, Mancio J, Alashi A, Hutt Centeno E, et al. Non-invasive detection of coronary inflammation using computed tomography and prediction of residual cardiovascular risk (the CRISP CT study): a post-hoc analysis of prospective outcome data. *Lancet.* (2018) 392:929–39. doi: 10.1016/S0140-6736(18)31114-0

13. Agatston AS, Janowitz WR, Hildner FJ, Zusmer NR, Viamonte M Jr., Detrano R. Quantification of coronary artery calcium using ultrafast computed tomography. *J Am Coll Cardiol.* (1990) 15:827–32. doi: 10.1016/0735-1097(90)90282-T

14. Blankstein R, Gupta A, Rana JS, Nasir K. The implication of coronary artery calcium testing for cardiovascular disease prevention and diabetes. *Endocrinol Metab.* (2017) 32:47–57. doi: 10.3803/EnM.2017.32.1.47

15. Obaid DR, Calvert PA, Gopalan D, Parker RA, Hoole SP, West NE, et al. Atherosclerotic plaque composition and classification identified by coronary computed tomography: assessment of computed tomography-generated plaque maps compared with virtual histology intravascular ultrasound and histology. *Circ Cardiovasc Imaging.* (2013) 6:655–64. doi: 10.1161/CIRCIMAGING.112.000250

16. Sangiorgi G, Rumberger JA, Severson A, Edwards WD, Gregoire J, Fitzpatrick LA, et al. Arterial calcification and not lumen stenosis is highly correlated with atherosclerotic plaque burden in humans: a histologic study of 723 coronary artery segments using nondecalcifying methodology. *J Am Coll Cardiol.* (1998) 31:126–33. doi: 10.1016/S0735-1097(97)00443-9

17. Elias-Smale SE, Proenca RV, Koller MT, Kavousi M, van Rooij FJ, Hunink MG, et al. Coronary calcium score improves classification of coronary heart disease risk in the elderly: the Rotterdam study. *J Am Coll Cardiol.* (2010) 56:1407–14. doi: 10.1016/j.jacc.2010.06.029

18. Razavi A, Iftekhar Uddin S, Dardari Z, Berman D, Budoff M, Miedema M, et al. Coronary artery calcium for risk stratification of sudden cardiac death: the coronary artery calcium consortium. *JACC Cardiovasc Imaging.* (2022). doi: 10.1016/j.jcmg.2022.02.011

19. McClelland RL, Jorgensen NW, Budoff M, Blaha MJ, Post WS, Kronmal RA, et al. 10-year coronary heart disease risk prediction using coronary artery calcium and traditional risk factors: derivation in the MESA (multi-ethnic study of atherosclerosis) with validation in the HNR (Heinz Nixdorf Recall) Study and the DHS (Dallas Heart Study). *J Am Coll Cardiol.* (2015) 66:1643–53. doi: 10.1016/j.jacc.2015.08.035

20. Nakazato R, Gransar H, Berman DS, Cheng VY, Lin FY, Achenbach S, et al. Statins use and coronary artery plaque composition: results from the International Multicenter CONFIRM Registry. *Atherosclerosis.* (2012) 225:148–53. doi: 10.1016/j.atherosclerosis.2012.08.002

21. Gottlieb I, Miller JM, Arbab-Zadeh A, Dewey M, Clouse ME, Sara L, et al. The absence of coronary calcification does not exclude obstructive coronary artery disease or the need for revascularization in patients referred for conventional coronary angiography. *J Am Coll Cardiol.* (2010) 55:627–34. doi: 10.1016/j.jacc.2009.07.072

22. Min JK, Shaw LJ, Devereux RB, Okin PM, Weinsaft JW, Russo DJ, et al. Prognostic value of multidetector coronary computed tomographic angiography for prediction of all-cause mortality. *J Am Coll Cardiol.* (2007) 50:1161–70. doi: 10.1016/j.jacc.2007.03.067

23. Min JK, Dunning A, Lin FY, Achenbach S, Al-Mallah M, Budoff MJ, et al. Age- and sex-related differences in all-cause mortality risk based on coronary computed tomography angiography findings results from the International Multicenter CONFIRM (Coronary CT Angiography Evaluation for Clinical Outcomes: An International Multicenter Registry) of 23,854 patients without known coronary artery disease. *J Am Coll Cardiol.* (2011) 58:849–60. doi: 10.1016/j.jacc.2011.02.074

24. Miller JM, Rochitte CE, Dewey M, Arbab-Zadeh A, Niinuma H, Gottlieb I, et al. Diagnostic performance of coronary angiography by 64-row CT. *N Engl J Med.* (2008) 359:2324–36. doi: 10.1056/NEJMoa0806576

25. Senior R, Reynolds HR, Min JK, Berman DS, Picard MH, Chaitman BR, et al. Predictors of left main coronary artery disease in the ISCHEMIA trial. *J Am Coll Cardiol.* (2022) 79:651–61. doi: 10.1016/j.jacc.2021.11.052

26. Stone PH, Maehara A, Coskun AU, Maynard CC, Zaromytidou M, Siasos G, et al. Role of low endothelial shear stress and plaque characteristics in the prediction of nonculprit major adverse cardiac events: the PROSPECT Study. *JACC Cardiovasc Imaging.* (2018) 11:462–71. doi: 10.1016/j.jcmg.2017.01.031

27. Lee SE, Sung JM, Rizvi A, Lin FY, Kumar A, Hadamitzky M, et al. Quantification of coronary atherosclerosis in the assessment of coronary artery disease. *Circ Cardiovasc Imaging.* (2018) 11:e007562. doi: 10.1161/CIRCIMAGING.117.007562

28. Halon DA, Azencot M, Rubinshtein R, Zafrir B, Flugelman MY, Lewis BS. Coronary computed tomography (CT) angiography as a predictor of cardiac and noncardiac vascular events in asymptomatic type 2 diabetics: a 7-year population-based cohort study. *J Am Heart Assoc.* (2016) 5:e003226. doi: 10.1161/JAHA.116.003226

29. Laufer EM, Mingels AM, Winkens MH, Joosen IA, Schellings MW, Leiner T, et al. The extent of coronary atherosclerosis is associated with increasing circulating levels of high sensitive cardiac troponin T. *Arterioscler Thromb Vasc Biol.* (2010) 30:1269–75. doi: 10.1161/ATVBAHA.109.200394

30. Feng YJ, Chen C, Fallon JT, Lai T, Chen L, Knibbs DR, et al. Comparison of cardiac troponin I, creatine kinase-MB, and myoglobin for detection of acute ischemic myocardial injury in a swine model. *Am J Clin Pathol.* (1998) 110:70–7. doi: 10.1093/ajcp/110.1.70

31. Lee KK, Bularga A, O'Brien R, Ferry AV, Doudesis D, Fujisawa T, et al. Troponin-guided coronary computed tomographic angiography after exclusion of myocardial infarction. *J Am Coll Cardiol.* (2021) 78:1407–17. doi: 10.1016/j.jacc.2021.07.055

32. Thomsen C, Abdulla J. Characteristics of high-risk coronary plaques identified by computed tomographic angiography and associated prognosis: a systematic review and meta-analysis. *Eur Heart J Cardiovasc Imaging.* (2016) 17:120–9. doi: 10.1093/ehjci/jev325

33. Stone PH, Saito S, Takahashi S, Makita Y, Nakamura S, Kawasaki T, et al. Prediction of progression of coronary artery disease and clinical outcomes using vascular profiling of endothelial shear stress and arterial plaque characteristics: the PREDICTION Study. *Circulation.* (2012) 126:172–81. doi: 10.1161/CIRCULATIONAHA.112.096438

34. Arbab-Zadeh A, Nakano M, Virmani R, Fuster V. Acute coronary events. *Circulation.* (2012) 125:1147–56. doi: 10.1161/CIRCULATIONAHA.111.047431

35. Kim U, Leipsic JA, Sellers SL, Shao M, Blanke P, Hadamitzky M, et al. Natural history of diabetic coronary atherosclerosis by quantitative measurement of serial coronary computed tomographic angiography: results of the PARADIGM Study. *JACC Cardiovasc Imaging.* (2018) 11:1461–71. doi: 10.1016/j.jcmg.2018.04.009

36. Lee SE, Chang HJ, Sung JM, Park HB, Heo R, Rizvi A, et al. Effects of statins on coronary atherosclerotic plaques: the PARADIGM Study. *JACC Cardiovasc Imaging.* (2018) 11:1475–84. doi: 10.1016/j.jcmg.2018.04.015

37. Davies MJ. Acute coronary thrombosis–the role of plaque disruption and its initiation and prevention. *Eur Heart J.* (1995) 16(Suppl. L):3–7. doi: 10.1093/eurheartj/16.suppl_L.3

38. Arbab-Zadeh A, Fuster V. The myth of the "vulnerable plaque": transitioning from a focus on individual lesions to atherosclerotic disease burden for coronary artery disease risk assessment. *J Am Coll Cardiol.* (2015) 65:846–55. doi: 10.1016/j.jacc.2014.11.041

39. Nakamura M, Nishikawa H, Mukai S, Setsuda M, Nakajima K, Tamada H, et al. Impact of coronary artery remodeling on clinical presentation of coronary artery disease: an intravascular ultrasound study. *J Am Coll Cardiol.* (2001) 37:63–9. doi: 10.1016/S0735-1097(00)01097-4

40. Achenbach S, Ropers D, Hoffmann U, MacNeill B, Baum U, Pohle K, et al. Assessment of coronary remodeling in stenotic and nonstenotic coronary atherosclerotic lesions by multidetector spiral computed tomography. *J Am Coll Cardiol.* (2004) 43:842–7. doi: 10.1016/j.jacc.2003.09.053

41. Kashiwagi M, Tanaka A, Kitabata H, Tsujioka H, Kataiwa H, Komukai K, et al. Feasibility of noninvasive assessment of thin-cap fibroatheroma by multidetector computed tomography. *JACC Cardiovasc Imaging.* (2009) 2:1412–9. doi: 10.1016/j.jcmg.2009.09.012

42. Ito T, Terashima M, Kaneda H, Nasu K, Matsuo H, Ehara M, et al. Comparison of *in vivo* assessment of vulnerable plaque by 64-slice multislice computed tomography versus optical coherence tomography. *Am J Cardiol.* (2011) 107:1270–7. doi: 10.1016/j.amjcard.2010.12.036

43. Motoyama S, Kondo T, Sarai M, Sugiura A, Harigaya H, Sato T, et al. Multislice computed tomographic characteristics of coronary lesions in acute coronary syndromes. *J Am Coll Cardiol.* (2007) 50:319–26. doi: 10.1016/j.jacc.2007.03.044

44. Ozaki Y, Okumura M, Ismail TF, Motoyama S, Naruse H, Hattori K, et al. Coronary CT angiographic characteristics of culprit lesions in acute coronary syndromes not related to plaque rupture as defined by optical coherence tomography and angioscopy. *Eur Heart J.* (2011) 32:2814–23. doi: 10.1093/eurheartj/ehr189

45. Kim SY, Kim KS, Seung MJ, Chung JW, Kim JH, Mun SH, et al. The culprit lesion score on multi-detector computed tomography can detect vulnerable coronary artery plaque. *Int J Cardiovasc Imaging.* (2010) 26:245–52. doi: 10.1007/s10554-010-9712-2

46. Cademartiri F, Mollet NR, Runza G, Bruining N, Hamers R, Somers P, et al. Influence of intracoronary attenuation on coronary plaque measurements using multislice computed tomography: observations in an ex vivo model of coronary computed tomography angiography. *Eur Radiol.* (2005) 15:1426–31. doi: 10.1007/s00330-005-2697-x

47. Voros S, Rinehart S, Qian Z, Vazquez G, Anderson H, Murrieta L, et al. Prospective validation of standardized, 3-dimensional, quantitative coronary computed tomographic plaque measurements using radiofrequency backscatter intravascular ultrasound as reference standard in intermediate coronary arterial lesions: results from the ATLANTA (assessment of tissue characteristics, lesion morphology, and hemodynamics by angiography with fractional flow reserve, intravascular ultrasound and virtual histology, and noninvasive computed tomography in atherosclerotic plaques) I study. *JACC Cardiovasc Interv.* (2011) 4:198–208. doi: 10.1016/j.jcin.2010.10.008

48. Maurovich-Horvat P, Hoffmann U, Vorpahl M, Nakano M, Virmani R, Alkadhi H. The napkin-ring sign: CT signature of high-risk coronary plaques? *JACC Cardiovasc Imaging.* (2010) 3:440–4. doi: 10.1016/j.jcmg.2010.02.003

49. Finn AV, Nakano M, Narula J, Kolodgie FD, Virmani R. Concept of vulnerable/unstable plaque. *Arterioscler Thromb Vasc Biol.* (2010) 30:1282–92. doi: 10.1161/ATVBAHA.108.179739

50. Otsuka K, Fukuda S, Tanaka A, Nakanishi K, Taguchi H, Yoshikawa J, et al. Napkin-ring sign on coronary CT angiography for the prediction of acute coronary syndrome. *JACC Cardiovasc Imaging.* (2013) 6:448–57. doi: 10.1016/j.jcmg.2012.09.016

51. Ferencik M, Schlett CL, Ghoshhajra BB, Kriegel MF, Joshi SB, Maurovich-Horvat P, et al. A computed tomography-based coronary lesion score to predict acute coronary syndrome among patients with acute chest pain and significant coronary stenosis on coronary computed tomographic angiogram. *Am J Cardiol.* (2012) 110:183–9. doi: 10.1016/j.amjcard.2012.02.066

52. Mori H, Torii S, Kutyna M, Sakamoto A, Finn AV, Virmani R. Coronary artery calcification and its progression: what does it really mean? *JACC Cardiovasc Imaging.* (2018) 11:127–42. doi: 10.1016/j.jcmg.2017.10.012

53. Kataoka Y, Wolski K, Uno K, Puri R, Tuzcu EM, Nissen SE, et al. Spotty calcification as a marker of accelerated progression of coronary atherosclerosis: insights from serial intravascular ultrasound. *J Am Coll Cardiol.* (2012) 59:1592–7. doi: 10.1016/j.jacc.2012.03.012

54. Ehara S, Kobayashi Y, Yoshiyama M, Shimada K, Shimada Y, Fukuda D, et al. Spotty calcification typifies the culprit plaque in patients with acute myocardial infarction: an intravascular ultrasound study. *Circulation.* (2004) 110:3424–9. doi: 10.1161/01.CIR.0000148131.41425.E9

55. Burke AP, Weber DK, Kolodgie FD, Farb A, Taylor AJ, Virmani R. Pathophysiology of calcium deposition in coronary arteries. *Herz.* (2001) 26:239–44. doi: 10.1007/PL00002026

56. Joshi NV, Vesey AT, Williams MC, Shah AS, Calvert PA, Craighead FH, et al. 18F-fluoride positron emission tomography for identification of ruptured and high-risk coronary atherosclerotic plaques: a prospective clinical trial. *Lancet.* (2014) 383:705–13. doi: 10.1016/S0140-6736(13)61754-7

57. Pijls NH, Van Gelder B, Van der Voort P, Peels K, Bracke FA, Bonnier HJ, et al. Fractional flow reserve. A useful index to evaluate the influence of an epicardial coronary stenosis on myocardial blood flow. *Circulation.* (1995) 92:3183–93. doi: 10.1161/01.CIR.92.11.3183

58. Pijls NH, De Bruyne B, Peels K, Van Der Voort PH, Bonnier HJ, Bartunek JKJJ, et al. Measurement of fractional flow reserve to assess the functional severity of coronary-artery stenoses. *N Engl J Med.* (1996) 334:1703–8. doi: 10.1056/NEJM199606273342604

59. Jensen JM, Botker HE, Mathiassen ON, Grove EL, Ovrehus KA, Pedersen KB, et al. Computed tomography derived fractional flow reserve testing in stable patients with typical angina pectoris: influence on downstream rate of invasive coronary angiography. *Eur Heart J Cardiovasc Imaging.* (2018) 19:405–14. doi: 10.1093/ehjci/jex068

60. Norgaard BL, Hjort J, Gaur S, Hansson N, Botker HE, Leipsic J, et al. Clinical use of coronary CTA-derived FFR for decision-making in stable CAD. *JACC Cardiovasc Imaging.* (2017) 10:541–50. doi: 10.1016/j.jcmg.2015.11.025

61. Chinnaiyan KM, Safian RD, Gallagher ML, George J, Dixon SR, Bilolikar AN, et al. Clinical use of CT-derived fractional flow reserve in the emergency department. *JACC Cardiovasc Imaging.* (2020) 13:452–61. doi: 10.1016/j.jcmg.2019.05.025

62. Matsumura-Nakano Y, Kawaji T, Shiomi H, Kawai-Miyake K, Kataoka M, Koizumi K, et al. Optimal cutoff value of fractional flow reserve derived from coronary computed tomography angiography for predicting hemodynamically significant coronary artery disease. *Circ Cardiovasc Imaging.* (2019) 12:e008905. doi: 10.1161/CIRCIMAGING.119.008905

63. Nous FMA, Geisler T, Kruk MBP, Alkadhi H, Kitagawa K, Vliegenthart R, et al. Dynamic myocardial perfusion CT for the detection of hemodynamically significant coronary artery disease. *JACC Cardiovasc Imaging.* (2022) 15:75–87. doi: 10.1016/j.jcmg.2021.07.021

64. Branch KR, Haley RD, Bittencourt MS, Patel AR, Hulten E, Blankstein R. Myocardial computed tomography perfusion. *Cardiovasc Diagn Ther.* (2017) 7:452–62. doi: 10.21037/cdt.2017.06.11

65. Rief M, Chen MY, Vavere AL, Kendziora B, Miller JM, Bandettini WP, et al. Coronary artery disease: analysis of diagnostic performance of CT perfusion and MR perfusion imaging in comparison with quantitative coronary angiography and SPECT-multicenter prospective trial. *Radiology.* (2018) 286:461–70. doi: 10.1148/radiol.2017162447

66. Li Y, Yu M, Dai X, Lu Z, Shen C, Wang Y, et al. Detection of hemodynamically significant coronary stenosis: CT myocardial perfusion versus machine learning CT fractional flow reserve. *Radiology.* (2019) 293:305–14. doi: 10.1148/radiol.2019190098

67. Nakamura S, Kitagawa K, Goto Y, Omori T, Kurita T, Yamada A, et al. Incremental prognostic value of myocardial blood flow quantified with stress dynamic computed tomography perfusion imaging. *JACC Cardiovasc Imaging.* (2019) 12:1379–87. doi: 10.1016/j.jcmg.2018.05.021

68. van Assen M, De Cecco CN, Eid M, von Knebel Doeberitz P, Scarabello M, Lavra F, et al. Prognostic value of CT myocardial perfusion imaging and CT-derived fractional flow reserve for major adverse cardiac events in patients with coronary artery disease. *J Cardiovasc Comput Tomogr.* (2019) 13:26–33. doi: 10.1016/j.jcct.2019.02.005

69. Yu L, Lu Z, Dai X, Shen C, Zhang L, Zhang J. Prognostic value of CT-derived myocardial blood flow, CT fractional flow reserve and high-risk plaque features for predicting major adverse cardiac events. *Cardiovasc Diagn Ther.* (2021) 11:956–66. doi: 10.21037/cdt-21-219

70. Gijsen F, Katagiri Y, Barlis P, Bourantas C, Collet C, Coskun U, et al. Expert recommendations on the assessment of wall shear stress in human coronary arteries: existing methodologies, technical considerations, and clinical applications. *Eur Heart J.* (2019) 40:3421–33. doi: 10.1093/eurheartj/ehz551

71. Davies PF. Hemodynamic shear stress and the endothelium in cardiovascular pathophysiology. *Nat Clin Pract Cardiovasc Med.* (2009) 6:16–26. doi: 10.1038/ncpcardio1397

72. Lee JM, Choi G, Koo BK, Hwang D, Park J, Zhang J, et al. Identification of high-risk plaques destined to cause acute coronary syndrome using coronary computed tomographic angiography and computational fluid dynamics. *JACC Cardiovasc Imaging.* (2019) 12:1032–43. doi: 10.1016/j.jcmg.2018.01.023

73. Torii R, Stettler R, Raber L, Zhang YJ, Karanasos A, Dijkstra J, et al. Implications of the local hemodynamic forces on the formation and destabilization of neoatherosclerotic lesions. *Int J Cardiol.* (2018) 272:7–12. doi: 10.1016/j.ijcard.2018.06.065

74. Papafaklis MI, Bourantas CV, Theodorakis PE, Katsouras CS, Naka KK, Fotiadis DI, et al. The effect of shear stress on neointimal response following sirolimus- and paclitaxel-eluting stent implantation compared with bare-metal stents in humans. *JACC Cardiovasc Interv.* (2010) 3:1181–9. doi: 10.1016/j.jcin.2010.08.018

75. van der Giessen AG, Schaap M, Gijsen FJ, Groen HC, van Walsum T, Mollet NR, et al. 3D fusion of intravascular ultrasound and coronary computed tomography for *in-vivo* wall shear stress analysis: a feasibility study. *Int J Cardiovasc Imaging.* (2010) 26:781–96. doi: 10.1007/s10554-009-9546-y

76. Park JB, Choi G, Chun EJ, Kim HJ, Park J, Jung JH, et al. Computational fluid dynamic measures of wall shear stress are related to coronary lesion characteristics. *Heart.* (2016) 102:1655–61. doi: 10.1136/heartjnl-2016-309299

77. Oikonomou EK, West HW, Antoniades C. Cardiac computed tomography: assessment of coronary inflammation and other plaque features. *Arterioscler Thromb Vasc Biol.* (2019) 39:2207–19. doi: 10.1161/ATVBAHA.119.312899

78. Liu Y, Sun Y, Hu C, Liu J, Gao A, Han H, et al. Perivascular adipose tissue as an indication, contributor to, and therapeutic target for atherosclerosis. *Front Physiol.* (2020) 11:615503. doi: 10.3389/fphys.2020.615503

79. Antonopoulos AS, Margaritis M, Coutinho P, Shirodaria C, Psarros C, Herdman L, et al. Adiponectin as a link between type 2 diabetes and vascular NADPH oxidase activity in the human arterial wall: the regulatory role of perivascular adipose tissue. *Diabetes.* (2015) 64:2207–19. doi: 10.2337/db14-1011

80. Antonopoulos AS, Sanna F, Sabharwal N, Thomas S, Oikonomou EK, Herdman L, et al. Detecting human coronary inflammation by imaging perivascular fat. *Sci Transl Med.* (2017) 9:aal2658. doi: 10.1126/scitranslmed.aal2658

81. Li P, Xu L, Yang L, Wang R, Hsieh J, Sun Z, et al. Blooming artifact reduction in coronary artery calcification by a new de-blooming algorithm: initial study. *Sci Rep.* (2018) 8:6945. doi: 10.1038/s41598-018-25352-5

82. Fujimoto S, Kondo T, Kodama T, Fujisawa Y, Groarke J, Kumamaru KK, et al. A novel method for non-invasive plaque morphology analysis by coronary computed tomography angiography. *Int J Cardiovasc Imaging.* (2014) 30:1373–82. doi: 10.1007/s10554-014-0461-5

83. Conte E, Mushtaq S, Pontone G, Li Piani L, Ravagnani P, Galli S, et al. Plaque quantification by coronary computed tomography angiography using intravascular ultrasound as a reference standard: a comparison between standard and last generation computed tomography scanners. *Eur Heart J Cardiovasc Imaging.* (2020) 21:191–201. doi: 10.1093/ehjci/jez089

84. Ghekiere O, Salgado R, Buls N, Leiner T, Mancini I, Vanhoenacker P, et al. Image quality in coronary CT angiography: challenges and technical solutions. *Br J Radiol.* (2017) 90:20160567. doi: 10.1259/bjr.20160567

85. Einstein AJ, Henzlova MJ, Rajagopalan S. Estimating risk of cancer associated with radiation exposure from 64-slice computed tomography coronary angiography. *JAMA.* (2007) 298:317–23. doi: 10.1001/jama.298.3.317

86. Maaniitty T, Stenstrom I, Uusitalo V, Ukkonen H, Kajander S, Bax JJ, et al. Incidence of persistent renal dysfunction after contrast enhanced coronary CT angiography in patients with suspected coronary artery disease. *Int J Cardiovasc Imaging.* (2016) 32:1567–75. doi: 10.1007/s10554-016-0935-8

87. Schuijf JD, Wijns W, Jukema JW, Atsma DE, de Roos A, Lamb HJ, et al. Relationship between noninvasive coronary angiography with multi-slice computed tomography and myocardial perfusion imaging. *J Am Coll Cardiol.* (2006) 48:2508–14. doi: 10.1016/j.jacc.2006.05.080

88. Gaemperli O, Schepis T, Valenta I, Koepfli P, Husmann L, Scheffel H, et al. Functionally relevant coronary artery disease: comparison of 64-section CT angiography with myocardial perfusion SPECT. *Radiology.* (2008) 248:414–23. doi: 10.1148/radiol.2482071307

89. Kolossvary M, Karady J, Kikuchi Y, Ivanov A, Schlett CL, Lu MT, et al. Radiomics versus visual and histogram-based assessment to identify atheromatous lesions at coronary CT angiography: an *ex vivo* study. *Radiology.* (2019) 293:89–96. doi: 10.1148/radiol.2019190407

90. Oikonomou EK, Siddique M, Antoniades C. Artificial intelligence in medical imaging: a radiomic guide to precision phenotyping of cardiovascular disease. *Cardiovasc Res.* (2020) 116:2040–54. doi: 10.1093/cvr/cvaa021

91. Ferrannini E, Manca ML, Ferrannini G, Andreotti F, Andreini D, Latini R, et al. Differential proteomics of cardiovascular risk and coronary artery disease in humans. *Front Cardiovasc Med.* (2021) 8:790289. doi: 10.3389/fcvm.2021.790289

92. Nakazato R, Gransar H, Berman DS, Cheng VY, Lin FY, Achenbach S, et al. Relationship of low- and high-density lipoproteins to coronary artery plaque composition by CT angiography. *J Cardiovasc Comput Tomogr.* (2013) 7:83–90. doi: 10.1016/j.jcct.2013.01.008

93. Danad I, Fayad ZA, Willemink MJ, Min JK. New applications of cardiac computed tomography: dual-energy, spectral, and molecular CT imaging. *JACC Cardiovasc Imaging.* (2015) 8:710–23. doi: 10.1016/j.jcmg.2015.03.005

94. Si-Mohamed SA, Congi A, Ziegler A, Tomasevic D, Tatard-Leitman V, Broussaud T, et al. Early prediction of cardiac complications in acute myocarditis by means of extracellular volume quantification with the use of dual-energy computed tomography. *JACC Cardiovasc Imaging.* (2021) 14:2041–2. doi: 10.1016/j.jcmg.2021.04.008

95. Sandfort V, Persson M, Pourmorteza A, Noel PB, Fleischmann D, Willemink MJ. Spectral photon-counting CT in cardiovascular imaging. *J Cardiovasc Comput Tomogr.* (2021) 15:218–25. doi: 10.1016/j.jcct.2020.12.005

96. Si-Mohamed SA, Boccalini S, Lacombe H, Diaw A, Varasteh M, Rodesch PA, et al. Coronary CT angiography with photon-counting CT: first-in-human results. *Radiology.* (2022) 303:303–13. doi: 10.1148/radiol.211780

frontiers | Frontiers in Cardiovascular Medicine

TYPE Original Research
PUBLISHED 18 August 2022
DOI 10.3389/fcvm.2022.917026

OPEN ACCESS

EDITED BY
Michail Papafaklis,
University Hospital of Ioannina, Greece

REVIEWED BY
Alexandros Kasiakogias,
Royal Brompton Hospital,
United Kingdom
Harminder Gill,
King's College London,
United Kingdom

*CORRESPONDENCE
Minjie Lu
coolkan@163.com
Shoujun Li
drlishoujunfw@163.com

SPECIALTY SECTION
This article was submitted to Cardiovascular Imaging, a section of the journal Frontiers in Cardiovascular Medicine

RECEIVED 10 April 2022
ACCEPTED 26 July 2022
PUBLISHED 18 August 2022

CITATION
Zhuang B, Yu SQ, Feng Z, He F, Jiang Y, Zhao S, Lu M and Li S (2022) Left ventricular strain derived from cardiac magnetic resonance can predict outcomes of pulmonary valve replacement in patients with repaired tetralogy of Fallot.
Front. Cardiovasc. Med. 9:917026.
doi: 10.3389/fcvm.2022.917026

Left ventricular strain derived from cardiac magnetic resonance can predict outcomes of pulmonary valve replacement in patients with repaired tetralogy of Fallot

Baiyan Zhuang[1], Shiqin Yu[1], Zicong Feng[2], Fengpu He[3], Yong Jiang[4,5], Shihua Zhao[1], Minjie Lu[1,6]* and Shoujun Li[2]*

[1]Department of Magnetic Resonance Imaging, Cardiovascular Imaging and Intervention Center, Fuwai Hospital, State Key Laboratory of Cardiovascular Disease, National Center for Cardiovascular Diseases, Chinese Academy of Medical Sciences and Peking Union Medical College, Beijing, China, [2]Pediatric Cardiac Surgery Center, Fuwai Hospital, State Key Laboratory of Cardiovascular Disease, National Center for Cardiovascular Diseases, Chinese Academy of Medical Sciences and Peking Union Medical College, Beijing, China, [3]Department of Cardiovascular Surgery, The First Affiliated Hospital, Zhejiang University College of Medicine, Hangzhou, China, [4]Department of Echocardiography, Fuwai Hospital, State Key Laboratory of Cardiovascular Disease, National Center for Cardiovascular Diseases, Chinese Academy of Medical Sciences and Peking Union Medical College, Beijing, China, [5]Department of Echocardiography, Fuwai Hospital Chinese Academy of Medical Sciences, Shenzhen, China, [6]Key Laboratory of Cardiovascular Imaging (Cultivation), Chinese Academy of Medical Sciences, Beijing, China

Purpose: Several adults with repaired tetralogy of Fallot (rToF) undergo pulmonary valve replacement (PVR) to reduce the right ventricular volume and retain right ventricular function. However, there is currently no consensus on the ideal time for PVR surgery in asymptomatic patients with rTOF with pulmonary regurgitation (PR). Clinical outcomes after PVR are also indeterminate. Recently, myocardial strain and strain rate derived from cardiac magnetic resonance (CMR) feature tracking were found to be more sensitive to right ventricular dysfunction than conventional parameters and therefore may add prognostic value in patients with rToF. We aimed to analyze whether pre-PVR left ventricular (LV) strain and strain rate detected by CMR feature tracking are associated with midterm outcomes after PVR in patients with rToF.

Methods: Seventy-eight asymptomatic patients with rToF who required PVR due to moderate or severe PR were prospectively enrolled between January 2014 and June 2020. CMR cine sequences were obtained, and feature tracking parameters were measured preoperatively. Adverse events were documented during the follow-up. Receiver operating characteristic analysis was performed to determine the cutoff value. Kaplan–Meier curves were drawn with log-rank statistics; moreover, univariate and multivariate Cox proportional hazards regression analyses and Harrel C-indices were analyzed.

Results: During 3.6 ± 1.8 years of follow-up, 25 adverse events were recorded. Kaplan–Meier survival curves and univariate Cox analysis verified that patients with significantly reduced radial strain (RS), circumferential strain (CS), longitudinal strain (LS), RS rate at systole and diastole (RSRs and RSRe), and circumferential and LS rates at diastole (CSRe and LSRe) had worse event-free survival. After multivariate correction, only LS and LSRe remained significantly associated with adverse outcomes (hazard ratio = 1.243 [1.083–1.428] and 0.067 [0.017–0.258], respectively, all $p < 0.05$). The cutoff values of LS and LSRe were −12.30 (%) and 1.07 (s^{-1}), respectively.

Conclusion: The LV strain and strain rate prior to PVR are important prognostic factors for adverse events after PVR in rToF.

KEYWORDS

strain rate, strain, cardiac magnetic resonance imaging, pulmonary valve replacement, repaired tetralogy of Fallot

Introduction

Tetralogy of Fallot (ToF) is one of the most common types of congenital heart disease, affecting 356 per million live births (1). When surgical repair of ToF (rToF) is performed in early childhood, the natural history of the disease dramatically changes and survival in adulthood improves. However, pulmonary regurgitation (PR) usually occurs after rToF, leading to poor prognosis. There is 40–85% of patients who develop moderate to severe PR in 5–10 years after repair (2, 3). Pulmonary valve replacement (PVR) was introduced to reduce late complications, prior symptoms, and worsening function (4). Although an increasing number of studies have reported PVR as the treatment of choice for severe PR after rToF, the effects of PVR on ventricular remodeling remain controversial.

The guidelines issued by the AHA/ACC and ESC recommend the right and left ventricular end-diastolic volume index (RVEDVI and LVEDVI), tricuspid regurgitation (TR), arrhythmia, and other cardiac function and clinical parameters to determine the timing of PVR surgery (4, 5). The AHA/ACC recommends that adults with previous ToF and severe PR undergo PVR surgery when they have moderate to severe RV dysfunction or enlargement. ESC experts believed that normalization of RV size after reintervention is unlikely as soon as the end-systolic index exceeds 80 ml/m^2 and the end-diastolic volume index exceeds 160 ml/m^2; however, this cutoff for reintervention may not correlate with clinical benefit. A more sensitive parameter that can predict adverse outcomes at an earlier stage may help identify the optimal time for PVR surgery (6).

In comparison with the traditional measurements, including ejection function (EF) and ventricular volume, the myocardial strain detected by cardiac magnetic resonance (CMR) feature tracking, which reflects myocardial deformation, has added value to predict the outcome of various cardiovascular diseases (7, 8). Although without impaired EF, myocardial strain could still be a sensitive parameter for evaluating ventricular dysfunction and may add clinical value during follow-up (9).

Owing to ventricular coupling, LV strain is also implicated in RV volume overload (10). Thus, LV strain has the potential to provide valuable information prior to PVR. However, there is little data and no consensus on the use of CMR feature tracking to help determine the timing of surgical intervention for PR in patients with rToF (6).

To date, there have been studies comparing the changes in strain and strain rate before and after PVR (11–13) or the relationship between strain and ventricular function parameters (5, 14, 15); however, few of these studies analyzed the relationship between strain and post-PVR surgical outcomes. We aimed to comprehensively evaluate the predictive value of LV strain and strain rate using a custom feature-tracking algorithm applied to a conventional CMR cine in asymptomatic patients with rToF and PVR. We assumed that LV strain and strain rate could have a potential predictive value.

Materials and methods

Patient enrolment

This prospective study was conducted at our hospital. The study protocol was approved by the ethics committee of our hospital. All participants provided written informed consent prior to enrolment.

Data definition

Asymptomatic patients were defined as those who maintained a functional status in New York Heart Association

class I or II without arrhythmia or heart failure symptoms/signs that cause syncope (16).

The severity of PR was divided into absent, trivial, mild, moderate, and severe by transthoracic echocardiography (16). Patients underwent follow-up through either a clinic or *via* telephone inquiring with patients or their contacts every 3 months after enrolment. Adverse events that occurred after PVR surgery were recorded. Adverse events included sudden cardiac death (unexpected death either within 1 h of the onset of cardiac symptoms without progressive cardiac deterioration, when asleep, or within 24 h of last being seen alive) (17), cardiac transplantation, application of implantable cardioverter defibrillator (ICD) (18), heart failure (19), and arrhythmia-induced syncope ("syncope caused by arrhythmias" was adjudicated based on clinical symptom and ECG monitor). The syncope cases were defined position-independent, with few prodromal symptoms, and may occur with cyanosis, dyspnea, arrhythmias, weak heart sounds, and associated ECG-detected arrhythmias) (20, 21), reoperation for PVR, sustained atrial or ventricular arrhythmias analyzed by 24-h Holter monitoring (last $\geq$ 30s but not causing syncope), and cardiac catheterization ablation (22).

Inclusion and exclusion criteria

Patients with rToF who were candidates for PVR were initially screened for this study from January 2014 to June 2020. According to the indications for PVR in asymptomatic patients with moderate or severe PR after rToF recommended by Boston Children's Hospital in 2013 (22), asymptomatic patients with moderate to severe pulmonary valve regurgitation after rToF (regurgitation fraction by CMR $\geq$ 25%) meeting at least two of the following conditions were included: (1) RVEDVI $>$ 150 ml/m^2, (2) RV end-systolic volume index (RVESVI) $>$ 80 ml/m^2, (3) RVEF $<$ 47%, (4) LVEF $<$ 55%, (5) QRS duration $>$ 160 ms, (6) sustained tachyarrhythmia related to right heart volume load, and (7) the presence of other hemodynamically significant lesions.

The following exclusion criteria were established: (1) obvious symptoms, (2) the presence of residual severe right ventricle outflow tract obstruction (RVOTO; ECG calculated gradient $\geq$ 60 mmHg), (3) RV pressure surpassing or equal to LV pressure, (4) ICD insertion or history of PVR, (5) contraindications for CMR or surgery, and (6) incomplete or poor-quality CMR (9).

Standard imaging protocol

CMR examinations were performed on a 3.0 T system within 6 months prior to PVR surgery using a 3.0 T scanner (Ingenia, Philips Healthcare, Best, Netherlands) with front and back surface coils and retrospective ECG triggering for capture of the entire cardiac cycle by the same senior operator. Cine images were obtained using a balanced steady-state free precession (SSFP) sequence, including 2-chamber, 4-chamber, and short-axis acquisitions with 25 image frames per cardiac cycle. The short-axis scans covered the entire LV (nine slices; the following standard acquisition parameters used for routine clinical imaging were applied: field of view, 321 $\times$ 321 mm^2; matrix, 184 $\times$ 256; slice thickness, 6 mm; TR/TE/flip-angle: 3 ms/1.6 ms/45°; temporal resolution, 43 ms; and parallel acquisition technique factor, 2). The two-dimensional phase-contrast images perpendicular to the main pulmonary artery (PA) were used for quantification of the PR fraction (field of view, 350 $\times$ 321 mm^2; matrix, 140 $\times$ 123; slice thickness, 6 mm; TR/TE/flip-angle: 4.9 ms/2.9 ms/10°; parallel acquisition technique factor, 1).

Surgery

All PVR surgeries were completed under cardiopulmonary bypass with mild hypothermia or a beating heart (without right-to-left shunt) by the same surgeon. A longitudinal incision was made in the pulmonary artery trunk or the position where the patch was previously placed. The replacement valve was inserted in the orthotropic position.

Data analysis

The LV and RV cardiac function analysis and strain analysis were measured using CVI 42 software (Circle Cardiovascular Imaging Inc., Calgary, Canada) with the help of artificial intelligence (with more than 3 years of work experience and more than 600 cases of cardiac MRI analysis) (23). The endocardial and epicardial borders of the LV were semi-automatically defined using the AI function of the CVI following manual adjustments. Measurements included RA and LA volumes, diastolic and systolic RV and LV volumes, mass, ventricular stroke volumes, and EFs. The ventricular volumes and mass were indexed by body surface area (BSA) into RA volume index (RAVI), LA volume index (LAVI), LVEDVI, LV end-systolic volume index (LVESVI), indexed RVEDVI, and RVESVI. Heart rate and QRS duration were obtained using electrocardiography. The PR fraction was calculated from the CMR flow velocity mapping. The severity of RVOTO was reflected by the pulmonary artery systolic gradient from the ECG. RV mass/volume ratio was calculated to reflect the degree of right ventricular hypertrophy (RVH). The RV pressure was measured using TR.

The global cardiac strain and strain rate representing the average of the entire heart were calculated from CMR cine images using the mature feature tracking software CVI 42

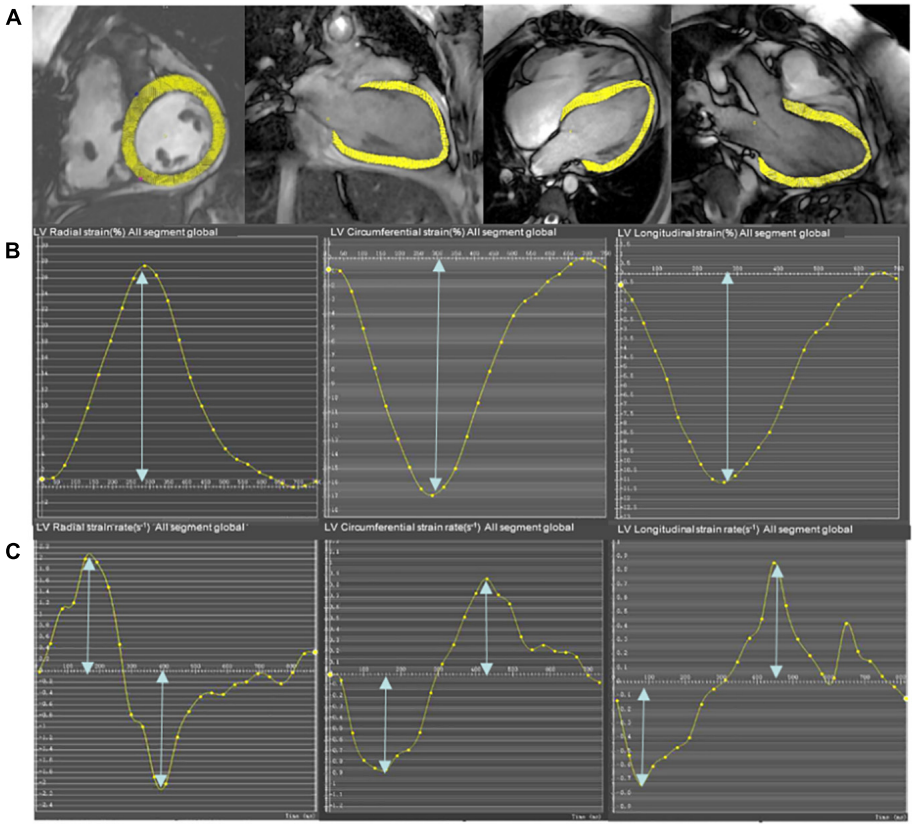

FIGURE 1
Representative short-axis and long-axis images **(A)**, strain curves **(B)**, and strain rate curves **(C)** in a participant who underwent pulmonary valve replacement (PVR). The epicardial and endocardial borders (excluding papillary muscles and trabeculae) at end-diastole are semi-manually defined in the LV 4-chamber, LV 2-chamber, and LV 3-chamber to calculate longitudinal strain and strain rate. The entire LV short-axis SSFP cine images are used to calculate radial and circumferential strain and strain rate.

version 5.12. The method has been described in detail in a previous study (15). In brief, the LV 4-chamber, LV 3-chamber, and LV 2-chamber were selected for post-processing to calculate the peak longitudinal strain (LS), peak systolic strain rate, and peak early diastolic strain rate (LSRe). The entire LV short-axis SSFP cine images were analyzed for radial strain (RS), circumferential strain (CS), peak systolic strain rate (RSRs and CSRs), and early diastolic strain rate (RSRe and CSRe). The endocardial and epicardial borders of the LV were semi-automatically defined using the AI function of the CVI following manual adjustments. The peak radial, circumferential, and LSs of the LV were identified as the highest or lowest peak of the global strain curve. Similarly, the peak systolic and early diastolic strain rates of the LV were calculated as the highest or lowest peak of the global strain rate curve (**Figure 1**) (24).

Inter- and intra-reproducibility

Intra- and inter-observer reliabilities were assessed in 20 randomly selected patients using Bland–Altman plots. Intra-observer reliability was derived from repeated measurements by one radiologist (**) after at least 1 week of blinding to previous results. Inter-observer reliability was independently assessed by two radiologists with more than 3 years of work experience and more than 650 cases of cardiac MRI analysis (** and AA), where one radiologist measured once and then a second radiologist measured again (blinded to the first radiologist's measurements).

Statistics

Statistical analyses were performed using SPSS Statistics (version 22.0; IBM Corp., Armonk, NY, United States) and MedCalc (version 18.2.1, Ostend, Belgium). Continuous data were descriptively reviewed and statistically analyzed using the Kolmogorov–Smirnov test to check for normality of the continuous variables. Continuous variables were described as means ± standard deviations or as median values with interquartile range, with respect to the normality of distribution. Comparisons between demographic and strain

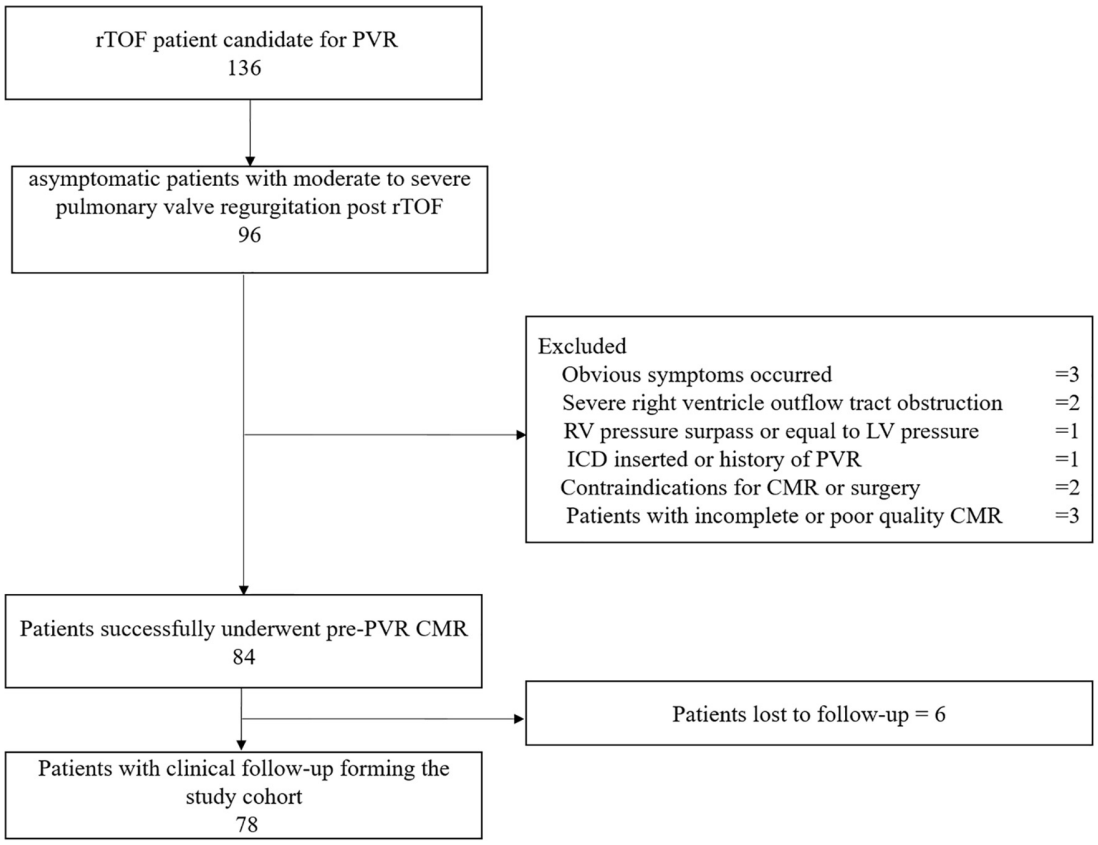

FIGURE 2
This flow chart shows the number of patients at each stage of the study. PVR, pulmonary valve replacement; ICD, implantable cardioverter defibrillator; ToF, Tetralogy of Fallot; CMR, cardiac magnetic resonance.

variables determined in the adverse event and non-adverse event groups were performed using either Student's *t*-test or Wilcoxon rank-sum test on the basis of whether the data were normally distributed (24). The Bonferroni method was used to correct multiple comparisons. Categorical variables were summarized by frequencies and percentages and compared between patients with and without the outcomes using the chi-squared test or Fisher's exact test.

To visualize the difference in event-free survival between different patient categories, Kaplan–Meier curves were drawn, followed by the log-rank test. The optimal preoperative strain and strain rate cutoffs were identified using receiver operating characteristic (ROC) curve analysis using the Youden index. The ROC curve was then drawn with the corresponding calculated area under the curve (AUC). The parameters satisfying the pH assumption were included in the univariate Cox regression analysis. Univariate Cox regression analysis was used to evaluate the predictive value of the strain and strain rate. Multivariate analysis Cox regression (forward LR) was performed for those parameters that were confirmed to be statistically significant in univariate analysis ($P < 0.05$) to identify the independent risk factors of prospective adverse events. Harrel C-indices were used to compare the relative predictive abilities of strain and strain rate. Statistical significance was set at $P < 0.05$.

Results

Characteristics of study participants

From January 2014 to June 2020, 78 asymptomatic patients with rToF with moderate or severe PR (21.5 years old, 44% male) were included for analysis with an average follow-up duration of 3.6 ± 1.8 years. The reasons for failure to be included are detailed in the study flowchart (**Figure 2**). The patients involved in our study did not have coronary artery anatomy abnormalities; only two patients had aortic arch abnormalities (patent ductus arteriosus). Demographic, surgical, ECG, and CMR parameters are summarized in **Table 1**. If appropriate, the parameters were indexed to BSA. On average, the age of the patients who underwent primary rToF was 3 (interquartile range [IQR]: 0–9) years. The most common approach was the transannular patch ($n = 56$). The mean QRS duration (150.78 ± 30.89 ms) was extended. On average,

TABLE 1 Baseline demographic, electrocardiographic and CMR parameters of the study subjects ($n = 78$).

Variable		
Male		44%
Height (cm)		1.53 ± 0.5
Weight (kg)		55.57 ± 15.52
Body surface area (m^2)		1.57 ± 0.27
Age at surgical repair (years)		3 (0–9)
Age at PVR (years)		21.5 (14–32)
Age at CMR (years)		21.5 (14–32)
Cardiac symptoms prior to PVR		63 (80.7%)
Transannular patch		56 (71.7%)
NYHA Class I or II prior to PVR		65 (83.3%)
NYHA Class III or IV prior to PVR		14 (17.9%)
Prescribed cardiac medications prior to PVR		9 (11.5%)
≥3previous cardiac operations		9 (11.5%)
Related familial genetic syndromes		5 (6.4%)
Valve types		
	Bioprosthesis	47 (60.2%)
	Homograft	12 (15.3%)
	mechanical valve	30 (38.5%)
Electrocardiogram		
	QRS duration (ms)	150.78 ± 30.89
	Heart rate (beats/min)	76.68 ± 14.55
	Sustained atrial arrhythmias prior to PVR	12 (15.3%)
	Sustained ventricular arrhythmias prior to PVR	0
Echocardiography		
	Tricuspid systolic pressure gradient (mmHg)	31.4 (25.5, 43.2)
	Tricuspid diastolic pressure gradient (mmHg)	2 (1.4, 3.2)
	Tricuspid systolic velocity (m/s)	2.8 (2.6, 3.275)
	Tricuspid diastolic velocity (m/s)	0.7 (0.6, 0.9)
	≤Mild tricuspid regurgitation	39 (50%)
	≥Moderate tricuspid regurgitation	34 (43.6%)
	Pulmonary valve systolic pressure gradient (mmHg)	15.2 (7.8, 25.5)
	Pulmonary valve diastolic pressure gradient (mmHg)	19.97 ± 8.6
	Pulmonary valve systolic velocity (m/s)	2.09 ± 0.72
	Pulmonary valve diastolic velocity (m/s)	2.3 (2, 3.15)
	≤Mild pulmonary valve regurgitation	0
	≥Moderate pulmonary valve regurgitation	78 (100%)
	Aortic valve systolic pressure gradient (mmHg)	3.6 (2.6, 4.8)
	Aortic valve diastolic pressure gradient (mmHg)	1 (0.875, 1.2)
	Aortic valve systolic velocity (m/s)	0.95 ± 0.25
	Aortic valve diastolic velocity (m/s)	0.9 (0.7, 1.8)
	≤Mild aortic valve regurgitation	14 (17.9%)
	≥Moderate aortic valve regurgitation	2 (2.6%)
CMR parameters pre-PVR		
	Pulmonary regurgitation fraction (%)	49.98 ± 18.58
	LV end-diastolic volume (ml)	142.01 ± 54.00
	LV end-systolic volume (ml)	75.51 ± 44.60
	LV ejection fraction (%)	50.47 ± 10.94
	LV mass-ED (g)	67.60 ± 26.64
	LVEDVI (ml/m^2)	89.98 ± 25.86
	LVESVI (ml/m^2)	47.48 ± 22.71

(Continued)

10.3389/fcvm.2022.917026

TABLE 1 Continued

Variable		
	RV end-diastolic volume (ml)	263.56 ± 91.42
	RV end-systolic volume (ml)	164.07 ± 72.53
	RV ejection fraction (%)	38.37 ± 12.53
	RVEDVI (ml/m^2)	168.80 ± 54.36
	RVESVI (ml/m^2)	104.42 ± 43.06
	RV mass-ED (g)	64.28 ± 30.22
	RV mass index (g/m^2)	41.12 ± 19.74
	RV mass/RV end-diastolic volume ratio (g/ml)	0.40 ± 0.20
	RV/LV end-diastolic volume ratio (g/ml)	2.00 ± 0.74
Additional procedures with PVR		
	Tricuspid repair	26 (33.3%)
	Patent ductus arteriosus cut and suture	2 (2.5%)
	Ventricular septal defect closure	13 (16.7%)
	Atrial septal defect closure	3 (3.8%)
	Pulmonary angioplasty	11 (14.1%)
	Right ventricular outflow tract muscle resection	7 (8.9%)
	Aortic valve replacement	5 (6.4%)
	Prior aortopulmonary shunt	1 (1.3%)
	Subaortic septum resection	2 (2.7%)

PVR, Pulmonary valve replacement; CMR, cardiac magnetic resonance imaging; LV, left ventricle; RV, right ventricular; LVEDVI, indexed LV end-diastolic volume; LVESVI, indexed LV end-systolic volume; RVEDVI, indexed RV end-diastolic volume; RVESVI, indexed RV end-systolic volume.

patients had slightly reduced LVEF (50.47 ± 10.94%) and RVEF (38.37 ± 12.53%). Meanwhile, the RVEDVI and RVESVI were significantly enlarged (168.8 ± 54.36 and 104.42 ± 43.06 ml/m^2, respectively). The mean PR fraction was 49.98 ± 18.58%.

Outcomes and cardiac magnetic resonance parameters

A total of 25 (32%) patients had noted adverse events (cardiovascular death, 3; ICD for ventricular tachycardia combined with atrioventricular block, 1; heart failure, 9; syncope caused by arrhythmias, 6; sustained atrial or ventricular arrhythmias, 4; and cardiac catheterization ablation for atrial fibrillation, 2), and 53 (68%) patients did not have any adverse events. Significant differences were noted between the two groups in LV RS, CS, and LS (all $p < 0.001$; Table 2 and Figure 3). The values in patients with adverse events were lower. Similarly, patients with adverse events noted tended to have lower absolute preoperative LV RSRs (1.37 ± 0.31 vs. 1.88 ± 0.59 s^{-1}, $p < 0.001$) and RSRe (−1.2 ± 0.57 vs. −2.28 ± 0.93 s^{-1}, $p < 0.001$). Furthermore, patients with adverse events noted had lower absolute preoperative CSRe (0.90 ± 0.26 vs. 1.23 ± 0.33 s^{-1}, $p < 0.001$) and LSRe (0.79 ± 0.31 vs. 1.34 ± 0.35 s^{-1}, $p < 0.001$) than those without adverse events. Significant differences were also observed in heart rate, age at surgical repair, age at PVR, LVEF, LVESVI, RVESVI, RV mass, and RV mass index between the two groups (Table 2). However, the QRS duration and PR fraction between the two groups did not exhibit a significant difference.

Predictors for adverse events

After ROC analysis, the corresponding cutoff values, sensitivity, specificity, and AUC of clinical parameters, different preoperative function parameters, strains, and strain rates for predicting adverse outcomes were obtained (Table 3). We found that the AUCs of the strain parameters were the best among the abovementioned parameters. The cutoff values of RS, CS, and LS were 22.2% (68.00% sensitivity, 92.45% specificity), −12.35% (88.00% sensitivity, 96.23% specificity), and −12.3% (96.00% sensitivity, 73.58% specificity), respectively. With regard to strain rates, the cutoff values of RSRs, RSRe, CSRe, and LSRe were 1.69 s^{-1} (92.00% sensitivity, 60.38% specificity), −1.65 s^{-1} (88.00% sensitivity, 75.47% specificity), 0.84 s^{-1} (56.00% sensitivity, 90.57% specificity), and 1.07 s^{-1} (92.00% sensitivity, 67.92% specificity), respectively. The AUCs of RS, CS, LS, RSRs, RSRe, CSRe, and LSRe were 0.863, 0.959, 0.916, 0.792, 0.889, 0.788, and 0.871, respectively (Figure 4 and Table 3).

The Kaplan–Meier survival curves (Figure 5) verified that patients with significantly reduced RS, CS, LS, RSRs, RSRe, CSRe, and LSRe had worse event-free survival than those who did not have a significant reduction. The 5-year event-free

10.3389/fcvm.2022.917026

TABLE 2 Comparison of baseline parameters and LV strain parameters (mean ± SD/median and interquartile range) between patients with or without adverse events.

Variable	Event ($n = 25$)	No event ($n = 53$)	*P-value*
Male	46%	44%	0.385
Age (years)	22.81 ± 10.62	29.12 ± 13.37	0.069
Height (cm)	1.62 ± 0.15	1.62 ± 0.13	0.730
Weight (kg)	55.08 ± 15.34	56.56 ± 16.13	0.648
Body surface area (m^2)	1.57 ± 0.28	1.58 ± 0.25	0.615
Age at surgical repair (years)	9 (3, 16)	2 (0, 7)	0.002
Age at PVR (years)	31 (16, 43)	20 (14, 28)	0.025
Age at CMR (years)	30 (15, 43)	20 (14, 27)	0.035
Predicted RV pressure by TR, mmHg	57.27 ± 14.95	53.74 ± 9.66	0.290
QRS duration (ms)	147.84 ± 31.1	156.56 ± 30.27	0.438
Heart rate (bpm)	74.5 ± 12.2	81.04 ± 17.86	0.034
Mean pulmonary valve area (mm^2)	9.01 ± 3.65	7.68 ± 3.59	0.043
Pulmonary regurgitation fraction (%)	52.95 ± 18.5	48.64 ± 18.65	0.645
Predicted RV pressure by TR (mmHg)	57.27 ± 14.95	53.74 ± 9.66	0.560
LV LGE	5 (24%)	2 (3.77%)	0.012
LAVI (ml/m^2)	47.6 (31.4, 68.0)	29.7 (23.2, 38.9)	<0.001
LVEDV (ml)	135.69 ± 50.7	154.65 ± 59.05	0.042
LVESV (ml)	69.65 ± 43.96	87.23 ± 44.38	0.020
LV ejection fraction (%)	53.21 ± 10.66	44.99 ± 9.51	0.001
LV mass at end-diastole (g)	65.49 ± 27.2	71.8 ± 25.49	0.152
LVEDVI (ml/m^2)	86.49 ± 21.04	96.97 ± 32.87	0.122
LVESVI (ml/m^2)	43.87 ± 20.5	54.7 ± 25.49	0.035
LV mass index (g/m^2)	44.81 ± 13.26	41.66 ± 12.76	0.186
LV mass/volume (g/ml)	0.5 ± 0.18	0.5 ± 0.15	0.868
RV LGE	1 (4%)	1 (1.89%)	0.547
RAVI (ml/m^2)	57.6 (35.4, 78.0)	39.7 (21.2, 52.9)	<0.001
RVEDV (ml)	258.99 ± 82.16	272.54 ± 108.54	0.609
RVESV (ml)	158.62 ± 66.33	174.75 ± 83.76	0.453
RV ejection fraction (%)	39.97 ± 12.19	35.24 ± 12.84	0.058
RVEDVI (ml/m^2)	165.76 ± 45.12	174.77 ± 69.69	0.500
RVESVI (ml/m^2)	100.21 ± 36.59	112.68 ± 53.4	0.034
RV mass (g)	68.59 ± 26.78	59.97 ± 33.66	0.045
RV mass index (g/m^2)	43.54 ± 15.94	38.69 ± 23.54	0.024
RV mass/RV end-diastolic volume ratio (g/ml)	0.27 ± 0.1	0.24 ± 0.14	0.053
RV/LV end-diastolic volume ratio (g/ml)	1.95 ± 0.75	2.04 ± 0.66	0.728
RS (%)	21.67 ± 5.06	31.85 ± 8.9	<0.001
CS (%)	−10.46 ± 2.11	−16.64 ± 2.91	<0.001
LS (%)	−8.36 ± 2.93	−14.04 ± 2.79	<0.001
RSRs (s^{-1})	1.37 ± 0.31	1.88 ± 0.59	<0.001
CSRs (s^{-1})	−0.76 (−0.66, −1.00)	−0.98 (−0.84, −1.14)	0.007
LSRs (s^{-1})	−0.66 ± 0.31	−1.35 (−0.79, −1.62)	<0.001
RSRe (s^{-1})	−1.2 ± 0.57	−2.28 ± 0.93	<0.001
CSRe (s^{-1})	0.90 ± 0.26	1.23 ± 0.33	<0.001
LSRe (s^{-1})	0.79 ± 0.31	1.44 (0.94, 1.63)	<0.001

PVR, Pulmonary valve replacement; CMR, cardiac magnetic resonance imaging; LV, left ventricle; RV, right ventricular; LVEDVI, indexed LV end-diastolic volume; LVESVI, indexed LV end-systolic volume; RVEDVI, indexed RV end-diastolic volume; RVESVI, indexed RV end-systolic volume; LGE, late gadolinium enhancement.

cumulative survival rates were 68.6, 91, and 94% for patients with a preoperative RS of > 22.2% ($p < 0.001$), preoperative CS of < −12.35% ($p < 0.001$), and preoperative LS of < −12.3% ($p < 0.001$), respectively. As for the strain rate, the 5-year event-free cumulative survival rates were 74, 82.4, and 65.2% for patients with a preoperative RSRs of > 1.69 s^{-1} ($p < 0.001$),

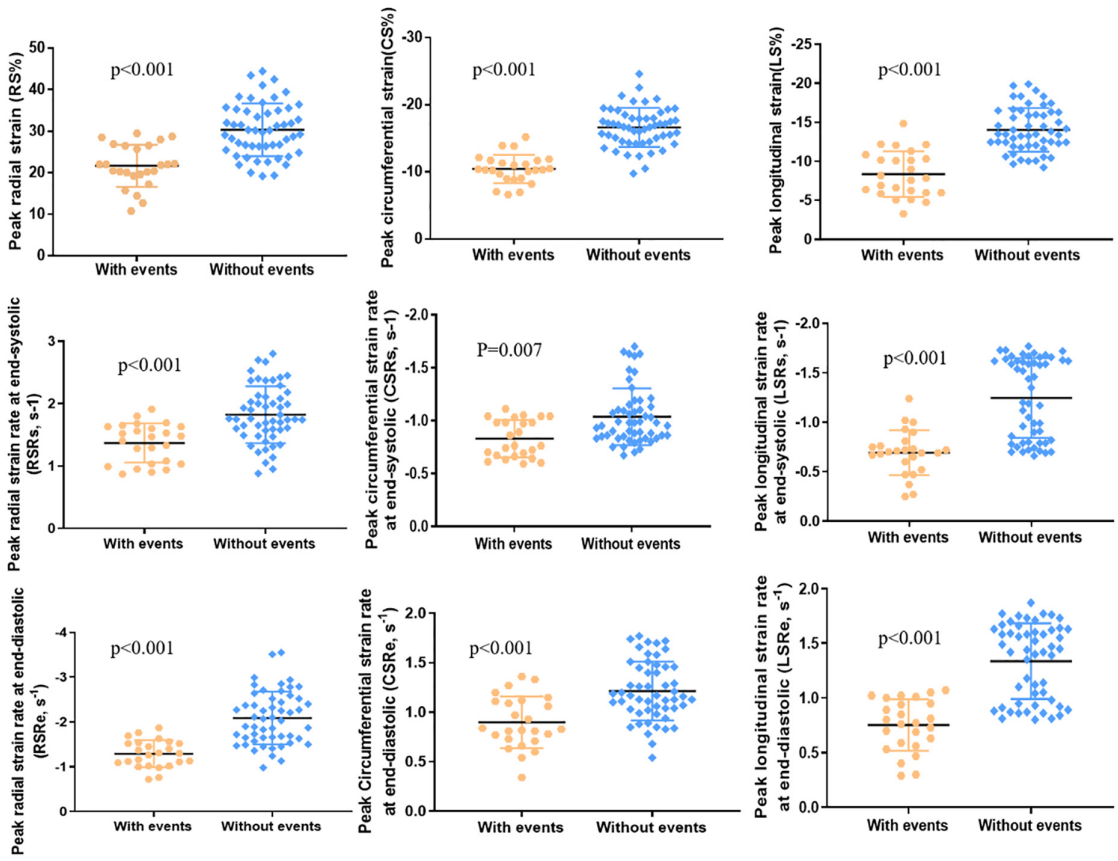

FIGURE 3
LV peak radial strain (RS), peak circumferential strain (CS), peak longitudinal strain (LS), peak radial strain rate at end-systole (RSRs), peak circumferential strain rate at end-systole (CSRs), peak longitudinal strain rate at end-systole (LSRs), peak radial strain rate at end-diastole (RSRe), peak circumferential strain rate at end-diastole (CSRe), and peak longitudinal strain rate at end-diastole (LSRe) in patients with adverse events ($n = 25$) and patients without adverse events ($n = 53$).

preoperative RSRe of $< -1.65\ s^{-1}$ ($p < 0.001$), and preoperative CSRe of $\geq 0.84\ s^{-1}$ ($p = 0.004$), respectively. The median survival time was 62% for patients with a preoperative LSRe of $> 1.07\ s^{-1}$ ($p < 0.001$).

In univariate Cox analysis, both strain (RS, CS, and LS) and strain rate (RSRs, RSRe, CSRe, and LSRe) were significantly associated with adverse outcomes in patients with rToF after PVR (Table 4). The HRs of RS, CS, LS, RSRs, RSRe, CSRe, and LSRe were 0.845, 1.336, 1.342, 0.198, 2.450, 0.199, and 0.053, respectively. The C-indices of RS, CS, LS, RSRs, RSRe, CSRe, and LSRe were 0.811, 0.826, 0.801, 0.73, 0.624, 0.805, 0.75, 0.683, and 0.834, respectively. After multivariate correction, the predictive values of preoperative LS and LSRe remained statistically significant. Specifically, multivariate Cox regression analysis identified LS (HR = 1.243 [1.083–1.428]) and LSRe (HR = 0.067 [0.017–0.258]) as strong predictors of adverse events (Table 5).

Regarding cardiac function parameters, in the univariate Cox analysis, RVESVI, LVEDVI, and LVESVI were associated with worse outcomes after PVR, whereas RVEDVI, RVEF, and LVEF were not. In addition to NYHA class III or IV prior to PVR, severe tricuspid regurgitation, ≥ 3 previous cardiac surgeries, sustained atrial arrhythmias prior to PVR, and the time interval between PVR and endpoint were related to adverse events after PVR (Table 4). However, after multiple multivariate corrections, only the predictive values of preoperative LS and LSRe remained significant (Table 5).

Intra- and inter-observer reliability

In a subgroup of 20 patients, reliability of strain was generally high with an intra-observer difference of approximately $0.01 \pm 0.28\%$–$0.12 \pm 0.26\%$, and an inter-observer difference of approximately $0.01 \pm 0.24\%$–$0.15 \pm 0.31\%$. Similarly, intra- and inter-observer differences were also small for strain rates (approximately 0.01 ± 0.35–$0.13 \pm 0.24\ s^{-1}$ and 0.01 ± 0.29–$0.10 \pm 0.30\ s^{-1}$, respectively; Bland–Altman plots are presented in Supplementary Figures 1, 2).

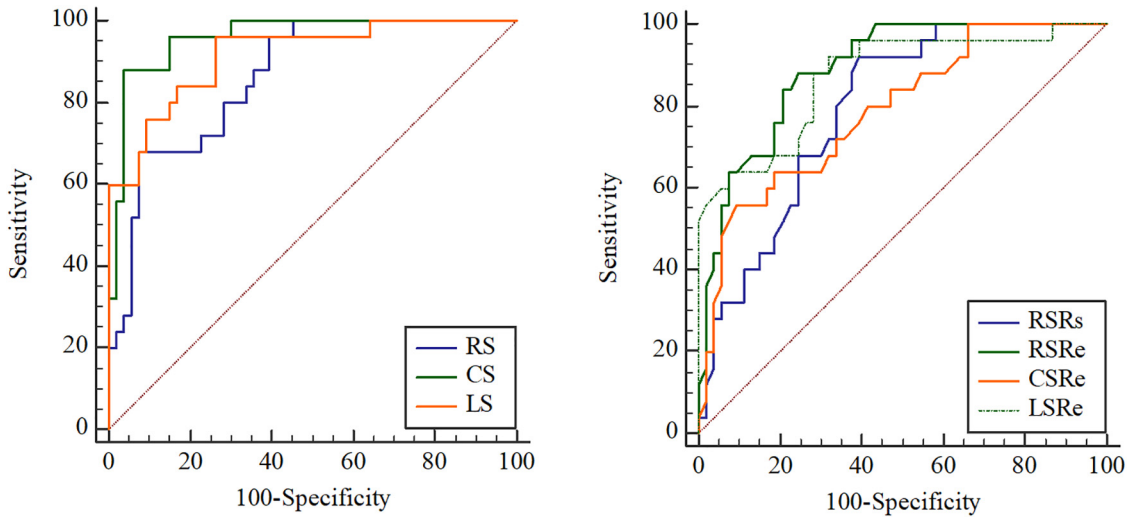

FIGURE 4
Receiver operating characteristic (ROC) curve analysis of the prognostic performance of peak radial strain (RS), peak circumferential strain (CS), peak longitudinal strain (LS), peak systole radial strain rate (RSRs), peak early diastole radial strain rate (RSRe), peak circumferential strain rate at end-diastole (CSRe), and peak early diastole longitudinal strain rate (LSRe) in asymptomatic patients with repaired tetralogy of Fallot (rToF) who required pulmonary valve replacement (PVR) for moderate or severe pulmonary regurgitation.

TABLE 3 Receiver operating characteristic (ROC) curve analysis.

Variable	AUC	Youden index J	Associated criterion	Sensitivity (%)	Specificity (%)	*P-value*
RS (%)	0.863 (0.766–0.93)	0.6045	≤22.20	68.00	92.45	<0.001
CS (%)	0.959 (0.888–0.99)	0.8423	>−12.35	88.00	96.23	<0.001
LS (%)	0.916 (0.831–0.96)	0.6958	>−12.30	96.00	73.58	<0.001
RSRs (s^{-1})	0.792 (0.685–0.87)	0.5238	≤1.69	92.00	60.38	<0.001
CSRs (s^{-1})	0.873 (0.779–0.93)	0.5902	>−0.78	76.00	83.02	<0.001
LSRs (s^{-1})	0.691 (0.576–0.79)	0.3857	>−0.79	48.00	90.57	<0.001
RSRe (s^{-1})	0.889 (0.798–0.94)	0.6347	>−1.65	88.00	75.47	<0.001
CSRe (s^{-1})	0.788 (0.681–0.87)	0.4657	≤0.84	56.00	90.57	<0.001
LSRe (s^{-1})	0.871 (0.775–0.93)	0.5992	≤1.07	92.00	67.92	<0.001
LVEDVI (ml/m^2)	0.596 (0.455–0.737)	0.2113	>97.48	40.00	81.13	0.181
LVESVI (ml/m^2)	0.635 (0.497–0.774)	0.2913	>51.07	48.00	81.13	0.055
RVEDVI (ml/m^2)	0.548 (0.403–0.693)	0.1223	>190.33	36.00	76.23	0.519
RVESVI (ml/m^2)	0.638 (0.498–0.778)	0.2226	>108.42	60.00	62.26	0.053
LV mass-ED (g)	0.58 (0.397–0.764)	0.1849	>62.00	60.00	58.49	0.374
LV mass/volume (g/ml)	0.475 (0.287–0.662)	0.1592	>0.44	48.00	67.92	0.778
RV mass-ED (g)	0.716 (0.558–0.873)	0.3358	>63.11	60.00	73.58	0.017
RV mass index (g/m^2)	0.763 (0.619–0.906)	0.4015	>35.81	76.00	64.15	0.004
RV mass/volume (g/ml)	0.743 (0.597–0.89)	0.2596	>0.18	92.00	33.96	0.007
RV/LV end-diastolic volume ratio	0.506 (0.317–0.695)	0.1623	≤1.04	20.00	96.23	0.948
Predicted RV pressure by TR (mmHg)	0.495 (0.326–0.664)	0.1693	>48.36	73.68	43.24	0.957
QRS duration (ms)	0.562 (0.374–0.749)	0.155	>166	37.50	78.00	0.494
Mean pulmonary valve area (mm^2)	0.609 (0.438–0.779)	0.2249	>8.25	64.00	58.49	0.229
Pulmonary regurgitation fraction (%)	0.473 (0.284–0.661)	0.1311	>67.26	22.73	90.38	0.761

RS, peak radial strain; CS, peak circumferential strain; LS, peak longitudinal strain; RSRs, peak systolic radial strain rate; RSRe, peak early diastolic radial strain rate; CSRs, peak systolic circumferential strain rate; CSRe, peak early diastolic circumferential strain rate; LSRs, peak systolic longitudinal strain rate; LSRe, peak early diastolic longitudinal strain rate; LVEDVI, indexed LV end-diastolic volume; LVESVI, indexed LV end-systolic volume; RVEDVI, indexed RV end-diastolic volume; RVESVI, indexed RV end-systolic volume; LGE, late gadolinium enhancement.

TABLE 4 Univariate associations of clinical and cardiac magnetic resonance (CMR) characteristics with adverse events.

Predictors	Exp (B)	95.0% CI for Exp (B)		*P-value*
		Lower	Upper	
RVEF (%)	0.981	0.953	1.011	0.208
RVEDVI (ml/m^2)	1.005	1.000	1.011	0.070
RVESVI (ml/m^2)	1.011	1.003	1.019	0.006
RAVI (ml/m^2)	1.010	0.958	1.035	0.136
RV LGE	1.625	0.870	3.846	0.145
LVEF (%)	0.979	0.953	1.005	0.109
LVEDVI (ml/m^2)	1.017	1.003	1.031	0.014
LVESVI (ml/m^2)	1.025	1.009	1.042	0.002
LAVI (ml/m^2)	1.007	0.998	1.015	0.116
LV LGE	1.971	0.778	4.997	0.153
BSA (m^2)	1.239	0.228	6.725	0.804
Heart rate beats (min)	1.022	0.99	1.055	0.174
QRSduration (ms)	1.006	0.994	1.018	0.366
Pulmonary regurgitation fraction (%)	1.013	0.991	1.035	0.262
Age at PVR (y)	1.023	0.989	1.058	0.181
Time interval between PVR and end point, y	0.827	0.77	0.888	<0.001
Age at surgical repair (y)	1.028	0.994	1.063	0.108
Time interval between rTOF and end point, y	1	0.998	1.002	0.843
mechanical valve	(−)	(−)	(−)	0.052
Bioprosthesis	2.919	0.971	8.774	0.056
Homograft	1.014	0.247	4.159	0.984
NYHA Class III or IV prior to PVR	3.829	1.711	8.572	0.001
Predicted RV pressure by TR (mmHg)	1.009	0.972	1.048	0.642
Servere tricuspid regurgitation	2.841	1.059	7.623	0.038
≥3previous cardiac operations	3.645	1.494	8.894	0.004
Pulmonary gradent at systolic (mmHg)	1.010	0.978	1.043	0.527
Presence of ventricular septum defect	0.619	0.230	1.662	0.341
Presence of associated anomalies	1.293	0.676	2.472	0.437
Related familial genetic syndromes	0.045	0	82.316	0.418
Sustained atrial arrhythmias before PVR	2.683	1.099	6.552	0.030
Sustained ventricular arrhythmias before PVR	/	/	/	/
LV mass/volume, g/ml	1.268	0.091	17.767	0.860
RV mass (g)	1.003	0.994	1.013	0.470
RV mass index (g/m^2)	1.003	0.990	1.017	0.625
RV mass/volume (g/ml)	0.831	0.052	13.143	0.895
RV/LV end-diastolic volume ratio	1.040	0.577	1.873	0.897
RS (%)	0.845	0.732	0.911	<0.001
CS (%)	1.336	1.199	2.091	<0.001
LS (%)	1.342	1.065	1.612	<0.001
RSRs (s^{-1})	0.198	0.026	0.871	0.002
CSRs (s^{-1})	18.406	2.195	154.379	0.007
LSRs (s^{-1})	14.898	4.320	51.373	<0.001
RSRe (s^{-1})	2.450	1.659	3.618	<0.001
CSRe (s^{-1})	0.199	0.061	0.643	0.007
LSRe (s^{-1})	0.053	0.016	0.176	<0.001

CI, confidence intervals; RS, peak radial strain; CS, peak circumferential strain; LS, peak longitudinal strain; RSRs, peak systolic radial strain rate; RSRe, peak early diastolic radial strain rate; CSRs, peak systolic circumferential strain rate; CSRe, peak early diastolic circumferential strain rate; LSRs, peak systolic longitudinal strain rate; LSRe, peak early diastolic longitudinal strain rate; LVEDVI, indexed LV end-diastolic volume; LVESVI, indexed LV end-systolic volume; RVEDVI, indexed RV end-diastolic volume; RVESVI, indexed RV end-systolic volume.

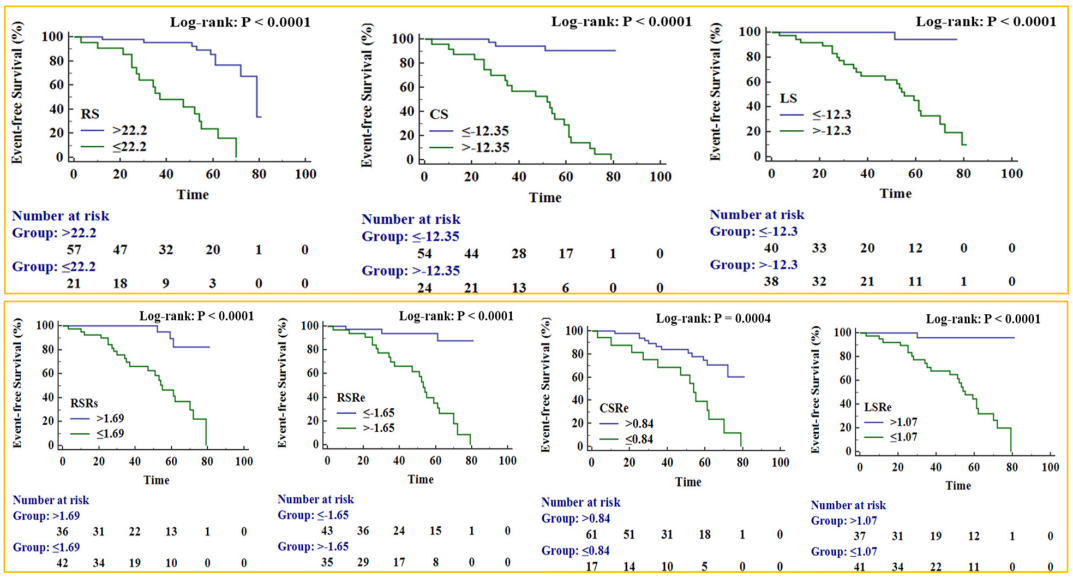

FIGURE 5
Kaplan–Meier survival curves for patient subgroups stratified by peak radial strain (RS), peak circumferential strain (CS), peak longitudinal strain (LS), peak systole radial strain rate (RSRs), peak early diastole radial strain rate (RSRe), peak circumferential strain rate at end-diastole (CSRe), and peak early diastole longitudinal strain rate (LSRe).

Discussion

In the present study, we found the following findings: (1) factors, including conventional volume parameters of both ventricles, ≥ 3 previous cardiac surgeries, severe TR, sustained atrial arrhythmias prior to PVR, and NYHA III/IV, were all associated with outcomes of PVR in patients with rToF; (2) preoperative LV RS, CS, LS, RSRs, CSRe, RSRe, and LSRe were significantly associated with adverse outcomes after PVR surgery in patients with rToF, suggesting that they serve as a novel index for risk stratification assessment in patients with rToF after PVR; and (3) multiple variable analysis demonstrated that patients with the highest incidence of adverse events were those with a severe reduction in LV LS and/or LSRe prior to PVR surgery.

Progressive PR is one of the most common complications occurring after rToF, despite the current treatment strategies used to treat ToF, demonstrating long-term survival (30-year survival rate between 68.5 and 90.5%) (25). In response to longstanding regurgitation, the RV progressively dilates to adapt to the increasing load (26), and the patients' exercise tolerance progressively reduces. In such situations, PVR is an effective method to help restore pulmonary valve function and improve cardiac function while alleviating symptoms (27). Our study confirmed for the first time that a severe decrease in RS, CS, LS, RSRs, RSRe, and LSRe was associated with an increase in the incidence of adverse outcomes during a midterm follow-up. Among these, LS and LSRe before PVR were the strongest risk factors for postoperative outcomes. After adjusting for other clinical and cardiac function parameters, these strain parameters maintained their prognostic values. This was supported by several CMR feature tracking-derived myocardial function indices, in which LSRe was utilized in the assessment of LV diastolic function and proved to be the most stable parameter with high reproducibility at both intra- and inter-observer levels (28).

Several factors influence the prognosis of PVR, most of which are clinical indicators or surgery-related factors. Jang et al. (29) conducted a retrospective study of 131 PVRs to explore the midterm clinical results of PVR after rToF. In univariate analysis, they found that the type of valve implanted, large valve implantation, and young age for rToF (<15 years) were risk factors for repeated PVR. Dorobantu et al. found that PVR after 35 years of age was associated with worse outcomes (30). In our study, we ascertained that the age for surgical repair of the ToF and PVR was significantly higher in patients with no events than in those with events; however, this difference did not affect the outcomes after PVR. Moreover, Jang et al. (29) found that the type of implanted valve and valve size were risk factors, whereas our study did not. The use of only biological valves may be the culprit, whereas, in our study, the patients used mechanical valves as well as homogenous valves, in addition to biological valves. We did not record this data in terms of valve size.

Furthermore, in our study, the pre-PVR LV and RVEF were not associated with adverse events, whereas previous studies, including the INDICTOR study (31), found that RVEF has a predictive value for mortality ($P = 0.03$). The reason may be that the RVEF values of our study, in both the event and no

TABLE 5 Multiple multivariable Cox to evaluate the associations of clinical and cardiac magnetic resonance (CMR) characteristics with adverse events.

	Exp(B)	95.0% CI for Exp(B)		*P-value*
		Lower	Upper	
RS (%)				
CS (%)				
LS (%)	1.243	1.083	1.428	0.002
RSRs (s^{-1})				
RSRe (s^{-1})				
CSRe (s^{-1})				
LSRe (s^{-1})	0.067	0.017	0.258	<0.001
LSRe (s^{-1})	0.067	0.017	0.258	<0.001
LS (%)	1.243	1.083	1.428	0.002
LVEDVI (ml/m^2)				
LVESVI (ml/m^2)				
RVEDVI (ml/m^2)				
RVESVI (ml/m^2)				
LSRe (s^{-1})	0.067	0.017	0.258	<0.001
LS (%)	1.243	1.083	1.428	0.002
RV mass-ED (g)				
RV mass index (g/m^2)				
RV mass/volume (g/ml)				
RV/LV end-diastolic volume ratio				
LSRe (s^{-1})	0.083	0.016	0.437	0.003
LS (%)	1.274	1.041	1.561	0.019
RVOT area (cm^2)				
Pulmonary regurgitation fraction (%)				
Predicted RV pressure by TR (mmHg)				
Severe tricuspid regurgitation				
LSRe (s^{-1})	0.066	0.017	0.262	<0.001
LS (%)	1.256	1.089	1.447	0.002
Age at surgical repair (years)				
Age at PVR (years)				
≥3previous cardiac operations				
Related familial genetic syndromes				
NYHA Class III or IV prior to PVR				
LSRe (s^{-1})	0.093	0.023	0.371	0.001
LS (%)	1.29	1.098	1.515	0.002
QRS duration (ms)				
Heart rate (beats/min)				
Sustained atrial arrhythmias prior to PVR				

Multivariate analysis Cox regression (forward LR) was carried out for those parameters who were confirmed statistically significant in univariate analysis and important function and clinical parameters. CI, confidence intervals; RS, peak radial strain; CS, peak circumferential strain; LS, peak longitudinal strain; RSRs, peak systolic radial strain rate; RSRe, peak early diastolic radial strain rate; CSRe, peak early diastolic circumferential strain rate; LSRe, peak early diastolic longitudinal strain rate; LVEDVI, indexed LV end-diastolic volume; LVESVI, indexed LV end-systolic volume; RVEDVI, indexed RV end-diastolic volume; RVESVI, indexed RV end-systolic volume.

event groups, were relatively low (<40%), and our study had a shorter average follow-up time (3.6 vs. 9.5 years). Similar to the INDICTOR study, we found that LVESVI and atrial arrhythmias prior to PVR are related to prognosis; however, we did not find the predicted value of the RV mass-to-volume ratio and RV systolic blood pressure, as mentioned in their study. In addition, we found that LVEDVI and RVESVI were correlated with prognosis, which is consistent with the findings of other studies. However, after incorporating the strain parameter into the multivariate analysis, the predictive value of these parameters ceased to exist.

Moreover, Roderick et al. found that prolonged QRS duration prior to PVR is the main determinant of the poor long-term follow-up outcome of patients with ToF (32); however, our study did not find such a result. Some studies found that VO^2 peak (%), which assesses the degree of exercise tolerance, may be a useful predictor of adverse events after PVR (33, 34). Although we were not able to obtain the results of the cardiopulmonary exercise experiment, we also concluded that patients with NYHA III/IV have a poor prognosis based on the NYHA classification, which correlates with the study conducted by Anna et al. (35). Anna et al. also found that ≥ 3 previous cardiac surgeries were associated with worse outcomes, which is consistent with the findings of our study. Their study also found that older age at rToF and greater BSA at PVR were factors influencing poor prognosis; however, this phenomenon was not observed in our study.

One study demonstrated that in multivariate analysis, severe preoperative TR (HR = 2.49; 95% confidence interval [CI], 1.11–5.52), right ventricular end-systolic volume (HR = 1.02; 95% CI, 1.01–1.03), and age at PVR can predict adverse events (36). However, in our study, the value of severe preoperative TR and right ventricular end-systolic volume to predict adverse events was only found in the univariate analysis. In the multivariate analysis, these parameters were not useful. Age at PVR was not significantly different between univariate and multivariate analyses.

This study had some limitations that must be highlighted. For instance, our study was conducted in one medical center with a relatively small sample size; thus, in addition to GLS, the feasibility of other parameters, such as GCS, should be further explored. Large-sample multicenter studies with possible confounders are required to validate and improve the power of assessing events. Another limitation of the study is the cardiac endpoint utilized, which includes a wide range of heterogeneous events from hard to softer ones. Moreover, it was determined that the number of outcomes was modest, although this is the largest study of patients with rToF after PVR (31). The number of hard events was small because the sample size was small, and contrastingly, partly because the cardiac function of such patients significantly improved after PVR (13). In addition, due to limited research conditions, we did not report inter-study reproducibility. However, inter-study reproducibility of strain measured by CMR feature tracking has been reported in a

previous study, showing a satisfactory coefficient of variation and intraclass correlation coefficient (37). Lastly, it was shown that significant differences were noted in all strain and strain rate values between different vendors. Because we only provided the strain and strain rate data of the Circle CVI software (38), the data of other vendors, such as TomTec Arena, QStrain Medis, and Segment Medviso, still need to be further supplemented by other studies.

In conclusion, PVR in patients with rToF has relatively low mortality and fewer adverse events. Preoperative LV RS, CS, LS, RSRs, RSRe, CSRe, and LSRe were significantly associated with adverse outcomes after PVR. In particular, LS and LSRe assessed with CMR are independent predictors of survival in patients with rToF after PVR and offer incremental information for risk stratification beyond clinical parameters, biomarkers, and standard CMR parameters.

Data availability statement

The raw data supporting the conclusions of this article will be made available by the authors, without undue reservation.

Ethics statement

The studies involving human participants were reviewed and approved by Fuwai Hospital Ethics Department. Written informed consent to participate in this study was provided by the participants or their legal guardian/next of kin.

Author contributions

SZ, SL, and ML: guarantors of integrity of entire study. BZ, SY, ZF, and ML: literature research. BZ, SY, FH, and YJ: clinical studies. BZ and ML: statistical analysis. BZ, SZ, SL, and ML: manuscript editing. All authors have study concepts/study design or data acquisition or data analysis/interpretation, manuscript drafting or manuscript revision for important intellectual content, approval of final version of submitted manuscript, and agreed to ensure any questions related to the work are appropriately resolved.

Funding

This work was supported by the Construction Research Project of the Key Laboratory (Cultivation) of Chinese Academy of Medical Sciences (2019PT310025), the National Natural Science Foundation of China (81971588), the Youth Key Program of High-level Hospital Clinical Research (2022-GSP-QZ-5), the Capital Health Research and Development of Special (2020-2-4034), and the Clinical and Translational Fund of Chinese Academy of Medical Sciences (2019XK320063). The Capital Health Research and Development of Special Fund (2022-1-4032, SL).

Conflict of interest

The authors declare that the research was conducted in the absence of any commercial or financial relationships that could be construed as a potential conflict of interest.

Publisher's note

All claims expressed in this article are solely those of the authors and do not necessarily represent those of their affiliated organizations, or those of the publisher, the editors and the reviewers. Any product that may be evaluated in this article, or claim that may be made by its manufacturer, is not guaranteed or endorsed by the publisher.

Supplementary material

The Supplementary Material for this article can be found online at: https://www.frontiersin.org/articles/10.3389/fcvm.2022.917026/full#supplementary-material

SUPPLEMENTARY FIGURE 1
Bland–Altman analysis for intra-observer reproducibility of strain and strain rate (the blue line indicates the mean value; the dashed red line indicates 95% CI).

SUPPLEMENTARY FIGURE 2
Bland–Altman analysis for inter-observer reproducibility of strain and strain rate (the blue line indicates the mean value; the dashed red line indicates 95% CI).

References

1. Hoffman JI, Kaplan S. The incidence of congenital heart disease. *J AmColl Cardiol.* (2002) 39:1890–900. doi: 10.1016/S0735-1097(02)01886-7

2. Mercer-Rosa L, Yang W, Kutty S, Rychik J, Fogel M, Goldmuntz E. Quantifying pulmonary regurgitation and right ventricular function in surgically repaired tetralogy of Fallot: a comparative analysis of echocardiography and magnetic resonance imaging. *Circ Cardiovasc Imaging.* (2012) 5:637–43. doi: 10.1161/CIRCIMAGING.112.972588

3. Mouws EMJP, de Groot NMS, van de Woestijne PC, de Jong PL, Helbing WA, van Beynum IM, et al. Tetralogy of Fallot in the current era. *Semin Thorac Cardiovasc Surg.* (2019) 31:496–504. doi: 10.1053/j.semtcvs.2018.10.015

4. Stout KK, Daniels CJ, Aboulhosn JA, Bozkurt B, Broberg CS, Colman JM, et al. 2018 AHA/ACC Guideline for the management of adults with congenital heart disease: a report of the American college of cardiology/American heart association task force on clinical practice guidelines. *Circulation.* (2018) 139:e698–800. doi: 10.1161/CIR.0000000000000602

5. Baumgartner H, De Backer J, Babu-Narayan SV, Budts W, Chessa M, Diller GP, et al. 2020 ESC Guidelines for the management of adult congenital heart disease. *Eur Heart J.* (2021) 42:563–645. doi: 10.15829/1560-4071-2021-4702

6. Sabate Rotes A, Bonnichsen CR, Reece CL, Connolly HM, Burkhart HM, Dearani JA, et al. Long-term follow-up in repaired tetralogy of fallot: can deformation imaging help identify optimal timing of pulmonary valve replacement? *J Am Soc Echocardiogr.* (2014) 27:1305–10. doi: 10.1016/j.echo.2014.09.012

7. Buss SJ, Breuninger K, Lehrke S, Voss A, Galuschky C, Lossnitzer D, et al. Assessment ofmyocardial deformation with cardiac magnetic resonance strain imaging improves risk stratification in patients with dilated cardiomyopathy. *Eur Heart J Cardiovasc Imaging.* (2015) 16:307–15. doi: 10.1093/ehjci/jeu181

8. De Siqueira MEM, Pozo E, Fernandes VR, Sengupta PP, Modesto K, Gupta SS, et al. Characterization and clinical significance of right ventricular mechanics in pulmonary hypertension evaluated with cardiovascular magnetic resonance feature tracking. *J Cardiovasc Magn Reson.* (2016) 18:1–12. doi: 10.1186/s12968-016-0258-x

9. Kraigher-Krainer E, Shah AM, Gupta DK, Santos A, Claggett B, Pieske B, et al. Impaired systolic function by strain imaging in heart failure with preserved ejection fraction. *J Am Coll Cardiol.* (2014) 63:447–56. doi: 10.1016/j.jacc.2013.09.052

10. Menting ME, van den Bosch AE, McGhie JS, Eindhoven JA, Cuypers JA, Witsenburg M, et al. Assessment of ventricular function in adults with repaired Tetralogy of Fallot using myocardial deformation imaging. *Eur Heart J Cardiovasc Imaging.* (2015) 16:1347–57. doi: 10.1093/ehjci/jev090

11. Jing L, Wehner GJ, Suever JD, Charnigo RJ, Alhadad S, Stearns E, et al. Left and right ventricular dyssynchrony and strains from cardiovascular magnetic resonance feature tracking do not predict deterioration of ventricular function in patients with repaired tetralogy of Fallot. *J Cardiovasc Magn Reson.* (2016) 18:49. doi: 10.1186/s12968-016-0268-8

12. Schmidt B, Dick A, Treutlein M, Schiller P, Bunck AC, Maintz D, et al. Intra- and inter-observer reproducibility of global and regional magnetic resonance feature tracking derived strain parameters of the left and right ventricle. *Eur J Radiol.* (2017) 89:97–105. doi: 10.1016/j.ejrad.2017.01.025

13. Heng EL, Gatzoulis MA, Uebing A, Sethia B, Uemura H, Smith GC, et al. Immediate and midterm cardiac remodeling after surgical pulmonary valve replacement in adults with repaired tetralogy of Fallot: a prospective cardiovascular magnetic resonance and clinical study. *Circulation.* (2017) 136:1703–13. doi: 10.1161/CIRCULATIONAHA.117.027402

14. Monti CB, Secchi F, Capra D, Guarnieri G, Lastella G, Barbaro U, et al. Right ventricular strain in repaired tetralogy of Fallot with regards to pulmonary valve replacement. *Eur J Radiol.* (2020) 131:109235. doi: 10.1016/j.ejrad.2020.109235

15. Kutty S, Deatsman SL, Russell D, Nugent ML, Simpson PM, Frommelt PC, et al. Pulmonary valve replacement improves but does not normalize right ventricular mechanics in repaired congenital heart disease: a comparative assessment using velocity vector imaging. *J Am Soc Echocardiogr.* (2008) 21:1216–21. doi: 10.1016/j.echo.2008.08.009

16. He F, Feng Z, Chen Q, Jiao Y, Hua Z, Zhang H, et al. Whether pulmonary valve replacement in asymptomatic patients with moderate or severe regurgitation after tetralogy of fallot repair is appropriate: a case-control study. *J Am Heart Assoc.* (2019) 8:e010689. doi: 10.1161/JAHA.118.010689

17. Halliday BP, Baksi AJ, Gulati A, Ali A, Newsome S, Izgi C, et al. Outcome in dilated cardiomyopathy related to the extent, location, and pattern of late gadolinium enhancement. *JACC Cardiovasc Imaging.* (2019) 12(8 Pt. 2):1645–55. doi: 10.1016/j.jcmg.2018.07.015

18. Li ZL, He S, Xia CC, Peng WL, Li L, Liu KL, et al. Global longitudinal diastolic strain rate as a novel marker for predicting adverse outcomes in hypertrophic cardiomyopathy by cardiac magnetic resonance tissue tracking. *Clin Radiol.* (2021) 76:e19–78. doi: 10.1016/j.crad.2020.08.019

19. Stacey RB, Vera T, Morgan TM, Jordan JH, Whitlock MC, Hall ME, et al. Asymptomatic myocardial ischemia forecasts adverse events in cardiovascular magnetic resonance dobutamine stress testing of high-risk middle-aged and elderly individuals. *J Cardiovasc Magn Reson.* (2018) 20:75. doi: 10.1186/s12968-018-0492-5

20. Writing Committee Members, Shen WK, Sheldon RS, Benditt DG, Cohen MI, Forman DE, et al. 2017 ACC/AHA/HRS guideline for the evaluation and management of patients with syncope: a report of the American college of cardiology/American heart association task force on clinical practice guidelines and the heart rhythm society. *Heart Rhythm.* (2017) 14:e155–217. doi: 10.1016/j.hrthm.2017.03.004

21. Brignole M, Moya A, de Lange FJ, Deharo JC, Elliott PM, Fanciulli A, et al. 2018 ESC Guidelines for the diagnosis and management of syncope. *Eur Heart J.* (2018) 39:1883–948. doi: 10.5603/KP.2018.0161

22. Geva T. Indications for pulmonary valve replacement in repaired tetralogy of Fallot: the quest continues. *Circulation.* (2013) 128:1855–7. doi: 10.1161/CIRCULATIONAHA.113.005878

23. Zhuang B, Li S, Xu J, Zhou D, Yin G, Zhao S, et al. Age- and sex-specific reference values for atrial and ventricular structures in the validated normal chinese population: a comprehensive measurement by cardiac MRI. *J Magn Reson Imaging.* (2020) 52:1031–43. doi: 10.1002/jmri.27160

24. Zhuang B, Cui C, Sirajuddin A, He J, Wang X, Yue G, et al. Detection of myocardial fibrosis and left ventricular dysfunction with cardiac MRI in a hypertensive swine model. *Radiol Cardiothorac Imaging.* (2020) 2:e190214. doi: 10.1148/ryct.2020190214

25. van der Ven JPG, van den Bosch E, Bogers A, Helbing WA. Current outcomes and treatment of tetralogy of Fallot. *F1000Res.* (2019) 8:F1000 Faculty Rev-1530.

26. Scherptong RW, Mollema SA, Blom NA, Kroft LJ, de Roos A, Vliegen HW, et al. Right ventricular peak systolic longitudinal strain is a sensitive marker for right ventricular deterioration in adult patients with tetralogy ofFallot. *Int J Cardiovasc Imaging.* (2009) 25:669–76. doi: 10.1007/s10554-009-9477-7

27. Giardini A, Specchia S, Coutsoumbas G, Donti A, Formigari R, Fattori R, et al. Impact of pulmonary regurgitation and right ventricular dysfunction on oxygen uptake recovery kinetics in repaired tetralogy of Fallot. *Eur J Heart Fail.* (2006) 8:736–43. doi: 10.1016/j.ejheart.2006.01.012

28. Yim D, Mertens L, Morgan CT, Friedberg MK, Grosse-Wortmann L, Dragulescu A. Impact of surgical pulmonary valve replacement on ventricular mechanics in children with repaired tetralogy of Fallot. *Int J Cardiovasc Imaging.* (2017) 33:711–20. doi: 10.1007/s10554-016-1046-2

29. Jang W, Kim YJ, Choi K, Lim HG, Kim WH, Lee JR. Mid-term results of bioprosthetic pulmonary valve replacement in pulmonary regurgitation after tetralogy of Fallot repair. *Eur J Cardio Thorac Surg.* (2012) 42:e1–8. doi: 10.1093/ejcts/ezs219

30. Dorobantu DM, Sharabiani MTA, Taliotis D, Parry AJ, Tulloh RMR, Bentham JR, et al. Age over 35 years is associated with increased mortality after pulmonary valve replacement in repaired tetralogy of Fallot: results from the UK national congenital heart disease audit database. *Eur J Cardiothorac Surg.* (2020) 58:825–31. doi: 10.1093/ejcts/ezaa069

31. Geva T, Mulder B, Gauvreau K, Babu-Narayan SV, Wald RM, Hickey K, et al. Preoperative predictors of death and sustained ventricular tachycardia after pulmonary valve replacement in patients with repaired tetralogy of Fallot enrolled in the INDICATOR Cohort. *Circulation.* (2018) 138:2106–15. doi: 10.1161/CIRCULATIONAHA.118.034740

32. Scherptong RW, Hazekamp MG, Mulder BJ, Wijers O, Swenne CA, van der Wall EE, et al. Follow-up after pulmonary valve replacement in adults with tetralogy of Fallot: association between QRS duration and outcome. *J Am Coll Cardiol.* (2010) 56:1486–92. doi: 10.1016/j.jacc.2010.04.058

33. Hwang TW, Kim SO, Kim MS, Jang SI, Kim SH, Lee SY, et al. Short-Term change of exercise capacity in patients with pulmonary valve replacement after tetralogy of Fallot repair. *Korean Circ J.* (2017) 47:254–62. doi: 10.4070/kcj.2016.0226

34. Babu-Narayan SV, Diller GP, Gheta RR, Bastin AJ, Karonis T, Li W, et al. Clinical outcomes of surgical pulmonary valve replacement after repair of tetralogy of Fallot and potential prognostic value of preoperative cardiopulmonary exercise testing. *Circulation.* (2014) 129:18–27. doi: 10.1161/CIRCULATIONAHA.113.001485

35. Sabate Rotes A, Eidem BW, Connolly HM, Bonnichsen CR, Rosedahl JK, Schaff HV, et al. Long-term follow-up after pulmonary valve replacement in repaired tetralogy of Fallot. *Am J Cardiol.* (2014) 114:901–8. doi: 10.1016/j.amjcard.2014.06.023

36. Bokma JP, Winter MM, Oosterhof T, Vliegen HW, van Dijk AP, Hazekamp MG, et al. Severe tricuspid regurgitation is predictive for adverse events in tetralogy of Fallot. *Heart.* (2015) 101:794–9. doi: 10.1136/heartjnl-2014-306919

37. Morton G, Schuster A, Jogiya R, Kutty S, Beerbaum P, Nagel E. Inter-study reproducibility of cardiovascular magnetic resonance myocardial feature tracking. *J Cardiovasc Magn Reson.* (2012) 14:43. doi: 10.1186/1532-429X-14-43

38. Dobrovie M, Barreiro-Perez M, Curione D, Symons R, Claus P, Voigt JU, et al. Inter-vendor reproducibility and accuracy of segmental left ventricular strain measurements using CMR feature tracking. *Eur Radiol.* (2019) 29:6846–57. doi: 10.1007/s00330-019-06315-4

frontiers | Frontiers in Cardiovascular Medicine

TYPE Original Research
PUBLISHED 20 September 2022
DOI 10.3389/fcvm.2022.930015

OPEN ACCESS

EDITED BY
Italo Porto,
Università degli Studi di Genova, Italy

REVIEWED BY
Francesco Pelliccia,
Sapienza University of Rome, Italy
Jaroslaw Zalewski,
Jagiellonian University Medical College, Poland

*CORRESPONDENCE
Giovanni Luigi De Maria
Giovanniluigi.Demaria@ouh.nhs.uk

†These authors have contributed equally to this work and share first authorship

‡These authors have contributed equally to this work and share senior authorship

SPECIALTY SECTION
This article was submitted to Cardiovascular Imaging, a section of the journal Frontiers in Cardiovascular Medicine

RECEIVED 27 April 2022
ACCEPTED 25 August 2022
PUBLISHED 20 September 2022

CITATION
Kotronias RA, Fielding K, Greenhalgh C, Lee R, Alkhalil M, Marin F, Emfietzoglou M, Banning AP, Vallance C, Channon KM and De Maria GL (2022) Machine learning assisted reflectance spectral characterisation of coronary thrombi correlates with microvascular injury in patients with ST-segment elevation acute coronary syndrome. *Front. Cardiovasc. Med.* 9:930015. doi: 10.3389/fcvm.2022.930015

Machine learning assisted reflectance spectral characterisation of coronary thrombi correlates with microvascular injury in patients with ST-segment elevation acute coronary syndrome

Rafail A. Kotronias[1,2†], Kirsty Fielding[3†], Charlotte Greenhalgh[3], Regent Lee[4], Mohammad Alkhalil[2,5], Federico Marin[1], Maria Emfietzoglou[2], Adrian P. Banning[1], Claire Vallance[3‡], Keith M. Channon[1,2‡] and Giovanni Luigi De Maria[1,2*‡]

[1]Oxford Heart Centre, National Institute for Health and Care Research (NIHR) Biomedical Research Centre, Oxford University Hospitals, Oxford, United Kingdom, [2]Department of Cardiovascular Medicine, University of Oxford, Oxford, United Kingdom, [3]Department of Chemistry, University of Oxford, Oxford, United Kingdom, [4]Nuffield Department of Surgical Sciences, University of Oxford, Oxford, United Kingdom, [5]Cardiothoracic Centre, Freeman Hospital, Newcastle, Translational and Clinical Research Institute, Newcastle University, Newcastle upon Tyne, United Kingdom

Aims: We set out to further develop reflectance spectroscopy for the characterisation and quantification of coronary thrombi. Additionally, we explore the potential of our approach for use as a risk stratification tool by exploring the relation of reflectance spectra to indices of coronary microvascular injury.

Methods and results: We performed hyperspectral imaging of coronary thrombi aspirated from 306 patients presenting with ST-segment elevation acute coronary syndrome (STEACS). Spatially resolved reflected light spectra were analysed using unsupervised machine learning approaches. Invasive [index of coronary microvascular resistance (IMR)] and non-invasive [microvascular obstruction (MVO) at cardiac magnetic resonance imaging] indices of coronary microvascular injury were measured in a sub-cohort of 36 patients. The derived spectral signatures of coronary thrombi were correlated with both invasive and non-invasive indices of coronary microvascular injury. Successful machine-learning-based classification of the various thrombus image components, including differentiation between blood and thrombus, was achieved when classifying the pixel spectra into 11 groups. Fitting of the spectra to basis spectra recorded for separated blood components confirmed excellent correlation with visually inspected thrombi. In the 36

patients who underwent successful thrombectomy, spectral signatures were found to correlate well with the index of microcirculatory resistance and microvascular obstruction; R^2: 0.80, $p < 0.0001$, $n = 21$ and R^2: 0.64, $p = 0.02$, $n = 17$, respectively.

Conclusion: Machine learning assisted reflectance spectral analysis can provide a measure of thrombus composition and evaluate coronary microvascular injury in patients with STEACS. Future work will further validate its deployment as a point-of-care diagnostic and risk stratification tool for STEACS care.

KEYWORDS

coronary thrombus, STEACS, reflectance spectroscopy, machine learning, coronary microvascular injury, coronary microvascular dysfunction (CMD)

Introduction

ST-segment elevation acute coronary syndrome (STEACS) presentation is secondary to atherosclerotic plaque disruption (erosion or rupture) leading to a prothrombotic milieu with subsequent thrombotic occlusion of the culprit artery and consequent myocardial necrosis. The introduction of primary percutaneous coronary intervention (pPCI) services, has led to significant reductions in mortality following a STEACS (1). Despite prompt coronary blood flow restoration, subsequent cardiac failure is on the rise due to a variety of pathological mechanisms culminating into suboptimal downstream myocardium perfusion (1, 2). Coronary microvascular injury is a key mechanism of prognostic importance that is predominantly, yet not exclusively, related to atherothrombotic material embolisation following mechanical flow restoration (2–5).

Coronary thrombus aspiration with manual thrombectomy can be used in patients with high thrombus burden (6), with a patient level meta-analysis of randomised studies identifying a trend towards better clinical outcomes (7). Beyond its potential therapeutic role, thrombus retrieval may prove useful for stratified medicine approaches in STEACS care. Indeed, erythrocyte-rich, macroscopically red coronary thrombi were associated with worse reperfusion and a poorer clinical outcome compared to platelet-rich macroscopically white thrombi (8, 9). Despite its attractive simplicity, qualitative categorisation of thrombi to "white" and "red" is subjective and non-standardised and often not visually feasible as thrombi can present a mixed of "red" and "white" texture (10). Therefore, a quantitative analytical method that is systematic, reproducible and clinically feasible could serve as an important stratification tool for STEACS care during pPCI.

Our group has validated one such approach using reflectance spectroscopy (11). In brief, analysis of the spectrum of visible light reflected from a sample provides information about its molecular composition (12). We have shown that reflectance spectroscopy of the sample can rapidly (near real-time) and reliably identify visually red thrombi and can discriminate between patients with significant and insignificant microvascular injury (11). In this work, we expand our earlier work by spatially resolving the reflectance spectral analysis and using the well-known classification technique of *k*-means clustering (13) in order to automatically quantify the aspirated thrombus and characterise its composition on a pixel by pixel basis. We also explore the potential risk stratification role of reflectance spectroscopy by correlating the thrombus spectra with established invasive and non-invasive indices of coronary microvascular injury.

Materials and methods

Patients presenting with a STEMI between June 2012 and December 2020 at the Oxford Heart Centre were recruited in the prospective OxAMI (Oxford Acute Myocardial Infarction) cohort study (14). The current study includes prospectively enrolled participants who underwent manual thrombectomy during primary percutaneous coronary intervention (pPCI) followed by microvascular injury phenotyping (**Figure 1**). The detailed study flow diagram is shown in **Supplementary Figure 1**. The study protocol was approved by the local ethics committee (10/H0408/24) and conducted in accordance with the Declaration of Helsinki.

Abbreviations: MR, index of microcirculatory resistance; LV, left ventricular; MVO, microvascular obstruction; pPCI, primary percutaneous coronary intervention; STEACS, ST-segment elevation acute coronary syndrome.

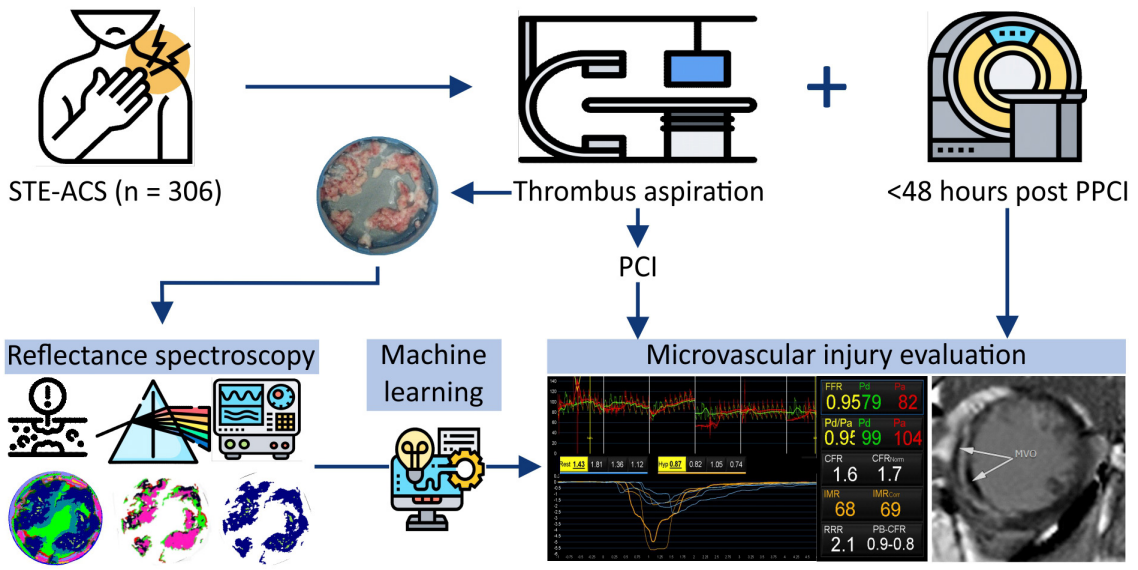

FIGURE 1
Experimental design.

Manual thrombectomy

Primary percutaneous coronary intervention was performed in standard fashion with the use of adjunctive manual thrombectomy at the operator's discretion in participants with high thrombus burden. After flow was established in the culprit artery with a 0.014' angioplasty wire, manual thrombectomy was performed using a conventional 6 French compatible thrombus aspiration catheter - Export (Medtronic), Vmax (Stron Medical), or Hunter (IHT Cordynamic). The chosen thrombectomy device was advanced proximal to the culprit lesion under fluoroscopic guidance and then manoeuvred gently forward and backward while vacuum-based-suction was applied with a 20 ml Luer-lock syringe connected to the proximal hub of the thrombectomy catheter. The aspirate was filtered using a 40 μm pore cell strainer (BD Falcon, Milan, Italy) and collected thrombotic debris was gently washed with normal saline to remove excess blood. The debris within the filter was frozen at −80°C. For this study, a thrombectomy was considered "successful" when the actual aspirated thrombus was representative of the expected thrombus based on the angiographic thrombus burden (see Section "Angiographic analysis").

Angiographic analysis

Intracoronary thrombus burden was angiographically evaluated in five grades after flow restoration as previously described (15). Thrombosis In Myocardial Infarction (TIMI) flow and myocardial blush were assessed as previously reported (16, 17).

Microvascular injury evaluation

Microvascular injury evaluation in OxAMI is performed by two modalities; invasive coronary physiology at the end of the pPCI and cardiac magnetic resonance imaging within 48 h following pPCI (4).

Invasive assessment of the infarct-related artery was performed with commercially available pressure wire technology (Pressure Wire X, Abbott, CA, United States or Certus, St. Jude Medical, MN, United States) and a thermodilution technique as previously described (**Supplementary material**). The index of microcirculatory resistance (IMR), a well-described index of microvascular injury in STEMI (14), was computed as:

$$IMR = hyperaemic\ Pd(mmHg)\ x\ average\ transit\ time\ (s)$$

where, *Pd* is the mean distal coronary pressure.

Based on established literature, *IMR* was dichotomized using the clinically significant threshold of 40 U (18).

Non-invasive evaluation by cardiac magnetic resonance imaging was performed as described previously (4) using a 3.0 Tesla scanner (either MAGNETOM TIM Trio or MAGNETOM Verio, Siemens Healthcare, Erlangen, Germany). Microvascular obstruction and infarct size were evaluated and quantified

by late gadolinium enhancement (LGE) (**Supplementary material**). The quantification of infarct size (IS) as a percentage of left ventricular (LV) mass, was performed by setting the signal intensity threshold at 5 standard deviations (SDs) above the mean signal intensity of the remote reference myocardium (19). Microvascular obstruction was identified as the hypointense area within the LGE region and quantified by manual delineation. MVO is expressed as a percentage of LV mass and was dichotomised using the prognostically significant threshold of 1.55% (20). Image analyses were performed on the Cvi42 image analysis software (Circle Cardiovascular Imaging Inc., Calgary, Canada).

Quantification of thrombus composition by hyperspectral imaging (Experiment A)

The experimental setup for the hyperspectral imaging measurements is shown in **Supplementary Figure 2**. The cell strainer containing the frozen thrombus sample was illuminated by four 20 W halogen lamps and the reflected light was imaged with the IMEC Snapscan Hyperspectral imaging camera (IMEC, Belgium). Typically, acquisition can be performed in approximately 1 min. For each pixel in the image, the reflected light intensity was recorded at 150 wavelengths across the range 470–900 nm (see **Supplementary material f**or further detail). Spectral images were also acquired for frozen samples of plasma and red blood cells, and for an empty filter and water ice. These were used as basis spectra in the fitting procedure described below.

Two distinct approaches were used to quantify the composition of the material imaged in each pixel based on the pixel's reflectance spectrum. In the first method, we used an unsupervised machine learning method known as *k*-means clustering (21, 22) to classify the pixels into a user-defined number of groups. Full details of this approach are provided in the **Supplementary material**. The outcome of this analysis is a set of characteristic "*k*-fractions" for each hyperspectral image, which quantify the spectral composition of pixels identified as thrombus.

In the second approach, we made the assumption that the spectrum for a given pixel can be written as a linear combination of the basis spectra $S_{plasma}(\lambda)$, $S_{RBCs}(\lambda)$, $S_{filter}(\lambda)$, and $S_{ice}(\lambda)$ recorded for plasma and red blood cells from healthy volunteer and for the filter base and water ice, respectively. The pixel spectra were fitted to the following expression:

$$S_{thrombus}(\lambda) = c_0 + c_{plasma}S_{plasma}(\lambda) + c_{RBCs}S_{RBCs}(\lambda) + c_{filter}S_{filter}(\lambda) + c_{ice}S_{ice}(\lambda). \quad (1)$$

where c_{plasma}, c_{RBCs}, c_{filter}, and c_{ice} are the fitting coefficients for each basis spectrum, proportional to the weighting of the relevant component in the measured spectrum, and c_0 is a constant offset. Within this analysis the composition of each pixel is characterised by the set of five fitting coefficients.

Correlation between thrombus spectral images and microvascular injury (Experiment B)

The relationship between spectral data (in the form of *k*-fractions f_k for each sample) and microvascular injury indices (IMR and MVO) was modelled by fitting the thrombus pixel data set to a range of linear and non-linear multiple linear regressions models. The four models used were:

$$y_{fit} = c_0 + c_1 f_1 + c_2 f_2 + \ldots + c_k f_k \quad (2)$$

$$y_{fit} = c_0 f_1^{c_1} f_1^{c_2} \ldots f_k^{c_k} \quad (3)$$

$$y_{fit} = c_0\, exp\{-(c_1 f_1 + c_2 f_2 + \ldots + c_k f_k)\} \quad (4)$$

$$y_{fit} = c_0[1 - exp\{-(c_1 f_1 + c_2 f_2 + \ldots + c_k f_k)\}] \quad (5)$$

where y_{fit} is the fitted value of MVO or IMR, f_k are the *k*-fractions extracted from the spectral image of the patient's thrombus sample, and c_k are fitting coefficients.

Initially, the above analysis was performed using data from all patients for whom thrombectomy had been attempted (see **Supplementary Figure 3**). However, it soon became apparent that in many cases sub-optimal thrombectomy was achieved such that the collected thrombus was only a small fraction of the total *in situ* coronary thrombus. The presence of these unrepresentative samples within the data set tends to mask the correlations under study to a significant degree. To address this, we developed a thresholding method (described in detail in the **Supplementary material**) to identify samples from patients for whom thrombectomy had been "successful," and repeated the analysis using only these patient samples ($n = 36$).

Statistical analysis

Following normality assumption evaluation, variables were expressed either as mean ± standard deviation or median (25th to 75th percentile) and categorical variables as numbers (percentage). Multiple linear regression analyses were performed to model the relationship between spectral data and microvascular injury indices. Goodness of fit was evaluated

using the co-efficient of determination (R^2). An R^2 value above 0.2 was considered biologically notable. All p-values are two-sided whilst $p < 0.05$ was considered statistically significant. All analyses were conducted in MATLAB 2020a (23).

Results

In experiment A, a total of 306 patients underwent manual thrombectomy during pPCI yielding a cohort with clinical and procedural characteristics representative of contemporary STEMI patients (Table 1). In experiment B, a cohort of $n = 36$ patients had microvascular injury evaluation and thrombus aspirate samples representative of the angiographic thrombus burden (Figure 2). The clinical and procedural characteristics were comparable to the wider cohort (Table 1).

TABLE 1 Clinical, procedural, and coronary microvascular injury characteristics.

	Experiment A	Experiment B
Total number	**306**	**36**
Clinical		
Age, years	62 ± 12	61 ± 11
Male gender, *n* (%)	251 (82)	28 (78)
Hypertension, *n* (%)	130 (42)	14 (39)
Hypercholesterolemia, *n* (%)	118 (39)	17 (49)
Diabetes, *n* (%)	43 (14)	4 (11)
Smoker, *n* (%)	211 (70)	31 (86)
Previous cardiology history, *n* (%)	54 (18)	3 (8)
Family history of IHD, *n* (%)	123 (40)	16 (44)
Procedural		
Ischemic time, minutes	262 (122, 273)	202 (101, 234)
Late presenter 6 h, *n* (%)	52 (17)	3 (8)
Culprit vessel		
LAD, *n* (%)	138 (45)	15 (42)
LCX, *n* (%)	31 (10)	1 (3)
RCA, *n* (%)	136 (44)	20 (55)
Angiographic thombus score > 3, *n* (%)	238 (82)	27 (85)
TIMI flow–pre-PCI, *n* (%)		
0	237 (78)	28 (78)
1	28 (9)	7 (19)
2	24 (8)	0 (0)
3	15 (5)	1 (3)
TIMI flow–post-PCI, *n* (%)		
0	0 (0)	0 (0)
1	3 (1)	0 (0)
2	44 (14)	2 (6)
3	258 (85)	34 (94)
Myocardial blush grade, *n* (%)		
0	12 (4)	3 (9)
1	28 (10)	3 (9)
2	164 (56)	17 (52)
3	86 (30)	10 (30)
GpIIb/IIIa inhibitor use, *n* (%)	39 (13)	8 (22)
Complete ST segment resolution, *n* (%)	219 (74)	28 (74)
Coronary microvascular injury		
IMR (U)	50 (22, 69)	49 (19, 61)
IMR > 40 U, *n* (%)	77 (40)	8 (36)
MVO (%)	3 (0, 4)	2 (0,4)
MVO > 1.55%, *n* (%)	63 (39)	8 (44)
Severe CMD (IMR > 40U and MVO), *n* (%)	22 (22)	2 (25)

CMD, coronary microvascular dysfunction; GPIIbIIIa, glycoprotein IIbIIIa; IHD, ischaemic heart disease; IMR, index of microcirculatory resistance; IQR, interquartile range; LAD, left anterior descending; LCx, left circumflex; MVO, microvascular obstruction; PCI, percutaneous coronary intervention; RCA, right coronary artery; TIMI, thrombolysis in myocardial infarction.

Quantification of thrombus composition by hyperspectral imaging (Experiment A)

Figure 3 shows examples of the hyperspectral images obtained for two selected thrombus samples. Within the image data, we have information on a spectrum of 150 wavelengths within each pixel. Colour images of the samples are shown on left, with spectra for a few selected pixels within each image shown to the right of the images.

The k-means analysis described in Section "Quantification of thrombus composition by hyperspectral imaging (Experiment A)" and in the Supplementary material was successfully employed across the full data set of sample spectral images, with false colour images generated using the pixel groups assigned by the k-means clustering algorithm showing good correspondence with conventional photographs of each sample. Two examples are shown in Figure 4, for two patients identified as having low and high IMR and MVO values, respectively. The left panel of the figure shows photographs of the thrombus samples for the two patients (Figures 4A,E), false colour images showing the pixels assigned to each of the 11 k-groups (Figures 4B,F), the same images with all non-thrombus pixels set to zero (Figures 4C,G), and finally, the results of the second k-means analysis with $K = 7$ (i.e., seven k-groups) carried out only on the thrombus pixels (Figures 4D,H). Note that the choice of 11 and 7 groups for the spectra is explained in the Supplementary material. The central panel of Figure 4 shows screenshots from invasive coronary physiology measurements and the right-hand panel shows the cardiac MRI scans used to determine MVO for the two patients.

We note that when using $K = 11$ in the initial k-means analysis on the complete data set, the algorithm, the clustering algorithm was successful in differentiating between the various materials present within the sample, including distinguishing blood and thrombus in blood-contaminated samples. The clusters with $k = 9$ and $k = 11$ were assigned to thrombus and used to generate the images shown in Figures 4C,D. Notably, the spectrum corresponding to the $k = 11$ cluster closely resembles that of the known spectrum of red blood cells, which is dominated by the absorption spectrum of haemoglobin.

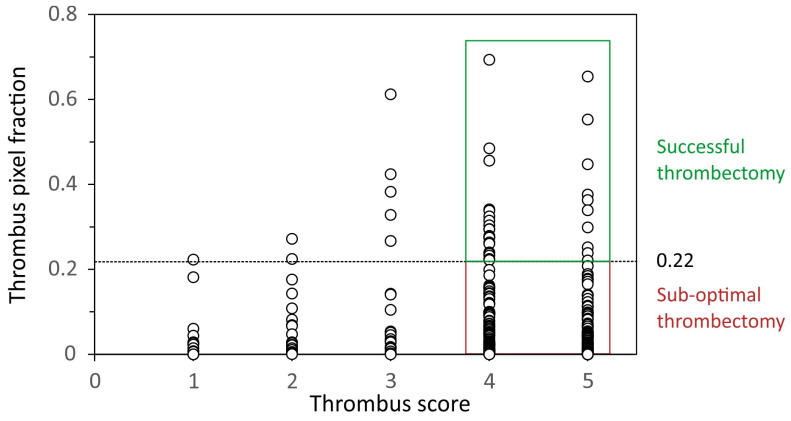

FIGURE 2
Plot of the thrombus area within each spectral image (expressed as a fraction) against Thrombosis In Myocardial Infarction (TIMI) thrombus score. A threshold thrombus area fraction of 0.22 was used as the minimum value to define successful thrombectomy in patients with thrombus scores of 4 and 5.

As noted in the Section "Materials and methods," in an alternative analysis the reflectance spectra of plasma, RBCs, empty filter, and water ice were used as basis spectra to perform a linear fit to the spectrum of each image pixel (Eq. 1). **Figure 5** shows an example output of the basis function fitting analysis, in which the best-fit coefficients for each spectral component (basis spectrum) are plotted separately as colour maps. Good fits were obtained to Eq. 1, as determined from χ^2 values and visual inspection, suggesting that these components account for most of the features observed in the reflectance spectra.

Correlation between thrombi spectra and microvascular injury (Experiment B)

Microvascular injury evaluation by CMR and/or IMR was performed in 36 patients, revealing a varied spectrum of microvascular injury in this cohort that was comparable to the injury noted in the wider cohort. As explained in Section "Correlation between thrombus spectral images and microvascular injury (Experiment B)," four different linear regression analyses were performed (Eqs 2–5) in order to model the relationship between the microvascular injury indices and the spectral imaging parameters (k-fractions) extracted from the thrombus pixels using k-means clustering. The power model (Eq. 3) was not able to fit the data well, and will not be considered further. The results of the analysis using Eqs (2, 4, 5) are shown in **Figure 6**.

The third model (Eq. 4), which assumes an exponential dependence of IMR and MVO on the k-fractions, performed best in predicting IMR (R^2: 0.80, $p < 0.0001$, $n = 21$) and MVO (R^2: 0.64, $p = 0.02$, $n = 17$).

Discussion

Coronary microvascular dysfunction in the STEACS setting is prognostically important (4, 5, 18), and its early and reliable identification during pPCI can guide stratification of adjunct therapies (24–26). Early work has shown that macroscopically red thrombi are associated with an adverse prognostic outcome (8, 9). Our proof-of-concept work established the feasibility of reflectance spectroscopy as a novel standardised tool for intraprocedural risk stratification. This study expands on our preliminary findings (11) by applying a robust, automated, near real-time analytical technique for coronary thrombus reflectance spectral characterisation and exploring its diagnostic role by correlating it with established coronary microvascular function indices.

In this work we have employed for the first time spatially resolved reflectance spectral analysis of coronary thrombus samples, in which reflectance spectra are recorded for every pixel in the image of each sample. This capability has enabled us to use advanced processing methods to: (i) phenotype the spectral signature of aspirated thrombi through machine learning approaches (unsupervised k-means clustering); and (ii) use the results of the clustering analysis to determine the regions of the images corresponding to aspirated thrombus area in an automated fashion. We have shown that separation of the pixel spectra into 11 groups allows the successful assignment of the various image components (thrombus, blood, water ice, filter, etc.).

Having developed a reliable method for determining the amount of aspirated thrombus, we observed that the adjunctive use of manual thrombectomy in patients with high angiographic thrombus burden only rarely led to aspiration of thrombus amounts larger than those aspirated

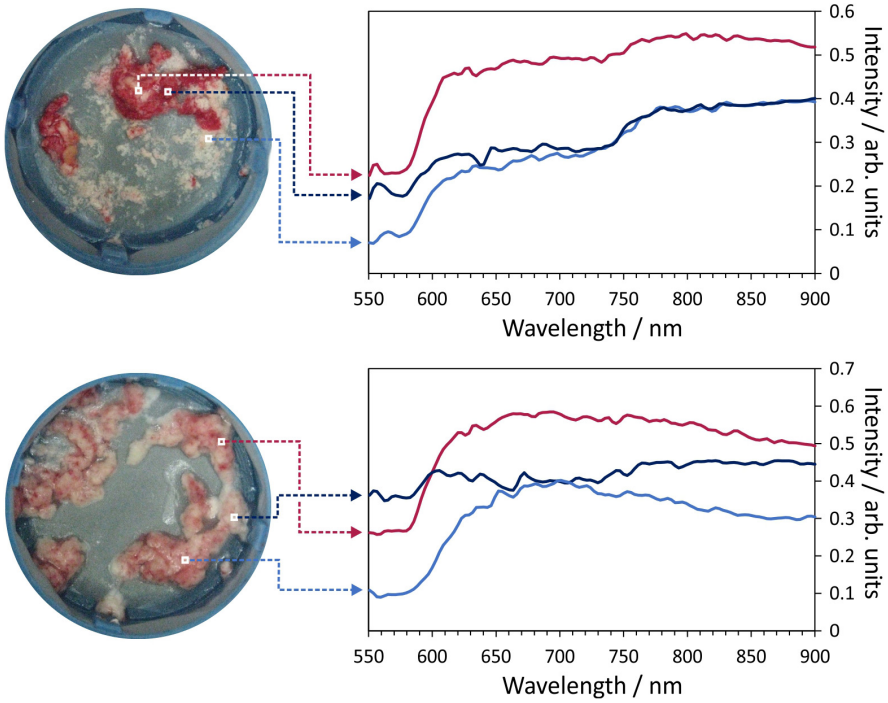

FIGURE 3
Example hyperspectral images for two thrombus samples. Each image pixel contains a 150-wavelength reflectance spectrum which characterises the composition of the material being imaged. Example spectra for the marked pixels are shown on the right of the figure.

from patients with low angiographic thrombus burden. This suggests that manual thrombectomy is infrequently effective at modifying thrombus burden, corroborating earlier work (27). Indeed, residual thrombus has been associated with worse microvascular dysfunction in STEACS (28), and sub-optimal thrombectomy has been put forth as one of the reasons that thrombus modification in STEACS was clinically inefficacious (7).

Finally, we have shown that the reflectance spectral signatures of the aspirated coronary thrombi show clear and reliable correlation with the degree of microvascular injury, as measured by MVO and IMR. The observed correlations are not perfect, highlighting that thrombus composition is one of the multiple factors influencing the extent of microvascular injury (29). Nonetheless, our work complements and improves on our earlier findings, which showed that spectrally identified red-cell content was able to modestly segregate patients with clinically significant and insignificant microvascular injury following a STEACS (11). Taking these two studies together, our work has shown that reflectance spectroscopy can offer a standardised, rapid, and reliable technique for identifying and stratifying patients with significant microvascular injury in cases where representative amounts of coronary thrombus are available for analysis.

Limitations

Firstly, we note that while the present work was carried out on frozen samples collected as part of the OxAMI study, the method is easily extendable to fresh samples. Further work is also underway which employs alternative spectroscopic and spectrometric methods with greater discriminating power. Together these methods have the potential to lead to a novel, high throughput, and non-destructive tool to study the pathobiology of coronary thrombus.

It is also worth mentioning that the 8 years over which patients were enrolled in the OxAMI study saw changes in pharmacotherapy that could have influenced aspirated thrombus composition. However, 97% of participants were pre-loaded with DAPT prior to their PPCI and 93% had intraprocedural bivalirudin administered. Adjunctive pharmacotherapy in the form of GpIIb/IIIa was used in 13% of all patients and a comparable 22% in patients from cohort B. Indeed, GpIIb/IIIa was predominantly (72%) used as a bailout strategy after thrombus aspiration. Nonetheless this is unlikely to confound our endpoint as insights from the T-TIME randomised trial show that intracoronary thrombolysis had no effect on microvascular injury indices (30).

Finally, from an external validity perspective, our approach can be applied to the small number of STEACS

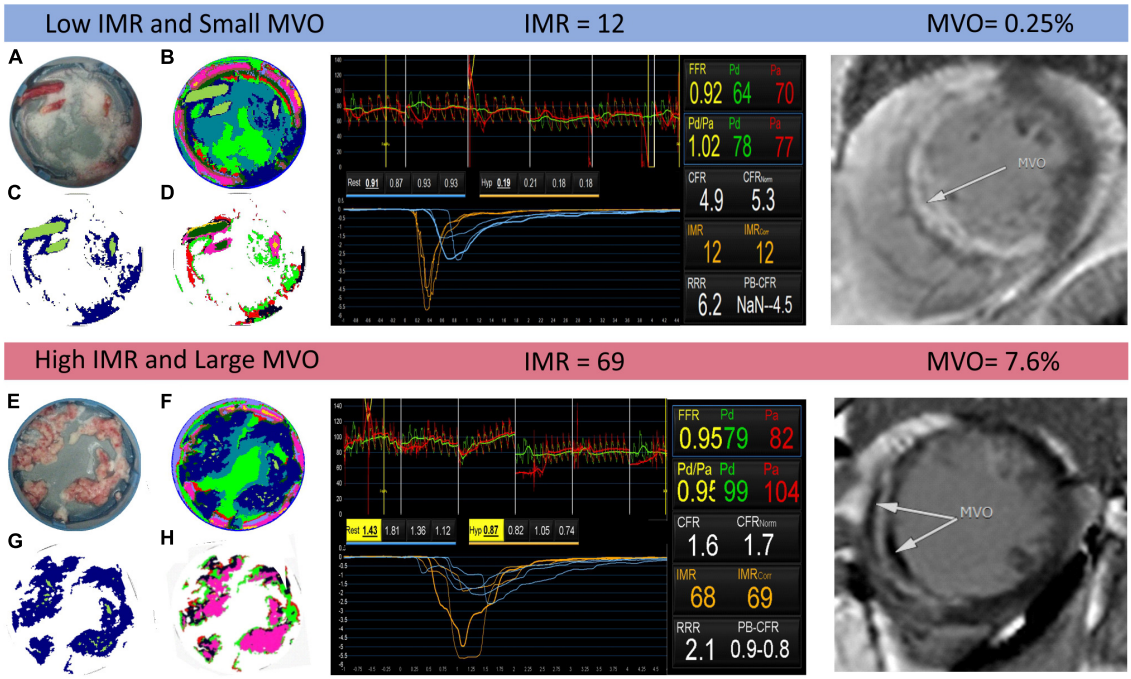

FIGURE 4
Example output of the *k*-means clustering analysis for two patients identified as having low and high index of coronary microvascular resistance (IMR) (centre panel) and small and large microvascular obstruction (MVO) (right panel), respectively. In the left panel, images **(A,E)** are photographs of the thrombus samples for each patient; images **(B,F)** show the results of the $K = 11$ *k*-means clustering analysis, with each colour corresponding to a different cluster; images **(C,G)** are the same as images **(B,F)** but with all non-thrombus pixels set to zero; and images **(D,H)** show the results of a second *k*-means clustering analysis with $K = 7$, performed only on thrombus pixels.

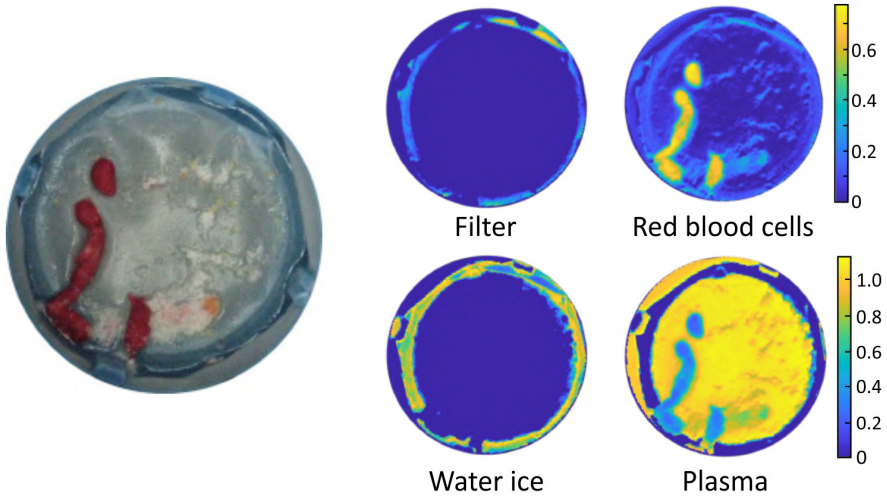

FIGURE 5
Example output of the basis function fitting process. The image on the left is a photograph of the sample. The false colour images show the fitted contributions to the spectral image from the filter, water ice, plasma, and red blood cells.

patients undergoing manual thrombectomy in contemporary practice (31). However, the early phase RETRIEVE-AMI (NCT05307965) and NATURE (NCT04969471) trials exploring novel tools for thrombus retrieval offer an excellent opportunity for our technology, as they address the drawbacks that underpin the dwindling use of aspiration thrombectomy and aim to define and refine its exact role in the expanding landscape of intraprocedural risk stratification tools for STEACS care.

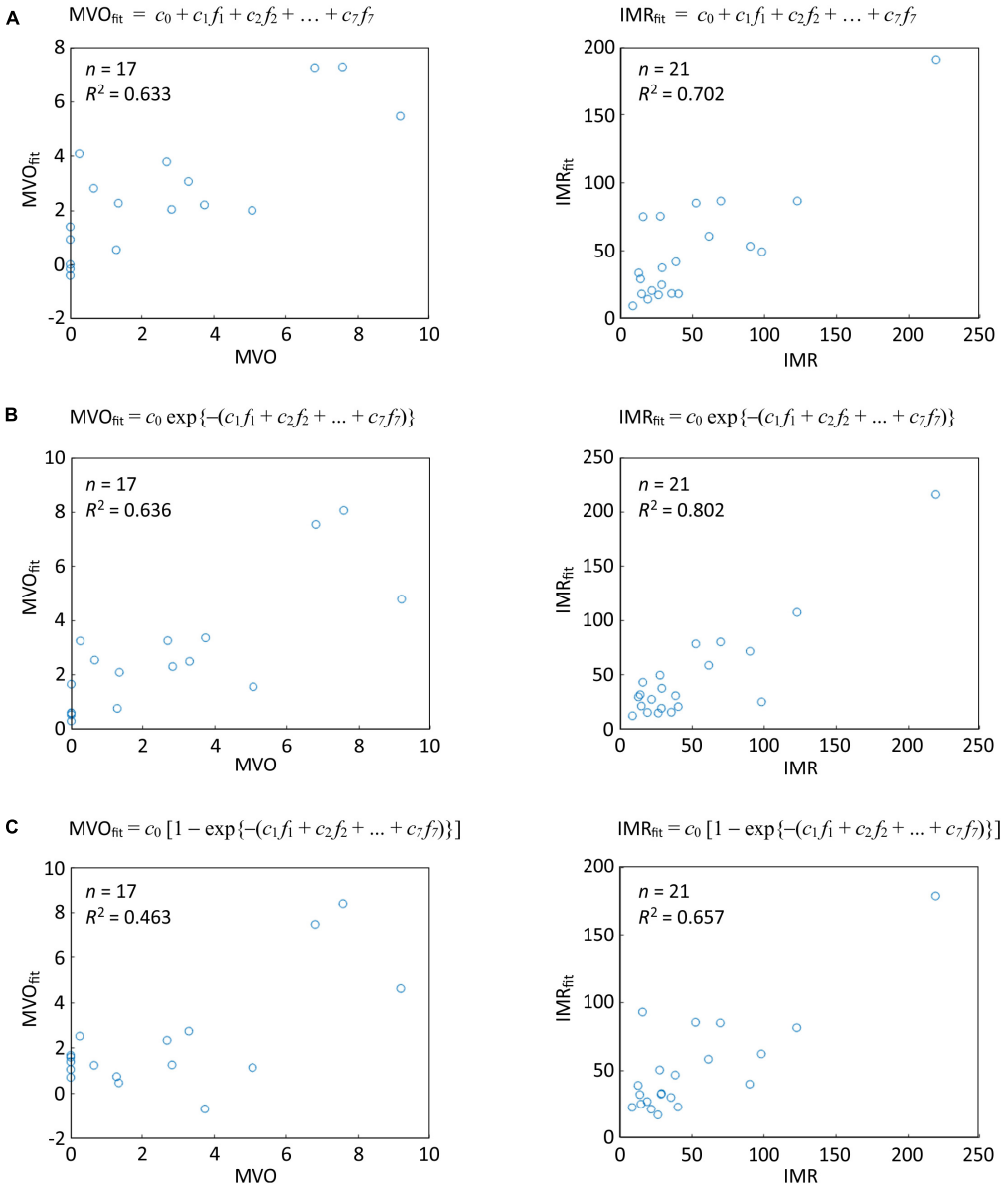

FIGURE 6
Linear regression analysis of correlations between thrombus spectral parameters predicted microvascular injury and actual microvascular injury indices for the thresholded data set of Oxford Acute Myocardial Infarction (OxAMI) samples. The plots show fits of the thrombus pixel k-fractions determined from the spectral images in the thresholded data set to **(A)** Eq. 2; **(B)** Eq. 4; and **(C)** Eq. 5. Note that the fitting coefficients c_k are different for each fit. Sample number n and R^2 value are shown for each correlation. Equivalent plots for the full OxAMI data set can be found in **Supplementary Figure 3**.

While we acknowledge that the correlations between spectral data and clinical parameters observed in the present study are somewhat limited by the small number of patients included in the thresholded data set, we are working to address this by employing alternative approaches involving analysis of plasma from coronary aspirate. These newer approaches do not require thrombectomy and can therefore be generalised to all patients undergoing pPCI.

Conclusion

We have shown that reflectance spectral imaging of coronary thrombus combined with machine learning approaches enables the determination of parameters correlating with thrombus composition, including automated quantification of thrombus area within the images. We have also shown for the first time that spectral signatures of coronary

thrombi correlate with microvascular injury indices in patients with STEACS. Further validation of this point-of-care system in future studies will potentially enable the integration of reflectance spectroscopy into the diagnostic workflow of STEACS and facilitate the stratified deployment of adjunct treatment therapies.

Data availability statement

The datasets presented in this article are not readily available because a patent based on some of the data/approaches included in this article has been filed. Requests to access the datasets should be directed to GD, GiovanniLuigi.Demaria@ouh.nhs.uk.

Ethics statement

The studies involving human participants were reviewed and approved by NRES Committee South Central – Oxford C (REC Number: 10/H0408/24). The patients/participants provided their written informed consent to participate in this study.

Author contributions

RK: methodology, investigation, writing – original draft, review and editing, visualisation, project administration, and funding acquisition. KF: methodology, investigation, formal analysis, visualisation, writing – review and editing, and project administration. CG: formal analysis, visualisation, and writing – review and editing. RL, MA, FM, and ME: investigation and writing – review and editing. AB: investigation, resources, writing – review and editing, and funding acquisition. CV and GD: conceptualisation, methodology, investigation, resources, writing – original draft, review and editing, supervision, project administration, and funding acquisition. KC: conceptualisation, methodology, investigation, resources, writing – review and editing, project administration, and funding acquisition. All authors contributed to the article and approved the submitted version.

Funding

This work was supported by British Heart Foundation (BHF; grant CH/16/1/32013), BHF Centre of Research Excellence, Oxford (RG/13/1/30181), Oxfordshire Health Services Research Committee, and the National Institute for Health Research (NIHR) Oxford Biomedical Research Centre. This work was also supported by an Engineering and Physical Sciences Research Council (EPSRC) Impact Acceleration Account Grant (EPSRC IAA Grant: D4D00010). RK, Academic Clinical Fellow, was at the time this work was conducted funded by Health Education England (HEE)/National Institute for Health Research (NIHR).

Acknowledgments

The authors would like to acknowledge the OxAMI study investigators for funding acquisition, project administration, participant recruitment and data collection as well as the Oxford Heart Centre Catheterisation Laboratory team and Yujun Ng for their support of the study. **Figure 1** has been designed using resources from Flaticon.com. Icons made by Eucalyp, Freepik, Nikita Golubev, and Voysla from Flaticon.com.

Conflict of interest

Author RK reports grants from Medtronic and Terumo Inc. outside the submitting work. Author AB reports grants from Boston Scientific and personal fees from Boston Scientific, Abbott, Medtronic, and Phillips outside the submitted work. Author GD reports consultancy fee from Miracor Medical SA, speaker fees from Miracor Medical SA and Abbott, and grants from Miracor Medical SA, Abbott, Philips, Medtronic, and Terumo outside the submitted work. In addition, Authors GD, KC, CV, RL, and MA have a patent PCT/US20/55240 pending relevant to this work.

The remaining authors declare that the research was conducted in the absence of any commercial or financial relationships that could be construed as a potential conflict of interest.

Publisher's note

Author disclaimer

The views expressed in this publication are those of the authors and not necessarily those of the NIHR, NHS, or the United Kingdom Department of Health and Social Care.

Supplementary material

The Supplementary Material for this article can be found online at: https://www.frontiersin.org/articles/10.3389/fcvm.2022.930015/full#supplementary-material

References

1. Szummer K, Wallentin L, Lindhagen L, Alfredsson J, Erlinge D, Held C, et al. Improved outcomes in patients with ST-elevation myocardial infarction during the last 20 years are related to implementation of evidence-based treatments: Experiences from the SWEDEHEART registry 1995-2014. *Eur Heart J.* (2017) 38:3056–65. doi: 10.1093/eurheartj/ehx515

2. Montecucco F, Carbone F, Schindler TH. Pathophysiology of ST-segment elevation myocardial infarction: Novel mechanisms and treatments. *Eur Heart J.* (2015) 37:1268–83. doi: 10.1093/eurheartj/ehv592

3. De Maria GL, Alkhalil M, Wolfrum M, Fahrni G, Borlotti A, Gaughran L, et al. Index of microcirculatory resistance as a tool to characterize microvascular obstruction and to predict infarct size regression in patients with STEMI undergoing primary PCI. *JACC Cardiovasc Imaging.* (2019) 12:837–48. doi: 10.1016/j.jcmg.2018.02.018

4. Scarsini R, Shanmuganathan M, De Maria GL, Borlotti A, Kotronias RA, Burrage MK, et al. Coronary microvascular dysfunction assessed by pressure wire and CMR after STEMI predicts long-term outcomes. *JACC Cardiovasc Imaging.* (2021) 14:1948–59. doi: 10.1016/j.jcmg.2021.02.023

5. Kotronias RA, Terentes-Printzios D, Shanmuganathan M, Marin F, Scarsini R, Bradley-Watson J, et al. Long-term clinical outcomes in patients with an acute ST-segment- elevation myocardial infarction stratified by angiography-derived index of microcirculatory resistance. *Front Cardiovasc Med.* (2021) 8:717114. doi: 10.3389/fcvm.2021.717114

6. Neumann F-J, Sousa-Uva M, Ahlsson A, Alfonso F, Banning AP, Benedetto U, et al. 2018 ESC/EACTS Guidelines on myocardial revascularization. *Eur Heart J.* (2018) 40:87–165. doi: 10.1093/eurheartj/ehy855

7. Jolly SS, James S, Džavík V, Cairns JA, Mahmoud KD, Zijlstra F, et al. Thrombus aspiration in ST-segment-elevation myocardial infarction: An individual patient meta-analysis: Thrombectomy trialists collaboration. *Circulation.* (2017) 135:143–52. doi: 10.1161/CIRCULATIONAHA.116.025371

8. Quadros AS, Cambruzzi E, Sebben J, David RB, Abelin A, Welter D, et al. Red versus white thrombi in patients with ST-elevation myocardial infarction undergoing primary percutaneous coronary intervention: Clinical and angiographic outcomes. *Am Heart J.* (2012) 164:553–60. doi: 10.1016/j.ahj.2012.07.022

9. Yunoki K, Naruko T, Inoue T, Sugioka K, Inaba M, Iwasa Y, et al. Relationship of thrombus characteristics to the incidence of angiographically visible distal embolization in patients with ST-segment elevation myocardial infarction treated with thrombus aspiration. *JACC Cardiovasc Intervent.* (2013) 6:377–85. doi: 10.1016/j.jcin.2012.11.011

10. Mahmoud KD, Zijlstra F. Thrombus aspiration in acute myocardial infarction. *Nat Rev Cardiol.* (2016) 13:418–28. doi: 10.1038/nrcardio.2016.38

11. De Maria GL, Lee R, Alkhalil M, Borlotti A, Kotronias R, Langrish J, et al. Reflectance spectral analysis for novel characterization and clinical assessment of aspirated coronary thrombi in patients with ST elevation myocardial infarction. *Physiol Meas.* (2020) 41:045001. doi: 10.1088/1361-6579/ab81de

12. Akter S, Hossain MG, Nishidate I, Hazama H, Awazu K. Medical applications of reflectance spectroscopy in the diffusive and sub-diffusive regimes. *J Near Infrared Spectrosc.* (2018) 26:337–50. doi: 10.1177/0967033518806637

13. Amigo JM. *Hyperspectral imaging*. Amsterdam: Elsevier (2019).

14. De Maria GL, Cuculi F, Patel N, Dawkins S, Fahrni G, Kassimis G, et al. How does coronary stent implantation impact on the status of the microcirculation during primary percutaneous coronary intervention in patients with ST-elevation myocardial infarction? *Eur Heart J.* (2015) 36:3165–77. doi: 10.1093/eurheartj/ehv353

15. Sianos G, Papafaklis MI, Daemen J, Vaina S, van Mieghem CA, van Domburg RT, et al. Angiographic stent thrombosis after routine use of drug-eluting stents in ST-segment elevation myocardial infarction: The importance of thrombus burden. *J Am College Cardiol.* (2007) 50:573–83. doi: 10.1016/j.jacc.2007.04.059

16. TIMI Study Group. The Thrombolysis in Myocardial Infarction (TIMI) trial: Phase I findings. *N Engl J Med.* (1985) 312:932–6. doi: 10.1056/NEJM198504043121437

17. Van 't Hof AW, Liem A, Suryapranata H, Hoorntje JC, de Boer M-J, Zijlstra F. Angiographic assessment of myocardial reperfusion in patients treated with primary angioplasty for acute myocardial infarction: Myocardial blush grade. *Circulation.* (1998) 97:2302–6. doi: 10.1161/01.CIR.97.23.2302

18. Carrick D, Haig C, Ahmed N, Carberry J, Yue May VT, McEntegart M, et al. Comparative prognostic utility of indexes of microvascular function alone or in combination in patients with an acute ST-segment-elevation myocardial infarction. *Circulation.* (2016) 134:1833–47. doi: 10.1161/CIRCULATIONAHA.116.022603

19. Eitel I, Desch S, Fuernau G, Hildebrand L, Gutberlet M, Schuler G, et al. Prognostic significance and determinants of myocardial salvage assessed by cardiovascular magnetic resonance in acute reperfused myocardial infarction. *J Am College Cardiol.* (2010) 55:2470–9. doi: 10.1016/j.jacc.2010.01.049

20. de Waha S, Patel MR, Granger CB, Ohman EM, Maehara A, Eitel I, et al. Relationship between microvascular obstruction and adverse events following primary percutaneous coronary intervention for ST-segment elevation myocardial infarction: An individual patient data pooled analysis from seven randomized trials. *Eur Heart J.* (2017) 38:3502–10. doi: 10.1093/eurheartj/ehx414

21. Forgy EW. Cluster analysis of multivariate data : Efficiency versus interpretability of classifications. *Biometrics.* (1965) 21:768–9.

22. Lloyd S. Least squares quantization in PCM. *IEEE Trans Inform Theory.* (1982) 28:129–37. doi: 10.1109/TIT.1982.1056489

23. MATLAB. *MATLAB* . Natick, MA: The Mathworks Inc. (2020).

24. De Maria GL, Alkhalil M, Borlotti A, Wolfrum M, Gaughran L, Dall'Armellina E, et al. Index of microcirculatory resistance-guided therapy with pressure-controlled intermittent coronary sinus occlusion improves coronary microvascular function and reduces infarct size in patients with ST-elevation myocardial infarction: The Oxford Acute Myocardial Infarction - Pressure-controlled Intermittent Coronary Sinus Occlusion study (OxAMI-PICSO study). *EuroIntervention.* (2018) 14:e352–9. doi: 10.4244/EIJ-D-18-00378

25. Scarsini R, Terentes-Printzios D, Shanmuganathan M, Kotronias RA, Borlotti A, Marin F, et al. Pressure-controlled intermittent coronary sinus occlusion improves the vasodilatory microvascular capacity and reduces myocardial injury in patients with STEMI. *Catheter Cardiovasc Interv.* (2021) 99:329–39. doi: 10.1002/ccd.29793

26. Maznyczka AM, Oldroyd KG, McCartney P, McEntegart M, Berry C. The potential use of the index of microcirculatory resistance to guide stratification of patients for adjunctive therapy in acute myocardial infarction. *JACC Cardiovasc Interv.* (2019) 12:951–66. doi: 10.1016/j.jcin.2019.01.246

27. Bhindi R, Kajander OA, Jolly SS, Kassam S, Lavi S, Niemela K, et al. Culprit lesion thrombus burden after manual thrombectomy or percutaneous coronary intervention-alone in ST-segment elevation myocardial infarction: The optical coherence tomography sub-study of the TOTAL (ThrOmbecTomy versus PCI ALone) trial. *Eur Heart J.* (2015) 36:1892–900. doi: 10.1093/eurheartj/ehv176

28. Higuma T, Soeda T, Yamada M, Yokota T, Yokoyama H, Izumiyama K, et al. Does residual thrombus after aspiration thrombectomy affect the outcome of primary PCI in patients with ST-segment elevation myocardial infarction?: An optical coherence tomography study. *JACC Cardiovasc Intervent.* (2016) 9:2002–11. doi: 10.1016/j.jcin.2016.06.050

29. Sezer M, van Royen N, Umman B, Bugra Z, Bulluck H, Hausenloy DJ, et al. Coronary microvascular injury in reperfused acute myocardial infarction: A view from an integrative perspective. *J Am Heart Assoc.* (2018) 7:e009949. doi: 10.1161/JAHA.118.009949

30. Maznyczka AM, McCartney PJ, Oldroyd KG, Lindsay M, McEntegart M, Eteiba H, et al. Effects of intracoronary alteplase on microvascular function in acute myocardial infarction. *J Am Heart Assoc.* (2020) 9:e014066. doi: 10.1161/JAHA.119.014066

31. Secemsky EA, Ferro EG, Rao SV, Kirtane A, Tamez H, Zakroysky P, et al. Association of physician variation in use of manual aspiration thrombectomy with outcomes following primary percutaneous coronary intervention for ST-elevation myocardial infarction: The national cardiovascular data registry CathPCI registry. *JAMA Cardiol.* (2019) 4:110–8. doi: 10.1001/jamacardio.2018.4472

frontiers | Frontiers in Cardiovascular Medicine

TYPE Original Research
PUBLISHED 08 November 2022
DOI 10.3389/fcvm.2022.974161

OPEN ACCESS

EDITED BY
Erhan Tenekecioglu,
University of Health Sciences, Turkey

REVIEWED BY
Andrew Kei-Yan Ng,
The University of Hong Kong,
Hong Kong SAR, China
Mauro Chiarito,
Humanitas University, Italy

*CORRESPONDENCE
Alexander Tindale
alexander.tindale09@imperial.ac.uk

SPECIALTY SECTION
This article was submitted to Cardiovascular Imaging, a section of the journal Frontiers in Cardiovascular Medicine

RECEIVED 20 June 2022
ACCEPTED 26 October 2022
PUBLISHED 08 November 2022

CITATION
Tindale A and Panoulas V (2022) Real-world intravascular ultrasound (IVUS) use in percutaneous intervention-naïve patients is determined predominantly by operator, patient, and lesion characteristics.
Front. Cardiovasc. Med. 9:974161.
doi: 10.3389/fcvm.2022.974161

Real-world intravascular ultrasound (IVUS) use in percutaneous intervention-naïve patients is determined predominantly by operator, patient, and lesion characteristics

Alexander Tindale[1,2]* and Vasileios Panoulas[1,2]

[1]Royal Brompton and Harefield Hospitals, Guy's and St Thomas' NHS Foundation Trust, London, United Kingdom, [2]National Heart and Lung Institute, Imperial College London, London, United Kingdom

Background: Intravascular Ultrasound (IVUS) has been shown to improve clinical outcomes in patients undergoing percutaneous intervention (PCI) in numerous trials. However, it is still underutilized outside of trial settings, and most trials include a significant proportion of patients with prior PCI. The aim of this study is to look at real-world use and outcomes in PCI-naïve patients who undergo IVUS-guided intervention.

Methods and results: Prospectively collected data from 10,574 consecutive patients undergoing their index PCI was retrospectively analyzed. 455 (4.3%) patients underwent IVUS, with a median follow-up of 4.6 years. Patients undergoing IVUS had higher levels of comorbidities including diabetes (27.5% vs. 19.7%, $p < 0.001$), hypertension (58.0% vs. 47.9%, $p < 0.001$), hypercholesterolemia (51.6% vs. 39.2%, $p < 0.001$) and were generally older (65.9 ± 14.5 vs. 64.5 ± 13.4 years, $p = 0.031$) with higher mean baseline creatinine levels (95.4 ± 63.3 vs. 87.8 ± 46.1 μmol/L). The strongest predictor of IVUS use was the operating consultant graduating from medical school after the year 2000 [OR 14.5 (3.5–59.8), $p < 0.001$] and the presence of calcific lesions [OR 5.2 (3.4–8.0) $p < 0.001$]. There was no significant difference in MACE nor 1-year mortality between patients undergoing IVUS-guided or angiography-only PCI on unadjusted analysis [OR 1.04 (0.73—1.5), $p = 0.81$, OR 1.055 (0.65–1.71) $p = 0.828$] nor mortality throughout the study period (HR 0.93 (0.69—1.26), $p = 0.638$). This held true for stents longer than 28 mm. Propensity matched analysis of patients similarly showed

no mortality difference between arms for all patients and those with longer stents (p = 0.564 and p = 0.919).

Conclusion: The strongest predictors of IVUS use in PCI-naïve patients are the operator's year of graduation from medical school and proxy measures of calcific lesions. On both matched and adjusted analysis there was no evidence of improved mortality nor reduced MACE in this specific retrospective cohort, although this may well be explained by significant selection bias.

KEYWORDS

IVUS (intravascular ultrasound), PCI—percutaneous coronary intervention, real-world, regression analysis, propensity matching

Introduction

The use of intravascular ultrasound (IVUS) has steadily increased since its development in the late 1980s (1), and this use was accelerated by the evolution of effective drug-eluting stents (DES) a decade later (2). Subsequently, there have been numerous large-scale randomized trials assessing the effectiveness of IVUS in the drug-eluting stent era.

In general, these show that IVUS-guided PCI reduces major adverse cardiac events (MACE) in a variety of different settings. These include complex coronary artery disease (3), all-comers with follow-up periods of up to 3 years (4) and patients requiring stents longer than 28 mm (5, 6). The largest synthesis looked at 31 studies, including both randomized and observational trials, and demonstrated that MACE was lower with IVUS use with the suggestion of mortality benefit when including observational data (7).

As a result of this evidence, IVUS has grown in popularity and is now a class IIa recommendation in the latest ESC guidelines (8). However, outside of trials, IVUS use remains heterogenous and often low. For example, IVUS is used in 12% of PCI cases in the UK (9), but 80% of such cases in Japan (10).

Furthermore, a significant proportion of patients in these trials have undergone previous revascularization, ranging from 11 to 48% (11). There is limited literature on the effect of IVUS in PCI-naïve patients.

Therefore, the aims of this study are threefold. Firstly, we begin with a descriptive analysis to examine which patient, procedural and operator characteristics are associated with IVUS use in PCI-naïve patients, to shed light on the relative underuse of IVUS.

Secondly, we analyze the clinical outcomes of all PCI-naïve patients who received second generation drug-eluting stents of any length with and without IVUS optimization.

Thirdly, in light of the evidence from a recent analysis concerning IVUS effectiveness in long stents, we perform subgroup analysis for patients with implanted stents of longer than 28 mm.

Materials and methods

Study population and design

This was an observational study to determine associations between patient and operator characteristics and IVUS use, in addition to associations between IVUS use and favorable clinical outcomes. The study population was 10,574 consecutive patients undergoing their first PCI with second-generation stent implantation at Harefield Hospital between January 1st 2011 and January 1st 2021. The study flow-chart is shown in **Figure 1**. Patients who underwent optical coherence tomography (OCT) were excluded.

Clinical and outcome data

The majority of clinical data, including patient characteristics and comorbidities, were taken from the audit data collected for every PCI patient at our institution. Blood gas analysis, hematology tests and laboratory biochemistry tests were taken from our own hospital's database. Health outcomes data including survival was obtained by linking patients' NHS numbers to the NHS spine, in collaboration with the Office for National Statistics (ONS).

The primary outcome measures were 1-year mortality and 1-year MACE, which is a patient-oriented composite endpoint encompassing all-cause mortality, unplanned revascularization, stroke and myocardial infarction (MI). Secondary outcome measures were a composite of device endpoints that includes cardiovascular (CV) death, MI and target-lesion revascularization (TLR). These were chosen in line with the Academic Research Consortium's (ARC) guidelines for

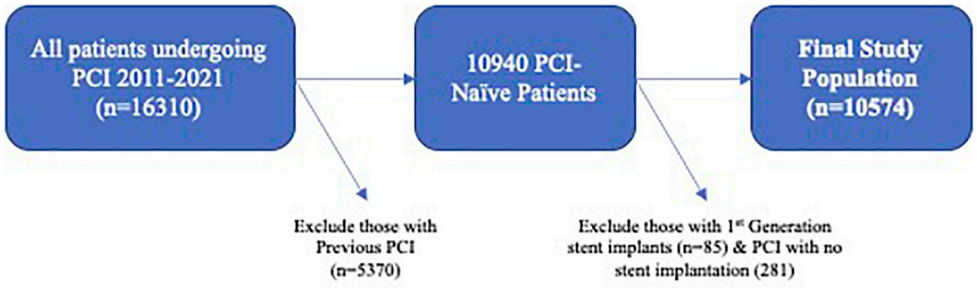

FIGURE 1
Study flow-chart.

outcome reporting in cardiovascular trials (12). When the cause of death was unknown, it was listed as a cardiovascular death for the purposes of analysis in line with the ARC guidance.

Ethics

All patient-identifiable information was removed before analysis. Our local audit office assigned institutional support for this project. As this was analysis of anonymized information taken from required audit data we were advised that no further ethical approval was required.

Statistical analysis

Univariate analysis was performed using Student's *t*-test for comparing the means of normally distributed data and Mann-Whitney U if not normally distributed. Chi-squared and Fisher's tests were used for categorical data. Fisher's exact test was used if the expected value in any group was less than five. Regression analysis was performed using binary logistic regression for dichotomous outcome variables and cox proportional hazards and Kaplan-Meier curves for survival data, as appropriate. These tests were performed in *SPSS* (IBM SPSS Statistics, version 28 (IBM Corp., Armonk, N.Y., USA) and *R* (R Foundation for Statistical Computing, Vienna, Austria).

Propensity matching was performed using *R*. The method used was 1:1 nearest neighbor matching without replacement, where distance was defined by using a propensity score estimated by logistic regression. The covariates used for propensity matching were age, ACS, previous ACS, previous CABG, hypercholesterolemia, smoking status, diabetes, hypertension, cardiac arrest, out of hospital cardiac arrest (OOHCA), maximum stent length per vessel, devices used for calcific lesions, devices used for calcium modification, number of stents used, year of procedure, hemoglobin, white blood cell concentration, sodium, potassium, urea, creatinine, consultant age band and consultant operator.

Statistical significance was established at $p < 0.05$ (2-tailed) for all tests. All data is reported according to the STrengthening the Reporting of OBservational studies in Epidemiology (STROBE) guidelines (13).

Results

The general landscape of intravascular ultrasound use

In total, 10,574 PCI-naïve patients underwent an initial percutaneous intervention at Harefield Hospital with second generation DES implantation. The full baseline characteristics can be seen in **Table 1**. Notably 75.3% of procedures were for acute coronary syndromes (ACS), and of these, 77% were treated for ST elevation myocardial infarction (STEMI).

IVUS was used in 455 patients, or 4.3% of cases. **Figure 2** shows IVUS procedures (for all patients) over time, showing a general trend upwards since 2011. Median follow-up for all included patients was 1,691 days (IQR 753–2796).

Univariate analysis showing associations with intravascular ultrasound use

Univariate analysis of different patient and procedural characteristics are show in **Table 1**. IVUS use was more prevalent in chronic rather than ACS: 50.1% of patients in the IVUS group were treated for ACS compared to 76.4% in the non-IVUS group ($p < 0.001$). However, the IVUS group had significantly higher rates of diabetes (27.5% vs. 19.7%, $p < 0.001$), hypertension (58.0% vs. 47.9%), hypercholesterolemia (51.6% vs. 38.7%, $p < 0.001$) and were generally older (65.9 ± 14.5 vs. 64.5 ± 13.4 years, $p = 0.031$) with higher mean baseline creatinine levels (95.4 ± 63.3 vs. 87.8 ± 46.1 μmol/L).

In contrast, IVUS use was less prevalent in patients with markers of acute illness, with lower prevalence in patients with

TABLE 1 Baseline characteristics and univariate analysis of patients undergoing index PCI 2011–202.

	All patients (n = 10,574)	IVUS not used (n = 10,119)	IVUS used (n = 455)	P
Patient characteristics				
Male sex	7,825 (74.0)	7,746 (74.0)	351 (74.7)	0.544
Age (years)	64.5 (13.4)	64.5 (13.4)	65.9 (14.5)	0.031
Weight (Kg)	83.2 (127.3)	84.0 (146.6)	80.7 (18.0)	0.67
Systolic BP	133.2 (188)	130.9 (155.9)	129.2 (28.5)	0.884
Previous ACS	1,105 (10.5)	1,008 (10.0)	97 (21.3)	< 0.001
Previous CABG	630 (6.0)	587 (5.8)	43 (9.5)	0.001
Hypercholesterolemia	4,150 (39.2)	3,915 (38.7)	235 (51.6)	< 0.001
Current smoker	2,491 (23.6)	2,431 (24.0)	60 (13.2)	< 0.001
Ex-Smoker	2,696 (25.5)	2,536 (25.1)	160 (35.2)	< 0.001
Diabetes	2,121 (20.1)	1,996 (19.7)	125 (27.5)	< 0.001
HTN	5,115 (48.4)	4,851 (47.9)	264 (58.0)	< 0.001
Procedure details				
ACS	7,961 (75.3)	7,733 (76.4)	228 (50.1)	< 0.001
STEMI	6,132 (58.0)	6,007 (59.4)	125 (27.5)	< 0.001
NSTEMI	1,829 (17.3)	1,726 (17.0)	103 (22.6)	< 0.001
Cardiac arrest	808 (7.6)	786 (7.8)	22 (4.8)	0.021
OOHCA	483 (4.6)	472 (4.7)	11 (2.4)	0.025
Longest stented/treated segment	24.8 (10.8)	23.4 (27.5)	27.5 (14.8)	< 0.001
Max stent length per vessel	25.8 (16.2)	24.6 (14.9)	30.0 (19.8)	< 0.001
Max balloon diameter	4.7 (23.5)			0.501
Number stents used	1.5 (0.9)	1.4 (0.9)	2.1 (1.4)	< 0.001
Devices for calcium	467 (4.4)	357 (3.5)	110 (24.2)	< 0.001
Calcium modification only	360 (3.4)	269 (2.7)	91 (20)	< 0.001
Vessels treated				
PCI LMS	393 (3.7)	374 (3.7)	19 (4.2)	0.597
PCI LAD	4,656 (44.0)	4,463 (44.1)	193 (42.4)	0.478
PCI LCx	2,207 (20.9)	2,102 (20.8)	105 (23.1)	0.237
PCI RCA	3,277 (31.0)	2,135 (31.0)	142 (31.2)	0.918
PCI grafts	158 (1.5)	153 (1.5)	5 (1.1)	0.690
Blood gas at time of procedure				
pH	7.4 (0.1)	7.40 (0.08)	7.41 (0.07)	0.071
BE	-1.2 (4.2)	-1.7 (4.4)	-0.3 (4.6)	< 0.001
HCO3	23.6 (3.1)	23.1 (3.4)	24.1 (3.4)	< 0.001
Lactate	2.1 (1.9)	2.3 (2.4)	1.8 (1.7)	< 0.001
Glucose BG	8.6 (3.5)	8.7 (3.7)	8.6 (3.5)	0.549
Laboratory blood values				
Hb	120.0 (43.6)	113 (49.6)	119.7 (38.8)	0.004
WCC	11.0 (5.0)	11.1 (4.7)	10.0 (6.9)	< 0.001
Sodium	136.0 (3.6)	136.0 (3.5)	136.1 (3.9)	0.531
Potassium	4.1 (0.5)	4.1 (0.5)	4.2 (0.4)	0.002
Urea	6.6 (3.4)	6.6 (3.2)	7.3 (4.1)	< 0.001
Creatinine	86.5 (44.0)	87.8 (46.1)	95.4 (63.3)	< 0.001
Bilirubin	12.0 (6.9)	12.0 (6.6)	12.8 (8.4)	0.025
ALT	51.0 (134.6)	49.3 (128.7)	54.9 (149.5)	0.416
Albumin	38.6 (5.0)	38.6 (5.1)	38.5 (5.3)	0.775
ALP	79.6 (37.3)	78.4 (35.0)	78.6 (5.3)	0.048
CRP	19.6 (41.8)	18.6 (40.8)	26.1 (50.6)	0.004
Trop I ng/L	14463.6 (27833.9)	14233.8 (24746)	15112.3 (35030.8)	0.652

(Continued)

TABLE 1 (Continued)

	All patients (n = 10,574)	IVUS not used (n = 10,119)	IVUS used (n = 455)	P
Mg	0.8 (0.1)	0.8 (0.1)	0.8 (0.1)	0.316
Cholesterol	4.9 (1.3)	4.9 (1.3)	4.6 (1.3)	0.002
Operator characteristics				
Consultant 1st operator	6,985 (66.1)	6,636 (65.6)	349 (76.7)	< 0.001
Operator's year of qualification				< 0.001
Before 1990	2,502 (23.7)	2,473 (24.4)	29 (6.4)	
1990–1999	5,838 (55.2)	5,588 (55.2)	250 (54.9)	
Post 2000	2,234 (21.1)	2,058 (20.3)	176 (38.7)	
Operator's case numbers	1510.7 (1004.2)	1492.0 (998.1)	1928.9 (1047)	< 0.001

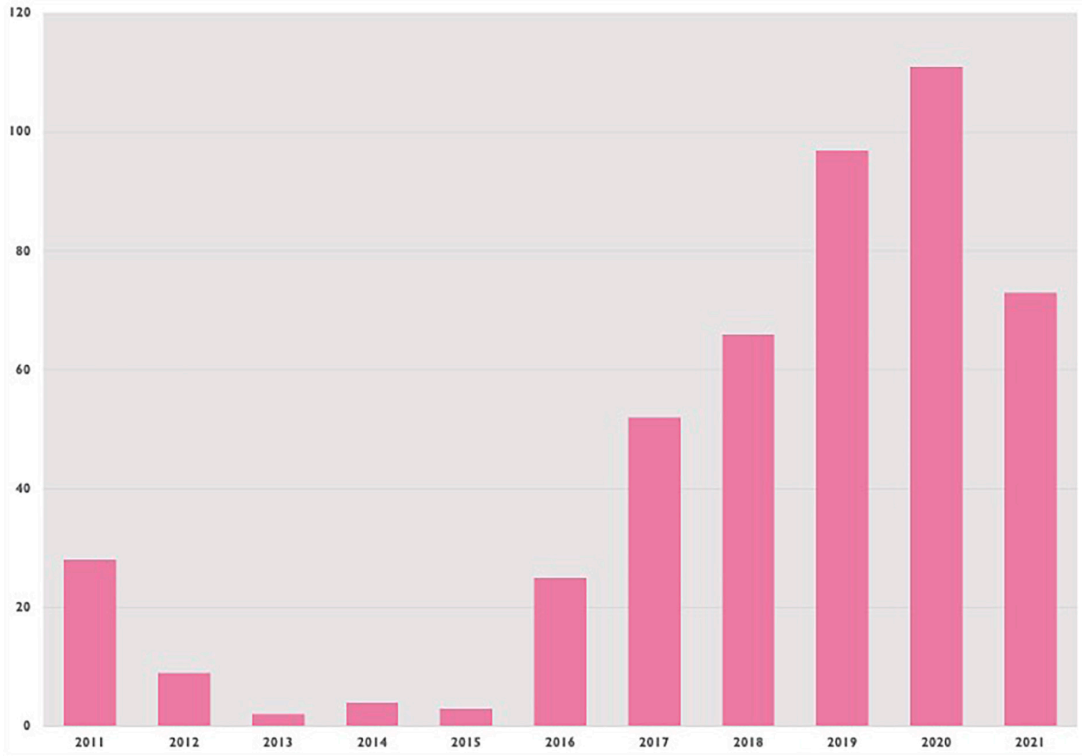

FIGURE 2
Absolute number of IVUS procedures performed in PCI-naive patients by year.

STEMIs and cardiac arrests. Related to this, patients undergoing IVUS-guided PCI had significantly lower mean lactate levels than those without IVUS guidance (1.8 ± 1.7 vs. 2.3 ± 2.4 mmols/L, $p < 0.001$).

Moreover, both longer length and higher complexity of coronary lesions were associated with choice of IVUS use, but there was no significant difference in the which vessel was treated nor vessel diameter between groups. The mean length of implanted stent per vessel was 30.0 ± 19.8 mm in the IVUS group vs. 24.6 (14.6) mm in the non-IVUS group ($p < 0.001$). Furthermore, patients undergoing IVUS had a higher mean numbers of stents (2.1 ± 1.4 vs. 1.4 ± 0.9, $p < 0.001$) and significantly higher rates of concomitant calcium modification device use. These include intracoronary laser, rotational atherectomy and shockwave lithotripsy: 19.8% of patients in the IVUS group had concomitant calcium modification vs. 2.6% in the non-IVUS group ($p < 0.001$). The variable "devices for calcium" was deemed positive if any calcium modification device or other devices that may be used in calcific lesions such as microcatheters.

Finally, there were large differences in the operator characteristics, with IVUS being favored heavily by more recently qualified consultants, discussed in the multivariate analysis section below.

TABLE 2 Multivariate analysis of IVUS use.

Variable	*P*	*OR*	Lower 95% CI	Upper 95% CI
Age (years)	0.046	0.987	0.974	1
Prev CABG	0.036	0.573	0.341	0.963
Calcific Lesions	< 0.001	5.223	3.383	8.064
STEMI	< 0.001	0.337	0.234	0.485
Qualified before 1990	< 0.001			
Qualified 1990–1999	0.026	5.397	1.227	23.735
Qualified 2000-	< 0.001	14.493	3.509	59.865
Operator case number	< 0.001	1.001	1	1.001
Year	0.005	1.101	1.03	1.178
Max stent length per vessel (mm)	0.012	0.987	0.977	0.997
Number stents used	< 0.001	1.593	1.374	1.847
Constant	0.004	0		

Multivariate analysis of factors associated with intravascular ultrasound use

The largest single predictor of IVUS use was the year that the operating consultant graduated from medical school (Table 2). Consultants graduating after 2000 were almost 15 times more likely to use IVUS than those graduating before 1990, even adjusting for the year that the procedure was performed (OR 14.5 (3.5–59.8), $p < 0.001$). The next most powerful predictor was the presence of calcific lesions, which led to a five-fold increase in the odds of IVUS use [OR 5.2 (3.4–8.0) $p < 0.001$]. The presence of STEMI made IVUS use around a third as likely [OR 0.34 (0.23–0.49), $p < 0.001$].

Unadjusted and adjusted outcomes of intravascular ultrasound use

Unadjusted outcomes are listed in Table 3. Adjusted outcomes are shown visually in Figure 3.

Adjusting for significant comorbidities, there was no significant difference in MACE at 1 year using IVUS [OR 1.04 (0.73—1.5), $p = 0.81$], 1-year mortality [OR 1.055 (0.65–1.71) $p = 0.828$] nor mortality throughout the study period [HR 0.93 (0.69—1.26), $p = 0.638$]. Furthermore, there was no difference in the device endpoint of MI/Death/TLR at 1 year [OR 1.15 (0.85–1.56) $p = 0.361$].

In chronic coronary syndromes, IVUS use was associated with higher rates of 1-year mortality [OR 2.34 (1.44–3.78), $p < 0.001$] but not the composite endpoint [OR 1.336 (0.95—1.88), $p = 0.098$].

However, in ACS there was no difference in either primary endpoint [composite endpoint: OR 0.953 (0.668—1.36), $p = 0.792$, 1-year-mortality: OR 0.748 (0.41—1.38), $p = 0.356$].

Finally, there was again no significant difference in outcome with IVUS use for patients with stented segments longer than 28 mm in either 1-year mortality [OR 1.287 (0.79—2.10), $p = 0.314$] nor MACE [OR 1.262 (0.894—1.78), $p = 0.186$].

Propensity-matched analysis of patients receiving intravascular ultrasound and associated outcomes

Propensity matching was performed looking at all covariates that could be related to both treatment choices (IVUS or no IVUS) or treatment outcome. For completeness, we used all the covariates that were significantly different on univariate analysis.

After matching, there was excellent balance between the IVUS (treatment) and non-treatment groups. This is shown most clearly in Supplementary Figure 1, which shows the absolute mean difference between treatment groups and the Kolmogorov-Smirnov statistics.

Outcomes after propensity matching

There was no significant difference in Survival between propensity-matched groups via Kaplan-Meier analysis across the length of the study period ($p = 0.564$, Figure 4). This also held true for patients with stents longer than 28 mm ($p = 0.919$).

There were higher rates of MACE in IVUS arm of the propensity-matched cohort, driven primarily by increased rates of unplanned revascularisation (Table 4). This remained the case using double-robust multivariate analysis, where IVUS was associated with higher rates of MACE [OR 1.72 (1.2–2.4), $p = 0.003$].

Discussion

Despite the growing evidence from randomized trials that IVUS improves cardiovascular outcomes across an array of patient populations, use in the UK remains low. These trials contained a significant proportion of patients with a history of

TABLE 3 Unadjusted outcomes.

Outcome				
All patients	**All patients (*n* = 10,574)**	**IVUS not used (*n* = 10,119)**	**IVUS used (*n* = 455)**	***P***
Composite death/Stroke/MI/Unplanned revasc 1 year	2,058 (19.5)	1,963 (19.4)	95 (20.9)	0.436
Death 1 year	903 (8.5)	855 (8.4)	48 (10.5)	0.117
Stroke 1 year	8 (0.1)	8 (0.1)	0 (0)	0.549
MI 1 year	300 (2.8)	286 (2.8)	15 (3.3)	0.546
Unplanned revasc 1 year	1,000 (9.5)	961 (9.5)	39 (8.6)	0.509
Composite CV death/MI/TLR 1 year	1,241 (11.7)	1,181 (11.7)	60 (13.2)	0.326
TLR	262 (3.4)	352 (3.5)	10 (2.2)	0.142
Stent thrombosis	84 (0.8)	78 (0.8)	6 (1.3)	0.198
Stents longer than 28 mm	**All patients (*n* = 3,592)**	**IVUS not used (*n* = 3,370)**	**IVUS Used (*n* = 222)**	***P***
Composite death/Stroke/MI/Unplanned revasc 1 year	704 (19.6)	650 (19.3)	54 (24.3)	0.067
Death 1 year	304 (8.5)	279 (8.3)	25 (11.3)	0.122
Stroke 1 year	0 (0)	0 (0)	0 (0)	1
MI 1 year	101 (2.8)	94 (2.8)	7 (3.2)	0.751
Unplanned revasc 1 year	348 (9.7)	321 (9.5)	27 (12.2)	0.198
Composite CV death/MI/TLR	419 (11.7)	390 (11.6)	29 (13.1)	0.503
TLR	109 (3)	104 (3.1)	5 (2.3)	0.684
Stent thrombosis	40 (1.1)	38 (1.1)	2 (0.9)	1

previous PCI. Our study aimed to look at contemporary real-world use in the era of second generation drug-eluting stents to assess the patient, lesion and operator characteristics associated with IVUS use in addition to adjusted analyses of IVUS effect. Our analysis showed two main findings:

1. Operator characteristics are more important than patient characteristics in choosing who receives IVUS
2. Likely due to the large selection bias, there was no improvement in outcomes with IVUS use in this study

Operator characteristics are more important than patient characteristics in choosing who receives intravascular ultrasound

Outside of a trial population, it is unsurprising that with time and resource constraints there is selective deployment of IVUS technology. Our patient population was confined to those who had never undergone PCI. There were two reasons for this. The first was that we wanted to scrutinize PCI as practiced at our institution that would not be affected by practice from other institutions. The second, and most important reason, was that we wanted to examine the effect of IVUS on the stent that was implanted with IVUS assistance, without the potential confounding of previous metalwork in the coronary tree.

The patient characteristics are significantly different between the groups. Patients who underwent IVUS-guided PCI were older, more likely to be ex-smokers and to be diagnosed with hypercholesterolemia, diabetes, hypertension and chronic kidney disease. This translated into the calcific nature of the coronary lesions—although we do not have direct markers of calcium in our data, patients who underwent IVUS were significantly more likely to need procedural devices including microcatheters, and calcium modification devices such as rotablation or shockwave lithotripsy. In multivariate analysis, the use of calcium devices was associated with an almost five-fold increase in the odds of IVUS use.

Similarly, patients requiring IVUS were less likely to be suffering an acute coronary syndrome and had fewer concomitant markers of acute cardiovascular compromise, for example having lower mean lactate levels. None of these results are surprising either at an empirical or evidence-based level. Almost all observational data shows a similar bias in operators toward this kind of patient population where stent malapposition is more likely, such as a recent study of over 100 000 patients in the United States (14). As a dedicated heart attack center in the UK, 77% of our ACS patients require primary PCI for STEMI. The observational evidence does not suggest an overwhelming benefit of IVUS use in this type of population

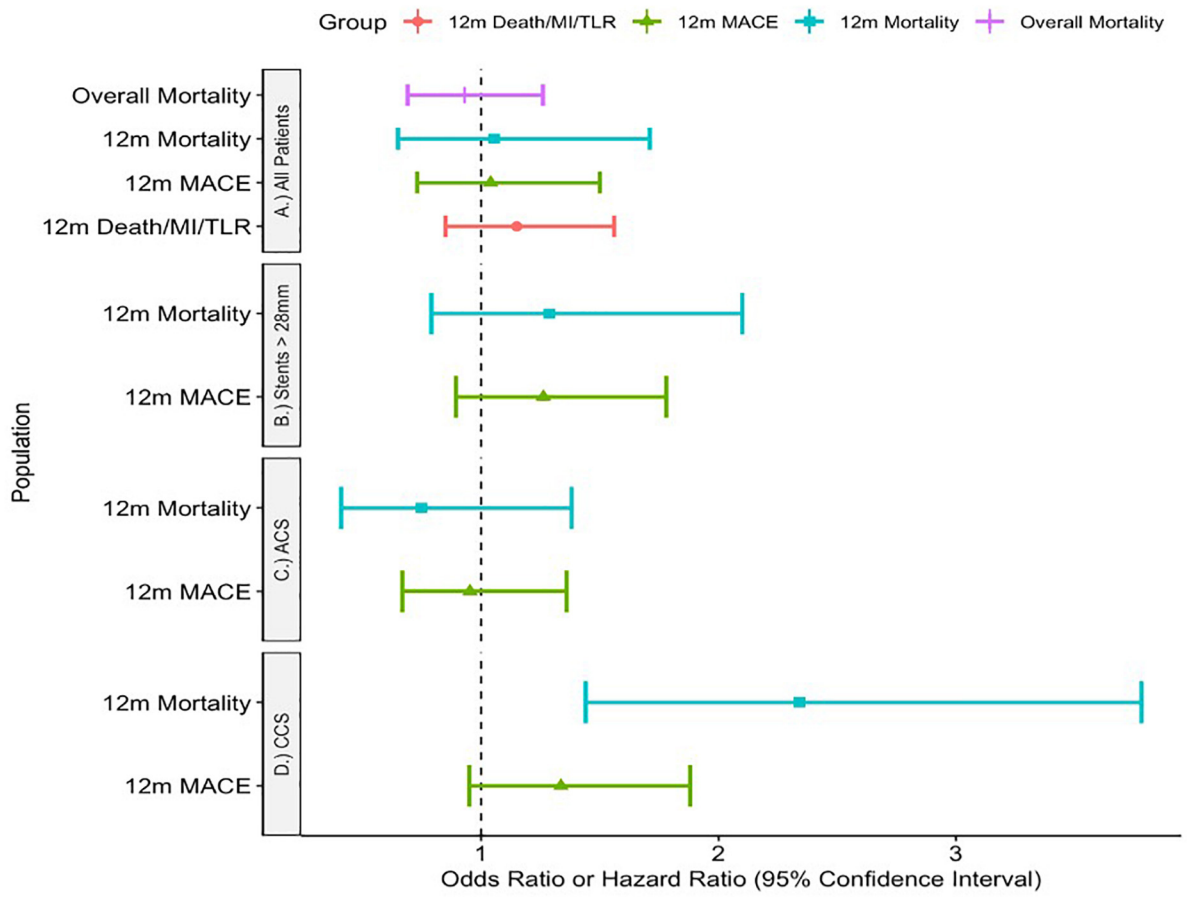

FIGURE 3
Adjusted outcome measures.

(15–17). In fact over-expansion of a stent in a thrombotic lesion can lead to distal embolization and microvascular obstruction.

However, a more important finding was that the strongest predictor of IVUS use in our patient population was the year that the consultant left medical school. In multivariate analysis, the odds of undergoing IVUS were almost 15-fold higher if the consultant in charge graduated from medical school after 2000 compared to before 1990. As mentioned before, IVUS use is low in the UK and the USA compared to Asian countries with similar GDP per capita. There are a number of postulated reasons for this, ranging from cost and different reimbursement patterns to fears surrounding increased complication rates, through to a lack of training of interventional cardiologists. Over half of interventional trainees in the United States report limited confidence and training with IVUS (18).

The findings of our physician characteristics that were associated with IVUS use, such as generation and procedural numbers, tally with previous data on the subject that show that both a physician's generation and patient numbers are associated with being an early adopter of technology (19). In order to maximize IVUS use in the correct patients, facilitating IVUS use for trainees and putting extra resources into training older and lower-volume operators may be a successful strategy.

The overall operator familiarity with IVUS can also affect the outcomes of patients when comparing image-guided with angiography-only PCI. Previous studies have noted the paradoxical relationship between IVUS use and patient outcomes on both an individual and population level. Operators in centers with high levels of intracoronary imaging become reliant on this technology and thus the outcomes of patients who undergo angiography-only PCI are worse because the operators are unfamiliar with the technique (20). The opposite is true in this case—our operators use IVUS in only 4.3% of cases, well below the 33% that would qualify a center as having low intracoronary imaging rates in the study above. Therefore, the operators are likely performing the angiography technique that is more comfortable and reliable, potentially leading to reduced differences between the study arms. However, it must be noted that, in clinical practice, the best operators are those who can accurately size a vessel using both angiography and intracoronary imaging modalities.

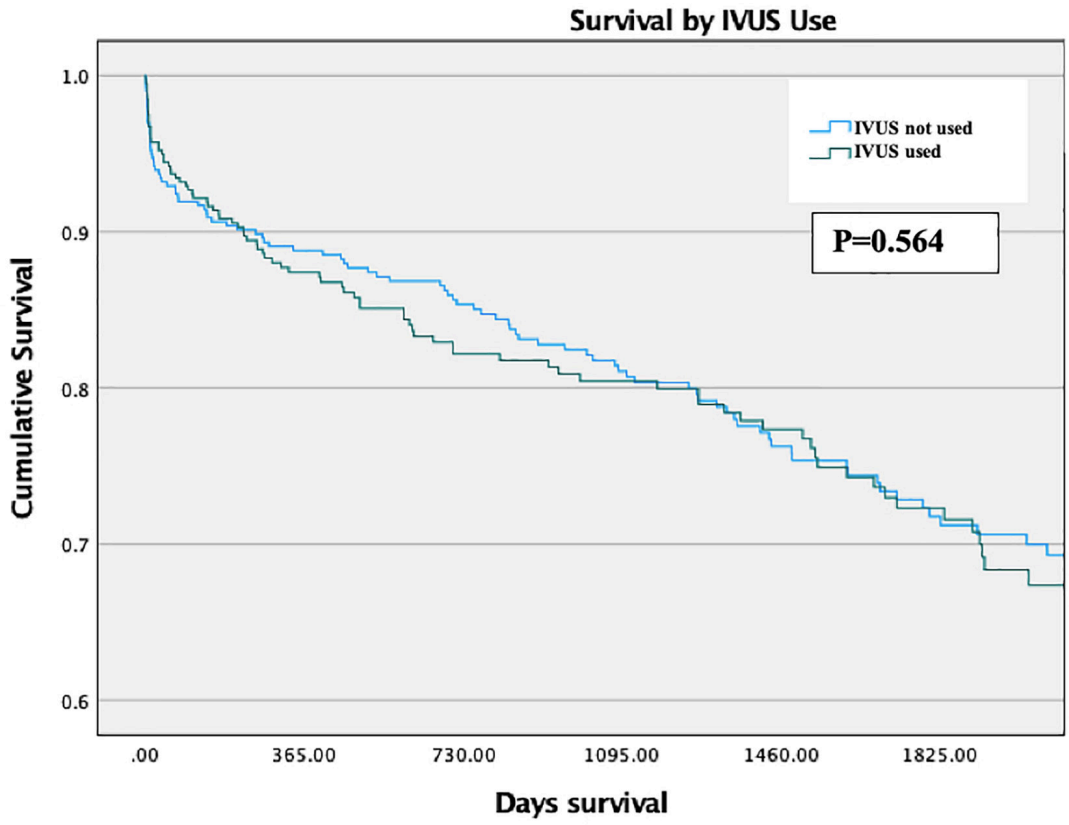

FIGURE 4
Survival by IVUS use (propensity matched groups).

There was no improvement in outcomes with intravascular ultrasound use in this study, probably due to the large selection bias and the high-risk population

The evidence base for IVUS use is strong and based on both observational data and numerous RCTs in the contemporary DES era. These trials have studied IVUS use in a variety of different scenarios. The first tranche examined medium-term outcome measures in patients with complex coronary disease, with the exception of the all-comers ULTIMATE trial. A meta-analysis synthesizing these trials showed that at 14 months mean follow-up, IVUS-guided PCI was associated with lower rates of cardiovascular mortality, target lesion revascularization and myocardial infarction (3).

The ULTIMATE trial (4) looked at all-comers and found significantly fewer instances of stent thrombosis and target vessel revascularization in the IVUS arm at 3 years follow-up. Further support for the benefit of IVUS at longer time points came in the shape of IVUS-XPL, which followed up patients for 5 years and demonstrated lower rates of major adverse cardiac events (5). These included death, target vessel MI and target-vessel revascularization. Finally, team members of the IVUS-XPL trial published a pooled analysis of the IVUS-XPL and ULTIMATE trials looking at patients who had $\geq$ 28 mm of stent inserted. There were significantly lower levels of MACE at 3 years, as reported in IVUS-XPL, although no reduction in cardiac death across 2,577 such patients and this was driven principally by TLR (6). Finally, a large-scale meta-analysis examining 31 trials, both randomized and observational trials, demonstrated that MACE was lower with IVUS use, although mortality was significantly reduced only when observational studies were included (7).

It was on this background that we began looking at patients without prior PCI. Each trial had a significant proportion of patients who had undergone prior revascularization. The lowest proportion of such patients was in IVUS-XPL, at 11%, and the greatest was almost 48% (15). The ULTIMATE trial was near the middle of this range at 18.7%. In no analysis did we find any significant improvements in patient outcomes with IVUS use, and in fact there was some suggestion of higher rates of unplanned revascularization. The same held true for patients with stents longer than 28 mm—a cut-off

TABLE 4 Outcomes for propensity-matched patients.

Outcomes in propensity matched patients

All patients	All patients (n = 794)	IVUS not used (n = 397)	IVUS used (n = 397)	P
Composite death/Stroke/MI/Unplanned revasc 1 year	162 (20.4)	64 (16.1)	98 (24.7)	0.003
Death 1 year	73 (9.2)	30 (7.6)	43 (10.8)	0.11
Stroke 1 year	2 (0.3)	1 (0.3)	1 (0.3)	1
MI 1 year	29 (3.7)	14 (3.5)	29 (3.7)	0.85
Unplanned revasc 1 year	71 (8.9)	23 (5.8)	48 (12.1)	0.002
Composite CV death/MI/TLR 1 year	111 (14.0)	52 (13.1)	59 (14.9)	0.474
TLR	7 (0.9)	2 (0.5)	5(1.3)	0.451
Stent thrombosis	4 (0.5)	0 (0)	4 (1)	0.124

chosen in line with the IVUS-XPL trial and subsequent pooled analysis with ULTIMATE.

The lack of benefit shown with IVUS use likely due to the large selection bias in patient choice, as well as the high-risk nature of our population. It seems implausible that patients with IVUS-guided PCI would be more likely to require revascularization. Secondly, our mortality rate is significantly higher than other all-comers trials such as ADAPT-DES (21) which probably reflects our status as a receiver of high-risk ACS patients for the region, as shown by a cardiac arrest rate of almost 8%. Furthermore, the end-goal of IVUS use appropriate stent expansion that may require multiple procedural elements and checks, which may well be harder to accomplish in the setting of ACS. This highlights how limited this study is at assessing outcomes due to its observational design, and the fact that IVUS use is driven by all of patient, lesion and operator characteristics.

In addition, although the propensity matching was technically very good, propensity matching is only as good as the fields that are inputted. Furthermore, the propensity-matched numbers were underpowered for outcome analysis. The data inputted is largely what is found in any interventional cardiology database, but which data is accessible is not necessarily the same as which data is optimal. There is no way to propensity match a physician's intuition for a patient, or how robust the patient looks in clinic. We can try to compensate with metrics including age, weight and important comorbidities, as we have done here, but it is never complete. This is the principal reason why RCTs exist, to exclude biases that we do not know even exist.

Therefore, the firm points that we can make in this paper are that patients who are undergoing their first PCI with a higher burden of comorbidity, in an elective setting, with lesions that are more calcified, being proceeded upon by more recently graduated cardiologists, are more likely to have IVUS used. As far as we can tell from our data, these patients are unlikely to fare better or worse compared to patients treated without IVUS when we control for these factors. We know that in other population settings, such as long stents implanted in patients with previous percutaneous revascularization, patients have better clinical outcomes with IVUS-guided angioplasty.

The strongest conclusion of this paper is that it is imperative to train more cardiologists to be comfortable with IVUS use in the UK, in order to use IVUS appropriately and in the settings that have shown to be beneficial by randomized controlled trials. The data from observational studies such as this are too confounded to suggest that there is no benefit to using IVUS in PCI-naïve patients.

Data availability statement

The original contributions presented in this study are included in the article/**Supplementary material**, further inquiries can be directed to the corresponding author.

Ethics statement

Ethical review and approval was not required for the study on human participants in accordance with the local legislation and institutional requirements. Written informed consent for participation was not required for this study in accordance with the national legislation and the institutional requirements.

Author contributions

AT: concept, data collection, statistical analysis, manuscript preparation, and text writing. VP: concept, manuscript preparation and text writing, edits, and statistical advice. Both authors contributed to the article and approved the submitted version.

Conflict of interest

The authors declare that the research was conducted in the absence of any commercial or financial relationships that could be construed as a potential conflict of interest.

Publisher's note

All claims expressed in this article are solely those of the authors and do not necessarily represent those of their affiliated organizations, or those of the publisher, the editors and the reviewers. Any product that may be evaluated in this article, or claim that may be made by its manufacturer, is not guaranteed or endorsed by the publisher.

Supplementary material

The Supplementary Material for this article can be found online at: https://www.frontiersin.org/articles/10.3389/fcvm.2022.974161/full#supplementary-material

SUPPLEMENTARY FIGURE 1
Propensity matching statistics.

References

1. Yock PG, Linker DT, Angelsen BA. Two-dimensional intravascular ultrasound: technical development and initial clinical experience. *J Am Soc Echocardiogr.* (1989) 2:296–304. doi: 10.1016/S0894-7317(89)80090-2

2. Ono M, Kawashima H, Hara H, Gao C, Wang R, Kogame N, et al. Advances in IVUS/OCT and future clinical perspective of novel hybrid catheter system in coronary imaging. *Front Cardiovasc Med.* (2020) 7:119. doi: 10.3389/fcvm.2020.00119

3. Elgendy IY, Mahmoud AN, Elgendy AY, Mintz GS. Intravascular ultrasound-guidance is associated with lower cardiovascular mortality and myocardial infarction for drug-eluting stent implantation – insights from an updated meta-analysis of randomized trials. *Circ J.* (2019) 83:1410–3. doi: 10.1253/circj.CJ-19-0209

4. Gao XF, Ge Z, Kong XQ, Kan J, Han L, Lu S, et al. 3-Year Outcomes of the ULTIMATE trial comparing intravascular ultrasound versus angiography-guided drug-eluting stent implantation. *JACC Cardiovasc Interv.* (2021) 14:247–57. doi: 10.1016/j.jcin.2020.10.001

5. Hong SJ, Mintz GS, Ahn CM, Kim JS, Kim BK, Ko YG, et al. Effect of intravascular ultrasound-guided drug-eluting stent implantation: 5-year follow-up of the IVUS-XPL randomized trial. *JACC Cardiovasc Interv.* (2020) 13:62–71. doi: 10.1016/j.jcin.2019.09.033

6. Hong SJ, Zhang JJ, Mintz GS, Ahn CM, Kim JS, Kim BK, et al. Improved 3-year cardiac survival after IVUS-guided long DES implantation: a patient-level analysis from 2 randomized trials. *JACC Cardiovasc Interv.* (2022) 15:208–16. doi: 10.1016/j.jcin.2021.10.020

7. Buccheri S, Franchina G, Romano S, Puglisi S, Venuti G, D'Arrigo P, et al. Clinical outcomes following intravascular imaging-guided versus coronary angiography-guided percutaneous coronary intervention with stent implantation: a systematic review and bayesian network meta-analysis of 31 studies and 17,882 patients. *JACC Cardiovasc Interv.* (2017) 10:2488–98. doi: 10.1016/j.jcin.2017.08.051

8. Neumann FJ, Sousa-Uva M, Ahlsson A, Alfonso F, Banning AP, Benedetto U, et al. ESC scientific document group. 2018 ESC/EACTS guidelines on myocardial revascularization. *Eur Heart J.* (2019) 40:87–165. doi: 10.1093/eurheartj/ehy855

9. Ludman PF. *National Audit Adult Interventional Procedures.* (2020). Available online at: https://www.bcis.org.uk/audit-results/ (accessed Oct 5, 2020).

10. Hibi K, Kimura K, Umemura S. Clinical utility and significance of intravascular ultrasound and optical coherence tomography in guiding percutaneous coronary interventions. *Circ J.* (2014) 79:24–33. doi: 10.1253/circj.CJ-14-1044

11. Claessen BE, Mehran R, Mintz GS, Weisz G, Leon MB, Dogan O, et al. Impact of intravascular ultrasound imaging on early and late clinical outcomes following percutaneous coronary intervention with drug-eluting stents. *JACC Cardiovasc Interv.* (2011) 4:974–81. doi: 10.1016/j.jcin.2011.09.011

12. Garcia-Garcia HM, McFadden EP, Farb A, Mehran R, Stone GW, Spertus J, et al. Standardized end point definitions for coronary intervention trials: the academic research consortium-2 consensus document. *Circulation.* (2018) 137:2635–50. doi: 10.1161/CIRCULATIONAHA.117.029289

13. von Elm E, Altman DG, Egger M, Pocock SJ, Gøtzsche PC, Vandenbroucke JP. The Strengthening the Reporting of Observational Studies in Epidemiology (STROBE) statement: guidelines for reporting observational studies. *Ann Intern Med.* (2007) 147:573–7. doi: 10.7326/0003-4819-147-8-200710160-00010

14. Mentias A, Sarrazin MV, Saad M, Panaich S, Kapadia S, Horwitz PA, et al. Long-term outcomes of coronary stenting with and without use of intravascular ultrasound. *JACC Cardiovasc Interv.* (2020) 13:1880–90. doi: 10.1016/j.jcin.2020.04.052

15. Nakatsuma K, Shiomi H, Morimoto T, Ando K, Kadota K, Watanabe H, et al. Intravascular ultrasound guidance vs. angiographic guidance in primary percutaneous coronary intervention for ST-segment elevation myocardial infarction - long-term clinical outcomes from the CREDO-Kyoto AMI registry. *Circ J.* (2016) 80:477–84. doi: 10.1253/circj.CJ-15-0870

16. Khalid M, Patel NK, Amgai B, Bakhit A, Khalid M, Kafle P, et al. In-hospital outcomes of angiography versus intravascular ultrasound-guided percutaneous coronary intervention in ST-elevation myocardial infarction patients. *J Community Hosp Intern Med Perspect.* (2020) 10:436–42. doi: 10.1080/20009666.2020.1800970

17. Ya'qoub L, Gad M, Saad AM, Elgendy IY, Mahmoud AN. National trends of utilization and readmission rates with intravascular ultrasound use for ST-elevation myocardial infarction. *Catheter Cardiovasc Interv.* (2021) 98:1–9. doi: 10.1002/ccd.29524

18. Mintz GS. Intravascular imaging, stent implantation, and the elephant in the room. *JACC Cardiovasc Interv.* (2017) 10:2499–501. doi: 10.1016/j.jcin.2017.09.024

19. Zachrison KS, Yan Z, Samuels-Kalow ME, Licurse A, Zuccotti G, Schwamm LH. Association of physician characteristics with early adoption of virtual health care. *JAMA Netw Open.* (2021) 4:e2141625. doi: 10.1001/jamanetworkopen.2021.41625

20. Ng AK, Ng PY, Ip A, Lam LT, Siu CW. Survivals of angiography-guided percutaneous coronary intervention and proportion of intracoronary imaging at population level: the imaging paradox. *Front Cardiovasc Med.* (2022) 9:792837. doi: 10.3389/fcvm.2022.79283

21. Witzenbichler B, Maehara A, Weisz G, Neumann FJ, Rinaldi MJ, Metzger DC, et al. Relationship between intravascular ultrasound guidance and clinical outcomes after drug-eluting stents: the assessment of dual antiplatelet therapy with drug-eluting stents (ADAPT-DES) study. *Circulation.* (2014) 129:463–70. doi: 10.1161/CIRCULATIONAHA.113.003942

frontiers | Frontiers in Cardiovascular Medicine

TYPE Original Research
PUBLISHED 13 September 2023
DOI 10.3389/fcvm.2023.1246759

OPEN ACCESS

EDITED BY
Arunark Kolipaka,
The Ohio State University, United States

REVIEWED BY
Juliet Varghese,
The Ohio State University, United States
Yu Ding,
The Ohio State University, United States

*CORRESPONDENCE
Sanaz Asadian
✉ asadian_s@yahoo.com

†These authors have contributed equally to this work and share first authorship

RECEIVED 10 July 2023
ACCEPTED 28 August 2023
PUBLISHED 13 September 2023

CITATION
Salmanipour A, Ghaffari Jolfayi A, Sabet Khadem N, Rezaeian N, Chalian H, Mazloomzadeh S, Adimi S and Asadian S (2023) The predictive value of cardiac MRI strain parameters in hypertrophic cardiomyopathy patients with preserved left ventricular ejection fraction and a low fibrosis burden: a retrospective cohort study.
Front. Cardiovasc. Med. 10:1246759.
doi: 10.3389/fcvm.2023.1246759

The predictive value of cardiac MRI strain parameters in hypertrophic cardiomyopathy patients with preserved left ventricular ejection fraction and a low fibrosis burden: a retrospective cohort study

Alireza Salmanipour[1†], Amir Ghaffari Jolfayi[1†], Nazanin Sabet Khadem[2], Nahid Rezaeian[1], Hamid Chalian[3], Saeideh Mazloomzadeh[1], Sara Adimi[1] and Sanaz Asadian[1*]

[1]Rajaie Cardiovascular Medical and Research Center, Iran University of Medical Sciences, Tehran, Iran, [2]Department of Radiology, School of Medicine, Iran University of Medical Sciences, Tehran, Iran, [3]Department of Radiology, Cardiothoracic Imaging, University of Washington, Seattle, WA, United States

Background: Prompt interventions prevent adverse events (AE) in hypertrophic cardiomyopathy (HCM). We evaluated the pattern and the predictive role of feature tracking (FT)-cardiac magnetic resonance (CMR) imaging parameters in an HCM population with a normal left ventricular ejection fraction (LVEF) and a low fibrosis burden.
Methods: The CMR and clinical data of 170 patients, consisting of 142 HCM (45 ± 15.7 years, 62.7% male) and 28 healthy (42.2 ± 11.26 years, 50% male) subjects, who were enrolled from 2015 to 2020, were evaluated. HCM patients had a normal LVEF with a late gadolinium enhancement (LGE) percentage below 15%. Between-group differences were described, and the potent predictors of AE were determined. A *P*-value below 0.05 was considered significant.
Results: LV global longitudinal, circumferential, and radial strains (GLS, GCS, and GRS, respectively) and the LV myocardial mass index (MMI) were different between the healthy and HCM cases (all *P*s < 0.05). Strains were significantly impaired in the HCM patients with a normal MMI. A progressive decrease in LVGLS and a distinct fall in LVGCS were noted with a rise in MMI. AE were predicted by LVGLS, LVGCS, and the LGE percentage, and LVGCS was the single robust predictor (HR, 1.144; 95% CI, 1.080–1.212; *P* = 0.001). An LVGCS below 16.2% predicted AE with 77% specificity and 58% sensitivity.
Conclusions: LV strains were impaired in HCM patients with a normal EF and a low fibrosis burden, even in the presence of a normal MMI. CMR parameters, especially FT-CMR values, predicted AE in our HCM patients.

KEYWORDS

hypertrophic cardiomyopathy (HCM), cardiac MRI, feature tracking, cardiac function, adverse events

Introduction

Hypertrophic cardiomyopathy (HCM) is an inherited disorder characterized by left ventricular (LV) hypertrophy and is unexplainable by other causes (1–3). HCM is the most common monogenic cardiovascular disorder, with an estimated prevalence of 1:250–500 in the adult population, predominantly affecting adolescents and young adults while rare in

children (4–6). The LV ejection fraction (EF), as an index of systolic function, often remains within the normal range in HCM despite disease progression (7).

Myocardial fibers are arranged in 3 different orientations as a continuum of 2 helical geometries, helping amplify myocyte contraction and cardiac function as a single unit. This superstructure deteriorates in HCM, resulting in faulty mechanics despite an apparently preserved EF. HCM diagnosis and characterization are based on echocardiography and magnetic resonance imaging (MRI), although cardiac magnetic resonance imaging (CMR) provides better identification and risk stratification by detecting *in vivo* fibrosis (8).

Several studies have examined imaging features that could better elucidate myocardial abnormalities and patient outcomes (9–12). One of these methods is the myocardial strain analysis by CMR to assess subclinical function impairment. Strains are reported in 3 directions: longitudinal, circumferential, and radial. The longitudinal strain represents subendocardial fiber deformation, while circumferential and radial strains reveal mid-myocardial and subepicardial fiber changes, respectively (13). Multiple parameters can affect LV myocardial strains in patients with HCM, including LVEF, the myocardial mass, the myocardial fibrosis burden, and the left ventricular outflow tract (LVOT) obstruction (14).

In the present study, utilizing the feasible cardiac magnetic resonance feature-tracking (CMR-FT) method, we aimed to define the myocardial strain pattern in HCM patients. Moreover, we investigated the role of CMR parameters in the prognostication of HCM patients with a normal LVEF and a low fibrosis burden.

Methods

The institutional research committee approved this study and waived the need for informed consent due to the retrospective design of this study.

Study population

The current investigation retrospectively enrolled 241 patients with HCM who underwent CMR between 2015 and 2020 in our institution. Additionally, the CMR findings of 28 healthy volunteers were retrieved from the center's normal CMR examination archives. Healthy subjects had a normal physical examination, no personal or family history of cardiac disease, and no cardiovascular risk factors, composed of hypertension, diabetes mellitus, and dyslipidemia.

Diagnostic criteria

All patients with a definite diagnosis of HCM, according to the American heart association/American college of cardiology guidelines for diagnosing and treating patients with hypertrophic cardiomyopathy, were enrolled (15).

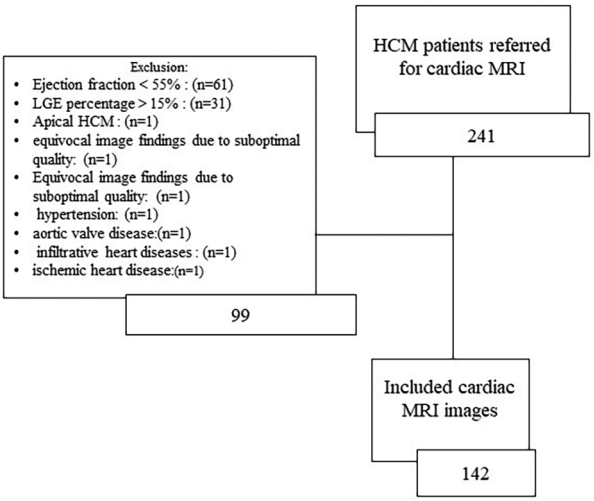

FIGURE 1
Diagram of the study population. HCM, hypertrophic cardiomyopathy; LGE, late gadolinium enhancement.

The exclusion criteria were an LVEF below 55%, a late gadolinium enhancement (LGE) percentage of more than 15%, hypertension, aortic valve disease, infiltrative heart diseases (e.g., Fabry disease, Danon disease, and cardiac amyloidosis), athlete's heart, ischemic heart disease, significant cardiac arrhythmias during CMR acquisition, and renal impairment (defined as an estimated glomerular filtration rate <30 ml/min precluding gadolinium injection). Also, other types of HCM, such as apical HCM, are excluded from the study. Furthermore, CMR studies that yielded equivocal findings due to suboptimal quality were excluded from the study (**Figure 1**).

Study population classification

The medical records of the patients were reviewed. Then, based on their transthoracic echocardiography (TTE)-measured LVOT gradient, the patients were classified into 2 groups: an LVOT gradient of less than 50 mm Hg and an LVOT gradient of 50 mm Hg or higher. TTE examinations with a maximum interval of 6 months from the CMR examination were selected for analysis. The former group was regarded as a no or mild LVOT obstruction group and the latter as a severe LVOT obstruction group (16, 17).

In another classification, the patients were divided based on their myocardial mass index (MMI) into normal and increased MMI categories. An MMI exceeding 81 g/m^2 for females and 85 g/m2 for males was regarded as increased (18).

CMR

CMR images were acquired using a 1.5-T MRI equipment (Siemens Avanto, Erlangen, Germany) with an 8-element phased-array receiver surface coil. A semi-automatic post-processing program (CVi42; Circle Cardiovascular Imaging Inc, Calgary, Canada) was applied for the measurements.

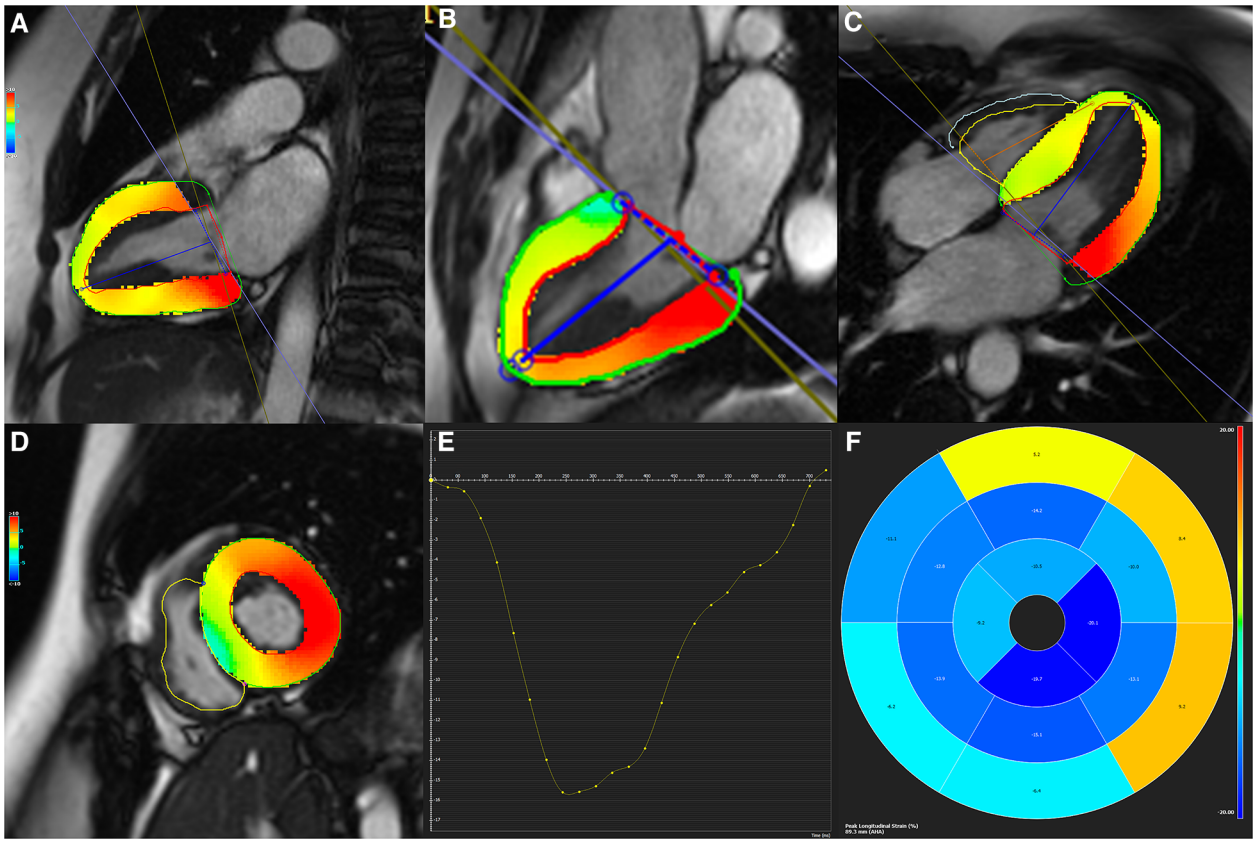

FIGURE 2
(A–D) Two-, three-, and four-chamber as well as short-axis cine functional sequences with defined endocardial and epicardial contours. (E) Strain curve, and (F) Bull's eye map are depicted for global circumferential and longitudinal strains.

CMR function

Electrocardiography-gated cine steady-state free precession in the 2-, 3-, and 4-chamber views, the right ventricular and LV outflow tracts planes, and a stack of short-axis slices covering LV during breath-hold at end-expiration (slice thickness = 8 mm, the field of view = 300 mm, flip angle = 65°, bandwidth = 925 Hz/Px, imaging matrix = 156 × 192, and repetition time/echo time = 2.7/1.2 ms) were acquired. Parallel imaging was utilized. The endocardial and epicardial borders were manually drawn in short-axis end-diastolic and end-systolic images and propagated throughout all ventricular slices. Functional parameters, composed of the EF, end-diastolic and end-systolic volumes, the LV mass index, the maximal septal thickness, the presence of the systolic anterior motion of the mitral valve, and the ratio of the asymmetric septal hypertrophy, were registered.

CMR-FT

LV end-diastolic and end-systolic frames of 2-, 3- and 4-chamber views and the short-axis plane were selected. Optimal brightness adjustment was done to ensure the best contrast to make accurate discrimination between the endocardium and the blood pool. The endocardial and epicardial contours were defined manually and propagated throughout the slices, and 3D LV strains, consisting of global longitudinal (GLS), global circumferential (GCS), and global radial (GRS) strains, were calculated utilizing the CMR-FT method (Figure 2). The absolute values of strains were utilized for analysis.

LGE imaging

LGE images were obtained 15 min after the injection of the gadolinium contrast agent, gadotetrate meglumine (Dotarem), applying the phase-sensitive inversion recovery sequence. Breath-held segmented single-shot protocol (slice thickness = 8 mm, the field of view = 320 mm, flip angle = 40°, bandwidth = 1,445 Hz/Px, imaging matrix = 192 × 192, and repetition time/echo time = 2.9/1.1 ms) with selecting the inversion time to null the normal myocardium (typically 200–250 ms) was applied. Considering a 5-standard deviation from the mean myocardial signal intensity, the LGE percentage was measured. The results were assessed visually and modified if needed.

LVOT evaluation

Based on echocardiographic findings obtained from patients' medical records, the patients' LVOT gradients were collected. Gradient measurement was performed based on the modified Bernoulli equation.

On CMR, cine LVOT images in at least 5 consecutive slices were acquired. The presence of the systolic anterior motion of the mitral valve and LVOT turbulence were registered.

Follow-up data

For each patient, we considered at least one follow-up. If a patient had several follow-ups, we considered the last one. A composite of adverse events, consisting of sudden cardiac death, aborted sudden cardiac death (unsuccessful cardiopulmonary resuscitation), implantable cardioverter defibrillator insertion, and deteriorated systolic function (an EF decline to <40%), was considered and registered.

Data collection

CMR measures were registered by two experts with more than five years of expertise (a cardiologist and a radiologist) in cardiovascular imaging. Readers were blind to the study population's data. Interobserver variability was reported, and both examiners' consensus resolved any conflicts.

Echocardiographic, clinical, and follow-up data, including physician visits, lab data, and imaging examinations, were collected by reviewing patients' medical records and/or telephone calls whenever needed.

Statistical analysis

SPSS version 22 (IBM incorporation) was utilized for statistical analysis. Categorical and continuous variables were reported as frequencies (percentages) and mean ± standard deviation (SD), respectively. The Kolmogorov–Smirnov test was utilized to assess the normality of distribution. Between-group comparisons were performed using the *t*, Mann–Whitney *U*, analysis of variances (ANOVA), and χ^2 tests, whichever was appropriate. The *post hoc* test of the least significant difference described the pattern of the intergroup changes. Univariate and multivariate Cox regression analyses were applied to evaluate the role of CMR parameters in revealing undesirable outcomes. For the definition of the cutoff point, specificity, and sensitivity of the predictor variables, the receiver operating characteristic (ROC) curve was utilized. Moreover, *P*-values below 0.1 for the univariate Cox regression analysis and 0.05 for the rest of the tests were considered statistically significant.

Results

Study population characteristics

CMR examinations of 170 patients, consisting of 142 subjects with HCM (mean ± SD age =45 y ± 15.7; 62.7% male) and 28 healthy subjects (mean ± SD age =42.2y ± 11.26; 50% male), were included. Interobserver variability was estimated to be 6.3% and the examiners' consensus-resolved conflicts.

The mean ± SD of the body surface area was 1.87 m^2 ± 0.14, and the mean ± SD of MMI was 59.57 g/m^2 ± 8.56 for the healthy subjects. No significant differences were observed in LVEF and end-diastolic and end-systolic volumes between the healthy population and the patients with HCM, whereas significant differences were noted between the 2 groups in LV MMI, LVGLS, LVGCS, and LVGRS (all *P*s < 0.05).

HCM patients characteristics in LVOT groups

Table 1 presents the demographic characteristics and the baseline CMR data of the patients with HCM in the two LVOT groups.

The difference in mean strain values was significant between the healthy controls and the HCM group. However, the mean strain values were not different between the 2 LVOT gradient groups ($P > 0.05$).

CMR-FT parameters in MMI groups

The 1-way ANOVA revealed a significant difference in all 3 strain parameters between the healthy controls and the HCM cases with normal and increased myocardial mass (all *P*s < 0.05). Between-group changes were evaluated by applying the *post hoc* least significant difference test, and the results are depicted in Figure 3.

The correlation between strain values and MMI

The Pearson correlation test revealed a moderate inverse linear correlation between MMI and LVGLS and LVGCS ($r = -0.4$ and $r = -0.32$, respectively; *P*s = 0.001). Scatter plots are demonstrated in Figure 4.

Follow-up data

The median (interquartile range) follow-up time was 25 months (23). Twenty-three patients developed adverse events. The results of the independent t-test analysis are depicted in Table 2. It was revealed that absolute values of LVGLS, LVGRS and LVGCS are considerably lesser in patients with adverse events than those without. Also, the myocardial mass index is significantly higher in patients with adverse events compared to others.

The results of the Cox regression analyses are depicted in Table 3. Variables with *P*-values below 0.1, consisting of LVGLS, LVGCS, and the LGE percentage, were entered into the

TABLE 1 Demographics, baseline CMR characteristics, and follow-up data of the study population.

Variables	LVOT Gradient < 50mmHg ($n = 69$)		LVOT Gradient > 50mmHg ($n = 73$)		*P*-value
Demographics					
Age (y) (mean ± SD)	45.4 ± 16.55		44.6 ± 14.94		0.7
Gender *n* (%)	Male	Female	Male	Female	0.8
	44 (63.8%)	25 (36.2%)	45 (61.6%)	28 (38.4%)	
BSA (m^2)	1.88 ± 0.24		1.85 ± 0.21		0.5
Positive family history	Negative	Positive	Negative	Positive	**0.03**
	38 (55%)	31 (45%)	24 (32.9%)	49 (67.1%)	
Diabetes	62 (90%)	7 (10%)	64 (87.7%)	9 (12.3%)	0.7
CMR findings					
LVEF (%) (mean ± SD)	61.4 ± 4		62.61 ± 4.6		0.1
LVEDVI (cc/m^2) (mean ± SD)	70.72 ± 15.59		72.63 ± 14.72		0.4
LVESVI (cc/m^2) (mean ± SD)	26.91 ± 6.52		27.38 ± 8.60		0.7
Main PA (mm) (mean ± SD)	23.96 ± 6.44		25.05 ± 4.50		0.2
Myocardial mass index (g/m^2) (mean ± SD)	67.90 ± 20.24		79.75 ± 27.45		**0.003**
Maximum septal diameter (mm) (mean ± SD)	17.48 ± 4.19		20.49 ± 4.34		**0.001**
ASH ratio	2.80 ± 1.10		3.05 ± 1.23		0.2
LGE percentage (mean ± SD)	6.43 ± 4.17		6.37 ± 3.76		0.9
LVGLS (mean ± SD)	14.21 ± 2.80		14.41 ± 2.86		0.6
LVGCS (mean ± SD)	17.30 ± 2.78		17.88 ± 3.25		0.2
LVGRS (mean ± SD)	47.34 ± 14.03		48.54 ± 15.88		0.6
Increased Myocardial Mass index	Negative	Positive	Negative	Positive	0.06
	56 (81.2%)	13 (18.8%)	48 (65.8%)	25 (34.2%)	
SAM	55 (79.7%)	14 (20.3%)	2 (2.7%)	71 (97.3%)	**0.001**
Follow up data					
Poor outcome	59 (85.5%)	10 (14.4 %)	60 (82.2%)	13 (17.8%)	0.2
Sudden cardiac death	68 (98.6%)	1 (1.4%)	72 (98.7%)	1 (1.3%)	0.9
Aborted sudden cardiac death	69 (100%)	0 (0%)	72 (98.7%)	1 (1.3%)	0.5
ICD insertion	63 (91.3%)	6 (8.7 %)	64 (87.7%)	9 (12.3%)	0.3
Follow up Systolic dysfunction	65 (94.2%)	4 (5.8%)	71 (97.2%)	2 (2.8%)	0.6

CMR: cardiac magnetic resonance, LVOT: left ventricle outflow tract, BSA: body surface area, LV: left ventricle, EF: ejection fraction, EDVI: end-diastolic volume index, ESVI: end-systolic volume index, PA: pulmonary artery, ASH: asymmetric septal hypertrophy, LGE: late gadolinium enhancement, GLS: global longitudinal strain, GCS: global circumferential strain, GRS: global radial strain, SAM: systolic anterior motion, ICD: implantable cardioverter defibrillator

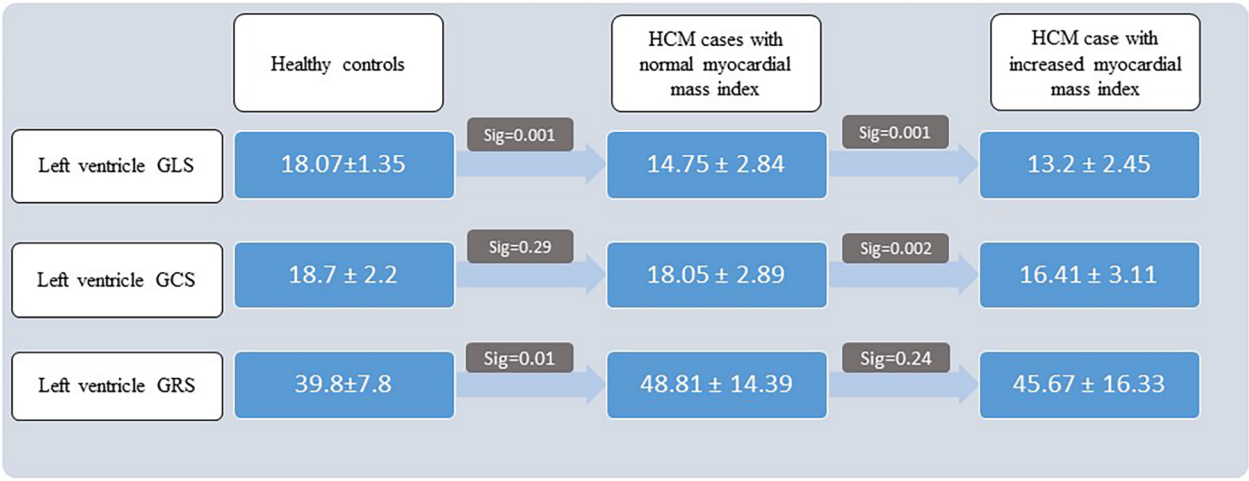

FIGURE 3
Results of *post hoc* least significant difference test. HCM, hypertrophic cardiomyopathy; GLS, global longitudinal strain; GCS, global circumferential strain; GRS, global radial strain.

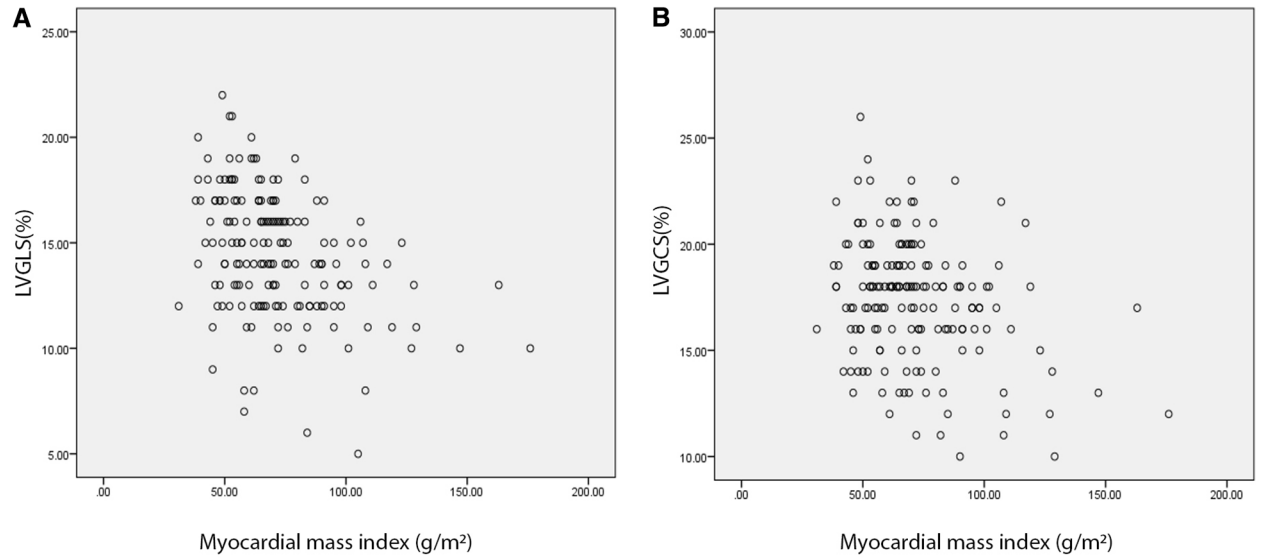

FIGURE 4
Scatter plots demonstrate a weak inverse correlation of absolute LVGLS (A) and LVGCS (B) values with myocardial mass index. Strain values are revealed on vertical and myocardial mass index on horizontal axes. LVGLS, left ventricle global longitudinal strain; LVGCS, left ventricle global circumferential strain.

TABLE 2 Global strains and myocardial mass index comparison among the two groups with and without adverse events.

Variables	Patients with adverse events	Patients without adverse events	*P*-value
LVGLS	−12.649 ± 2.50	−14.473 ± 2.82	**0.005**
LVGRS	41.943 ± 12.81	49.145 ± 15.11	**0.035**
LVGCS	−15.451 ± 3.52	−17.892 ± 2.79	**0.004**
Myocardial mass index	89.087 ± 31.48	71.025 ± 22.91	**0.002**

GLS, global longitudinal strain; GCS, global circumferential strain; GRS, global radial strain.
The statistically significant values are in bold.

TABLE 3 Results of Cox regression analyses.

Variable	Univariate			Multivariate		
	HR	95% CI	*P*-value	HR	95% CI	*P*-value
LVGLS	1.164	1.051–1.290	**0.004**			
LVGCS	1.146	1.082–1.213	**0.001**	**1.144**	**1.080–1.212**	**0.001**
LVGRS	1.004	0.982–1.027	0.7			
LVOT gradient	1.034	0.456–2.347	0.9			
LV myocardial mass index	1.002	0.993–1.012	0.6			
LGE percentage	1.096	0.995–1.209	**0.06**			

LV, left ventricle; GLS, global longitudinal strain; GCS, global circumferential strain; GRS, global radial strain; LVOT, left ventricle outflow tract; LGE, late gadolinium enhancement; HR, hazard ratio; CI, confidence interval.
The statistically significant values are in bold.

multivariate Cox regression. The results revealed that LVGCS was the single predictor of adverse events (HR, 1.144; 95% CI, 1.080–1.212; $P = 0.001$).

The ROC analysis determined a cutoff point of 16.2% for LVGCS to predict adverse events with 77% sensitivity and 58% specificity (area under the curve = 0.716; $P = 0.001$) (Figure 5).

Discussion

HCM is one of the prevalent causes of sudden cardiac death in young adults, hence the vital significance of its timely diagnosis and appropriate management strategy. In the present study, we investigated the CMR findings of 142 HCM patients with normal LV systolic function and a low myocardial fibrosis burden. Furthermore, we meticulously registered the follow-up data of the study population to determine whether CMR data could predict adverse events. Our principal findings are as follows:

A. The HCM and control groups were not statistically meaningfully different concerning LVEF and end-diastolic and end-systolic volumes, whereas the difference between them in all 3 global strain values and MMI constituted statistical significance.
B. In the HCM group, the severity of LVOT obstruction did not influence strain measurements.
C. LVGLS and LVGRS were impaired in the HCM group even if there was no increase in the myocardial mass. Along with an increase in the myocardial mass, a further decline in the LVGLS and LVGCS was detected.
D. Two of the strain values, LVGLS and LVGCS, and the LV myocardial LGE percentage predicted adverse events, with LVGCS being the single robust predictor.
E. An LVGCS value of 16.2% or less predicted adverse events with 77% sensitivity and 58% specificity.

Our results supported the notion that despite an unimpaired systolic function, abnormal myocardial deformation is present even without significant myocardial fibrosis. A previous study proved that CMR-FT parameters were impaired even in the carriers of HCM without the overt disease (19). Therefore, we suppose that CMR-derived strain values, influenced by myocardial fibers disarray, may reveal

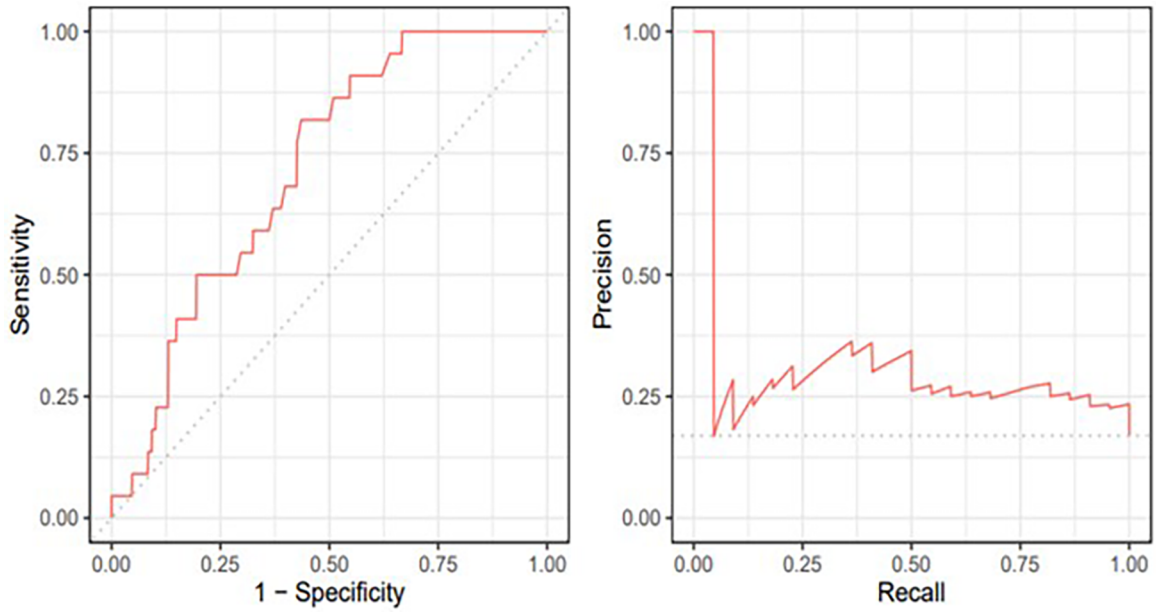

FIGURE 5
Receiver operating curve and precision-recall plots for left ventricle global circumferential strain.

subclinical function impairment and assist in prompt cardioprotective treatment.

Multiple factors may affect the measurement of strain values (20–22). According to previous investigations, we assumed that an increased LVOT gradient, indicative of LVOT obstruction, might influence strain parameters (22). Nonetheless, our analysis did not prove this assumption, which may partly be due to our selected HCM population with an unimpaired LVEF and a low fibrosis burden. We believe that further investigations are needed in this regard.

Our study is one of the first investigations to address the mechanical changes secondary to an abnormal MMI. Our selection of HCM patients without systolic dysfunction and with a low fibrosis burden enabled us to evaluate the net effect of the LV myocardial mass to a great extent. We found a decreased LVGLS and an increased LVGRS in our selected HCM patients with normal myocardial mass. On the other hand, when the myocardial mass increases, LVGCS decreases distinctly. We suppose that it could be due to increased myocyte disarrangement in enlarged myocardial mass, which especially results in LVGCS decline. These findings are in agreement with previous studies suggesting that myocardial disarray in patients with HCM is a limiting factor of myocardial compliance and contractile function (23). Nevertheless, the precise myocardial mechanics in different myocardial mass groups have yet to be elucidated.

Remarkably, our results revealed a moderate inverse linear correlation between the net values of LVGLS and LVGCS and MMI. Strain values indicate function, especially in our selected population, who exhibited no decline in EF values. In a previous study, Dohy et al. showed that while there is no linear correlation between LVEF and MMI, LVGLS, as a functional parameter, correlated with MMI (24). Therefore, we suppose that strain values could be sensitive and early indicators of function impairment in HCM patients.

Previous studies have investigated the role of CMR parameters in indicating the outcome of patients with HCM (25–27). Parameters such as the LGE percentage, regional CMR-FT measures, and 3D global strains were reported to be capable of revealing outcomes in HCM subjects. Similarly, we demonstrated that the LGE percentage, LVGLS, and LVGCS were predictors of adverse events in our selected HCM patients. We also found that LVGCS was an independent predictor of adverse events and managed to define a cutoff point of 16.2% with 77% sensitivity and 58% specificity for LVGCS to reveal adverse events. Our findings are in line with previous investigations concluding that an LGE percentage exceeding 15% and an LVGLS decline are valuable in the risk stratification of patients suffering from HCM (28, 29). The discriminative characteristic of our study is that we selected HCM patients with normal systolic function and a low fibrosis burden and demonstrated that even in these benign-appearing clinical phenotypes, we might take advantage of CMR-FT parameters to estimate the probability of future adverse events.Morever, we utilized the CMR-FT method to determine strain values. This method is now established to have excellent reproducibility and agreement with the known MRI tagging and fast strain-encoded CMR imaging techniques. In contrast to other methods, CMR-FT does not require additional sequences and is, thus, more feasible in clinical practice (30).

In the present study, we observed that patients with a positive family history were more likely to show an increased LVOT gradient. It is noteworthy that 60% of HCM patients with a positive family history have at least one of the eleven known sarcomere protein-encoding genes mutations. However, only 30% of HCM patients without positive family history have them (31). These genetic differences lead to significant phenotypic diversity in HCM, affecting various heart structures (32). Our finding confirms the genetic role in different HCM phenotypic subgroups.

Limitations

Despite its remarkable findings, the present investigation has some limitations. Firstly, the retrospective design of this study limited the data to available medical records and CMR images. Prospective studies with precise predefined clinical variables and CMR protocols may provide more reliable findings. For example, although the gold standard for LVOT gradient measurement is cardiac catheterization, we could not find the catheterization data in the medical records. Doppler echocardiography at rest and with provocative maneuvers were employed to estimate the highest LVOT gradient in our cases. However, previous studies' report of a good correlation between Doppler echocardiography estimations and cardiac catheterization results, convinced us to a great extent (33). Additionally, the use of novel CMR methods, including mapping techniques and 4D flow measurements, is warranted in the assessment of patients with HCM. Secondly, our study had a limited number of patients in each subgroup. Further large-scale multicentric investigations may provide more robust results in subgroup analysis. Finally, the number of the healthy population was a limitation in our investigation. We believe that more reliable results could be obtained by increasing age- and sex-matched healthy control subjects in future studies.

Conclusions

Cardiac MRI-derived strain measures are valuable in revealing subclinical functional alterations in HCM patients with unimpaired EF values and low fibrosis burdens. Furthermore, CMR-FT measures, distinctly LVGCS, are powerful predictors of the outcome in this patient population. It is noteworthy that the CMR-FT method can explain alterations in LV mechanics in different myocardial mass measures.

Data availability statement

The raw data supporting the conclusions of this article will be made available by the authors, without undue reservation.

Ethics statement

The studies involving humans were approved by Rajaie Cardiovascular Medical and Research Center, Iran University of Medical Sciences, Tehran, Iran. The studies were conducted in accordance with the local legislation and institutional requirements. Written informed consent for participation was not required from the participants or the participants' legal guardians/next of kin in accordance with the national legislation and institutional requirements.

Author contributions

SAs: Conceptualization, Methodology, Investigation, Writing. AG: Software, Validation, Formal Analysis, Investigation. AS: Software, Validation, Formal Analysis, Investigation. NS: Data curation. NR: Writing – original draft. HC: Writing. SM: Visualization. SAd: Supervision.

Funding

The author(s) declare that no financial support was received for the research, authorship, and/or publication of this article.

Conflict of interest

The authors declare that the research was conducted in the absence of any commercial or financial relationships that could be construed as a potential conflict of interest.

Publisher's note

All claims expressed in this article are solely those of the authors and do not necessarily represent those of their affiliated organizations, or those of the publisher, the editors and the reviewers. Any product that may be evaluated in this article, or claim that may be made by its manufacturer, is not guaranteed or endorsed by the publisher.

References

1. Elliott PM, Anastasakis A, Borger MA, Borggrefe M, Cecchi F, Charron P, et al. 2014 ESC guidelines on diagnosis and management of hypertrophic cardiomyopathy. *Kardiol Pol.* (2014) 72(11):1054–126. doi: 10.5603/KP.2014.0212

2. Gersh BJ, Maron BJ, Bonow RO, Dearani JA, Fifer MA, Link MS, et al. 2011 ACCF/AHA guideline for the diagnosis and treatment of hypertrophic cardiomyopathy: executive summary: a report of the American college of cardiology foundation/American heart association task force on practice guidelines. *Circulation.* (2011) 124(24):2761–96. doi: 10.1161/CIR.0b013e318223e230

3. Marian AJ, Braunwald E. Hypertrophic cardiomyopathy: genetics, pathogenesis, clinical manifestations, diagnosis, and therapy. *Circ Res.* (2017) 121(7):749–70. doi: 10.1161/CIRCRESAHA.117.311059

4. Maron BJ. Clinical course and management of hypertrophic cardiomyopathy. *N Engl J Med.* (2018) 379(7):655–68. doi: 10.1056/NEJMra1710575

5. McKenna WJ, Maron BJ, Thiene G. Classification, epidemiology, and global burden of cardiomyopathies. *Circ Res.* (2017) 121(7):722–30. doi: 10.1161/CIRCRESAHA.117.309711

6. Semsarian C, Ingles J, Maron MS, Maron BJ. New perspectives on the prevalence of hypertrophic cardiomyopathy. *J Am Coll Cardiol.* (2015) 65(12):1249–54. doi: 10.1016/j.jacc.2015.01.019

7. Marstrand P, Han L, Day SM, Olivotto I, Ashley EA, Michels M, et al. Hypertrophic cardiomyopathy with left ventricular systolic dysfunction: insights from the SHaRe registry. *Circulation.* (2020) 141(17):1371–83. doi: 10.1161/CIRCULATIONAHA.119.044366

8. He D, Ye M, Zhang L, Jiang B. Prognostic significance of late gadolinium enhancement on cardiac magnetic resonance in patients with hypertrophic cardiomyopathy. *Heart Lung*. (2018) 47(2):122–6. doi: 10.1016/j.hrtlng.2017.10.008

9. Cavus E, Muellerleile K, Schellert S, Schneider J, Tahir E, Chevalier C, et al. CMR Feature tracking strain patterns and their association with circulating cardiac biomarkers in patients with hypertrophic cardiomyopathy. *Clin Res Cardiol*. (2021) 110:1–13. doi: 10.1007/s00392-021-01848-5

10. Kinno M, Nagpal P, Horgan S, Waller AH. Comparison of echocardiography, cardiac magnetic resonance, and computed tomographic imaging for the evaluation of left ventricular myocardial function: part 2 (diastolic and regional assessment). *Curr Cardiol Rep*. (2017) 19:1–13. doi: 10.1007/s11886-017-0817-2

11. Li X, Shi K, Yang Z-g, Guo Y-k, Huang S, Xia C-c, et al. Assessing right ventricular deformation in hypertrophic cardiomyopathy patients with preserved right ventricular ejection fraction: a 3.0-T cardiovascular magnetic resonance study. *Sci Rep*. (2020) 10(1):1967. doi: 10.1038/s41598-020-58775-0

12. Shimada YJ, Hoeger CW, Latif F, Takayama H, Ginns J, Maurer MS. Myocardial contraction fraction predicts cardiovascular events in patients with hypertrophic cardiomyopathy and normal ejection fraction. *J Card Fail*. (2019) 25(6):450–6. doi: 10.1016/j.cardfail.2019.03.016

13. Bansal M, Sengupta PP. Longitudinal and circumferential strain in patients with regional LV dysfunction. *Curr Cardiol Rep*. (2013) 15:1–14. doi: 10.1007/s11886-012-0339-x

14. Kovacheva E, Gerach T, Schuler S, Ochs M, Dössel O, Loewe A. Causes of altered ventricular mechanics in hypertrophic cardiomyopathy: an in-silico study. *Biomed Eng Online*. (2021) 20(1):1–28. doi: 10.1186/s12938-021-00900-9

15. Cardiology ACo, Cardiology ACo, Association AH. 2020 AHA/ACC guideline for the diagnosis and treatment of patients with hypertrophic cardiomyopathy A report of the American college of cardiology/American heart association joint committee on clinical practice guidelines. *Circulation*. (2020) 142(25):E558–631. doi: 10.1161/CIR.0000000000000937

16. Maron MS, Olivotto I, Betocchi S, Casey SA, Lesser JR, Losi MA, et al. Effect of left ventricular outflow tract obstruction on clinical outcome in hypertrophic cardiomyopathy. *N Engl J Med*. (2003) 348(4):295–303. doi: 10.1056/NEJMoa021332

17. Maron MS, Olivotto I, Zenovich AG, Link MS, Pandian NG, Kuvin JT, et al. Hypertrophic cardiomyopathy is predominantly a disease of left ventricular outflow tract obstruction. *Circulation*. (2006) 114(21):2232–9. doi: 10.1161/CIRCULATIONAHA.106.644682

18. Petersen SE, Khanji MY, Plein S, Lancellotti P, Bucciarelli-Ducci C. European Association of cardiovascular imaging expert consensus paper: a comprehensive review of cardiovascular magnetic resonance normal values of cardiac chamber size and aortic root in adults and recommendations for grading severity. *Eur Heart J Cardiovasc Imaging*. (2019) 20(12):1321–31. doi: 10.1093/ehjci/jez232

19. Vigneault DM, Yang E, Jensen PJ, Tee MW, Farhad H, Chu L, et al. Left ventricular strain is abnormal in preclinical and overt hypertrophic cardiomyopathy: cardiac MR feature tracking. *Radiology*. (2019) 290(3):640–8. doi: 10.1148/radiol.2018180339

20. Sharifian M, Rezaeian N, Asadian S, Mohammadzadeh A, Nahardani A, Kasani K, et al. Efficacy of novel noncontrast cardiac magnetic resonance methods in indicating fibrosis in hypertrophic cardiomyopathy. *Cardiol Res Pract*. (2021) 2021:1–7. doi: 10.1155/2021/9931136

21. Rezaeian N, Hosseini L, Omidi N, Khaki M, Najafi H, Kasani K, et al. Feature-tracking cardiac magnetic resonance method: a valuable marker of replacement fibrosis in hypertrophic cardiomyopathy. *Pol J Radiol*. (2022) 87(1):263–70. doi: 10.5114/pjr.2022.116548

22. She Jq, Guo Jj, Yu Yf, Zhao Sh, Chen Yy, Ge My, et al. Left ventricular outflow tract obstruction in hypertrophic cardiomyopathy: the utility of myocardial strain based on cardiac MR tissue tracking. *J Magn Reson Imaging*. (2021) 53(1):51–60. doi: 10.1002/jmri.27307

23. Tseng WYI, Dou J, Reese TG, Wedeen VJ. Imaging myocardial fiber disarray and intramural strain hypokinesis in hypertrophic cardiomyopathy with MRI. *J Magn Reson Imaging*. (2006) 23(1):1–8. doi: 10.1002/jmri.20473

24. Dohy Z, Szabo L, Toth A, Czimbalmos C, Horvath R, Horvath V, et al. Prognostic significance of cardiac magnetic resonance-based markers in patients with hypertrophic cardiomyopathy. *Int J Cardiovasc Imaging*. (2021) 37:2027–36. doi: 10.1007/s10554-021-02165-8

25. Chen X, Pan J, Shu J, Zhang X, Ye L, Chen L, et al. Prognostic value of regional strain by cardiovascular magnetic resonance feature tracking in hypertrophic cardiomyopathy. *Quant Imaging Med Surg*. (2022) 12(1):627. doi: 10.21037/qims-21-42

26. O'Hanlon R, Grasso A, Roughton M, Moon JC, Clark S, Wage R, et al. Prognostic significance of myocardial fibrosis in hypertrophic cardiomyopathy. *J Am Coll Cardiol*. (2010) 56(11):867–74. doi: 10.1016/j.jacc.2010.05.010

27. Smith BM, Dorfman AL, Yu S, Russell MW, Agarwal PP, Mahani MG, et al. Relation of strain by feature tracking and clinical outcome in children, adolescents, and young adults with hypertrophic cardiomyopathy. *Am J Cardiol*. (2014) 114(8):1275–80. doi: 10.1016/j.amjcard.2014.07.051

28. Mentias A, Raeisi-Giglou P, Smedira NG, Feng K, Sato K, Wazni O, et al. Late gadolinium enhancement in patients with hypertrophic cardiomyopathy and preserved systolic function. *J Am Coll Cardiol*. (2018) 72(8):857–70. doi: 10.1016/j.jacc.2018.05.060

29. Makavos G, Kairis C, Tselegkidi ME, Karamitsos T, Rigopoulos AG, Noutsias M, et al. Hypertrophic cardiomyopathy: an updated review on diagnosis, prognosis, and treatment. *Heart Fail Rev*. (2019) 24:439–59. doi: 10.1007/s10741-019-09775-4

30. Bucius P, Erley J, Tanacli R, Zieschang V, Giusca S, Korosoglou G, et al. Comparison of feature tracking, fast-SENC, and myocardial tagging for global and segmental left ventricular strain. *ESC Heart Fail*. (2020) 7(2):523–32. doi: 10.1002/ehf2.12576

31. Gersh BJ, Maron BJ, Bonow RO, Dearani JA, Fifer MA, Link MS, et al. 2011 ACCF/AHA guideline for the diagnosis and treatment of hypertrophic cardiomyopathy: a report of the American college of cardiology foundation/American heart association task force on practice guidelines. *Circulation*. (2011) 124(24):e783–831. doi: 10.1161/CIR.0b013e318223e2bd

32. Baxi AJ, Restrepo CS, Vargas D, Marmol-Velez A, Ocazionez D, Murillo H. Hypertrophic cardiomyopathy from A to Z: genetics, pathophysiology, imaging, and management. *Radiographics*. (2016) 36(2):335–54. doi: 10.1148/rg.2016150137

33. Geske JB, Sorajja P, Ommen SR, Nishimura RA. Left ventricular outflow tract gradient variability in hypertrophic cardiomyopathy. *Clin Cardiol*. (2009) 32(7):397–402. doi: 10.1002/clc.20594

Frontiers in
Cardiovascular Medicine

Innovations and improvements in cardiovascular treatment and practice

Focuses on research that challenges the status quo of cardiovascular care, or facilitates the translation of advances into new therapies and diagnostic tools.

Discover the latest Research Topics

See more →

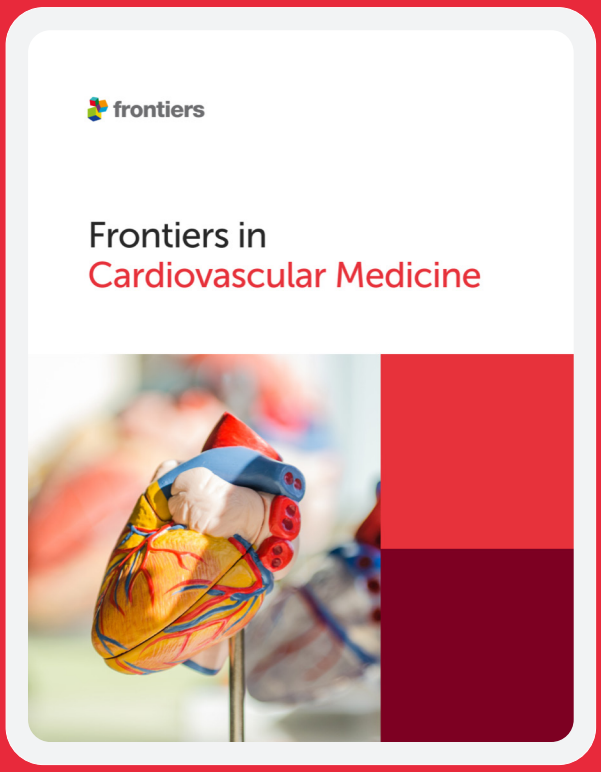

Frontiers

Avenue du Tribunal-Fédéral 34
1005 Lausanne, Switzerland
frontiersin.org

Contact us

+41 (0)21 510 17 00
frontiersin.org/about/contact